UNIVERSITÀ DEGLI STUDI DI MESSINA

Dipartimento di Scienze Chimiche, Biologiche, Farmaceutiche ed Ambientali

Doctor of Philosophy in "Chemical Science"

Foodomics: LC×LC approach in modern food science

PhD Thesis

Katia Arena

Tutor

Ivana Lidia Bonaccorsi

Coordinator

Prof.ssa Paola Dugo

XXIII Cycle (2017-2020)

Index

Abstract

The object of the research work investigated in this Ph.D. thesis was the development and implementation of advanced analytical techniques based on comprehensive two-dimensional liquid chromatography coupled to MS, in order to obtain a complete identification and characterization of bioactive molecules in complex natural products. Comprehensive two-dimensional LC (LC×LC), involving the coupling of two or more orthogonal or quasi-orthogonal separation systems, is an interesting alternative to classical 1D approach, being in many cases also selective and sensitive enough to detect minor components. The advantages of this technique compare to mono dimensional approach are: increased resolving power, enhanced identification potential, especially when coupled to mass spectrometry, reduction of ion enhancement or suppression phenomena during the ionization process in the source of MS. In addition, modern food analysis is direct to the characterization of as many components as possible in food and food-related materials. The use of "Foodomics" approach requires the employ of these advanced analytical techniques, able to offer capability to separate a high number of constituents, such as LC×LC separations. For this reason, most of the research have been focused on the characterization of polyphenols compounds in food samples and natural products.

1.0 Introduction

1.1 Liquid chromatography from the origin to modern techniques

The term “chromatography” according to the International Union of Pure and Applied Chemistry (IUPAC) refers to a physical method of separation, in which, compounds of the samples are selectively distributed in two immiscible phases [1]. The history of modern chromatography can be located to the beginning of the 20th century, when the Russian botanist Michail Tswett (1872–1919) using a packed column with a calcium carbonate as stationary phase, was able to separate coloured pigments from plant extracts [2]. In his experiments, Tswett put the sample at the head of the column that were carried out through the stationary phase using a flow of petroleum ether used as mobile phase. As the sample moved through the column, the extracts were separated into individual coloured bands. Once the pigments were well separated, the calcium carbonate was eluted from the column and the pigments recovered by extraction. Tswett called the technique “chromatography”, combining the Greek words “chroma” (colour) and “grafos” (writing). There was little interest in Tswett’s technique until late 60’s, when thanks to the development in columns, detectors and the works of Martin and Synge, who developed the liquid-liquid partition chromatography for the separation of acetyl derivatives of natural amino-acids, and defined a chromatographic theory by adding the theory of distillation in packed columns [3]. The column could be divided into a series of "theoretical tables", each one showing a partition balance between various phases (stationary phase and gas phase during distillation, stationary phase and liquid phase in chromatographic processes). The efficiency is related to the theoretical plates, so correlated to the length of the column, or otherwise, reversely proportional to the “equivalent height of the theoretical plate (HETP o H). This latter dependes to variables that influence the diffusion of solutes in the two phases, like the diameter of the particle of the column, so that a larger porosity size results in a more

relevant diffusibility of the compounds in the stationary phase, thus enhancing the H value. The new parameter to be taken into account in chromatography is the flow rate of the mobile phase, in particular the diffusion described above can be minimized if a high flow rate is applied. In this respect, the capability to use a very high flow rate without any pressure restrictions and maximize the chromatographic performance was the main reason for the faster development of gas chromatography (GC) compared to LC. In 1956 was introducted, by Van Deemeter et al., the relative equation for GC process [4].

$$H = A + \frac{B}{u} + Cu \qquad \textbf{(1)}$$

According to this formula, H is the sum of the three terms:

1) A refers to the influence of multi-path dispersion across the column, due to potential packing differences or particles with various dimensions so multiple diffusion channels are formed; this parameter is also called Eddy diffusion and could be calculated as $A=2\lambda d_p$, where λ refers to the quality of the packing and d_p is the diameter of the particle.

2) B is the longitudinal diffusion, which follows the solute gradient of concentration, resulting in the Gaussian shape of each chromatographic peak. It can be represented as $B=2\gamma D_M/u$, where γ is, as λ, a variable connected to potential differences in the stationary phase, D_M is the diffusivity of the solute in the mobile phase and u is the linear velocity of the mobile phase. To reduce the B factor, D_M should be kept to a minimum and a high flow rate should be used.

3) C is the resistance to mass transfer, considering both mobile (Cm) and stationary (Cs) phase transfer, then $C = C_m+C_s$, where $C_m=f_1K'd_p^2u/D_M$ and $C_s=f_2K'd_f^2u/D_s$. The parameters f_1 and f_2 are values related with the shape of the stationary phase, K' is the column capacity factor related to the solute

retention, d_p and d_f are respectively the particle diameter and the total packing, D_M and D_s are the diffusivity of the solute in the mobile and stationary phase, respectively, and u is the flow rate of the mobile phase. This term was not considered before by Martin and Synge, who expressed only a direct proportionality between chromatographic efficiency and flow rate [5].

Due to the presence of two different contributions, it has been possible to establish that there an optimal flow is obtained when both terms B and C were minimized. It corresponded to the minimum of the traced curve H against the linear velocity u (Figure 1).

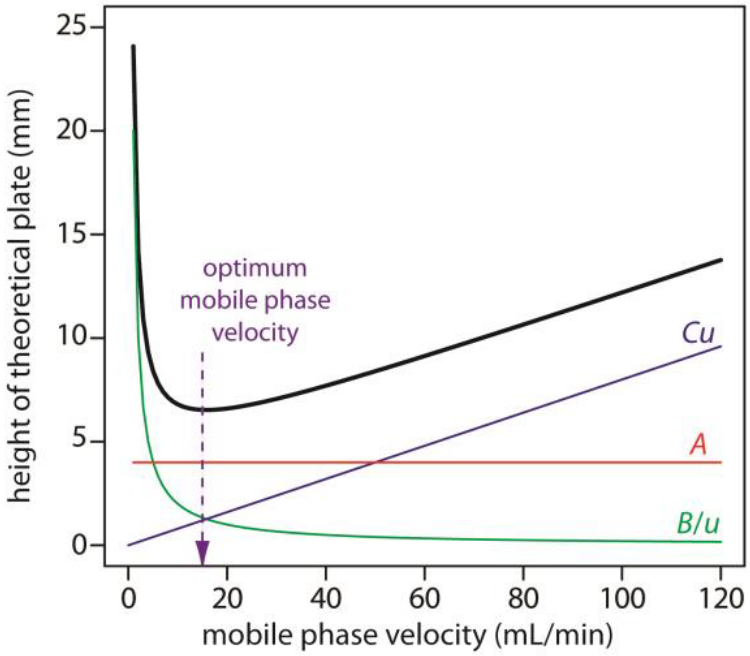

Figure 1. Typical Van Deemter plot

According to Van Deemter's equation it became obvious that the decrease of both particle diameter (dp) and stationary phase thickness (df) should cause a significant reduction of H, since both terms A and C are linked to these parameters. This was the work of Golay, who in 1958 wrote an article on open tubular columns equally coated with a thin layer of stationary phase, thereby removing the term A and making C

smaller due to the thinness of the stationary phase [6]. The direct result was an exponential increase in GC applications and open capillary tubular columns are re the most popular used nowdays. GC theory was promptly applied to LC, resulting in the development of high performance column packings for LC, substituting traditional 30-200 μm porous material with particles of less than 10 μm. The origin of modern LC is usually attributed to Horvath, who packed for the first time in 1965, a 1mm ID column with μ-porous particelles [7]. Based on column length, ID and particle dimensions, the mobile phase has been flushe into the column at different flow rates in the μL-mL/min range with relatively high back pressures. Therefore, high performance liquid chromatography or high pressure liquid chromatography (HPLC) has been the name of modern LC techniques, aiming to increase the separation of constituents and the repeatability of the method, thus enabling qualitative/quantitative analysis. The main columns used in LC have ID 2-2.1 mm or 4-4.6 mm and a length of 10-25 cm. Columns with smaller ID allow very low sample detection quantification but leading to a low sampling capacity. Bigger columns are generally utilized for preparatory LC. Table 1.1 shows the classification of analytical LC columns according to their ID [8].

The first stationary phases employed in LC by Tswett in 1903 were very polar chemicals such as cellulose, silica. In 1950 Martin and Howard discovered that very apolar components such as long chain fatty acids were not properly separated on a polar substrate, whatever the composition of the mobile phase used [9]. Subsequently, they combined a stationary phase in cellulose acetate and water in combination with a very apolar solvent such as octane to ensure good separation quality (high chromatographic resolution). New chromatography separation, in which the stationary phase was less polar than the mobile phase, was called reversed phase (RP) LC to differentiate it from conventional normal phase (NP) LC.

Table 1.1 Classification of LC columns according to their ID

Column designation	Typical I.D. (mm)
Preparative LC	Higher than 20
Semi- Preparative LC	6-20
Conventional LC	3-5
Narrow-bore LC	2
Micro LC	0.5-1
Capillary LC	0.1-0.5
Nano LC	0.01-0.1
Open tubular LC	0.005-0.05

In normal phase liquid chromatography (NP-LC), the stationary phase is more polar than the mobile phase. Retention is higher as the polarity of the mobile phase decreases, so polar analytes are retained more strongly than non-polar analytes. Opposite situation occurs in reverse phase liquid chromatography (RP-LC). NP-LC has been extensively utilized to separate different compounds, from non-polar to highly polar compounds. Even though RP-LC systems were earlier widely employed by scientists, NP-LC methods are still in a phase of turnaround. Hydrophilic interaction liquid chromatography (HILIC) is another mode of high performance liquid chromatography (HPLC) for the polar compounds separation. Due to various reasons, HILIC has been described as a variant of normal phase liquid chromatography, but the separation mechanism used in HILIC is more complex than that of NP-LC. The number of publications on HILIC has increased substantially since 2003 as highlighted in the well-constructed review of Hemström and Irgum [10].

Such as NP-LC, HILIC uses traditional stationary polar phases such as silica, amine or cyan [8-12], but the mobile phase adopted is quite similar to those used in RP-LC mode [10-12]. HILIC also enables the analysis of charged substances, as in ion chromatography (IC). Figure 2 shows how HILIC is complementary to other areas of chromatography and extends the range of separation options.

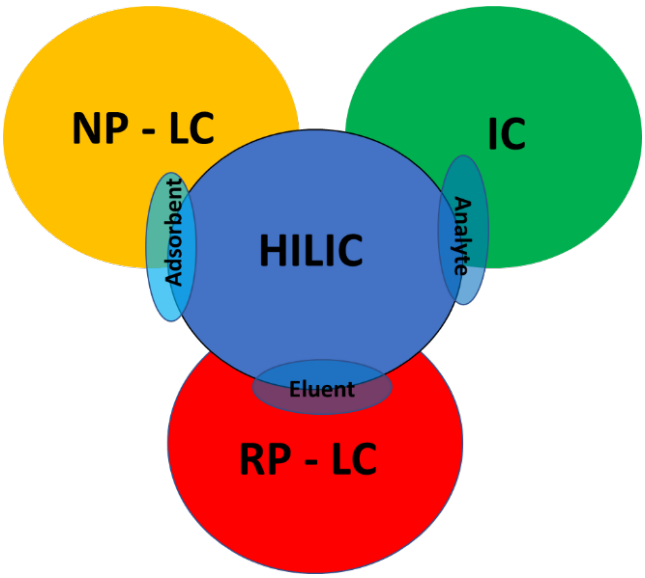

Figure 2. HILIC combines the characteristics of the three major methods in liquid chromatography

HILIC offers several specific benefits over traditional NP-LC and RP-LC. For example, it is suitable for the analysis of mixtures in complex systems that always elute close to void in reserved phase chromatography. Polar samples always exhibit good water phase solubility in the mobile aqueous phase used in HILIC, which bypasses the problems of poor solubility often found in NP-LC. Expensive ion pair reagents are not needed in HILIC and can be conveniently combined with mass spectrometry (MS), especially in electrospray ionization (ESI) mode. Unlike RP-LC, HILIC gradient elution starts with a low-polarity organic solvent and elutes polar analytes by increasing the aqueous polar content [13]. A recommendable mobile phase would contain high

organic concentration for enhanced sensitivity and would also exhibit good column retention for polar ionic compounds. Hydrophilic interaction liquid chromatography has proven to be the separation mode of choice for uncharged highly hydrophilic and amphiphilic compounds that are too polar to be well preserved in RP-LC but have insufficient charge to allow effective electrostatic retention in ion exchange chromatography. HILIC separation is currently gaining a lot of popularity as it resolves many separation problems that were previously hard to solve, such as the separation of small organic acids, basic drugs and many other neutral and charged substances. It has been successfully applied to the analysis of carbohydrates [14,15], peptides [16-18] and polar drugs [11,19], etc.

Several articles have discussed the mechanism and theoretical description of analyte retention in HPLC. Basically, there are three different ways to model the separation process. The first is the partitioning of the analyte between the mobile and stationary phase [20, 21]; the second is the adsorption of the analyte on the adsorbent surface [22, 23]; the third takes the selective adsorption of the organic mobile phase modifier on the adsorbent surface, and then by the partitioning of this analyte in the adsorbent layer [24]. The retention phenomenon in HPLC depends at the same time on several types of intermolecular interactions among solute and stationary phase, solute and mobile phase, and stationary and mobile phases. The current theory suggests that HILIC retention is due to partitioning. This phenomenon still lacks an in-depth theoretical explanation. In this method, the separation mechanism is dependent on the differential distribution of the solute molecules of the injected analyte between the mobile phase rich in acetonitrile and a layer enriched with water adsorbed on the stationary hydrophilic phase [25,26]. Therefore, the more hydrophilic the analyte, the more the distribution equilibrium is shifted towards the immobilized water layer on the stationary phase, the more the analyte is retained. This means that a separation based on the polarity of the compounds and the degree of solvation takes place.

1.2 General trends and recent development in LC

1.2.1 UHPLC techniques

Over the last years, chromatographers continued to focus their attention on reducing column particle diameters in order to improve chromatographic efficiency with reasonable flow rates, resulting in a considerable reduction in analysis time. As shown by Giddings in 1991 there is a linear correlation between the pressure drop (ΔP) and the linear velocity (u) in the column [27] (equation 1.2).

$$\Delta P = \frac{\varphi \eta u L}{d_p^2} \quad \textbf{(2)}$$

where φ, η, L and d are the flow resistance, mobile phase viscosity, column length and diameter of the particles, respectively. It has been proved that choosing a 25cm lengthy column packed with 5 μm particles, an inlet pressure less than 25bar is needed to perform the analysis, while reducing the particle diameter at 1 μm require an inlet pressure of 2000 bar [28,29]. Therefore, a significant upgrade of the instrumentation was essential: the pumps, the injection system and all connections had to be able to work at very high pressures (thousands of bar), instead detectors capable of acquiring a high acquisition speed had to be used. The name of the new instrumentation and new methods was ultra-high pressure (or ultra-high performance) LC (UPLC or UHPLC), a term coined by Jorgensen in 1997 [30] and used today to refer to a very fast separation with high efficiency and resolution. The heart of the UHPLC technique lies in columns with particles smaller than 2 μm. Observing Van Deemter's diagram for this type of columns (Figure 3), it is possible to see the flattening of the curve in the region of linear velocity of mobile phase greater than optimal, which means that these columns can run at high flow rates without any loss of efficiency.

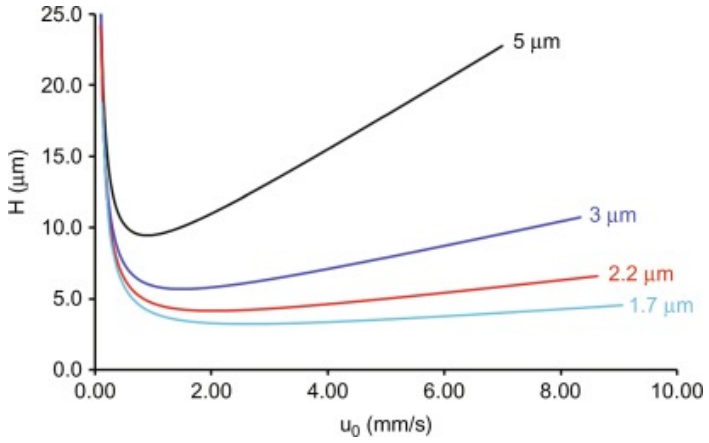

Figure 3. Van Deemter Plot at different d_p

Figure 3 shows similar performance for the other packing of columns, i.e. monolithic and with fused-core. The first was introduced roughly in the same years of sub-2µm particles and consists of a single piece of porous material such as organic polymers or silica, having a very limited flow resistance compared to a particle-packed column. Normally the diameter of the porous rod is about 1.5-2 µm (macroporosity) with porosity of 10-12 nm (mesoporosity), which minimizes the diffusion path and mass transfer effect. However, mesopores make these columns not very efficient for small molecules, on the contrary, they are largely still employed for the analysis of macromolecules, like in proteomics analysis [31]. The biggest problem with monolithic technology is the limited length of the column: a straight monolithic column longer than 15 cm cannot be prepared smoothly, thus limiting the number of theoretical plates per column. [32,33]. Fused core particles appeared on the market in 2006 and are also called as partially porous or core-shell particles to discern the difference with totally porous technology and the presence of a solid core in which analytes cannot penetrate. The biggest advantage of the fused core columns compared to columns of less than 2 µm is the lower backpressure so that these phases can be operated on a conventional LC instrument [34].

1.2.2 Multidimensional LC

Within the overview of LC trends, recent improvements in multidimensional techniques should be reported. Actually, multidimensional LC (MDLC) has a history almost as long as chromatography. The term is used to refer to the coupling of more than one column to separate sample compounds, where each mechanism of separation in each column being an independent separative dimension. The necessity to develop MDLC methods was born from the extreme complexity of several real samples, since the one-dimensional system was not able to fully resolve all the components of the sample mixture. For example, in the presence of biological or pharmaceutical samples, the separation of enantiomers is very important; therefore a first dimension (1D) is used to separate the diastereoisomers, and a properly time-controlled transfer of each peak into a second dimension enantioselective (2D) is used to resolve the enantiomers. Basically, there are two types of multidimensional LC approaches: the heart cutting (LC-LC) and comprehensive (LC×LC). The first one, allows ^{2}D separation for selected fractions of the sample only, while the second allows the two-dimensional (2D) separation of the whole matrix with a significant increase in resolving power, which is usually given by the total peak capacity (n_c), which is the number of analytes that can be theoretically separated.

The two approaches may be carried out both in off-line and on-line modes. In the former case, the fractions eluted from the first column are collected manually or from a fraction collector, concentrated if necessary, and re-injected in a second column. These solutions are certainly time-consuming, labor-intensive and difficult to automate. In addition, off-line sample treatments might be prone to contamination resulting not useful if quantitative trace analysis is required. This technique is most commonly employed when only specific parts of the first separation require secondary separation. In an on-line MDLC system instead, the two columns are connected through a special interface, usually a switching valve, which enables the transfer of the

fractions from the first column effluent to the second column. This approach should fulfill some specific criteria, like as compatibility of the ^{1}D mobile phase and the ^{2}D stationary phase, the miscibility of the solvent used in the two dimensions, and the elution time in the ^{2}D must be very fast, before the successive transfer. Stop flow approach, where the ^{1}D flow is temporarily interrupted during the elution in ^{2}D, allowed to go over this issue. Otherwise, a very high flow rate or a short column can be used to accelerate the separation in 2D, affecting the chromatographic efficiency according to Van Deemter's equation. However, the development of UHPLC and improvements in stationary column phase technology have made possible to perform very fast analyses without losing efficiency. Nonetheless, the need for a specific interface and software, the skill level of the operator and also the cost implications make online techniques less easy to use than the off-line approach which can be easily realized because both analytical dimensions can be optimized as two independent methods.

1.3 Detection systems

Detector choice is usually key for the achievement of a particular HPLC method. A certain variety are in daily use, including UV, fluorescence, electrochemistry, conductivity and refractive index detectors, each with their own particular advantages and drawbacks. Detectors may be classified:

- solute or solvent-property detectors
- selective or universal detectors
- mass or concentration sensitive detectors
-

1.3.1 Solute or solvent property detectors

This category covers whether the detector detects in solute property (analyte), e.g. for the UV detector, or a variation of some solvent properties (mobile phase) caused by the presence of an analyte, e.g. for the refractive index detector.

1.3.2 Selective or universal detectors

This category takes into consideration whether the detector responds to a specific analyte property of the analyte of interest or whether it will respond to a high number of analytes, regardless of their structural properties. According to the classification, it can be assumed that solute detectors are also typically selective while solvent detectors are general detectors.

UV absorption is the most used HPLC detection technique is probably UV absorption and has capacity both as a specific detector and as a general detector, according on the way it is utilized. If the wavelength of maximum absorption of the analyte (λmax) is given, it can be controlled, and the detector can be considered selective for these analytes. As UV absorptions are, however, typically broad, this form of detection is often not selective. If a diode instrument is used, it is possible to monitor more than one wavelength and measure the absorbance ratio. Agreement of the ratio measured by the "unknown" with that measured in a reference sample gives better confidence that the analyte of interest is being measured, although it does not yet provide absolute certainty.

A broadly used general detector is the refractive index detector that measures variations in the refractive index of the mobile phase as an analyte elutes from the column. If gradient elution is selected, the refractive index of the mobile phase changes as its composition changes, giving a constant baseline of the detector. The measurement of both position and intensity of a low intensity the analytical signal on a variable baseline

is less exact and less accurate than the same measurement on a constant baseline with zero baseline signal. It is usually recognized that general detectors are not as sensitive as specific detectors, showing a lower dynamic range and do not provide the best results when gradient elution is utilized.

1.3.3 Mass or concentration sensitive detectors

The last classification concerns how intense the detector response is proportional to the solute concentration or to the absolute amount of solute that reaches it. This class of detector is really important for quantitative goals. If the flow rate of the mobile phase is increased, the concentration of the analyte reaching the detector remains the same, but the amount of analyte increases. In these conditions, the intensity of the signal from this kind of detector will stay constant, even though the peak width will decrease, i.e. the the response area will decrease too. A variation in the flow rate will decrease the width of the response of a mass sensitive detector, unlike a concentration sensitive detector, the signal intensity will increase as the absolute quantity of analyte reaches the detector. As the overall response increases, this can be used to improve the quality of the signal obtained. In many experimental conditions, mass spectrometer works as a mass sensitive detector, and in others, like for example when LC-MS is used in electrospray ionization, it can be considered like a concentration sensitive detector. A benefit of the mass spectrometer as a detector is that it can provide differentiation of compounds with very similar retention characteristics or may enable the identification and/or quantitative determination of compounds that are only partially eluted chromatographically, or even those totally co-eluted. In general, an MS instrument consists of three basic components, namely the ion source, to generate ions from the sample, the mass analyzer, to separate them according to the mass-to-charge ratio (m/z), and the detector, to measure emerging ions.

1.3.4 MS ion sources

According with the ionization process that take place into the ion source, mainly divided in hard and soft ionization, the level of information obtained is different. Hard ionization process provides enough energy to the molecules that involves bonds break, releasing fragment ions having a mass-to-charge ratios lower than the molecular ion, driven the structural elucidation. On the contrary, soft ionization leads to a less fragmentation, therefore the resulting mass spectrum usually includes the molecular ion peak (in GC-MS) or the deprotonated molecular ion (LC-MS), given the molecular weight details. Immediately after its invention, it became obvious that this technique was well adapted for volatile and thermally stable compounds, but it precluded the study of large molecules. In addition, due to poor compatibility of the liquid phase with the vacuum region of an MS, hyphenation with gas chromatography was simpler than hyphenation with LC, which needed to elimination of the mobile phase prior the analyte enters in the mass spectrometer, thus compromising analytical performance. The turning point arrived with the discover of different ionization techniques, like as, the atmospheric pressure ionization (API) and in particular the electrospray ionization (ESI) and atmospheric pressure chemical ionization (APCI). Thanks to these new techniques, the elimination of the quantity of the solvent was much easier [35,36]. Nowadays, ESI and matrix assisted laser desorption ionization (MALDI) are the techniques of choice for the analysis of macromolecules. In the first case, the ionization arrives after the passage of the analytes into a needle keep at high voltage (kV) placed at the entrance to the MS. ESI is the best technique for very polar compounds, ranging from 100 to 150000 Da. On the contrary, MALDI produces only singly charged ions, and it is suitable for protein and carbohydrate characterization [37]. Finally, APCI is preferred to ESI for the medium polarity compounds comprised for 100 to 2000 Da. While ESI is liquid phase ionization, APCI is in gas phase conditions, after a nebulization promoted by nitrogen stream and the subsequent LC effluent vaporization at 350-550 °C.

1.3.5 MS analyzers

The analyzer can be considered the heart of MS, since characteristics such as analysis speed, mass range, resolution, mass accuracy, dynamic range and sensitivity depend on it. The most widely used mass analyzers, due their low cost, are the quadrupole (Q), ion-trap (IT) and time of flight (ToF), as well as a mix of hybrid instruments such as Q-ToF, IT-ToF and QqQ (triple quadrupole). In general, the ToF analyzer is distinguished by a very high resolution, mass accuracy, analysis speed and very wide mass range. On the contrary, quadrupole and ion trap are limited to a specific *m/z* range that arrive to detector according to the electric field applied [38]. In the Figure 4 a schematic representation of quadrupole and ion trap detector is showed. In detail, quadrupole is made up of 4 metal bars to which a combination of current and radiofrequency is applied in order to send only specific ions; in fact, in ion trap the radiofrequency (RF) is released by a ring electrode, while a direct or alternate current (DC or AC) can be applied to the terminal electrodes, so that at the beginning the ions are present together inside the trap and are ejected by applying the RF field in a similar way to the quadrupole analyzer.

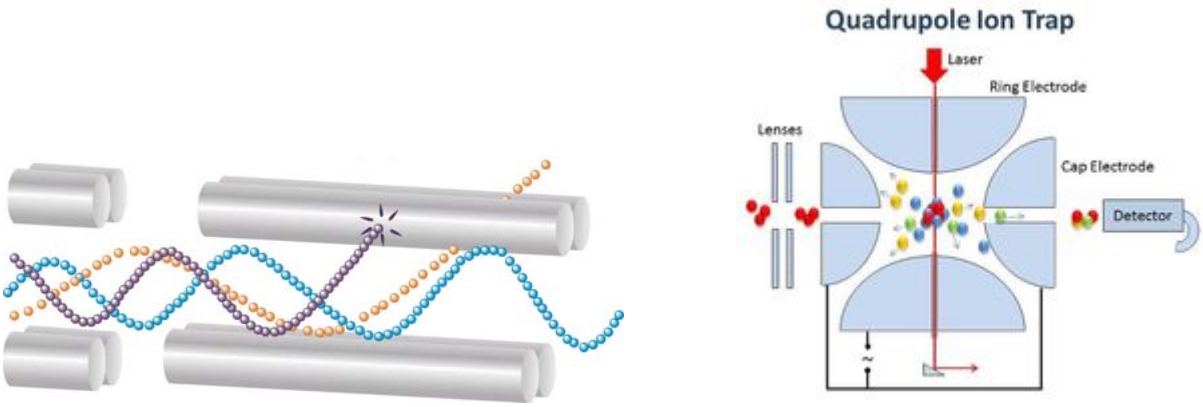

Figure 4. Schematic representation of quadrupole (on the left) and ion trap (on the right) analyzers.

Generally, MS systems can work in full scan mode (total ion current chromatogram, TIC), in tandem MS experiments or in selected ion monitoring mode (SIM) where only

ions with a given m/z value reach the detector by setting a specific RF on the quadrupole. SIM mode is used for the development of selective and sensitive quantitative method, due to the reduction of the baseline noise, i.e. the gain in the signal-to-noise ratio (S/N). In addition, the integration of the SIM spikes excludes any problem from totally or partially coeluted substances, as is the case with a PDA detector [39].

Nevertheless, the quantification, or even detection of a target trace component, in SIM mode can be tricky with high background ions of the same m/z values; in these cases, higher selectivity is achieved using MS/MS techniques. At this time, triple quadrupole (QqQ) instruments are the detector of choice for targeted analysis with high selectivity and sensitivity [40]. A schematic representation of this analyzer is shown in Figure 5.

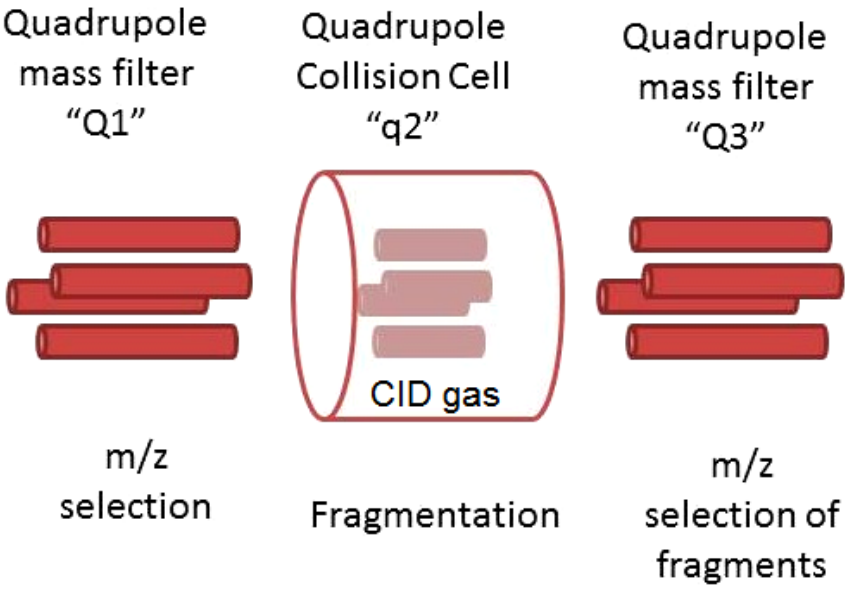

Figure 5. Schematic representation of triple quadrupole

While Q1 and Q3 work as true quadrupoles by filtering ions according to the combination of RF and DC, q2 operates like an ion trap where only one RF is applied to capture the ion. If both Q1 and Q3 operate both in SIM mode, by choosing a precursor or "parent" ion and a produced or "daughter" ion respectively, maximum selectivity and sensitivity is achieved in the so-called selected reaction monitoring (SRM) or multiple reaction monitoring (MRM) mode. Normally, the fragmentation

marked by the highest S/N is chosen as a quantifying transition for quantitative analysis, while a second (or even more) fragmentation is selected as a qualifying transition, necessary to evaluate with a high level of certainty the identification of the components. Furthermore, the ratio between the intensity of the two transitions is typical of the given component and must remain stable along the linearity range [41]. The very low detection limit reduces sample consumption and also shortens analysis time, minimizing the need for clean-up operations. If there is a need to monitor multiple components with similar fragmentation patterns, the neutral loss scan mode can be used to monitor the loss of a neutral molecule, such as water or carbon dioxide during fragmentation, so only transitions characterized by a specific difference between the precursor and the produced ion will result in a peak in the chromatogram. The very low detection limit reduces sample consumption and also shortens analysis time, minimizing the need for clean-up operations. If there is a need to monitor multiple components with similar fragmentation patterns, the neutral loss scan mode can be used to monitor the loss of a neutral molecule, such as water or carbon dioxide during fragmentation, so only transitions characterized by a specific difference between the precursor and the produced ion will result in a peak in the chromatogram. Also, to help elucidate the structure, the full scan spectrum of a precursor ion can be achieved in the product ion scan mode, in the same way that the precursor ion scan mode is adequate to provide identification of a component by giving the possible precursor for a selected product. Figure 6 shown the different way of working of a triple quadrupole [42].

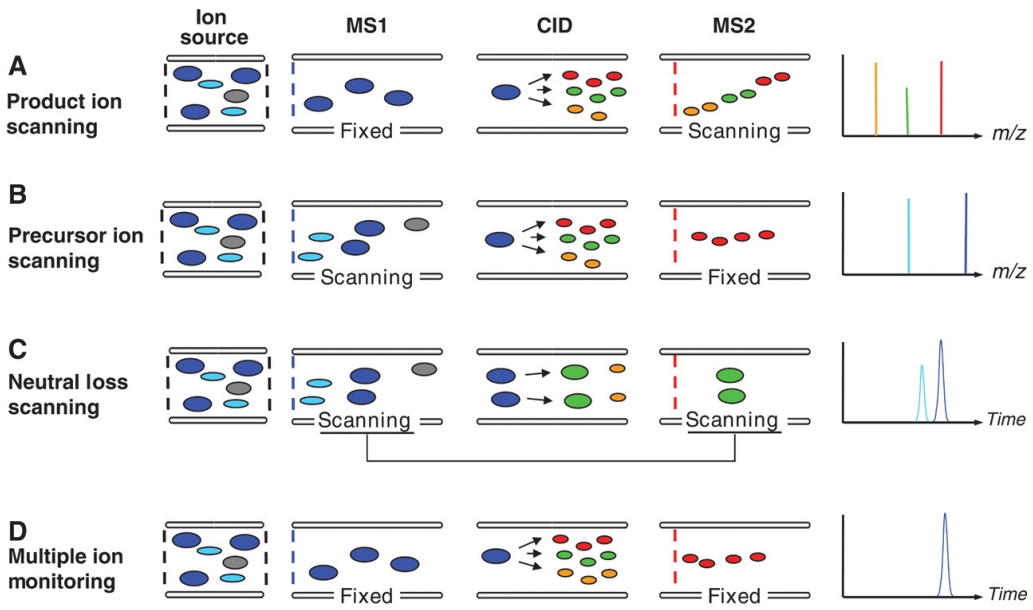

Figure 6. Different working step of the different mode for QqQ

Despite the high selectivity of tandem MS, the necessity for more powerful high-resolution separation methods increased over the years, with the interest in complex biological samples and metabolic profiles, so that the analyst's goal is to achieve the entire fingerprint of all metabolites in a biological sample. If the analyte of interest is not well separated, its mass spectrum is "contaminated" with ions coming from other non-specific compounds, hindering positive identification and, even more, reliable quantification, especially for trace components. The more recent analyzer is the orbitrap (OT), it is based on orbital trapping of the ions in an electrostatic field (figure 7), similar to the ion trap technology. The aim of the OT development was to achieve a high-performing research and routine instrument regarding resolution power and sensitivity. The OT is based on pulsed packages of ions, produced by the C-trap, that are introduced and captured into the analyzer. The ions are kept in an OT movement while the applied electrical field keeps the ions in oscillating movement and produces signals to receiver plates. The signals are Fourier transformed into mass spectral data. In order to obtain quality data, the time spent for each ion package in the OT is essential. Orbitrap mass spectrometers deliver a total possible maximum resolution (FWHM) of 1.000.000 at m/z 200 and a sub-1 ppm mass accuracy in a single compact

and easy-to-use instrument. These high-resolution accurate-mass systems detect a wide range of compounds and small molecules during both targeted and untargeted analyses, without losing selectivity or sensitivity. Simply put, when it comes to Orbitrap technology, there is no compromise [43-44].

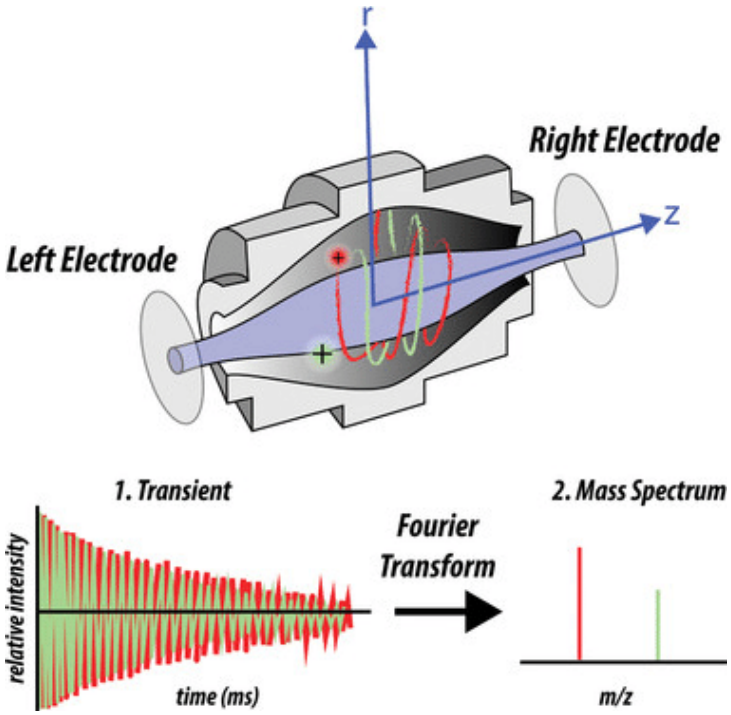

Figure 7. Schematic representation of orbitrap analyzers.

References

[1] M. Tswett. Ber. Dtsch. Botan. Ges. 1906, 24, 316-384.

[2] A. J .P. Martin. R. L. M. Synge, Biochem. J. 1941, 35, 1358.

[3] J. R. Peters. W.A. Ind. Eng. Chem. 1922, 14, 476-479.

[4] J. J. Van Deemter; F. J. Zuiderweg; A. Klinkenberg. Chem. Eng. Sc. 1956, 5, 271-289.

[5] A.T. James; A.J.P. Martin. Biochem. J. 1952, 50, 679-690.

[6] M. J. E. Golay. Gas Chromatography 1958, edit. by Desty, D.H., 36, Butterworths Sci. Pub., London, 1958.

[7] C. Horváth; S. R. Lipsky. Nature, 1966, 211, 748-749.

[8] Y. Saito; K. Jinno; T. Greibrokk. J. Sep. Sci 2004, 27,1379-1390.

[9] G. A. Howard; A.J.P. Martin. Biochem. J. 1950, 46, 532-538.

[10] P. Hemström; K. Irgum. J. Sep. Sci. 2006, 29, 1784–1821.

[11] R. Li; J. Huang. J. Chromatogr. A 2004, 1041,163–169.

[12] Y. Guo; S. Gaiki. J. Chromatogr. A 2005, 1074, 71–80.

[13] S. Cubbon; T. Bradbury; J. Wilson; J. Thomas-Oates. Anal. Chem. 2007, 79, 8911-8918.

[14] A. J. Alpert; M. Shukla; A. K. Shukla; L. R. Zieske; S. W. Yuen; M. A. J. Ferguson; A. Mehlert; M. Pauly; R. Orlando. J. Chromatogr. A 1994, 676, 191–202.

[15] S. C. Churms. J. Chromatogr. A 1996, 720, 151–166.

[16] A. R. Oyler; B. L. Armstrong; J. Y. Cha; M. X. Zhou; Q. Yang; R. I. Robinson; R. Dunphy; D. J. Burinsky. J. Chromatogr. A 1996,724, 378–383.

[17] T. Yoshida. J. Biochem. Biophys. Meth. 2004, 60, 265–280.

[18] Z. G. Hao; C. Lu; B. M. Xiao; N. D. Wenig; B. Parker; M. Knapp; C. Ho. J Chromatogr. A 2007, 1147, 165–171.

[19] M. A. Strege; S. Stevenson; S. M. Lawrence. Anal. Chem. 2000,72, 4629–4633.

[20] K. A. Dill. J. Phys. Chem. 1987, 91, 1980–1988.

[21] P. T. Ying; J. G. Dorsey; K. A. Dill. Anal. Chem. 1989, 61, 2540–2546.

[22] H. L. Wang; U. Duda; C. J. Radke. J. Colloid. Interface Sci. 1978, 66, 153–165.

[23] F. Riedo; E. S. Kováts. J. Chromatogr. A 1982, 239, 1–26.

[24] J. H. Knox; A. Pryde. J. Chromatogr. A 1975, 112, 171–188.

[25] A. J. Alpert. J. Chromatogr. A 1990, 499, 177–196.

[26] P. Hemström; K. Irgum. J. Sep. Sci. 2006, 29, 1784–1821.

[27] J. C. Giddings. Unified separation Science, Wiley, New York, 1991.

[28] L. A. Colon; J. M. Cintron; J. A. Anspach; A. M. Fermier; K. A.Swinney. Analyst, 2004, 129, 503-504.

[29] J. A. Anspach; T. D. Maloney; L. A. Colon. J. Sep. Sci. 2007, 30, 1207-1213.

[30] J. E. MacNair; K. C. Lewis; J. W. Jorgenson. Anal. Chem. 1997, 69, 983-989.

[31] I. Ali; V. D. Gaitonde; H. Y. Aboul-Enein. J. Chromatogr. Sci. 2009, 47, 432-442.

[32] N. Ishizuka; H. Kobayashi; H. Minakuchi; K. Nakanishi; K. Hirao; K. Hosoya; T. Ikegami; N. Tanaka. J. Chromatogr. A, 2002, 960, 85-96.

[33] N. Tanaka; H. Kobayashi; N. Ishizuka; H. Minakuchi; K. Nakanishi; K. Hosoya; T. Ikegami. J. Chromatogr. A, 2002, 965, 35-49.

[34] S. Fekete; D. Guillarme; M.W. Dong. LC GC N. Am. 2014, 32, 2-12.

[35] E. C. Horning; I. Carroll; K. D. Haegele; M. G. Horning; R. N. Stillwell. J. Chromatogr. Sci. 1974, 12, 725-729.

[36] C. M. Whitehouse; R. N. Dreyer; M. Yamashita; J. B. Fen. Anal. Chem. 1985, 57, 675-679.

[37] M. Karas; M. Glückmann; J. Schäfer. J. Mass Spectrom. 2000, 35, 1-12.

[38] G.L.Glish; R.W. Vachet. Nat. Rev. Drug Discov. 2, 140-150.

[39] P. Donato; F. Cacciola; P.Q. Tranchida; P. Dugo; L. Mondello. Mass Spectrom. Rev. 2012, 31, 523-559.

[40] D.C. Liebler; L. Zimmerman. J. Biochem. 2013, 52, 3797-3806.

[41] European Communities. "Commission Decision 2002/657/EC of 12 August 2002 implementing Council Directive 96/23/EC concerning the performance of analytical methods and the interpretation of results." Official Journal of the European Communities L 221.

[42] H. Farwanah; T. Kolter. eds. Lipidomics in Wiley Encyclopedia of Chemical Biology, John Wiley & Sons, Inc. New York, 200.

[43] A. Makarov; E. Denisov; A. Kholomeev; W. Balschun; O. Lange; K. Strupat; S. Horning. Anal. Chem. 2006, 78, 2113–2120.

[44] A. Makarov; M. Scigelova. J. Chromatogr. A 2010, 1217, 3938–3945.

2.0 Multidimensional Liquid Chromatography

Nowadays, the real world presenting different and heterogeneous samples in term of chemical composition. Matrices derivate of food, biological samples and pharmaceutical formulations are one of the more complex matrices; the most challenging step of the actual separation science is to overcome the traditional methods to obtain a comprehensive profile of all chemical classes.

Despite recent and important improvements in conventional LC, this technique has several limitations in terms of increased separation power and to overcome matrix effects.

The separation capability is represented by the peak capacity (n_c), which is the maximum number of the peaks that are distributes between the first and the last compounds of interest. It's a measure of the maximum number of components that can be separated during a single chromatographic run. The values of peak capacity should be considerably larger than the number of sample compounds [1].

In this regard, Davis and Giddings with the statistical theory of component have proved that peak resolution is seriously compromised when the number of components exceed 37% of the peak capacity [2]. To overcome this problem, a multidimensional system (MD) can be used. This latter is a combination of more dimensions with different separation mechanisms (orthogonal) that greatly improve the separation power, which is reflected in the increase in the peak capacity and the reduction of component co-eluted [3-4]. In MD-LC, the peak capacity can overcome values major of thousand. For high-resolution separation, multidimensional techniques are also very fast, with a peak-production rate (peak capacity divided by the analysis time) of about 1 peak per second, instead of to 1 peak per minute in high-resolution one dimensional LC (1D-LC) [5-6].

In MD-LC according with the way transfers from the primary column effluent to the second column, the two-dimensional liquid chromatography (2D-LC) can be classified in off-line or on-line mode. Off-line 2D-LC is the most used approach, due to the simple use. One or more fractions isolated in the first dimension (^{1}D) are manually or,

via a fraction collector, transferred after which they are separated from the initial solvent, re-dissolved in the different solvents if necessary, and re-injected in the second column. Instead, in the on-line 2D-LC setup, one or more fractions isolated in the first column are automatically transferred with the aid of a specific interface or modulator into the second dimension (^{2}D) [1]. Pros and cons of each approach are illustrated in Table 1.

Table 1: Pros and cons of Off-line and On-line MD-LC

Off-line MD-LC		**On-line MD-LC**	
Advantage	Disadvantage	Advantage	Disadvantage
- Very Simple - Conventional instrumentation - No problems related with immiscible solvents - Different separation mode can be applied - The sample concentration injected can be different in each dimension	- Times consuming -Possible sample contamination and artefact formation - Losses or degradation during solvent evaporation - Low analytical reproducibility	- High analytical reproducibility - Analysis time comparable to conventional LC (1-2 h) - Minor treatment of the sample	- More advanced instrumentation required - Need a specific modulator or interface - Need a specific software - Problems related with immiscible solvents - Problems related to coupled different separation mode in each dimension

On-line 2D-LC can be divided into heart-cutting (LC-LC) and comprehensive (LC×LC). In both techniques, the dimensions in the system are connected via a specific interface. The most important difference between the two approaches is the number of the ^{1}D fractions that are transferred in the ^{2}D. In addition, in the last decades, other set-ups are developed to improve the MD-LC technique. This part will be discussed in detail in the next paragraph.

2.1 Heart-cutting *versus* Comprehensive 2D-LC

In heart-cutting 2D-LC, only certain fractions of the analysis, containing the target compounds, are transferred into the ^{2}D. The result is one or more separations, that are useful for resolving the co-eluted peaks in a specific region(s) of the first dimension (Figure 1),

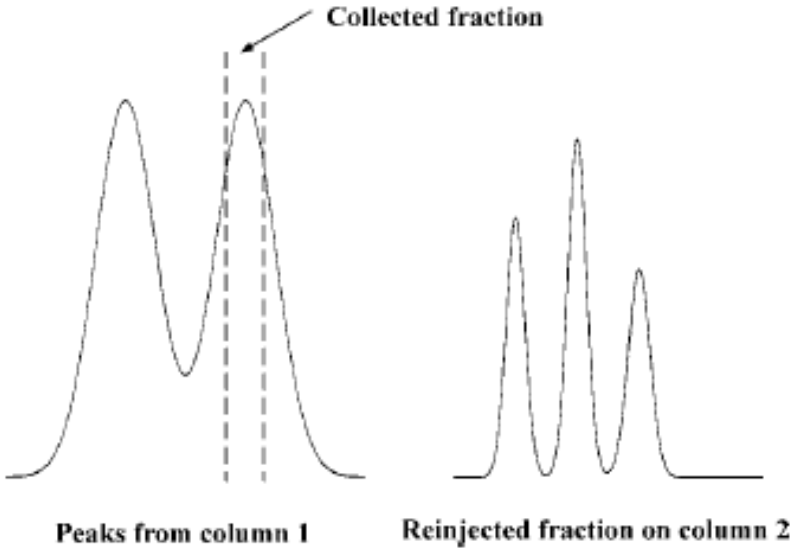

Figure 1. Heart-cutting separation mechanism.

The set-up can be simplified, using a fraction collector in which, the zone of interest, is collected. Then, the collected segment is re-injected in a different selectivity column. LC-LC has a long history, the first studies date back to 1943 with the isolation of plant chlorophyll extracts using an adsorption column; the procedure was carried out manually, the separation fractions from the first column were evaporated and re-

injected in a second different column [8]. Then, another approach of resolution of co-elution R,S-leucine and glycine was performed by Wachtel and Cassidy [9]. Tyrosine and phenylalanine were separated from glycine/leucine through the first column, each

fraction was concentrated and pre-separated in the second column containing a different ration of charcoal/paper adsorbent to separate the glycine and leucine.

Scott et al. [10] developed a LC-LC system for the elucidation of molecular constituents of body fluids, by cation exchange and anion exchange separations in ^{1}D and ^{2}D, respectively. In particular, the actual version of LC-LC was developed by Huber et al. [11] where a six-port valve was used to split the column effluent into another column (Figure 2).

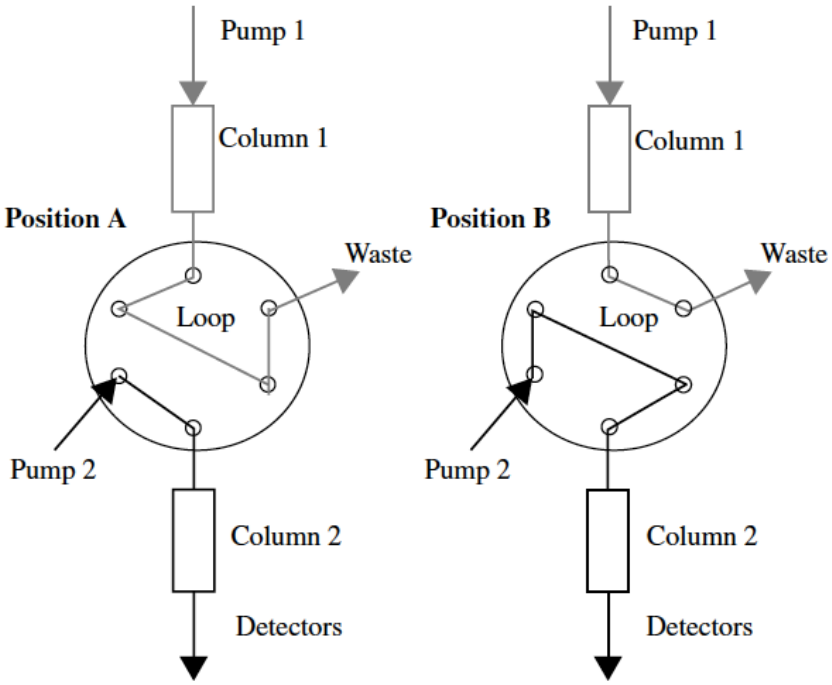

Figure 2. Typical six-port valves of Heart-cut 2D-LC.

In Comprehensive 2D-LC, the whole sample is subjected to two different separation steps in particular the same percentages of all sample compounds are analyzing in both columns and reach the detector. Another important characteristic is that the separation or resolution obtained in the ^{1}D should be maintained [12].

In the 1978, Erni and Frei [13] due to the low resolving power of 1D-LC to obtain a complete separation to complex samples, a 2D thin-layer chromatography (2D-TLC) was developed. The set-up constituted of a permeation (GP) column in the first dimension, coupled to RP-LC by means of an 8-port switching valve, equipped with

two identical sampling loops. The modulation time was 75 min and re-introduction of only seven fractions of 1.5 mL over a total analysis time of 10 h. Despite, this application has different limits can be considered as "pioneering" in the field of LC×LC. Subsequently, Bushey and Jorgenson [14] has modified the previous approach, increasing the sampling fractions. In addition, in order to reduce the extra-column broadening, the detector after the first dimension was removed as showed in figure 3.

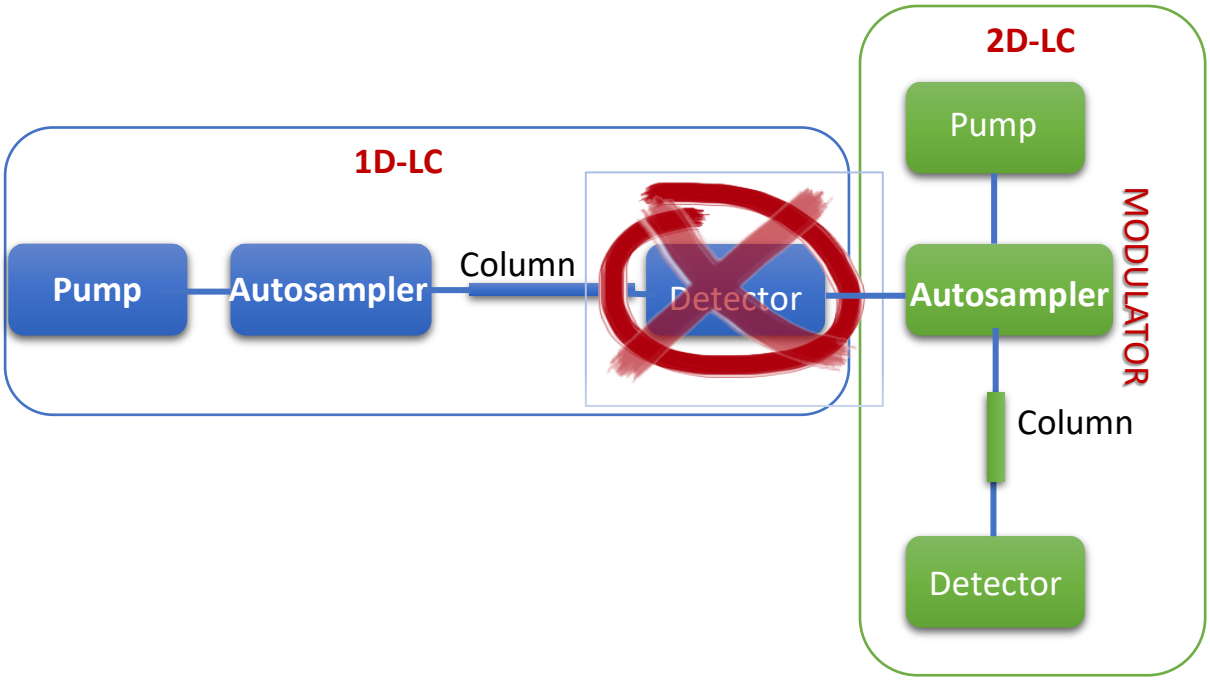

Figure 3. Schematic representation of LC×LC.

In the first dimension was used a microbore IEX column in gradient elution mode, with a flow rate of 5 µL m^{-1}. In the second dimension, a semi-preparative SEC column (250 mm × 9.4 mm I.D.) with 2.5 mL m^{-1} as flow rate was set. Finally, a valve equipped with two identical sample loops of 30 µL and a modulation time of 6 min was used. The orthogonality values have showed good results and the separation offered important information of the sample compounds. Another innovation respect to the past was to plot the analysis in a 3D representation, obtaining an easier data interpretation.

The other improvement of the development of set-up was the couples of the system to the mass spectrometer, in this regard Opiteck et al., were the first to use UV with ESI-MS for compounds identification of proteins and peptides by IEX×RP-LC [15] and SEC×RP-LC [16].

How is imaginable the development of set-up NP-LC×RP-LC is much more complex than RP-LC×RP-LC, due to the immiscible mobile phases. In this regard, the coupling of NP-LC to RP-LC is one of the most orthogonal system that can be realized. Murphy et al. [17] were the first to try to develop a NP-LC×RP-LC system for the separation of alcoholethoxylates, but the result wasn't optimum method because they used aqueous mobile phase in NP dimension. Finally, Dugo et al. [18] developed a true NP-LC×RP-LC set-up in order to separate oxygen heterocyclic fraction from cold-pressed lemon oil. A microbore diol column at a flow rate of 20 μL min^{-1} in isocratic mode and a monolithic C18 column at 4 mL min^{-1} were used in the first and in the second dimension, respectively. The two columns were linked by a two-position 10 ports high-pressure valve equipped with two identical 20 μL sample loops. The modulation time was 1 minute. In NP mode (^{1}D) the separation was achieved according to the polarity of compounds, while the fractions in the ^{2}D were eluted on the basis of the hydrophobicity by the C18 column. A few years later, Francois et al. [19] has developed a similar set-up by making some modifications, especially in the second dimension. A second pump, a column, a detector and a supplementary 10-port valve have been utilized to obtain a parallel column system. In this way, an increased peak capacity in the second dimension was obtained, doubling the modulation time up to 1 min. An interference signal, resulting from the solvent immiscibility, were reduced to the available separation space.

The best approach to eliminate the negative effect of the NP-LC×RP-LC approach, and to increase the separation power and the orthogonality, is the development of a specific interfaces for removing the ^{1}D mobile phases.

Another important approach in MDLC that have been developed over last years, is a HILIC approach in one of the two dimensions. This represent a variant of NP-LC but

use an aqueous mobile phase with a high percentage of organic solvent. The retention mechanism is determined by a partitioning process of the analyte between the acetonitrile-rich mobile phase and a water-enriched layer adsorbed onto the hydrophilic stationary phase. In this regard, thanks to the difference in selectivity, together with the aqueous mobile phases, HILIC mode allows a good partner to RP-LC, SEC and IEX in a comprehensive set-up.

Pros and cons of heart-cutting and comprehensive approach are illustrated in Table 2.

Table 2: Pros and cons of MD-LC techiniques *vs* Conventional LC

Heart cutting (LC-LC)		**Comprehensive (LC×LC)**	
Advantage	Disadvantage	Advantage	Disadvantage
- Better resolution and sensitivity - Use of different retention mechanism - Combination with MS and MS/MS	-Increase analyses time -Instrumental complexity	- Higher orthogonality and peak capacity -Ease of implementing automation - Minor risk of sample loss, deterioration and artifact formation	- Difficult to development of method - Decrease of sensitivity - Very rapid ^{2}D separation

2.2 Theoretical aspects

The theoretical aspects that explained the advantages of the multidimensional separation have been developed much later than the first published work.

Initially, Connors [20] assumed that the distribution of spots on a 2D-TLC plate could be modeled according a Poisson distribution of data on each retention axis. The theory was based of the equations that related the number of chromatographic systems needed to separate a specific number of compounds. The challenge of this work was to find separation systems that are not correlated. Due to the system employed, that doesn't base on the resolving power viz efficiency or the number of theoretical plates, it can't

apply for complex bio-separations. Further, Martin et al. [21] continued this study and offered a modern theoretical approach, that was further clarified in the modern years by Davis and Blumberg [22].

Finally, the most important theoretical aspects to consider in MD-LC are: peak capacity, orthogonality, resolution, sampling frequency, dilution factors and limit detection which will be discussed later.

2.2.1 Peak capacity

The reason of using multidimensional techniques is due to a better separation of the components than of a conventional method. The quality of separation can be evaluated by the peak capacity, this value was defined for the first time by Gibbings [23] in one-dimension, it corresponds to the maximum number of peaks separable in a specific part of the space. Few years later, the concept was introduced to multidimensional technique by Guiochon et al. [24,25] and Giddings [26,27]. The peak capacity in 2D separation is similar or slightly lower than the sum of peak capacities of each dimension. In particular, the 2D peak capacity is correlated to the separation mechanisms, if the systems are orthogonal the value of the peak capacity is higher.

In the first concept of peak capacity [23], Gibbings described the equation for an isocratic condition:

$$n_c = 1 + \frac{\sqrt{N}}{4Rs} \ln\left(\frac{k_1+1}{k_f+1}\right) \quad \textbf{(1)}$$

with N the efficiency, R_S the resolution and k_1 and k_f the retention factors of the first and the last eluting components. The value of R_S corresponds on the aim of the separation but is often taken as unity.

For the gradient mode, the peak capacity is generally higher than the isocratic analysis, considering that the bandwidths (w_i) are narrower. In the eqs. (2) and (3) are presented the general formula to calculate the gradient peak capacity.

$$n_c = 1 + \frac{t_g}{\varpi} \quad \textbf{(2)}$$

where, t_g is the gradient run time and ϖ is the average peak width (four or eight time the value of the standard deviation of a peak).

$$n_c = \frac{t_1 - t_f}{\varpi} \quad \textbf{(3)}$$

with t_1 and t_f correspond the retention times for the first and the last eluted peaks, respectively.

In the Eq. (2) the entire gradient run time is considering, instead unused space at both end part of the chromatogram is taken into account when using (3).

It is important to highlight these equations are valid when the peak width pattern over the entire chromatogram is very similar. When the operating conditions changing during the analysis, more complex procedures for the determinate the peak width ϖ are used to calculate the peak capacity. There are several theories and equations for the calculation of the peak capacity, and it is very difficult to choose the correct formula.

The key point is based on the theoretical value calculated by multiplication peak capacities of the separate dimensions.

$$n_{c,theoretical} = {}^1n_c \times {}^2n_c \quad \textbf{(4)}$$

where ${}^1n_c$ and ${}^2n_c$ is first- and second peak capacity, respectively. This eq. does not consider the deleterious effects due to the modulation processes as well as possible undersampling, practical peak capacity is necessary to calculate with the eq. (5) [28]:

$$^{2D}n_{c,practical} = \frac{^{1}n_c \times {}^{2}n_c}{\sqrt{1 + 3.35 \times \left(\frac{^{2}t_c \ {}^{1}n_c}{^{1}t_g}\right)^2}} \quad \textbf{(5)}$$

the parameter $^{2}t_c$ is the time of separation in ^{2}D, it is the same as the modulation time, instead $^{1}t_g$ is the ^{1}D gradient time. In this eq. is including the parameter <β> that taking into account undersampling.

But, to obtain a realistic peak capacity it is important to evaluate possible peak distribution along in the 2D space with to aim to estimate 2D coverage, the orthogonality degree (A_0) must be included in the final peak capacity (also known as effective).

$$^{2D}n_{c,effective} = {}^{2D}n_{c,practical} \times A_0 \quad \textbf{(6)}$$

2.2.2 Orthogonality

The major challenge in using the multidimensional peak capacity is to discover different set-ups that can spread the compounds across the separation space. It is possible, when the separation mechanism of the two columns is different or uncorrelated. The meaning of orthogonality is showed in Fig. 4 (a-b). where a comparison of NP × RP and NP × RP set-up is reported. Low correlation (high

orthogonality) is showed in the Fig. 4c for the separation of lemon oil where compounds are randomly distributed over the entire chromatogram space. On the contrary in Fig. 4d, the separation of steroids occurred in the linear mode. Due to the importance of the concept of orthogonality, different studies based of the mathematical point have been made.

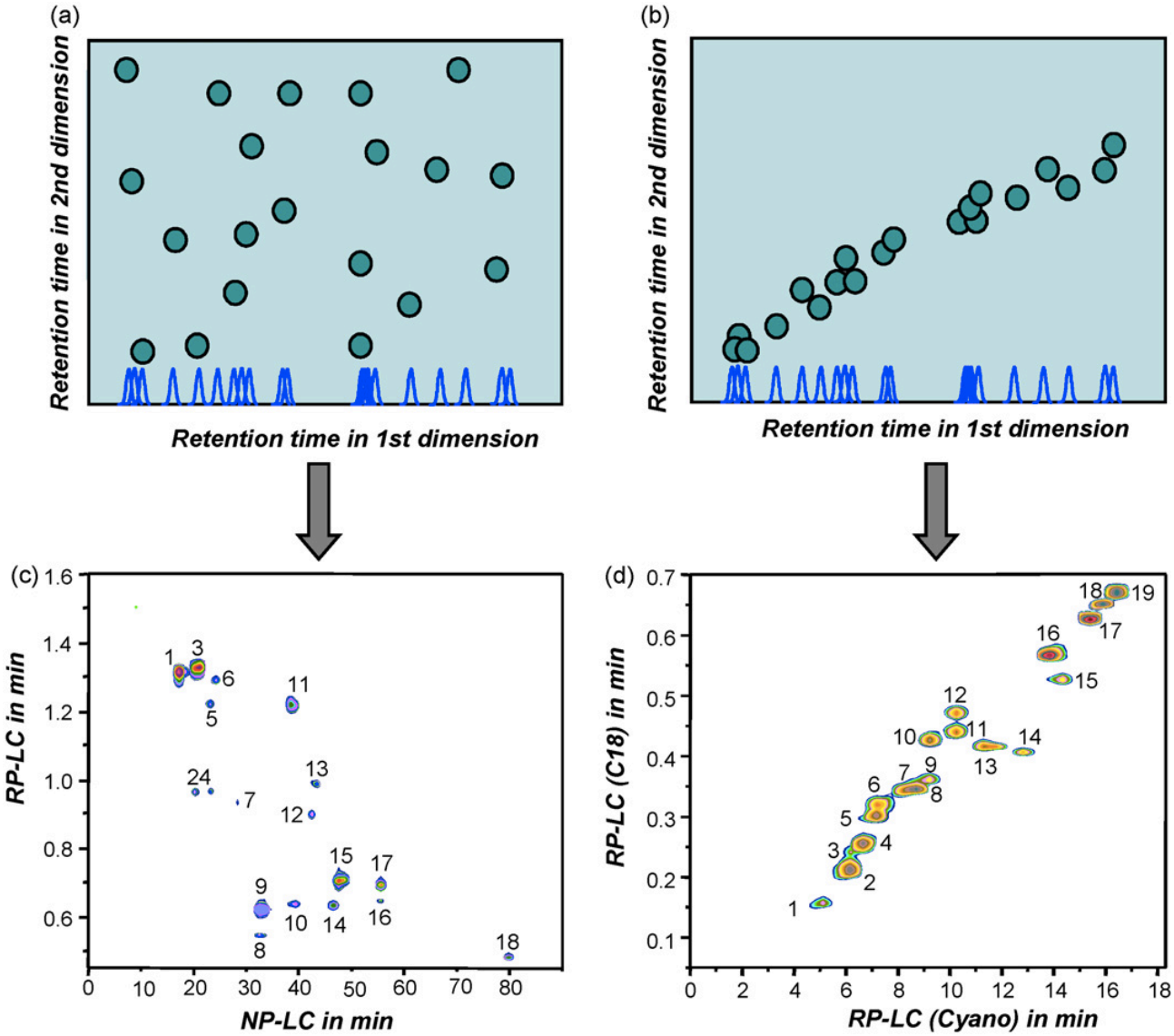

Figure 4. Representation of orthogonality in comprehensive LC. (a) Low correlation, high orthogonality; (b) high correlation, low orthogonality. Practical examples from reference [1]: (c) NP-LC×RP-LC separation of lemon oil. (d) RP-LC×RP-LC separation of steroids.

Liu et al. [29] proposed a geometric study to factor analysis in which a correlation matrix was developed from the solute retention parameters. The area of 2D space covered by the peaks was calculated for the orthogonality and then was used as a subtraction factor applied to the theoretical peak capacity in order to obtain the real value. [1]

Slonecker et al. [30-31] have studied the orthogonality by terms as informational similarity (IS) which is a measure of the global solute crowding and percentage of synentropy (PS) based on the amount of a cross-information.

Gilar et al. [32] explained orthogonality like the normalized area covered by each peak, after the normalization step of the retention time values obtained in both separations and correlated to the peak area of each blob.

The concept of orthogonality was resumed in 2014 by Camenzuli and Shoenmakers [33]. This procedure regards the distribution of each peak along the virtual lines that cross the 2D plot forming an asterisk, where Z_- , Z_+ (diagonal lines of the asterisk) and Z_1 , Z_2 (vertical and horizontal lines). Z parameters explain the use of the separation space in comparison of the correlated Z line, enabling semi-quantitatively diagnose areas of separation space where the sample constituents are plotted, reducing in practice orthogonality.

2.2.3 Resolution

The resolution for 2D separation presented by Peter et al. [34] was studied to calculate a resolution value and the separation quality for each set-up.

This parameter is calculated on the valley-to-peak ratio between two close peaks (peak 1 and peak 2), three maximum intensities are considered: the maximum of the peak 1 (*max1*) and peak 2 (*max2*), the highest point between the peaks (*S*) and the distance between max 1 and S, ($d_{1,S}$) and the distance between max 2 and S, ($d_{2,S}$).

$$d_{1,S} = \sqrt{(\Delta^1 t_{R1,S})^2 + (\Delta^2 t_{R1,S})^2} \quad \textbf{(7)}$$

$$d_{2,S} = \sqrt{(\Delta^1 t_{R2,S})^2 + (\Delta^2 t_{R2,S})^2} \quad \textbf{(8)}$$

being $\Delta^1 t_{R1,S}$ and $\Delta^2 t_{R1,S}$ and $\Delta^1 t_{R2,S}$ and $\Delta^2 t_{R2,S}$ are the differences on the retention time between max(1-2) and S in the first and second dimensions, respectively.

Intensity g is calculated by:

$$g = \frac{d_{1,S}h_{max2}+d_{2,S}h_{max1}}{d_{1,S}+d_{2,S}} \quad \textbf{(9)}$$

where h_{max1} and h_{max2} are the maximum height of the peaks 1 and 2.
The valley-to-peak ratio (V) is measured as:

$$V = \frac{f}{g} = \frac{(g-h_s)}{g} \quad \textbf{(10)}$$

Finally, resolution (R_s) is calculated as:

$$R_S = \sqrt{\frac{1}{2}\, ln\left(\frac{1-V}{2}\right)} \quad \textbf{(11)}$$

2.2.4 Sampling frequency

Sampling frequency or modulation periods is fundamental to maintain the ^{1}D resolution in a comprehensive configuration. For example, when sampling value is larger than the peak widths obtained in ^{1}D it follows a big reduction in the resolution in the first dimension resolving power, due to the mixing prior to the transfer into the second dimension. In particular, the peaks that were partially separated by the first column are collected in the same fraction and the partially separation is completely lost. To avoid this situation, a fast second dimension analyses is necessary. Consequently, the time for the separation in the second dimension is reduced and hence, the peak capacity of the second column is very low. Instead, the flow rate in the first dimension is very slow, below the Van Deemter's optimum value, in order to get

the widest possible peaks. In this way, the number of sampling for the primary peak is greater, but the main drawback is a reduced peak capacity in the first dimension.

In this regard, Murphy et al. [17] studied the effect of the sampling rate on the first dimension peak width through a modeled Gaussian peak as a histogram profile of the average concentration in each sampling period. Briefly, their theoretical and experimental data proved that is necessary three sampling along the peak, calculated a 8σ peak width for each peak. This value is valid when the sampling is "in-phase" therefore the sampling should start at the beginning of the peak. In the experimental analysis, this is very complicated and so a minimum value of four sampling is recommended. In addition, most studies are based on 4 σ peak widths values.

Seeley [35] investigated the sampling frequency for the modulators with several duty cycles for a theoretical study. In particular, when the effluent of the first dimension is collected in the entire sampling period, the duty cycle is equal to unity. This is the case when an interface of a two-position/8- or 10 ports switching valve equipped with two sampling loops is used, on the contrary when is used only one storage loop the duty cycle is less than 1.

Seeley also introduced the (average) peak broadening factor σ^* ($<\sigma *>$) by detailing parameters as sampling period τ_z and sampling phase Φ. The parameter τ_z is calculated by the sampling time t_s or modulation period and ${}^1\sigma$ of the first dimension peak, and Φ is the manner in which the primary peak is cut into fractions. The difference time between the center of the sampling cycle nearest to the peak maximum and the peak maximum, divided by the sampling period is the sampling phase (Φ). When the peak maximum was center in one of the sampling periods and for low duty cycles, the peak broadening greatly was reduced. Usually, for the most comprehensive separations the duty cycle is 1 and the peak broadening is independent of Φ. In conclusion, Seeley has deduced the same conclusion as Murphy et al.

Other important applications were introduced by the group of Carr [28, 36, 37], these are based on the effect of undersampling on the whole chromatogram, in contrast to all previous studies where focused on just a single couple of peaks. A new parameter based

on average ^{1}D peak broadening factor (β) was introduced. This value is correlated with the sampling time (t_s) and the standard deviation of the first dimension peaks prior to sampling ($^1\sigma$), typically used for calculation of the practical peak capacity (Eq. 5) [28].

2.2.5 Dilution factors and limit to detection

The principal drawback in MD-LC separation is due to the dilution factors, especially for the analyte detectability. The chromatography technique is always affected by dilution, and in comprehensive LC this problem is more evident due to the fraction from the ^{1}D which are injected into the ^{2}D by means of the interface. The result is a loss in sensitivity and decreasing detection limits, to reduce these effects a comprehensive configuration with interfaces that enable focusing or concentration before re-injection of the fractions is necessary.

The dilution factor (*DF*) in the ^{1}D can be calculated by Eq. 12

$$^1DF = \sqrt{2\pi}\,\frac{^1\sigma_{peak}\ ^1F}{^1V_{inj}} \qquad \textbf{(12)}$$

where $^1\sigma_{peak}$ represents the average SD of the peak in the ^{1}D, ^{1}F the flow in the ^{1}D and $^1V_{inj}$ the injection volume. To obtain the second dimension dilution factor [38], the total band broadening in ^{2}D needs to be considered by:

$$^2\sigma_{total} = \sqrt{\left(^2\sigma_{peak}\right)^2 + \left(\frac{^1F}{^2F}\right)^2 \left(\frac{1}{FF}\right)^2 \frac{\left(^2t_A\right)^2}{\delta_{inj}^2}} \qquad \textbf{(13)}$$

with ^2t_A depicting the analysis time in the ^{2}D and FF denotes the focusing factor which is the transferred volume (^{2}D injection volume) due to the focusing of the inlet of the second column or on a trap cartridge. The focusing factor can be calculated from [39]:

$$FF = \frac{^2k_{1e}+1}{^2k_{2e}+1} \quad \textbf{(14)}$$

here, $^2k_{1e}$ denotes the retention factor in the ^{2}D in the presence of the mobile phase of the ^{1}D and $^2k_{2e}$ represent the ^{2}D retention factor in the presence of ^{2}D mobile phase.
In conclusion, the total dilution in comprehensive set-up can be calculated multiplied ^{1}D and ^{2}D dilution factors.

$$^{2D}DF = {}^1DF \times {}^2DF \quad \textbf{(15)}$$

2.3 Method development in LC×LC

The success of a method development LC×LC can be attributed to several factors. Generally called as "the cardinal rules of 2D-LC method development" that detail the most important parameter like as column selection, sampling, mobile phases and gradient elution, sample loop volume, and finally the interface. Schoenmakers et al. [40] have suggested a protocol for the design of comprehensive LC separation system. The following paragraphs are focused on each important parameter for the development of comprehensive LC separations.

2.3.1 Column selection

The columns choice can be considered the most important parameter to the development of the 2D-LC separation method. This is fundamental to obtain an orthogonal separation. Ideally, the separation in ^{1}D should be characterized a highest separation power, in contrast the ^{2}D should be efficient, fast and compatible with the ^{1}D and the detector.

The first dimension can be operated under gradient or isocratic conditions, but the most important parameter is the flow very slow in order to obtain a sufficient number of samplings. In this contest the first column should be relatively long (100-250 mm) to obtain high efficiencies. On the contrary, the second column is very short (50 mm or less) which favors fast separations. The dimensions of the ^{2}D columns are important when the analysis is in gradient separations mode. Short column allows gradient with high volume ratios (t_G/t_0), while maintaining short cycle times and reducing the time needed to re-equilibrate a column after a gradient.

An example of a good setup is 1 mm ID of ^{1}D column in combination with 4.6 mm ID of ^{2}D column, in this way the separation in ^{1}D is obtained at low flow rate (i.e. 10 µL min^{-1}), reducing the ^{2}D injection volumes. Similarly, having a wider ^{2}D column increases the volume of the column used, so that larger volumes can be introduce without affecting the separation performance. Usually, the second column I.D. is larger than one used for the first separation (4-8 times [40]).

The second important parameter in the optimization of LC×LC system is the choice of the stationary phase used in each dimension. The majority of systems are developed using silica based fully-porous particles, functionalized with the chemistries but depend of the analytes of the samples. The column in ^{2}D is subjected to considerable stress due to a fast gradient with a high flow rate and often at elevated temperatures (> 50 °C) and changes in pressure in continuous injection cycles. For these reasons, robustness is an important parameter in ^{2}D columns.

2.3.2 Modulation Interfaces

The heart of comprehensive system is the transfer-interface, generally called modulator. It has the role of collect the fractions from the first dimension that are continuous re-injected into the second dimension. Over the years, several devices have been reported, but nowadays the most modulator used is a high-pressure (10 or 8-port, two position) switching valve, equipped with two identical sampling loops. While one

of the loops is filled, the other one is used as injector for the second separation. Different configurations have been developed using the same principle through a combination of 6-port valves. The loops sizes are chosen by the ^{1}D fractions quantity per sampling time. As an example, if the flow rate for the first dimension is set at 10 µL min^{-1} and the sampling time is 1 min, the sampling loops should be 10 µL.

The modulation strategies using the switching valves can be divided in two different categories [41]: 1) Simple valve-based modulation; 2) Valve-based modulation combined with assist technology.

Simple valve-based modulation

In this mode the fractions from the ^{1}D are directly transferred by sample loops into the ^{2}D column. The device employed is very simple, how previously described the effluents from the ^{1}D column is collected by the sample loop and then transferred to a ^{2}D column by a switching a two-position valve system. The modulation is based by the connection of one or more valves, using sample loops and steel tubes. Among the single valve type, the most used are the two-position 6-port valve, two-position 10-port valve, and two-position 8-port valve. The same modulation can also be obtained by using multiple valves such as 2 two-position 6-port valves or 2 two-position 10-port valves.

Nowadays, a new versatile technology using the multi heart-cutting (MHC) has been developed. It is composed by two six-position 14-ports valves with 12 parking loops and a two-position 4-port duo valve.

Finally, a new loop modulator was developed by Sandra [42]. It is characterized on 2 two-position 10-port valves with two ^{2}D parallel columns. In this case, the mobile phase for each 2D column was delivered by two independent pumps, which allowed carrying out the elution of 2D analysis with independent gradients, while the 2D analysis time was significantly enlarged, resulting in a considerable increase of peak capacity.

Valve modulation with assistant technology

In many cases, the simple modulation is not able to resolve the mismatch incompatibility of the mobile phase between the first and second dimensions. resulting in negative effects in the ^{2}D separation. Furthermore, the coupling of simple modulators with sample loops can reduce the sensitivity of detection in the ^{2}D due to the small volume of the fraction transferred in the high ^{2}D flow. Nevertheless, the disadvantage of a simple modulation could be overcome if the ^{1}D fractions is pre-treated before is collected or transferred into the second column. This step can resolve the incompatibility of the two dimensions, obtaining a better focus of the analytes on the head of the ^{2}D column. The goal of the new device is to obtain the focusing of the analytes and/or remove the ^{1}D mobile phase to reduce the immiscibility problems in the second separation. The desalting [43], the dilution [44,45], dilution and splitting [44,46], capture by trapping columns [47] and evaporation by vacuum are some of the most pre-treatment methods widely used in 2D instruments. The modulators with assistant technology design and their usage are very complex than the simple modulation and can be divided into two different categories: single-valve system and multi-valve systems.

Single valve modulation with assistant technology

The pre-treatment process involved in the single based-valve modulation is relatively simple. In most cases, the same configuration used for the simple valve-based modulation can be used just of the third pump that generates a make-up flow. Usually, this configuration is used when the mobile phase in both dimensions are partially compatible (RP-LC×RP-LC, HILIC×RP-LC). Adding a make-up flow a dilution of the ^{1}D fractions is obtained and its composition is the same as the initial gradient conditions of the ^{2}D separation. In this way, the eluent is dissolved in a compatible solvent before its separation in ^{2}D column. For example, this modulator is widespread when the ^{1}D mobile phase has a high content of organic solvent (HILIC mode) and should be diluted

by a make-up flow with water. Therefore, the analytes are focused on the head of the ^{2}D RP column, avoiding the negative effects on the ^{2}D separation.

Petersson et al. [48] has developed a new modulator, called "Fixed Solvent Modulator" (FSM), which not require a third pump to generate the dilution effect because the ^{2}D flow is split into two parts. A schematic representation of this modulator is showed in Figure 5. In this configuration, one part of the flows will go at the sample loop and the other part bypasses the modulator and both flows are combined in the modulator through a T connection, and then the fraction is injected in the second column. The drawback of this modulator is the difference time between the mobile phases flowing through the two paths, which changes the composition of the combined mobile phase compare to the composition of the mobile phase without bypass. Consequently, baseline shifts during the measurement and interferes with fewer intensive signals are formed.

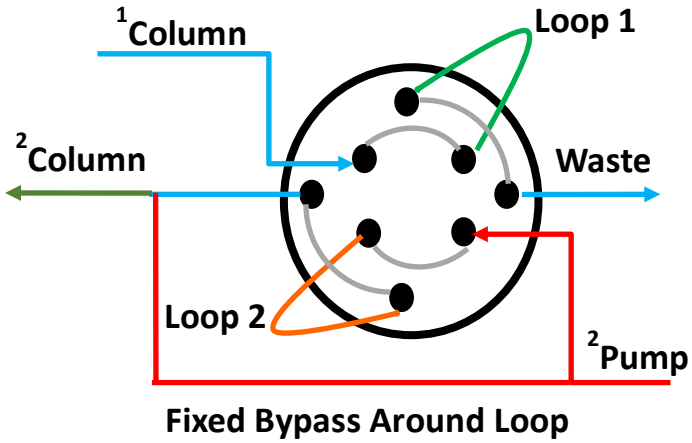

Figure 5. Schematic of eight ports two-position valve of a fixed solvent modulator (FSM)

To overcome this limitation, the FSM was modifier by Stoll et al [49], a new modulator called active solvent modulation (ASM), controlling the on and off to the bypass at each modulation time, showed in Figure 6. The split of ^{2}D mobile phase only happens at the step of the transfer of the fractions, reducing the negative effects on the ^{2}D separation.

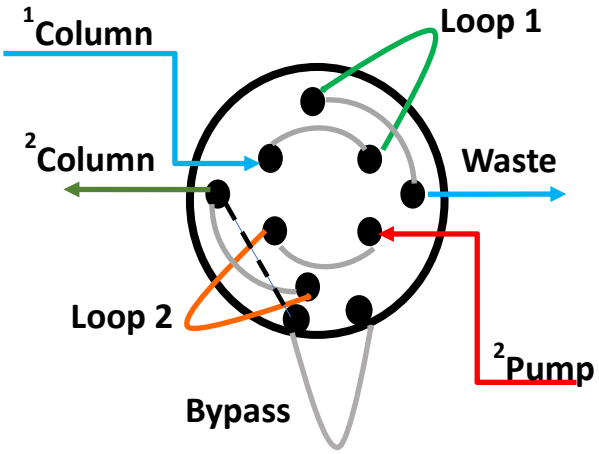

Figure 6. Schematic of ten ports four-position of active solvent modulator (ASM) valve

Therefore, another modulator for removing the incompatible among solvents was developed by Guan's group [50] and it is illustrated in Figure 7. It is based on a vacuum assistant evaporation device to achieve the desolvation of a ^{1}D solvent in the sample loop, allowing the successful coupling of NP-LC×RP-LC. The strategy for removing the incompatible solvent consists of a heat tape wrapped around the sample loop and a vacuum pump at the outlet of the sample loop.

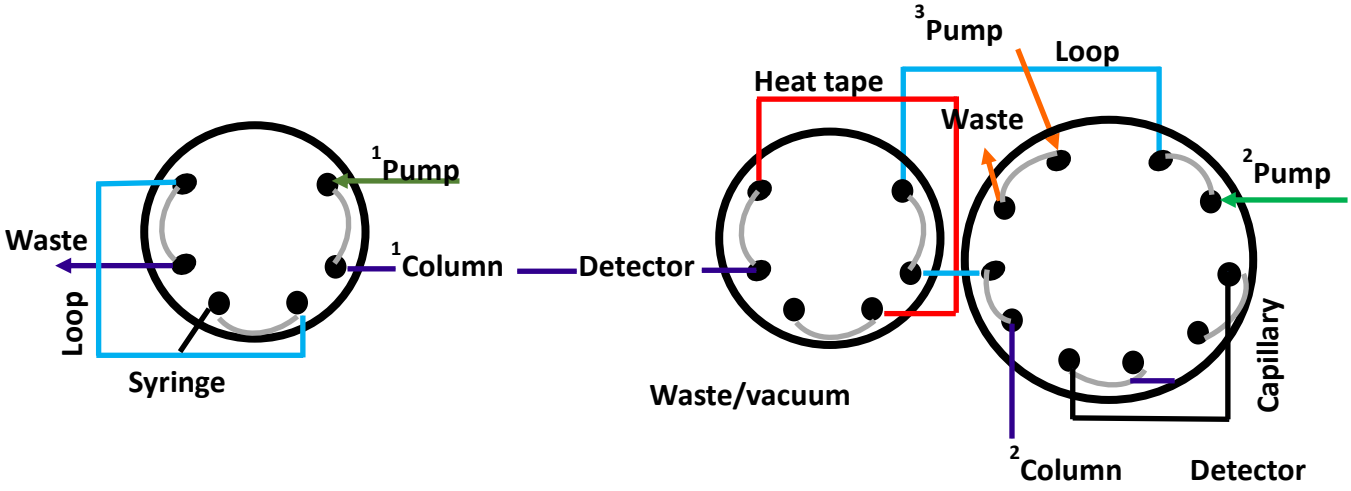

Figure 7. New modulator based on the vacuum system and heat tape.

In addition, Fornells et al. [51] has developed a different vacuum evaporation modulator, in which a concentrator module based on a porous hydrophobic membrane placed between the ^{1}D column and the modulator.

Another alternative method to increase the ^{1}D flow rate without loss of analytes consists in the use of the trapping columns, instead of the sample loops, or the trapping column with the addition of a make-up flow or so called "Stationary-Phase-Assisted Modulation (SPAM) (Figure 8),to allows the elimination of the solvent from the ^{1}D. The use of trapping columns enables to adjust the transfer volume to a large extent since the compounds interact with the stationary phase of the trapping column and will be retarded, while the solvent from the ^{1}D is eluted and removed into the waste. This allows an independent optimization of both dimensions with a better detection sensitivity. The main difference of the modulation with trapping columns with or without a make-up flow in RP×RP or HILIC×RP, lies in the complete elimination of the ^{1}D eluent. When using trapping columns alone, a part of the ^{1}D solvent remains in the interface due to the existence of dead volume in the trapping columns and the tubing that connect them to the valve. This could result in no, or low retention, of the analytes in the next separation. With the addition of the make-up flow, the dead volume problem can be resolved because the residual solvent is eliminated to improve the trapping of the analytes in the trapping column.

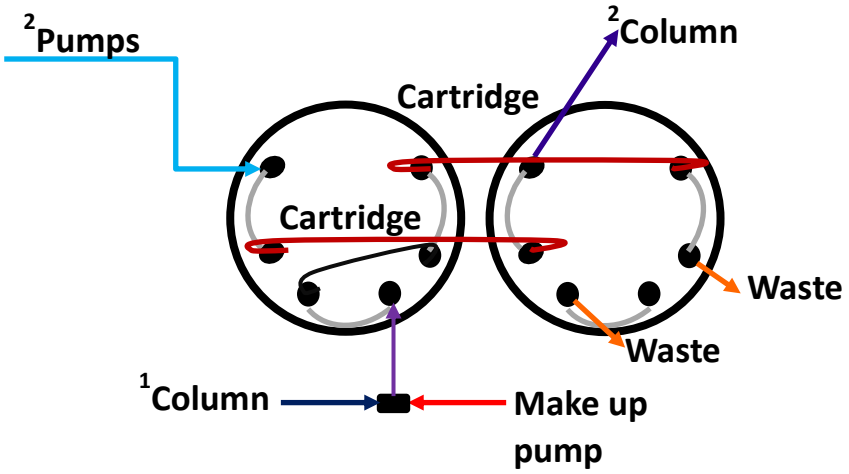

Figure 8. Schematic of Stationary-Phase-Assisted Modulation (SPAM)

In addition, to reduce solvent effect caused by the incompatible solvent present in dead volume of the trapping column, Chen's group designed a new improved version based on the FSM (in figure 5) [52] by using the short C18 trapping column instead of the sample loops. The flow rate from ^{2}D is divided into two streams, one part is conducted in the trapping column and the other one thought the splitting column. These two flows are fused after the modulator, just before the ^{2}D column and in this way the online dilution of the analyte is obtained. The dilution factor of the analytes could be modified by changing the length ratio between the trapping column and the splitting column, which influences the focusing performance on the head of the ^{2}D column. This modified resulted important to the coupling of RP-LC×HILIC. In conclusion, the assistant technology with the use of trapping columns is the best modulator to couple the most incompatible combinations.

Multi-valve modulation with assistant technology

The coupling of NP-LC×RP-LC or IEX×RP-LC led to a poor mobile phase compatibility. In this case more complex configurations are necessary to remove the effluents and solvent change. A multi-valve as a modulator may be a better choice because of the convenience to introduce a third mobile phase to produce a full solvent exchange, resulting in better separation in the ^{2}D column. In this contest Taihyun's group has developed a dual-valve modulator to coupled NP-LC with RP-LC for the analysis of block copolymers [53]. In this way the ^{1}D effluent from NP separation was collected in the sample loop at the left valve. The collected fraction was sent to a trapping column by switching the left valve six times in each modulation cycle. Consequently, the ^{1}D effluent collected in one modulation cycle was cut into six fractions in the water provided by a make-up pump, showed in figure 9.

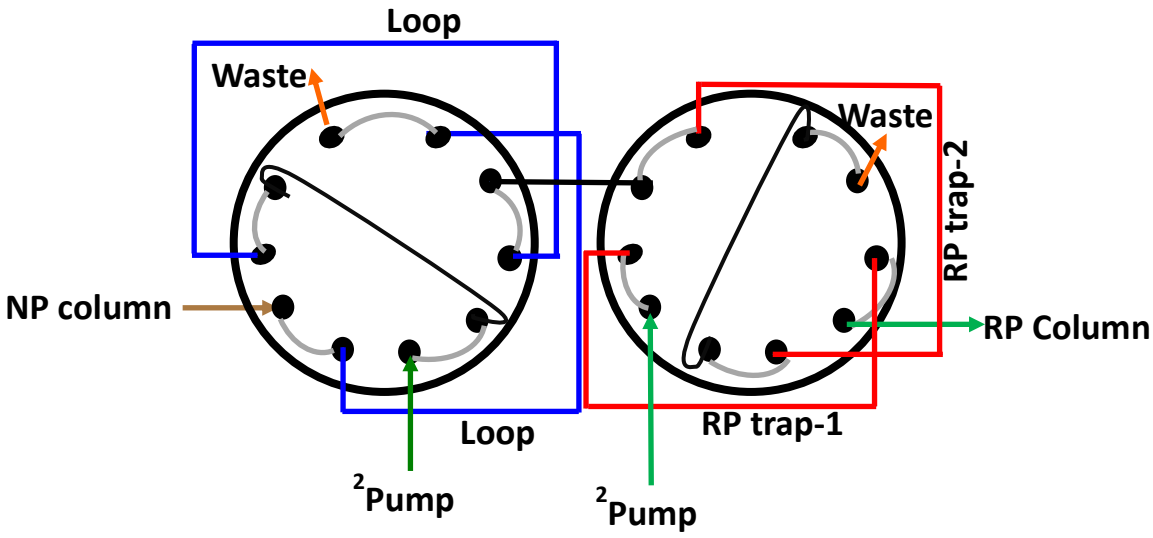

Figure 9. Dual-valve modulator to coupled NP-LC with RP-LC for the analysis of block copolymers.

In addition, Qui's group created a complex multi-valve modulator for the analysis of traditional Chinese medicine [54] including three valves, two of these valves were 2-position 10-port valves equipped with NP and RP trapping column and the other one was 2-position 6-port valve, one of this port valves was connected to a vacuum system.

The NP effluent from ^{1}D was collected on NP trapping column placed at valve A. The vacuum system was connected to the outlet of the ^{1}D column to remove the non-polar mobile phase in the NP trapping. Then, desorption of the captured analytes with hot acetonitrile was produced and after that the solution was diluted with water, resulting in a solvent exchange from NP to RP, and the analytes with aqueous solvent were transported to the RP trapping columns, producing an enrichment of the fraction.

Unger et al. [55] developed a dual ^{2}D separation system. The second dimension was controlled by two 2-position 10 port valves, each of these valves were equipped with two columns and two pumps. In this way, alternating the fraction collection and separation on four ^{2}D columns, next to, another 10-port 2-position valve was used for the equilibration of the columns with an isocratic flow for the desalting steps.

The system is based on four steps: 1) the column is connected to the other pump to allow the equilibration of the column; 2) the ^{1}D column is placed to the equilibrated ^{2}D

column; 3) Once the fraction is injected in the ^{2}D column a desalting step achieved using another time the isocratic pump 4) the ^{2}D separation is carried out.
The four steps could be done at the same time but in different ^{2}D columns.
Finally, Ji et al. [56] achieved a multi-valve modulator to coupling the HILIC with RP column based on a 2 position 10-port valve equipped with two sample loops and a 2-position 6-port valve. The innovation of this set-up is the very fast switches of the 6-port valve during the analysis. In this way the ^{2}D mobile phase passes the loop by turns.

2.3.3 Sampling

One of the drawbacks of the comprehensive LC is that the eluent of the first column must sample for a sufficient number of times, so that, the peaks in the first separation are not "deresolved". The effect of this problem can be related to the undersampling in the first dimension, particularly the zone that has been separated in the ^{1}D to be mixed with other resolved zones in the sample loop. It is necessary to either speed up the second dimension or slow down the first dimension. As discussed in the paragraph 2.3.4., the first-dimension peaks should be sampling at least three or four times. If the sampling rate is reduced to less than 1.5 times of ^{1}D peak width, the total peak area and retention time are minor as compared to a higher sampling rate but if the sampling frequency above four samples per peak width this becomes a deleterious effect.

2.3.4 Mobile phase compatibility

One of the most difficult challenges in developing LC×LC separations is the compatibility of the mobile phase in the two dimensions.
Negative effects can arise when the solvents are not fully miscible in both dimensions and difficulties in the combination of various separation modes may arise. This is the

case when one of the separation modes is RP-LC, HILIC or IEX, which uses an aqueous solution, while the other one is either NP-LC or SEC with the organic solvent as mobile phase and is not easily miscible with the previous solvents.

Another problem can be made from the differences in solvent strength of the sampled ^{1}D fraction and the ^{2}D mobile phase, especially if the eluent strength of the ^{1}D is too strong for retention to occur in the second column. The result is the so-called breakthrough phenomenon. Usually, a minor injection volume in the second dimension can minimize the impact of the sample solvent on the ^{2}D separation, another solution is the use of a ^{2}D column more retentive than the ^{1}D column, in this way on average the eluent used in the ^{1}D column will be weaker and so the solvent used in the second column will be stronger. Alternatively, different studies were proposed to replace the conventional loops based on "passive modulation". All approaches, in which the ^{1}D fraction is modified before injection in the second dimension, are called "active modulation". In this way, it is possible to increase the retention on the ^{2}D column head (focusing effect) and this improves peak-shape and enhances peak height. It is possible when replaced the empty loops with trap columns. This allows the reduction of the 2D injection volume and the possibility to modify the solvent.

2.3.5 Sample loop volumes

The volume of the sample loops determines the quantity of ^{1}D fraction that can be collected and the ^{2}D injection volume. Normally, to limit injection band-broadening effects, the volume injection should not exceed 15% of the column dead volume [57]. The most common approach to determining the loop volume is the product of the ^{1}D flow rate (^{1}F) and the sampling time (t_s)

$$^{2}V_{inj.} = t_s \times {}^{1}F \quad \textbf{(16)}$$

but when the ^{1}D effluent fills the sample loop the two-fold higher linear velocity at the center of the tube will cause some loss of sample when using the exact volume of the loop that calculated by Eq. (16)

To avoid this problem, it is generally a good practice to choose a loop volume that is around 30% larger than the volume calculated, to obtain more precise results.

In conclusion, it is important to understand that the volume of both loops doesn't need to be very accurate, but it should be exactly the same in both loops to get the two flow paths as similar as possible.

2.3.6 Elution modes in the second dimension

The elution mode in both dimensions could be separately optimized. In each dimension an isocratic mode or a gradient mode could be used. Compared to isocratic conditions, gradient elution is more used as it provides a significant improvement in peak capacity and orthogonality. In the second dimension, several types of gradients have been used in LC×LC as shown in Figure 10 [58]. In details:

a) **Full in fraction (FIF)** (Fig. 10a): the gradient program using a large range of mobile-phase compositions in a short time and is the same during the whole analysis. This offers high bandwidth suppression and is commonly used in LC×LC. The short run time in each modulation increase the probability of a wrap-around effect of some strongly retained compounds, which don't have enough time to be eluted within a single modulation and can continue elution into the next fraction(s). Another important consideration of this gradient is the distribution of the compounds, these not able to cover over the available bi-dimensional space but tend to cluster more or less around the line connecting the lower-left corner with the upper-right corner when the separation mechanisms in each dimension are similar.

b) **Segment in fraction (SIF) (**Fig.10b): the gradient consists of one or more fractions; in the first part the gradient has a lower concentration than the next segment where the concentration is higher. Despite the segment gradient is less steep than the FIF, provides significant bandwidth suppression, in addition the probability of wraparound effect is diminished thanks to several segment with various concentration ranges can be modified according to the retention of the sample.

c) **Parallel gradient (PG)** (Fig. 10c): the gradient uses a program independent of the ^{2}D run. For a single ^{2}D modulation, there is a quasi-isocratic elution and as post-gradient equilibration is not necessary within the individual cycle. The gradient can be modified on the basis of the retention characteristic to improve the ^{2}D space. One of the inconvenient of this gradient is the decrease of the total two-dimensional peak capacity due to the larger bandwidths.

d) **Shift gradient (SG)** (Fig. 10d): the gradient has a narrower range of the mobile-phase composition and continuously varies the concentration range according to the elution of the compounds. This can be classified as the combination between the FIF and the PG. The SG suppresses the bandwidth and decreases the probability of a wrap-around.

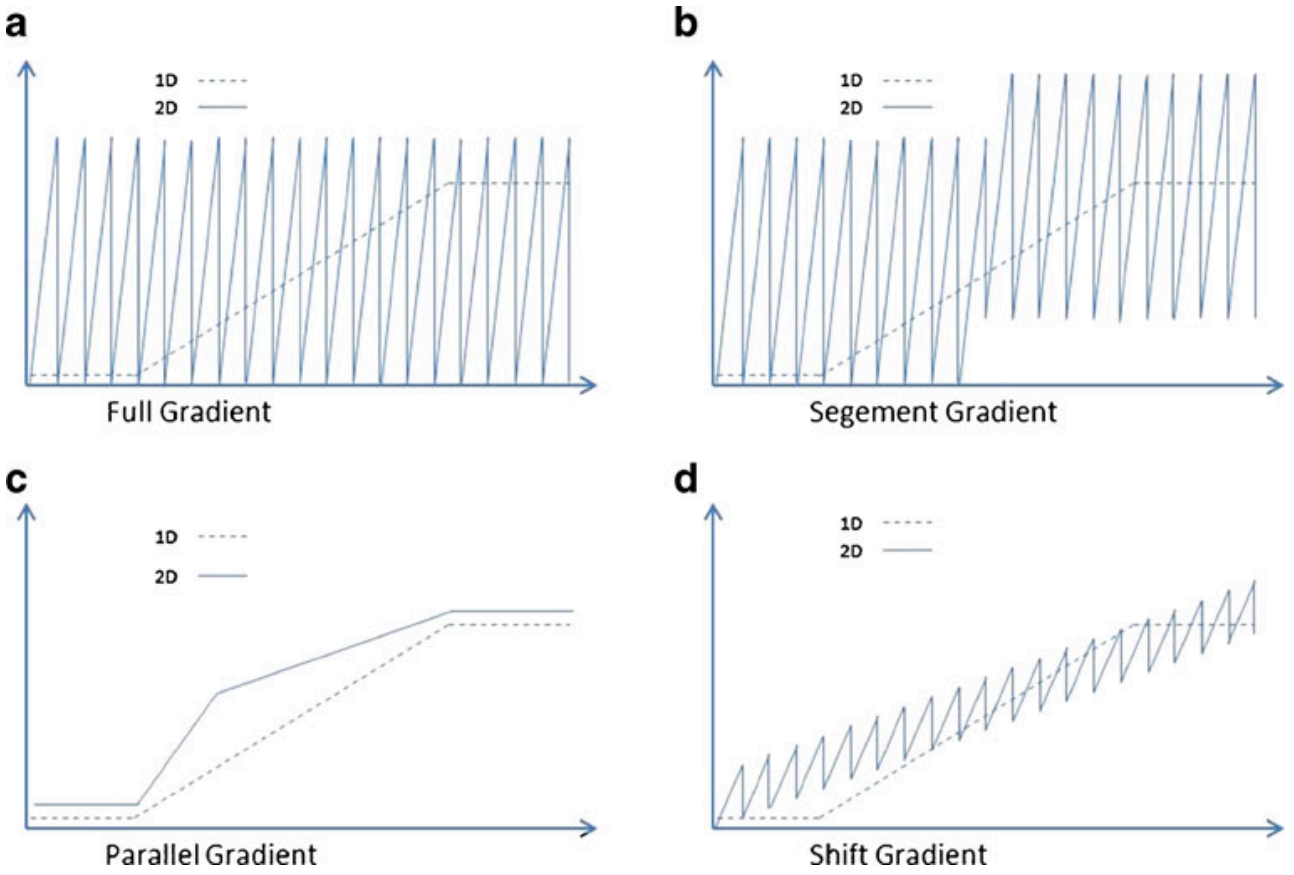

Figure 10: Second-dimension gradients in comprehensive two-dimensional liquid chromatography (LC×LC)

2.4 Detection

A comprehensive 2D-LC system can be easily coupled with all conventional LC detectors i.e. photo-diode array (PDA), mass spectrometry (MS), and evaporative light scattering (ELSD) detection. How discussed in cap. 1, these revelators give important information on the sample constituents. In the modern instrument the detector is placed after the second dimension but, a second detector to monitor the fraction in the first dimension can be added. It is important to know that this last option will lead to extra-column broadening. When a comprehensive 2D-LC approach is used, the acquisition rate of the detector must be very fast, due to the high speed of the ^{2}D separation. In the fast second dimension analyses, peak widths of a few seconds are common, and a detector acquisition rate of 5 Hz is necessary to obtain a reliable peak reconstruction

(6-10 points per peak) since no loss in resolution can be tolerated. As regards the analyzers, the high scanning rates and high resolution of the TOF MS is the best choice in 2D-LC system thanks to scan speed 20000 amu/sec.

When MS is used as detector, the very high flow rate used in the ^{2}D must be split to values up to 1 mL min^{-1}, and lower before the ion source, as these high values used to speed up the ^{2}D analysis are not tolerated. The flow splitting has a negative effect on sensitivity and produces peak broadening due to the addition of extra volume of the splitter. Regarding the MS, electrospray (ESI) and atmospheric pressure chemical (APCI) are the most used for online analyses, instead MALDI for the offline application.[1]. The quadrupole detector has been the most common used due to its ease of use, the relatively low cost, and ruggedness but it offers low resolution (typically 1 Da). In order to improve the resolution, enhanced sensitivity, as well as increase the mass accuracy over a wide dynamic range and performs MS/MS experiments and accurate quantification a several of hybrid instruments have been developed in the last years. These has been already fully detailed in cap.1

2.5 Data processing

In 2D-LC several data are produced within a short period of time. When this fast scan mode is used, the chromatograms are composed of a huge number of data points and generate very big files. These data are often visually represented in 2D plots or contour plots, where the retention time in the first and second dimensions are plotted along the *x*- and *y*- axes, respectively. The color of the spots is a proportional measure for the intensity of the compounds. Usually, an individual ^{2}D chromatogram is generated or the fractions produce one long second dimension chromatogram that is then broken down into the chromatograms of the individual runs. The data are converted to construct a matrix containing absorbance values as a function of first- and second-dimensions retention times after which the contour plots are created using specific software that is able to represent three-dimensional data (3D).

For the same reason, quantification in LC×LC is very difficult and rarely been calculated.

In this thesis, all the functions of a 2D software, called Chromsquare will be exploited for the different applications: comprehensive characterization (qualitative and quantitative approaches of target components or untargeted analyses of complex samples).

2.6 Recent Developments

As discussed in the previous paragraphs, MD-LC are typically divided into two main groups: comprehensive (separation of the several compounds of the matrix) and heart-cutting (separation of few constituents of the sample) mode. However, in the last decade different hybrid modes of 2D-LC separations were developed. Some set-up combines features of both heart-cutting and comprehensive separations, so called selective comprehensive (sLC×LC) and multi heart-cutting (mLC-LC).

The first approach is selective, which means that only selected parts of ^{1}D separation are cut or sampled in multidimensional manner (Figure 11). Fig 11 A shows as the ^{1}D effluent, containing the target compounds, is transferred to the subsequent dimension in many small fractions where a complete ^{2}D separation occurs as shown in Figure 10 B. This approach enables momentary storage of these fractions such that the sampling time in the ^{1}D need not be the same as the analysis time in the ^{2}D. In this example, samples of ^{1}D effluent are cut every 2 s, but each ^{2}D separation is occurred 20 s.

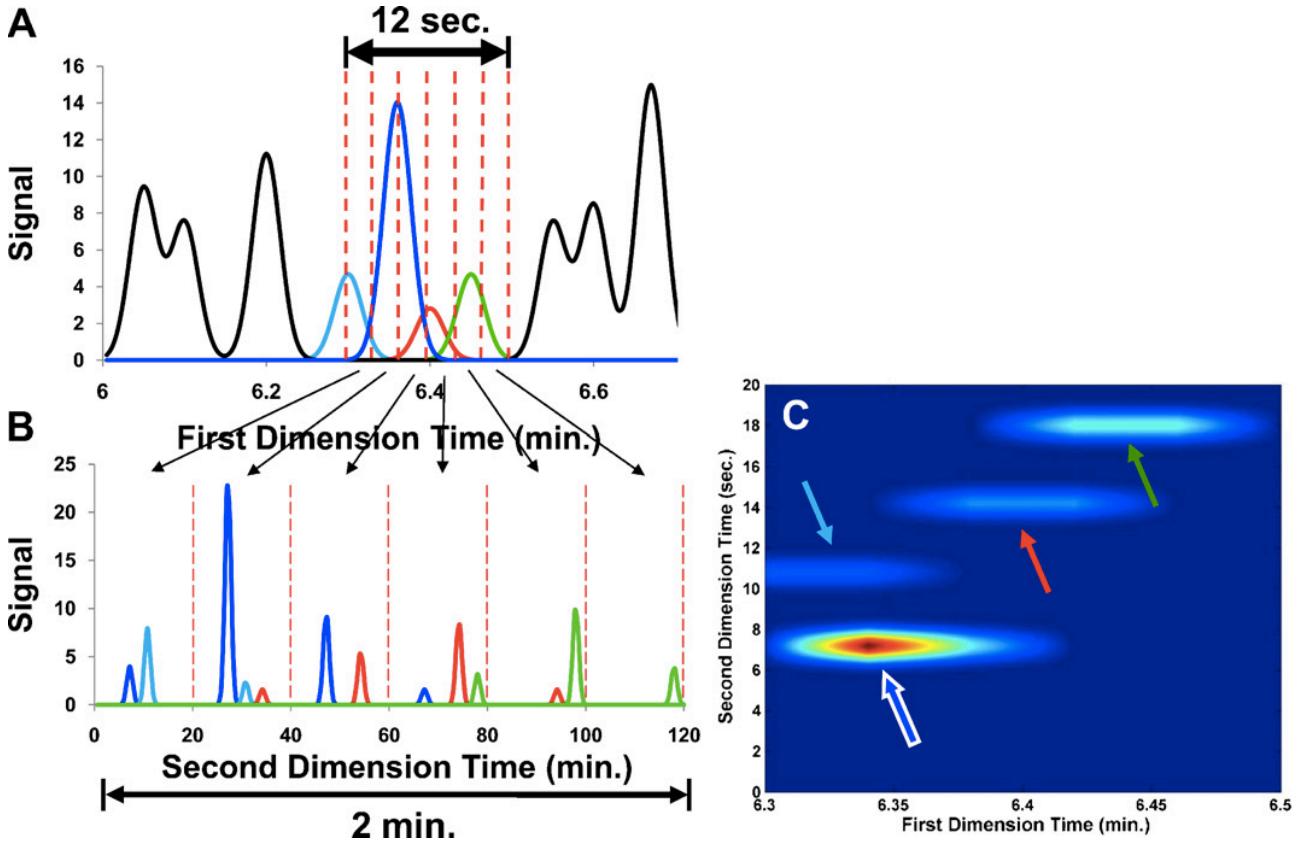

Figure 11. Selective comprehensive (sLC×LC) separation of the same complex matrix.

The sLC×LC instrument setup is very complex, because it allows the collection and transient storage of up to six fractions of one or more ^{1}D peaks, followed by serial injection of those fractions into a ^{2}D column for the next separation [59]. The benefit of sLC×LC is that a more detailed view of certain areas of the ^{1}D chromatogram is obtained, and that is possible transfer multiple small fractions of ^{1}D effluent in a region of interest preserving the resolution of target analytes developed by ^{1}D separation.

On the contrary, the principle of mLC-LC is to expand the single heart-cut approach, in such way that multiple regions of the ^{1}D separation specific region [60,61]. This approach is particularly utile when one uses a sampling interface that enables sampling of the ^{1}D separation and next ^{2}D separation of the transferred fractions to be executed in parallel, showed in Figure 12. The goal, this allows to choose many ^{1}D regions as need, provided that there is sufficient spacing between regions of interest.

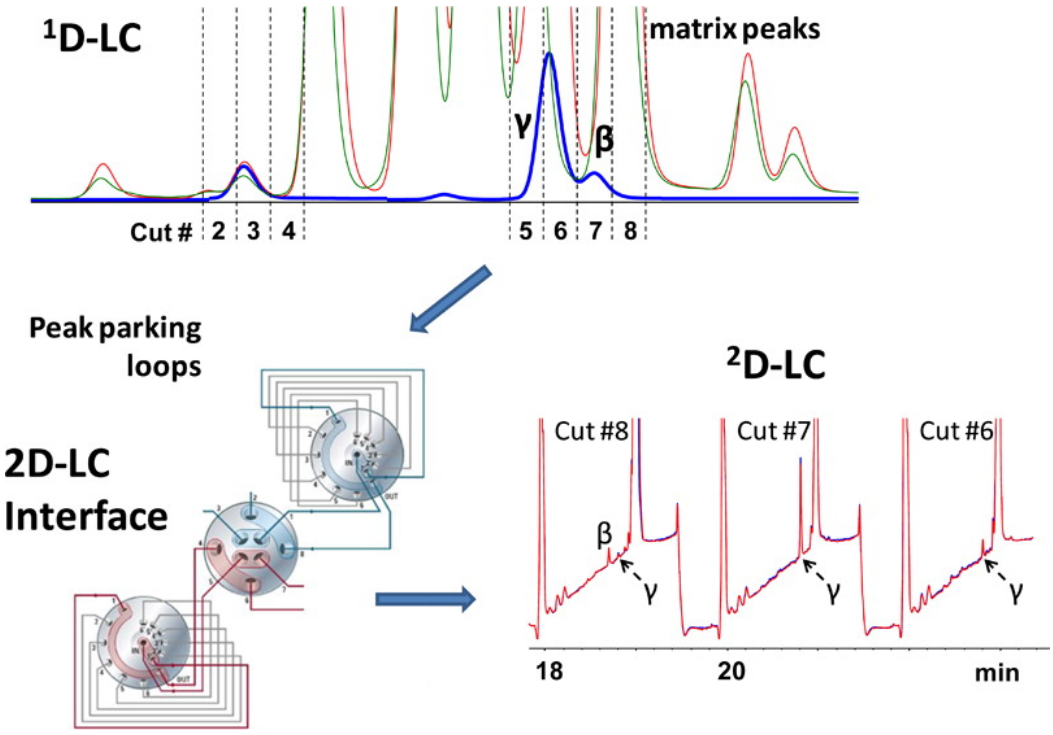

Figure 12. Multiple heart-cutting (mLC-LC) separation and 2D-LC interface.

Recently, a new modulation approach called Active Solvent Modulation (ASM) have been introduced by Stoll et al. [49]. In this case, two ports are added to a conventional valve used for 2D-LC with a bypass capillary (Figure 6). Therefore, two switching position are added to the common valves. Two of the positions have the same behavior of the passive modulation, where all of the ^{1}D effluent enter into the loops and all of the ^{2}D mobile phases passes through the other loop, transferring previously ^{1}D fraction collected into the ^{2}D column. On the contrary, in the other two additional positions the flow from the ^{2}D pump is spilt into two parts, one that enters through the loop and one that bypasses the loop, so that the ^{2}D eluent acts as a diluent for the collected fraction. The advantage of this configuration is the possibility to couple HILIC and RP mode bypassing the incompatibility of the solvents in the first and the second dimensions, respectively. Figure 13 shown a comparison of two plots with and without active solvent modulation. In the up part of the figure, the peaks marked in red are in breakthrough. These constituents are eluted during the dead time of each ^{2}D separation due to the solvent-strength mismatch. On the contrary, when ASM is applicated (bottom part of the figure 13) peaks in breakthrough are not present as the ^{1}D fraction

is diluted 1:2 with the same concentration of the mobile phases using the starting point in the ^{2}D gradient [62].

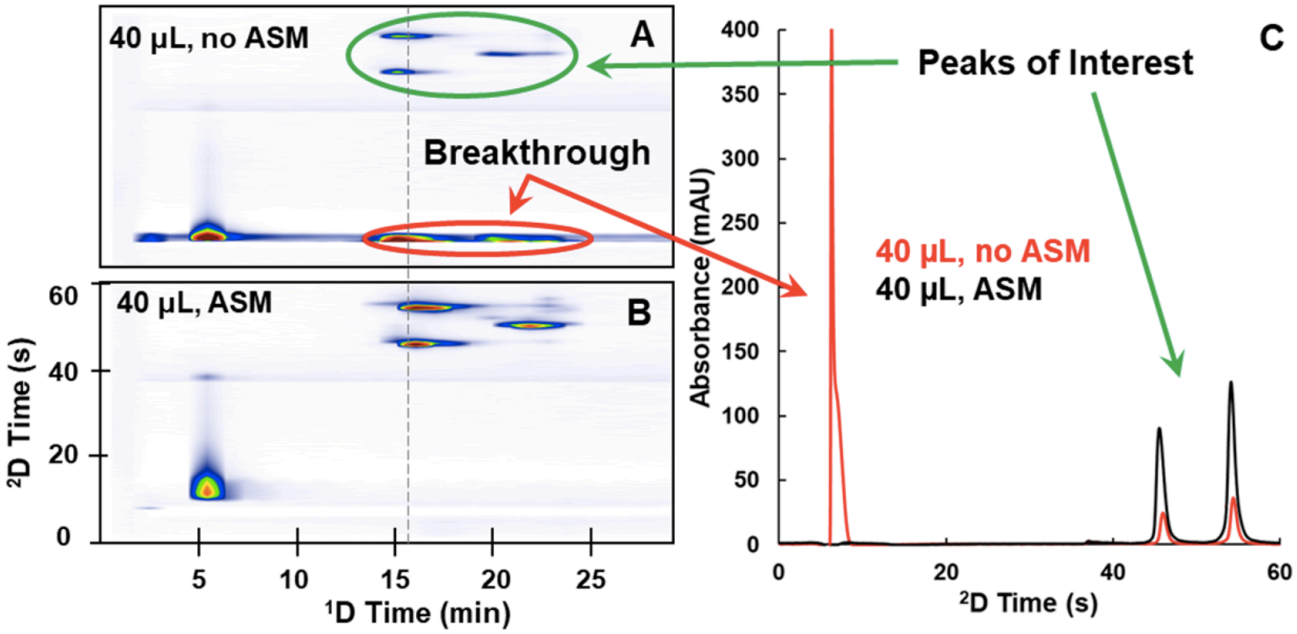

Figure 13. Hilic×RP separation of mAb fragment with (B) and without ASM (A)

Another very common active-modulation application is "Stationary-Phase-Assisted Modulation (SPAM) based on the use of trapping (or "enrichment") columns (Fig.8) instead of the loops. Normally, guard column consists of the same stationary phase of ^{2}D column. When the ^{1}D effluent is sampled by the modulator, the analytes are retained in the stationary phase of the trap columns and the ^{1}D solvent going to the waste. When the ^{2}D mobile phase enters into the trapping the analytes are eluted as sharp and concentrated bands and introduced into the second column. To facilitate this procedure, it is possible to add an additional pump, the "make-up pump", to decreases the elution strength of the ^{1}D effluent before entering the trap.

The advantages of SPAM can be resumed as follow:

- Reduced solvent incompatibility issues as the ^{1}D mobile phase is removed;
- Improved sensitivity due to the analyte focusing on the trapping cartridge;
- Minor ^{2}D injection volumes.

On the contrary, the disadvantages are:

- Potential loss of some analytes (incomplete recovery) due to the not sufficient retention which can be caused by the different chemical properties;
- and the dilution solvent may not always ensure complete trapping of all analytes [6].

How can see in Figure 14 a comparison of RPLC×RPLC-MS for the separation of steroids in bovine urine using (A) passive modulation and (B) SPAM are reported. An important increase of peak intensities and signal to noise ratio was obtained by using SPAM to passive modulation. The authors reported an increase in S/N ratio by a factor of 7 and were able to detect 76 compounds with SPAM application and "only" 36 for passive modulation.

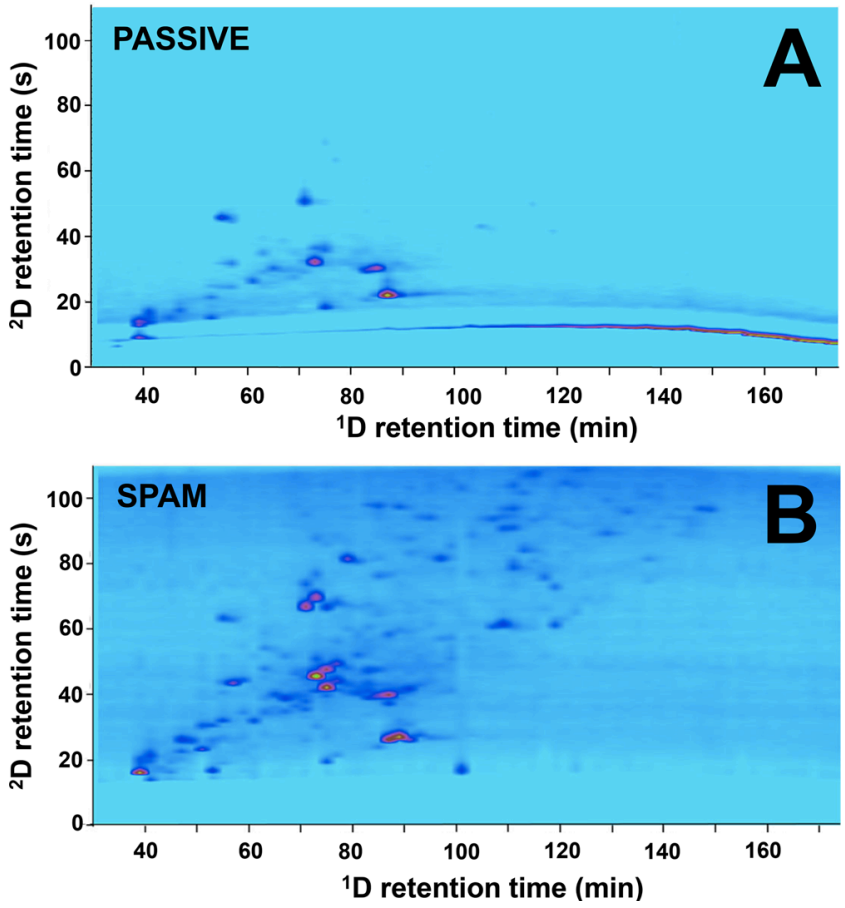

Figure 14: RPLC × RPLC-MS separation of steroids in bovine urine using (A) passive modulation and (B) stationary-phase assisted modulation (SPAM).

References

[1] I. Francois; K. Sandra; P. Sandra. Anal. Chim. Acta 2009, 641, 14-31.

[2] J. M. Davis; J. C. Giddings. Anal. Chem. 1983, 55, 418-424.

[3] H. J. Cortes (Ed.). Multidimensional Chromatography: Techniques and Applications, Marcel Dekker, New York, 1990.

[4] L. Mondello; C. Lewis; K.D. Bartle (Eds.). Multidimensional Chromatography, John Wiley and Sons, Chichester, 2001.

[5] E. Sommella; O. H. Ismail; F. Pagano; G. Pepe; C. Ostacolo; G. Mazzoccanti; M. Russo; E. Novellino; F. Gasparrini; P. Campiglia, J. Sep. Sci. 2017, 40, 2188-2197.

[6] B. W. J. Pirok; D. R. Stoll; P. J. Schoenmakers. Anal. Chem. 2019, 91, 240-263.

[7] S. A. Cohen; M. R. Schure. John Wiley and Sons Inc., Hoboken, New Jersey, 2008.

[8] W. M. Manning; H. H. Strain; J. Biol. Chem. 1943, 151, 1-19.

[9] J. L. Wachtel; H. G. Cassidy. J. Am. Chem. Soc. 1943, 65, 665-668.

[10] C. D. Scott, D. D. Chilcote, N. E. Lee. Anal. Chem. 1972, 44, 85-89.

[11] J. F. K. Huber; R. Van der Linden; E. Ecker; M. Oreans. J. Chromatogr. A. 1973, 83, 267-279.

[12] P. J. Schoenmakers; P. Marriott; J. Beens. LC–GC Eur. 2003, 16, 335-339.

[13] F. Erni, R. W. Frei. J. Chromatogr. 1978, 149, 561-569.

[14] M. M. Bushey; J. W. Jorgenson. Anal. Chem. 1990, 62, 161-167.

[15] G. J. Opiteck; K. C. Lewis; J. W. Jorgenson; R. J. Anderegg. Anal. Chem. 1997, 69, 1518-1524.

[16] G. J. Opiteck; J. W. Jorgenson; R. J. Anderegg. Anal. Chem. 1997, 69, 2283-2291.

[17] R. E. Murphy; M. R. Schure; J.P. Foley. Anal. Chem. 1998, 70, 1585-1594.

[18] P. Dugo; O. Favoino; R. Luppino; G. Dugo; L. Mondello. Anal. Chem. 2004, 76, 2525-2530.

[19] I. Francois; A. de Villiers; P. Sandra. J. Sep. Sci. 2006, 29, 492-498.

[20] K. A. Connors. Anal. Chem. 1974, 46, 53-58.

[21] M. Martin; D. P. Herman; G. Guiochon. Anal. Chem. 1986, 58, 2200-2207.

[22] J. M. Davis; L. M. Blumberg. J. Chromatogr. A 2005, 1096, 28-39.

[23] J. C. Giddings. Anal. Chem. 1967, 39, 1027-1028.

[24] G. Guiochon; L. A. Beaver; M. F. Gonnord; A. M. Siouff; M. Zakaria. J. Chromatogr. 1983, 255, 415-437.

[25] G. Guiochon; M. F. Gonnord; A. Siouffi; M. Zakaria. J. Chromatogr. 1982, 250, 1-4.

[26] J. C. Giddings. Anal. Chem. 1984, 56, 1258A-1270A.

[27] J. C. Giddings. Chromatogr. Commun. 1987, 10, 319-323.

[28] X. Li; D. R. Stoll; P. W. Carr. Anal. Chem. 2009, 81, 845-850.

[29] Z. Liu; D. G. Patterson Jr.; M. L. Lee. Anal. Chem. 1995, 67, 3840-3845.

[30] P. J. Slonecker; X. Li; T. H. Ridgway; J. G. Dorsey. Anal. Chem. 1996, 68, 682-689.

[31] M. Gray; G. R. Dennis; P. Wormell; R. A. Shalliker; P. Slonecker. J. Chromatogr. A 2002, 975, 285-297.

[32] M. Gilar; P. Olivova; A. E. Daly; J. C. Gebler. Anal. Chem. 2005, 77, 6426-6434.

[33] M. Camenzuli; P. J. Schoenmakers. Anal. Chim. Acta 2014, 838, 93-101.

[34] S. Peters; G. Vivo Truyols; P. J. Marriot; P. J. Schoenmakers. J. Chromatogr. A 2007, 1146, 232-241.

[35] J. V. Seeley. J. Chromatogr. A 2002, 962, 21-27.

[36] J. M. Davis; D. R. Stoll; P. W. Carr. Anal. Chem. 2008, 80, 461-473.

[37] J. M. Davis; D. R. Stoll; P. W. Carr. Anal. Chem. 2008, 80, 8122-8134.

[38] G. Vivò-Ttuyols; S. van der Wal; P. J. Schoenmakers. Anal. Chem. 2010, 82, 8525-8536.

[39] J. Lankelma; H. Poppe. J. Chromatogr. A 1978, 149, 587-598.

[40] P. J. Schoenmakers; G. Vivo-Truyols; W. M. C. Decrop. J. Chromatogr. A 2006, 1120, 282-290.

[41] Y. Chen; L. Montero; O. J. Schmitz. Trends in Anal. Chem. 2019, 120, 115647.

[42] I. François; A. de Villiers; B. Tienpont; F. David; P. Sandra. J. Chromatogr. A 2008, 1178, 33-42.

[43] B. W. J. Pirok; M. J. Den Uijl; G. Moro; S. V. J. Berbers; C. J. M. Croes; M. R. Van Bommel; P. J. Schoenmakers. Anal. Chem. 2019, 91, 3062-3069.

[44] D. R. Stoll; E. S. Talus; D. C. Harmes; K. Zhang. Anal. Bioanal. Chem. 2015, 407, 265-277.

[45] R. J. Vonk; A. F. Gargano; E. Davydova; H. L. Dekker; S. Eeltink; L. J. de Koning; P. J. Schoenmakers. Anal. Chem. 2015, 87, 5387-5394.

[46] S. Stephan; J. Hippler; T. Köhler, A. A. Deeb, T. C. Schmidt, O. J. Schmitz. Anal. Bioanal. Chem. 2016, 408, 6545-6555.

[47] S. Han; J. Huang; J. Hou; S. Wang. J. Sep. Sci. 2014, 37, 1525-1532.

[48] P. Petersson; K. Haselmann; S. Buckenmaier. J. Chromatogr. A 2016, 1468, 95-101.

[49] D. R. Stoll; K. Shoykhet; P. Petersson; S. Buckenmaier. Anal. Chem. 2017, 89, 9260-9267.

[50] H. Tian; J. Xu; Y. Xu; Y. Guan. J. Chromatogr. A 2006, 1137, 42-48.

[51] E. Fornells; B. Barnett; M. Bailey; E. F. Hilder; R. A. Shellie; M. C. Breadmore. Anal. Chim. Acta 2018, 1000, 303-309.

[52] Y. Z. Chen; Y. J. Wu; X. M. Liu; B. W. Li; D. P. Hu; S. Huang; M. Ma; B. Chen. J. Chromatogr. A 2019, 1583, 98-107.

[53] K. Im; H. W. Park; Y. Kim; B. Chung; M. Ree; T. Chang. Anal. Chem. 2007, 79, 1067-1072.

[54] J. F. Li, X. Yan, Y. L. Wu, M. J. Fang, Z. Wu, Y. K. Qiu. Anal. Chim. Acta 2017, 962, 114-120.

[55] K. Wagner; T. Miliotis; G. Marko-Varga; R. Bischoff; K. K. Unger. Anal. Chem. 2002, 74, 809-820.

[56] B. Ji; B. Xia; J. Liu; Y. Gao; L. Ding; Y. Zhou. J. Chromatogr. A 2016, 1466, 199-204.

[57] J. W Dolan. LCGC North Am. 2014, 32, 854–859.

[58] D. Li; O. J. Schmitz. Anal. Bioanal. Chem. 2013, 405, 6511–6517.

[59] S. R. Groskreutz; M. M. Swenson; L. B. Secor; D. R. Stoll. J. Chromatogr. A 2012, 1228, 31-40.

[60] K. Zhang; Y. Li; M. Tsang; N.P. Chetwyn. J. Sep. Sci. 2013, 36, 2986-2992.

[61] M. Pursch; S. Buckenmaier. Anal. Chem. 2015, 87, 5310-5317.

[62] D. R Stoll; D. C Harmes; G. O Staples; O. G. Potter; C. T Dammann; D. Guillarme; A. Beck. Anal. Chem. 2018, 90, 5923−5929.

[63] A. Baglai; M. H. Blokland; H. G. J. Mol; A. F. G. Gargano; S. van der Wal; P. J. Schoenmakers. Anal. Chim. Acta 2018, 1013, 87−97.

3.0 Foodomics

In the last years, the development of research has led to a good improvement in different fields thanks to the high-throughput, *omics* technologies.
Starting from the four major types of *omics* fields (genomics, transcriptomics, proteomics and metabolomics), a variety of *omics* subdisciplines (epigenomics, lipidomics, interactomics, metallomics, diseasomics etc.) have emerged.
The *omics* approach could represent a new approach to connect together, food components, food, diet, the health and the diseases; but this broad vision needs not only the application of advanced technologies but also a different view, the "*foodomics* approach"indeed. *Foodomics* in fact, is the comprehensive, high-throughput approach for the investigation of food science in the improvement of human nutrition. This new approach studies nutrition and food in terms of the food domain, as a whole nutrition domain, to reach the main objective: the improvement of human health and well-being [1].

3.1 Introduction to Foodomics

The connection of modern food science and nutrition with the fields such as pharmacology, medicine or biotechnology provides new challenges and opportunities. As result, researches in food science and nutrition are moving from classical methodologies to more advanced strategies for incorporate borrow methods well established in medical, pharmacological, and/or biotechnology research.
In this context, *foodomics* has been defined as a new discipline that studies the food and nutrition domains through the application of advanced omics technologies in order to improve consumer's well-being, health and confidence [2]. Thus, Foodomics is intended to be a global science that includes all of emerging working areas in which

food (including nutrition), advanced analytical techniques and bioinformatics are combined.

This science would help: to understand the gene-based differences among individuals in response to a specific dietary; to understand the biochemical, molecular, and cellular mechanisms that underlie the positive or negative effects of certain bioactive food components; to determine the effect of bioactive food constituents on molecular pathways; to know the identity of genes that are involved in the previous stage to the onset of the disease and so the possible molecular biomarkers; in the comprehensive assessment of food safety, quality, and traceability. The interest in Foodomics coincides with a clear change in medicine and biosciences toward prevention of future diseases through food intakes, and the development of the "functional foods" [3].

3.2 Foodomics applications: Challenges, advantages and drawbacks

The great analytical potential of foodomics can help to resolve many issues and questions related to traceability, food safety, quality, transgenic foods, new foods, functional foods, nutraceuticals etc. In this regards foodomics can resolve some of the new challenges that food safety, quality and traceability have to face. These challenges include the analyses of contaminants and allergens, in according to more powerful analytical technologies to guarantee food origin, traceability and quality; the discovery of biomarkers to detect unsafe products. As result, one of main challenges is to improve our limited understanding of the roles of a nutritional compound at molecular level for the design of strategies to manipulate cell functions through diet, which is expected to have a good impact on health human [4].

Foodomics could be an adequate strategy to investigate the complex issues correlated to the prevention of future diseases and health promotion through food intake. Nowadays, it's well known that health is strictly influenced by genetics. When the

combination of genetics and nutrition/lifestyle/environment is not balanced, poor health results are obtained. Foodomics could increase tool for detecting small changes induced by food ingredient(s) at different levels. The interest of this science coincides with a clear shift in medicine and biosciences toward prevention of future diseases through food intakes and the introduction of functional foods. Therefore, this science seems to be essential to understand how the bioactive compounds from diet interact at molecular and cellular levels, to provide better scientific information on their health benefits. As far as the analytical strategies used in Foodomics the great challenges arise, among other things, from the complexity of the food, the enormous natural variability, the large number of different nutrients and bioactive compounds, their very different concentrations and finally by the numerous targets with different characteristics that they may have.

The challenge of the Foodomics is to improve our limited knowledge on many biological processes that may have place at molecular level. In the future, the combination of Foodomics and Systems Biology can provide crucial information on, for example, host-microbiome interactions, nutritional immunology, food microorganisms including pathogens resistance.

3.3 Metabolomics

As discussed previously, the definition of Foodomics includes -omics technologies as transcriptomics, proteomics and metabolomics, for the study of food functionality and its effect on human health.

Metabolomics aims is to provide knowledge about the profile of the total metabolites present in biological sample (metabolome). The metabolome has been defined as “the full set of endogenous or exogenous low molecular weight metabolic entities of around <1000 Da”[5].

The study of the human metabolome includes hundreds of metabolites of chemical diversity, several ranges of concentrations and complex pathways of interrelation. These challenges can include different analytical approaches such as: ^{1}H nuclear

magnetic resonance spectroscopy (^{1}H-NMR), mass spectrometry (MS), which most times is coupled with separation techniques as GC and LC, and more recent hyphenation like with capillary electrophoresis (CE). ^{1}H-NMR has been applied for identifications of low molecular weight compounds. The extract compounds are dissolved in a deuterated solvent and the resonance frequencies of the hydrogen, in each metabolite, is measured. The advantages of using this technique are:

- minimal sample preparation,
- high reproducibility and identification of macromolecules (DNA, proteins). The problem arise as each metabolite gives multiple signals from the different hydrogen atoms and these signals often are overlaid, so the identification it is impossible. Furthermore, NMR technique is less sensitive than MS spectrometry [6].

Regard this latter, MS is more sensitive and selective in the quantification and identifications, from very low to high, molecular weight metabolites, with detection levels in the order of ng/mL or pg/mL.

The food metabolome can provide markers of dietary short- or long-term intake, more reliable than subjective dietary records [7]. Cultivars, food processing, or storage give high variability on phytochemical composition of plant-based foods. The approach of metabolomic minimize the limitations. Endogenous metabolites are dependent of change due to dietary components and their metabolomic study may be helpful to give markers of effect. Nowadays, even though human nutritional intervention studies using metabolomics approach are poor, attempts have been made on the search for markers of intake of polyphenol-rich foods. Dietary polyphenols have poor bio-availability and are subject extensive phase II metabolism in intestine and liver, where they are conjugated with glucuronide, sulfate and methyl moieties to facilitate their elimination in urine. A major fraction of this class reaches the colon where are degraded by intestinal microbiota in phenolic acids [3].

3.3.1 Metabolomics of Diet-Related Diseases

Lifestyle and diet are directly correlated for specific diseases. Epidemiological and clinical studies have highlighted that diseases with high rates of mortality, including diabetes, some cancers, and cardiovascular disease (heart disease and stroke), are related to diet. The group diet-related diseases include a wide variety of diseases and disorders that have effects in different systems and organs. There are low complexity alterations, restricted to a single organ or system such as dental disorders. Another group, more complex, that would include atherosclerosis, obesity, diabetes, osteoporosis and other systemic involvement and associated complications. Furthermore, cardiovascular disease and cancer, due of compromising vital organs such as liver, heart, kidneys and brain or due to their complications are the leading causes of mortality.

From the etiology point of view, two types of diet-related diseases could be described: cancer, cardiovascular diseases, and diabetes are corelated to disorder (especially excess) in the food intake, whereas the lack of constituents such as proteins, mineral and vitamins may give rise to specific complications known as deficiency diseases (Figure 1).

Food matrix is a complex mixture which does not act on single molecular targets, but modulates many biochemical pathways simultaneously, and the mechanisms for the diet-related pathogenesis involves complex interactions of different processes.

Finally, the application of “omics” science, in particular metabolomics has showed the metabolic change corelated to diet-related diseases and consequently of diet intervention in a global untargeted way.

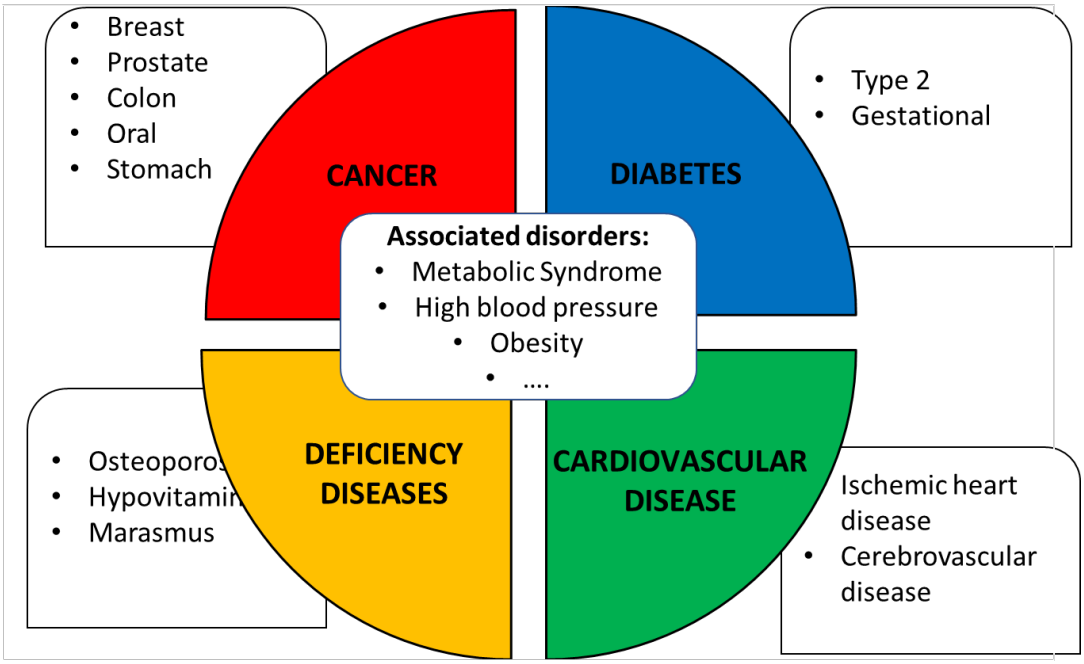

Figure 1. Diet-related diseases.

Nevertheless the latest innovation technologies, other studies are still needed, in particularly on the development of dietary ideal models that can explanation the sequence of events that start with the interaction between dietary habits and genetic adaptations, the changes induced in the metabolism and the diseases related, together with the potential therapeutics, therefore, providing a equilibrate in previously unbalanced organisms expanding the knowledge of the health status.

3.3.2 Analysis of Metabolome

The metabolome is constituted of small molecules, typically less than 1500 Da, coming from protein activity (catabolism and anabolism) in living system.

The principal approaches in metabolomics are:

- targeted analysis,
- metabolite profiling,
- metabolic fingerprinting.

Usually, the first one is the classical analytical approach to study metabolites. It is used to calculate the concentration of a limited number of known metabolites precisely. On the contrary, the second one is the measurement of a set of related metabolites, either chemically or biochemically, correlated among them. Finally, the last one take in consideration the total profile, or "fingerprints", as a unique pattern characterizing an image of the metabolism in a particular cell line or tissue. In conclusion metabolite fingerprinting is most useful in biomarker discovery.

Due to the huge amount of physico-chemical properties and the large differences in concentrations, different analytical techniques are required. The analyses generally are carried out thought GC-MS, LC-MS, CE-MS and or NMR. The metabolome study will be influenced on different factors according to the analytical approaches: selection of the sample, sample preparation and instrumentation. Despite the sensitivity in NMR is very poor, the elucidation capabilities are unquestionable; the NMR profile could contain qualitative and quantitative information on several of different small molecules present in the sample. Regarding GC separation, it is appropriate for volatiles metabolites such as: amino acids, monosaccharides, fatty acids, disaccharides and cholesterol. HPLC instead, has many advantages like minimum requirements of sample treatment and so minimum alteration of the metabolites during the analysis.

Especially, RP-LC is used for low and medium polarity metabolites, but it is not optimal for polar metabolites as sugars or amino acids, while HILIC mode and CE could offer a good separation for polar metabolites. Mass spectrometry-based approaches are more sensitive than NMR techniques, providing access to lower concentration metabolites.

3.4 Polyphenols

Nowadays, the natural polyphenolic compounds have an increasing interest, since a great amount of them can be found in plants, in beverages consumption, and vegetables. Their high level concentrations may reduce the risk of development of

several diseases, thanks to their antioxidant power. As well know, the metabolism of plants can be divided in primary and secondary; the substances that are essential to cells maintenance (lipids, carbohydrates, proteins and nucleic acids) are produced from the primary metabolism. On the contrary, constituents originated from several biosynthetic pathways are results of the secondary metabolism [8].

Polyphenols are constituted in one of the biggest and largely distributed groups of the secondary metabolites in plants [9] and are principally involved in defense against aggression by pathogens and against ultraviolet radiations. They are naturally found in the fruit, vegetables, cereals and beverages. For example, in the grapes, apple, berries, cherries and pear, could contains up to 200-300 mg of polyphenols per 100 grams fresh weight. In addition, the products obtained from these fruits, could also contain these compounds. For example, a glass of red wine or a cup of tea or coffee has about 100 mg of polyphenols.

Polyphenols presents in food can contribute to give the color, flavor, odor and bitterness. Therefore, as to the location in the plant (free in the soluble fraction of cell or bound to compounds of cell wall), with the chemical structure of these constituents, can be classified as: soluble (such as simple phenol, tannins and flavonoids) and insoluble (such as condensed tannins, phenolic acids and other phenolic compounds of low molecular weight bound to cell wall polysaccharides or proteins forming insoluble stable complex). Is well known, that long period of diets rich in polyphenols give some protection against cancers, cardiovascular diseases, osteoporosis, diabetes and neurodegenerative diseases [10,11] (Figure 2).

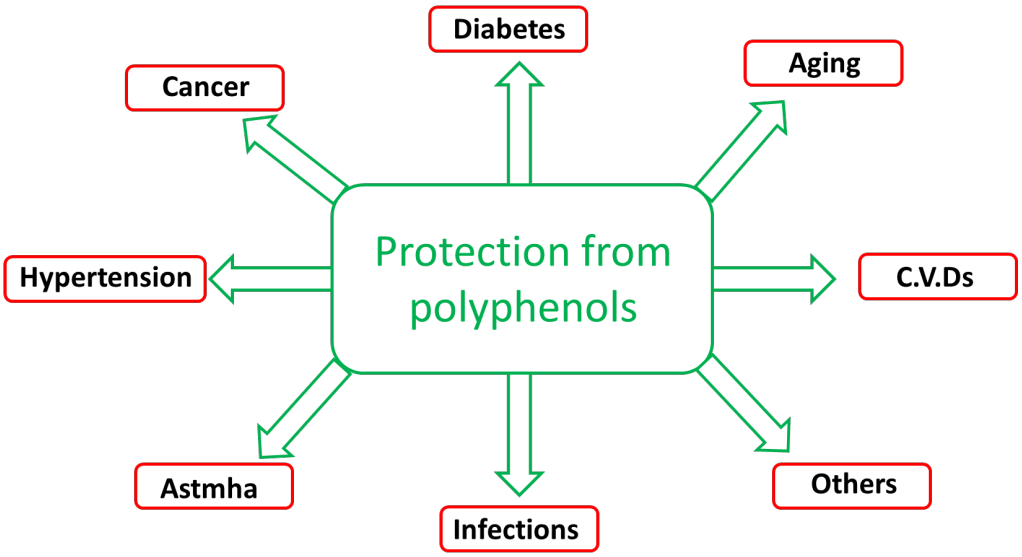

Figure 2. Polyphenols actions against several diseases.

3.4.1 Classes and structure of Polyphenols

In nature are present more than 8000 polyphenolic compounds in several plant species. In particular, all polyphenols compounds are derived from a common intermediate, the phenylalanine or shikimic acid. Usually, they occur in conjugated forms, with one or more sugar unity linked to hydroxyl groups, or direct linkages of the sugar to an aromatic carbon (mono- or poly-saccharide).

Polyphenols can be classified into various groups according to the number of phenol rings present and in function of structural elements that bind these rings to one another. The principal classes are: phenolic acids (that are divided in two big groups: Benzoic acid and Cinnamic acid), flavonoids, stilbenes and lignans [12]. The structures are showed in figure 3.

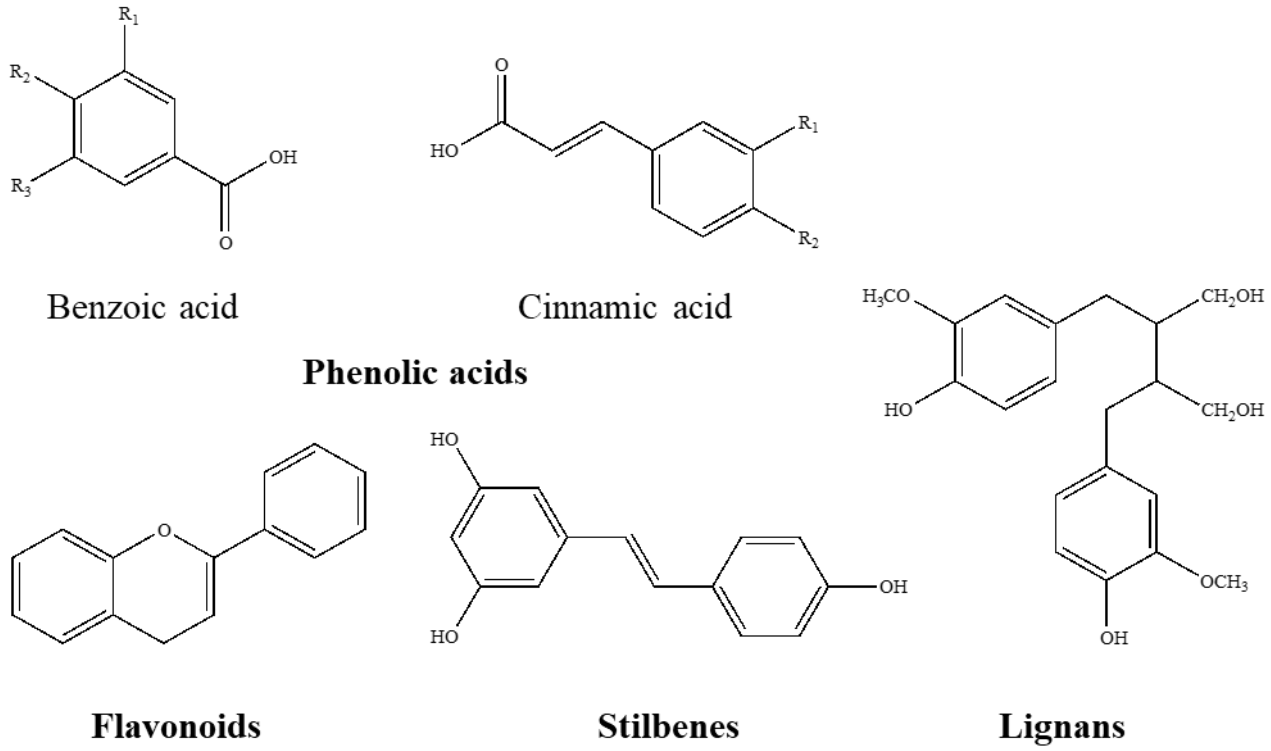

Figure 3. Chemical structures of the different classes of polyphenols

3.4.2 Phenolic acids

The phenolic acids are present mainly in foods and can be divided in two group: derivates of benzoic acid and derivates of cinnamic acid. These compounds are characterized by having a benzenic ring, one or more hydroxyl group, a carboxylic group and/or methoxyl groups in the structure. The general formula and names of the main benzoic and cinnamic acids are showed in figure 4 and 5, respectively. Usually, the benzoic acid has seven carbon atoms (C_6-C_1) and is contained in edible plants at low concentration. On the contrary could be found in high concentration in red fruits, black radish and onions, in the order of several tens of milligrams per kilogram fresh weight [13]. Cinnamic acids have nine carbon atoms (C_6-C_3), but the most common present in vegetable, are with seven and rarely are present in free form in the plants. They are normally in form of esters, along with a cyclic alcohol-acid, such as a quinic acid to form the isochlorogenic acid, neochlorogenic acid, cripto chlorogenic acid, a caffeoyl ester, which are the most important combination [14].

The phenolic acids could be about one-third of the polyphenols compounds in the human's diet [15]. As well know, these substances and their esters have high antioxidant activity, in particular hydroxybenzoic acid, hydroxycinnamic acid, caffeic acid and chlorogenic acid. This activity is usually determined by the number of hydroxyl groups found in the molecule. In general, the hydroxylated cinnamic acids are more effect than their benzoic acids counterparts [16].

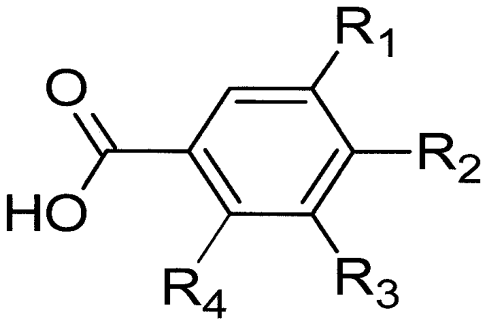

Salicylic acid (R_4 = OH, R_1, R_2, R_3 = H);
Gentisic acid (R_1, R_3 = OH; R_2, R_4 = H);
p-Hydroxybenzoic acid (R_2 = OH, R_1, R_3, R_4 = H);
Protocatechuic acid (R_1, R_2 = OH; R_3, R_4 = H);
Vanillic acid (R_1 = OCH_3, R_2 = OH; R_3, R_4 = H);
Gallic acid (R_1, R_2, R_3 = OH; R_4 = H);
Syringic acid (R_1, R_3 = OCH_3; R_2 = OH; R_4 = H)

Figure 4. The names and general structures of the main benzoic acids derivate.

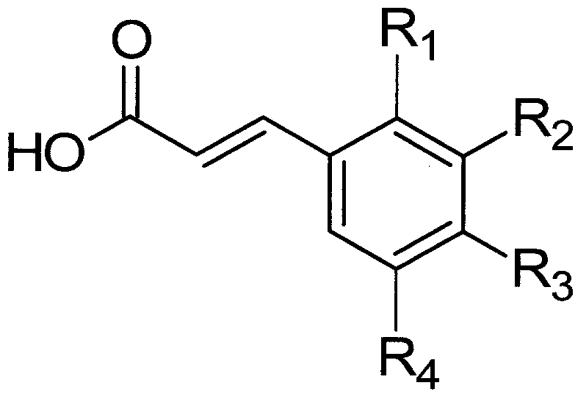

Ceramic acid (R_1 = R_2 = R_3 = R_4 = H)
o-Coumaric acid (R_1 = OH; R_2, R_3, R_4 = H)
m-Coumaric acid (R_2 = OH; R_1, R_3, R_4 = H)
p-Coumaric acid (R_3 = OH; R_1, R_2, R_4 = H)
Caffeic acid (R_2 = R_3 = OH; R_1, R_4 = H)
Ferulic acid (R_2 = OCH_3; R_3 = OH; R_1, R_4 = H)
Sinapic acid (R_2 = R_4 = OCH_3; R_3 = OH; R_1 =H)

Figure 5. The names and general structures of the main cinnamic acids derivate.

3.4.3 Flavonoids

These groups have a common basic structure consisting of two aromatic rings linked together with three carbon atoms forming an oxygenated heterocycle. More than 4000 varieties of flavonoids are known in nature and could be divided into 13 classes [16]. The manly are: flavonols, flavanols, flavones, isoflavones, anthocyanidins or anthocyanins and flavanones [9]. There are many structural variations according to the degree of hydrogenation and hydroxylation of the three rings of these compounds. There is also a sulfated and methylated derivative, conjugated with monosaccharides and disaccharides, resulting in complex with oligosaccharides, lipids, amines, organic acids and carboxylic acids [17]. The chemical structures of the main classes of flavonoids are showed in figure 6.

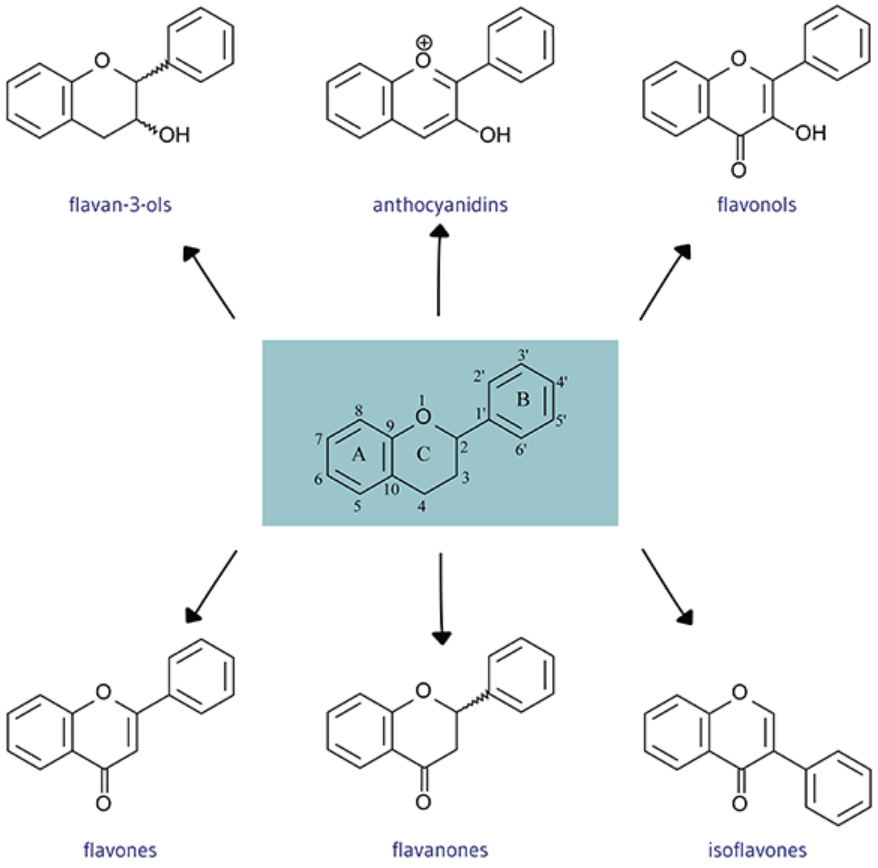

Figure 6. The general structures of the flavonoids.

Flavonoids are very important constituent in the human diet [18-19] and are most distributed in phenolic compounds in plant foods [14]. Additionally, the excellent antioxidant activity is correlated to the presence of hydroxyl group in position 3' and 4'of the B ring, that confer high stability to the formed radical by participating in the displacement of the electron and a double bond between carbons C2 and C3 of the ring C with the carbonyl group at the C4 position, which makes the displacement of an electron possible from the ring B [20]. It is important highlight that the effectiveness of the flavonoids decreases with the substitution of hydroxyl groups for sugars, due to the glycosides less antioxidants than their corresponding aglycons [21].

Flavonols are the most ubiquitous flavonoids in foods and the most abundant are quercetin and kaempferol. Usually they are present at low concentrations, around 15-30 mg/kg in fresh wt. Additionally, these compounds are present in glycosylated forms especially with glucose or rhamnose and less common galactose, arabinose, xylose, glucuronic acid.

Flavones are much less common than flavanols in fruit and vegetable. The most principal compounds of this groups are glycosides of luteolin and apigenin [22]. The flavanones most present in foods are naringenin in grapefruit, hesperetin in oranges and eriodictyol in lemon. Generally, the flavanones are glycosylated by a disaccharide at position 7: either a neohesperidose which gives a bitter taste or a rutinose, which is flavorless. Flavanols are present in the monomer form (catechins) and the polymer form (proanthocyanidins). The first ones founded in various types of fruit, such as apricots and in red wine. An infusion of green tea contains up to 200 mg catechins [23]. Catechin and epicatechin are the main flavanols in fruit, on the contrary gallocatechin, epigallocatechin gallate are found in seed of leguminous plants, in grapes [24,25].

Proantocyanidinis, are another subclass belonging of flavonoids, which are also known as condensed tannins and can be dimer, oligomers and polymers of catechins that are bound together by links between C4 and C8 or C6. Their mean degree of polymerization in foods is very difficult to determined. Through the formation of complexes with salivary proteins, condensed tannins are responsible for the astringent

character of fruit such as in grapes, peaches, kakis, pears, berries, etc) and the bitterness of chocolate [26]. This characteristic change particularly over the course of maturation and normally disappears when the fruit reaches ripeness. This behavior has been seen in the kaki fruit by polymerization reactions with acetaldehyde [27].

Anthocyanins are pigments presented in the vacuolar sap of the epidermal tissues of fruits and flowers and give the colors (pink, red, blue or purple) [28]. In nature they are present in different chemical forms, both colored and uncolored, in according to pH. In addition, anthocyanins are stabilized by the formation of complexes with other flavonoids. In the diet, these pigments are found in red wine, in some verities of cereals but in particular in fruits such as in the range to 2-4 g/kg fresh wt in blackcurrants or blackberries, but this value can increase in the fruit ripens.

3.4.4 Lignans

Lignans are biphenolic compounds that are formed of 2 phenylpropane units. In particular, the high quantitate of it is present in linseed, with secoisolariciresinol (up to 3.7 g/kg dry wt) and low quantities of matairesinol. Other vegetables, or cereals contain traces of lignans but concentrations in linseed are 1000 times as high as concentrations in these other food [29]. This group are metabolized to enterodiol and enterolactone by the intestinal microflora. The secoisolariciresinol and matairesinol, that are ingested as part our diet, don't take in account for the concentrations of the metabolites enterodiol and enterolactone that are measured in plasma and urine. Other lignans from plant are precursors of enterodiol and enterolactone but have not yet been identified [30].

3.4.5 Stilbenes

Stilbenes contain two phenyl moieties connected by a two-carbon methylene bridge. Occurrence of stilbenes in the human diet is very low. Most stilbenes in plants has a role as antifungal phytoalexins, compounds that are synthesized only in response to

infection. The major compound is resveratrol, that has anticarcinogenic effects and is found in low quantities in wine (0.3-7 mg aglycones/L and 15 mg glycosides/L in red wine) [31-33].

References

[1] F. Capozzi; A. Bordoni. Genes Nutr. 2013, 8, 1-4.

[2] A. Cifuentes. J. Chromatogr. A 2009, 1216, 7109-7110.

[3] A. Cifuentes (Ed.). Foodomics: Advanced Mass Spectrometry in Modern Food science and Nutrition, John Wiley and Sons, Inc., Hoboken, New Jersey, 2013.

[4] V. Garcia-Cana; C. Simò; C. Leon; A. Cifuentes. J. Pharm. Biomed. Anal.2010, 51, 290-304.

[5] E. Trujillo; C. Davis; J. Millner. J. Am. Diet. Assoc. 2006, 106, 403-413

[6] S. Becker; L. Kortz; C. Helmeschrodt; J. Thiery; U. Ceglarek. J. Chromatogr. B 2012, 883-883, 68-75.

[7] S. Primrose; J. Draper; R. Elsom; V. Kirkpatrick; J. C. Mathers; C. Seal; M. Beckmann; S. Haldar; J. H. Beattie; J. K. Lodge; M. Jenab; H. Keun; A. Scalbert. Brit. J. Nutr. 2011, 105, 1277-1283.

[8] M. L. Vickery; B. Vickery; Secondary plant metabolism, Macmillan Press., 1981.

[9] A. Scalbert; G. Williamson. J. Nutr. 2000, 130, 2073-2085.

[10] B. A. Graf; P. E. Milbury; J. B. Blumberg. J. Med. Food 2005, 8, 281-290.

[11] I. C. W. Arts; P. C. H. Hollman. Am. J. Clin. Nutr. 2005, 81, 317-325.

[12] J. P. Spencer; M. M. Abd El Mohsen; A. M. Minihane; J. C. Mathers. Br. J. Nutr. 2008, 99, 12-22.

[13] F. Shahidi; M. Naczk. Lancaster, PA: Technomic Publishing Co Inc, 1995.

[14] L. Bravo. Nutr. Rev. 1998, 56, 317-333.

[15] C. S. Yang; J. M. Landau; M. T. Huang; H. L. Newmark. 2001. Annu. Rev. Nutr. 2001, 21, 381-406.

[16] C. Sánchez-Moreno. Alimentaria 2002, 329, 29-40.

[17] G. G. Duthie; P. T. Gardner; J. A. M. Kyle. 2003 Proc. Nutr. Soc. 2003, 62, 599-603.

[18] M. G. L. Hertog; P. C. H. Hollman; D. P. Venema. J. Agric. Food Chem. 1992, 40, 1591-1598.

[19] S. V. Jovanovic; S. Steenken; M. Tosic; B. Marjanovic; M. G. Simic. J. Am. Chem. Soc. 1994, 116, 4846-4851.

[20] M. D. L. R. Giada. InTech 2013, 87-112.

[21] C. Rice-Evans; N. J. Miller; G. Paganga. Free Radic. Biol. Med. 1996, 20, 933 956.

[22] C. Manach; A. Scalbert; C. Morand; C. Rémésy; L. Jiménez. Am. J. Clin. Nutr. 2004, 79, 727-747.

[23] C. Lakenbrink; S. Lapczynski; B. Maiwald; U. H. Engelhardt. J Agric. Food Chem. 2000; 48:2848–52.

[24] I. C. W. Arts; B. van de Putte; P. C. H. Hollman. J. Agric. Food Chem. 2000, 48, 1746-1751.

[25] K. Reinli; G. Block. Nutr. Cancer 1996, 26, 123-148.

[26] C. Santos-Buelga; A. Scalbert. J. Sci. Food Agric. 2000, 80, 1094-1117.

[27] T. Tanaka; R. Takahashi; I. Kouno; G. Nonaka. J. Chem. Soc. 1994, 3013-3022.

[28] G. Mazza; E. Maniati. Boca Raton, FL: CRC Press, 1993.

[29] H. Adlercreutz; W. Mazur. Ann. Med. 1997, 29, 95-120.

[30] S. Heinonen; T. Nurmi; K. Liukkonen. J. Agric. Food Chem. 2001, 49, 3178-3186.

[31] A. Bertelli; A. A. E. Bertelli; A. Gozzini; L. Giovannini. Drugs Exp. Clin. Res. 1998, 24, 133-138.

[32] K. P. Bhat, J. M. Pezzuto. Ann. NY Acad. Sci. 2002, 957, 210–229.

[33] X. Vitrac; J. P. Moni; J. Vercauteren; G. Deffieux; J. M. Mérillon. Anal. Chim. Acta 2002, 458, 103-110.

4.0 Determination of the polyphenolic fraction of *Pistacia vera* L. kernel extracts by comprehensive two-dimensional liquid chromatography coupled to mass spectrometry detection

Pistachio (Pistacia vera L.) belongs to the Anacardiaceae family and it is a small tree species. It is native of the Middle East and Central Asia, but currently, it is cultivated also in California and in some Mediterranean countries, such as Greece and Italy. The most important pistachio producers are Iran, the USA, and Turkey. Besides being a delicious nut, pistachio, due to its whole some nutritional properties, could be considered as a functional food. According to the results of several studies, pistachios have been proven to have various groups of valuable phytochemicals such as anthocyanins, flavan-3-ols, proanthocyanidins, flavonols, isoflavones, flavanones, stilbenes, and phenolic acids, possessing excellent biological activities. The most common analytical technique employed for their analysis is represented by liquid chromatography coupled to photodiode array and mass spectrometry
detection. However, conventional LC can present some limits especially in terms of resolving power. In this contribution, as a powerful alternative, comprehensive two-dimensional liquid chromatography (LC×LC) was applied to the determination of the polyphenolic fraction of pistachio kernels from different geographical origins. A 150-mm micro-bore cyano column (2.7 μm dp) and 50-mm superficially porous C18 silica column (2.7 μm dp) in the first (^{1}D) and second (^{2}D) dimensions were employed, respectively. For boosting orthogonality, a shift ^{2}D gradient was investigated leading to an increase in the overall peak capacity.

The newly developed LC×LC method showed satisfactory linearity, sensitivity, precision and accuracy, which was then applied to sample quantitative analysis. A total of 51 different polyphenolic compounds were determined in the four samples investigated and 18 out of them are hereby reported for the first time.

4.1 Introduction

Pistachio (*Pistacia vera* L; Anacardiaceae) is native of aride zones of Central and West Asia and distributed throughout the Mediterranean basin. The genus Pistacia contains only 11 species among which P. vera, cultivated for its edible nuts, is by far the most important economically. Top producing countries are Iran, the USA, and Turkey, followed by Greece, Italy, and Spain. The seeds or pistachio nuts consist of a wooden shell and a yellow or green kernel, which has a papery seed coat (skin), the color of which ranges from yellow to green. The pistachio nut is mainly used as food ingredient (*e.g.*, in the manufacture of ice cream, pastries, fermented meats, puddings, and in confections) and is consumed natural and roasted [1], while the shells have been proposed as a raw material to prepare activated carbons [2].

Pistachio nuts are known to contain several classes of polyphenolic compounds, e.g., anthocyanins, flavan-3-ols, proanthocyanidins, flavonols, isoflavons, flavanones, stilbenes, and phenolic acids, which are responsible of many biological properties [3–6]. Specifically, anthocyanins possess antioxidant, anti-inflammatory, anti-carcinogenic [5, 6], and anti-angiogenic activities [7]; catechins are active in decreasing the oxidation of low-density lipoproteins (LDL) [8–10], whereas isoflavones show chemopreventive properties (partial agonists at the level of estrogen receptors) [11]. Several studies have been devoted to the characterization of the polyphenolic fraction of the various parts of *Pistacia vera* L. fruits *viz*. entire nuts, hull, or kernel extracts [12–26], most of them dealing with the Bronte [12–14, 19, 24, 25] and Turkey varieties [15, 16, 18, 21, 23, 26]. However, only in a few cases, quantitative data are reported with a limited characterization of the extracts [12–14, 17, 19, 20, 25]. The complete profile of the bioactive polyphenols in pistachio samples is rather difficult since they are characterized by an enormous structural variability. As a consequence, in the present study, a comprehensive liquid chromatography (LC×LC) method based on the use of reversed phase conditions in both separation systems (RP-LC×RP-LC-PDA-ESI/MS) was investigated for tackling such a task. Since from its

introduction in 1978 [27], LC×LC has experienced an ever growing number of applications and many of them have dealt with the characterization of the polyphenolic content in various food and natural products by using different stationary phases, especially for the first dimension (^{1}D) separations: polyethylenglycol [28, 29], polyamine [30], cyano [31–35], RP-Amide [36, 37], and diol [29, 38, 39]. It is notorious that RP-LC×RP-LC separations, carried out with a conventional full-in-fraction approach, are affected by low orthogonality arising from the similarity of the two separation modes. Interestingly, in this work, a novel approach based on the use of shift gradients is proposed allowing a promising "orthogonal" separation for the polyphenolic compounds occurring in the investigated samples.

The present study was carried out to exploit a thorough determination of the polyphenolic composition of four varieties of *Pistacia vera* kernels from different geographical origin. Particular attention has been given to polyphenolic composition of a Sicilian variety (Bronte pistachio) with respect to the other varieties investigated namely Turkey, California, and Iran. The main reason derives from the fact that since 2009 Bronte pistachio has received the Protected Designation of Origin (PDO) from the European Community as a recognition of the special procedure for cultivation and biodiversity conservation (annual production is roughly 30 tons which corresponds to 80% of the total Sicilian production) [12].

A preliminary investigation with the conventional LC-PDA-MS method was carried out in order to highlight the benefits arising from the hyphenation of the LC×LC to the MS detection, which resulted in more confident qualitative and quantitative results.

4.2 Experimental

4.2.1 Reagents and Materials

Water, acetonitrile (ACN), methanol (MeOH), and formic acid LC-MS grade were all purchased from Merck Life Science (Merck KGaA, Darmstadt, Germany).

Polyphenolic standards, namely, gallic acid, catechin, caffeic acid, genistin, eriodictiol, luteolin, and kaempferol, were purchased from Merck Life Science (Merck KGaA, Darmstadt, Germany). Stock solutions of 1000 mg L^{-1} were prepared for each standard by dissolving 10 mg of gallic acid, catechin, caffeic acid, genistin, and eriodyctiol in 10 mL of water and 10 mg of luteolin and kaempferol in 10 mL of methanol.
1D-LC separations were performed on an Ascentis Express C18 column (Merck Life Science, Merck KGaA, Darmstadt, Germany; 150 × 4.6 mm I.D., 2.7 µm dp).
LC×LC separations were conducted by using a ^{1}D Ascentis Express Cyano (ES-CN) column (Merck Life Science, Merck KGaA, Darmstadt, Germany); 150 × 1.0 mm I.D., 2.7 µm dp) and a second dimension (^{2}D) Ascentis Express C18 column (Merck Life Science, Merck KGaA, Darmstadt, Germany; 50 × 2.1 mm I.D., 2.7 µm dp).

4.2.2 Sample and sample preparation

Samples of unprocessed whole pistachio nuts from different geographical origins and varieties (Bronte, California, Iran, Turkey, Greece) were kindly provided by Pistì S.r.L. (Bronte, Italy). Samples (5 g) were initially shredded to increase the surface of extraction and then extracted three times with n-hexane (10 mL) for 6 h under constant agitation in order to remove the lipids [40]. After filtration, the residue was mixed with 50 mL of methanol/HCl 0.1% (*v/v*) and sonicated for 15 min. Afterwards, the sample solutions were centrifugated (3000×g, 20 min). After centrifugation, the pellet was extracted two more times by using the same procedure.
The acidic methanolic fractions were combined and evaporated by a rotary evaporator; the residue was dissolved in 20 mL of distilled water and extracted four times with 20 mL of ethyl acetate.
The organic phases were combined and dried with anhydrous Na_2SO_4 for 20 min. The dried extracts of pistachios were dissolved in methanol. The samples were filtered through a 0.45-µm Acrodisc nylon membrane (Merck Life Science, Merck KGaA, Darmstadt, Germany) prior to LC and LC×LC injection.

4.3 Instrumentation and software

LC and LC×LC analyses were performed on a Nexera-e liquid chromatograph (Shimadzu, Kyoto, Japan), consisting of a CBM-20A controller, four LC-30AD dual-plunger parallel flow pumps, a DGU-20A5R degasser, a CTO-20AC column oven, a SIL-30AC autosampler, and an SPD-M30A photo diode array (PDA) detector (1.0 uL detector flow cell volume).

The two dimensions were connected by means of two high speed/high pressure two-position, six-ports switching valves with micro-electric actuator (model FCV-32 AH, 1.034 bar; Shimadzu, Kyoto, Japan), placed inside the column oven and equipped with two 15-μL stainless steel loops. The Nexera-e liquid chromatograph was hyphenated to an LCMS-8050 mass spectrometer, through an ESI source (Shimadzu, Kyoto, Japan).

4.4 Analytical conditions

4.4.1 LC separation

One-dimensional LC (1D-LC) separations were run on the Ascentis Express C18 column. Mobile phases: (A) 0.1% formic acid in water (pH 3), (B) 0.1% formic acid in ACN.

Gradient: 0 min, 2% B; 5 min, 2% B; 20 min, 10% B; 60 min, 30% B; 80 min, 100% B. Mobile phase flow rate, 1 mL min^{-1} split to 0.4 mL/min prior to MS detection. Column oven, 30 °C. Injection volume, 2 μL.

4.4.2 LC×LC separations

For ^{1}D separations, the Ascentis Express ES-CN column was used. Mobile phases: (A) 0.1% formic acid in water (pH 3), (B) 0.1% formic acid in ACN.

Gradient: 0 min, 2%B; 5 min, 2% B; 20 min, 10% B; 60 min, 30% B; 80 min, 100% B (held for 20 min). Flow rate, 15 μL min^{-1} maintained by the use of a T-piece union placed between the mixer and the autosampler (at pumps, 75 μL min^{-1}). Column oven, 30 °C. Injection volume, 5 μL.

For ^{2}D separations, an Ascentis Express C18, 50 × 2.1 mm I.D., 2.7 μm d.p. partially porous column was used. The mobile phases employed were (A) 0.1% formic acid in water (pH 3) and (B) 0.1% formic acid in ACN. Shift gradient (SG) conditions: 0–8 min, 0–1 %B (gradient steepness:1%B); 8–80 min, 1–26 %B (gradient steepness: 6%B The flow rate employed was 0.8 mL min^{-1}. Backpressure values in the ^{2}D ranged from 546 bar (0%B) to 610 bar (26%B). Modulation time of the switching valves, 1.20 min. Loop internal volume, 20 μL. Column oven, 30 °C.

4.5 Detection conditions

PDA range, 200–400 nm; sampling rate, 12.5 Hz (1D-LC analyses) and 40 Hz (LC×LC analyses); time constant, 0.08 s (1D-LC analyses) and 0.025 s (LC×LC analyses).

Interface: ESI-MS in negative ionization mode. Mass spectral range in full scan mode: m/z 100–1200; event time, 0.5 (1D-LC analyses) and 0.2 s (LC × LC analyses); nebulizing gas (N_2) flow, 3 L min^{-1}; drying gas (N_2) flow, 15 L min^{-1}; heating gas flow (air), 10 L min^{-1} same; heat block temperature, 400 °C; desolvation line (DL) temperature, 250 °C; interface temperature, 300 °C; interface voltage, 3.50 kV; detector voltage, 1.80 kV.

4.6 Data handing

The LC×LC-LCMS-8050 system and the switching valves were controlled by the Shimadzu Labsolution software (ver. 5.65). LC×LC-Assist software (ver. 2.00) was used for setting up the shift gradient analyses. The LC×LC data were visualized and

elaborated into two and three dimensions using Chromsquare ver. 2.3 software (Shimadzu, Kyoto, Japan).

4.7 Construction of calibration curves

Since only a few polyphenolic compounds detected were commercially available, following a frequently adopted approach [41, 42], seven standards, representative of the chemical classes under study, were selected, namely gallic acid, catechin, caffeic acid, genistin, eriodyctiol, luteolin, and kaempferol. Standard calibration curves were prepared in a concentration range 0.1–50 mg L^{-1} with seven different concentration levels. Triplicate injections were made for each level, and a linear regression was generated. The calibration curves with the external standards were obtained using concentration (mg L^{-1}) with respect to the area obtained from the integration of the PDA peaks at a wavelength of 270 nm for benzoic acid-like and isoflavones, 278 nm for flavan-3-ol-like compounds, 325 nm for cinnamic acid-like compounds 336 nm for flavone-like compounds, 346 nm for flavanone like compounds, and 350 nm for flavonol-like compounds (Table 1). The amount of the compound was finally expressed in milligrams per gram of extract.

Table 1. Quantitative performance of the polyphenolic reference materials used in this study using the RP-LC×RP-LC system coupled to PDA detection

Reference material	Chemical class	Linearity		LoD	LoQ	Precision
		Standard curve	R^2	(□g/mL)	(□g/mL)	(RSD%)
Gallic acid	Benzoic acid-like	y=152566x-748573	0.9998	0.01	0.03	0.21
Catechin	Flavan-3-ol-like	y=86625x-258568	0.9993	0.03	0.09	0.42
Caffeic acid	Cinnamic acid-like	y=483992x-200000	0.9995	0.01	0.03	0.19
Genistin	Isoflavone-like	y=241149x-81444	0.9997	0.01	0.03	0.25
Eriodyctiol	Flavanone-like	y=45374x-148895	0.9998	0.02	0.06	0.08
Luteolin	Flavone-like	y=160589x-817577	0.9995	0.02	0.06	0.15
Kaempferol	Flavonol-like	y=161918x-688222	0.9999	0.01	0.03	0.18

4.8 Results and discussion

The knowledge in differences in polyphenolic profile can be useful to discriminate the geographic origin and preserve the authenticity of selected types of pistachios.
In this context, the evaluation of the bioactive components in pistachio extracts could be of remarkable value for improving human health and have a significant economic impact on pistachio food industry.

4.8.1 RP-LC-PDA-ESI-MS analysis of the polyphenolic fraction of in Pistacia vera extracts

Figure 1 shows the LC-PDA-MS analysis of four varieties of *Pistacia vera* kernels from different geographical origin, namely Bronte, Turkey, Iran, and California (peak identification of selected target compounds were highlighted) carried on a partially porous C18 column. Optimization of the mobile phase composition was initiated by choosing a suitable organic modifier, methanol and acetonitrile, and running a mixture of the seven standard compounds listed in the "Experimental" section. From the comparison of methanol based mobile phases and acetonitrile-based mobile phases, the latter resulted in higher separation efficiency and selectivity with reduced backpressure values. For the choice of mobile phase additive, the use of 0.1% formic acid at pH 3 provided the best sensitivity for all compounds in negative ionization mode.
As can be appreciated from Fig. 1, the chemical composition of the pistachio kernels is rather complex and a considerable number of compounds overlapped, despite the optimization of mobile phase was carried out (peak identification in Table 2). Therefore, the use of multiple dimensions (*i.e.*, separation and detection selectivity) was then exploited as a valuable method of choice for unraveling the investigated extracts aiming to identify the full suite of occurring compounds.

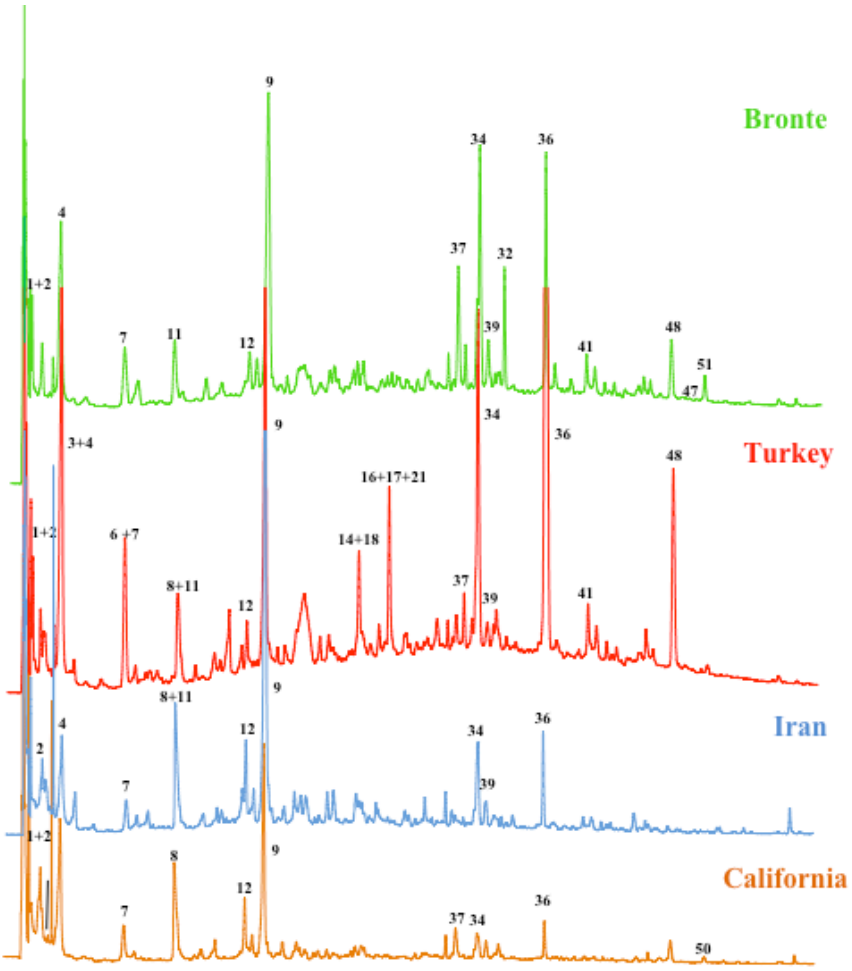

Figure 1: LC-PDA-MS analysis of four varieties of Pistacia vera kernels from different geographical origin, namely Bronte, Turkey, Iran, and California. Peak numbering as in Table 2.

4.8.2 Optimization of the RP-LC×RP-LC-PDA-ESI-MS analysis of the polyphenolic fraction in *Pistacia vera* extracts

To improve peak separation and resolution of overlapped components, an RP-LC×RP-LC system coupled to PDA and ESI-MS was investigated.

At first, each dimension was optimized independently. LC×LC separations imply to run ^{1}D under suboptimal chromatographic conditions in order to decrease the amount of the eluate transferred from the ^{1}D.

Table 2. Quantitative analysis (mg/kg) of polyphenols in pistachio samples. Results are expressed as mean ± S.D. of three replicates.

No	Trivial name	Bronte	California	Turchia	Iran
1	1-O-galloyl β-D-glucopyranose	24.3±1.2	33.2±1.5	13.4±1.9	-
2	Quinic Acid	10±0.8	12±1.0	21±1.2	26±1.2
3	Galloylquinic acid	-	-	34±0.7	-
4	Gallic acid	37±0.8	32±0.9	50±1.5	35±1.3
5	Cinnamic acid	12±0.6	11±0.9	14±0.7	-
6	Gallic acid der. I	-	-	33±1.0	-
7	Protocatechuic acid	32±1.2	27±1.5	30±1.8	26±1.4
8	Galloylshikinic acid	-	-	24±1.3	-
9	Catechin hexoside	52±0.3	40±0.6	55±0.8	51±0.9
10	Genistein 7-glucoside	7±1.8	-	<LoQ	<LoQ
11	Gallocatechin	18±1.5	-	14±1.5	20±1.2
12	Procyanidin dimer	23±0.8	18±0.9	24±0.4	26±0.8
13	Vanillin	-	-	14±1.3	-
14	Taxifolin hexoside	24±0.8	<LoQ	25±0.9	24±0.9
15	Gallic acid der. II	-	-	11±1.2	-
16	Quercetin glucoside	-	-	23±1.3	22±1.2
17	Catechin	14±1.5	12±1.9	28±1.2	10±1.8
18	Digalloylshikimic acid	-	-	10±1.8	-
19	Daidzein 7-glucoside	32±0.5	15±0.7	30±0.8	30±1.5
20	Digalloylquinic acid	-	-	10±1.6	11±1.8
21	Apigenin dihexoside	-	-	24±1.2	-
22	Quercetin rutinoside	12±0.8	-	11±1.0	10±1.1
23	3,7-Dimethylquercetin	11±1.2	14±1.2	15±1.5	15±1.6
24	Digalloylhexose	-	-	15±1.6	-
25	Epicatechin	15±1.6	13±1.6	11±1.8	12±1.9
26	Kaempferol dihexoside	-	-	24±1.3	-
27	Gallic acid der. III	30±0.5	-	27±0.5	25±1.8
28	Ellagic acid diglucoside	-	11±1.6	28±0.7	12±0.9
29	Gallic acid der. IV	-	-	10±1.7	-
30	Myricetin der.	-	-	23±1.5	12±1.9
31	Isorhamnetin glucuronide	24±1.2	22±1.3	13±1.5	26±1.5
32	Luteolin hexoside	30±0.8	<LoQ	15±1.6	<LoQ
33	Galloyl dihexoside	-	-	11±1.8	-
34	Eriodictyol 7-glucoside	52±0.5	18±1.4	61±0.3	25±0.7
35	Quercetin galloyl hexoside	12±1.5	11±1.8	12±1.8	<LoQ
36	Quercetin 3-glucoside	47±0.6	12±1.9	54±0.6	20±1.6
37	Dihydroquercetin	43±0.7	15±1.8	25±1.5	<LoQ
38	Tetragalloyl hexose	-	-	20±1.2	19±1.4
39	Ellagic acid	38±0.8	11±1.8	40±1.3	-
40	Hesperetin 7-rutinoside	11±1.7	12±1.6	37±0.6	18±0.9

41	Naringenin 7-neohesperidoside	12±1.8	17±1.8	38±0.8	16±1.3
42	Quercetin pentoside	13±1.5	-	9±1.8	13±1.5
43	Isorhamnetin dihexoside	12±1.5	33±0.8	31±0.9	35±0.6
44	Penta-O-galloyl-β-D glucose	-	-	<LoQ	<LoQ
45	Kaempferol 3-glucoside I	<LoQ	-	20±0.6	18±0.6
46	Kaempferol 3-glucoside II	-	-	21±0.7	-
47	Luteolin	11±1.7	-	15±1.8	-
48	Eriodictyol	44±0.9	-	50±1.0	-
49	Kaempferol	13±1.8	-	-	15±1.5
50	Luteolin diglucuronide	-	18±1.6	-	-
51	Apigenin	20±1.5	-	-	-

In this regard, in the ^{1}D, a micro-bore ES-CN column (1.0 mm I.D.) was employed. In these conditions, no compatibility issues arose from the mobile phases used in the two dimensions, apart from the "peak focusing" effects: to solve such an issue in the ^{2}D column a gradient program starting with 100% of the weaker solvent (water) was employed.

The optimization of individual ^{2}D separation conditions is also critical for achieving RP-LC×RP-LC separations. The ^{2}D available analysis time and re-equilibration time is equal to the modulation time and this time has to be kept as short as possible in order to get the maximum number of 2D analyses per ^{1}D peak, thus requiring very fast ^{2}D analyses [43]. In this work, a 2.1 mm I.D. C18 column was employed in the ^{2}D run at 0.8 mL/min; the choice of such a I.D. was highly beneficial to allow straightforward hyphenation to ESI-MS without the need of post ^{2}D flow-splitting.

With respect to NP-LC×RP-LC separations, the coupling of two RP-LC phases provides lower resolving power, due to the apparent similarity of the separation mechanisms in both dimensions. A potential solution to overcome such a limitation could be the development of tailored ^{2}D gradient elution strategies with the aim of improving the spreading of the solutes in the ^{2}D separation space [35]. In particular, a ^{2}D shift gradient (SG) approach employing a narrower range of organic solvent (gradually increasing of ACN) was investigated.

Due to the high polarity of polyphenolic compounds, a two SG step was considered: the first segment used a gradient steepness of only 1% per modulation cycle, starting

with 100% water for the first 8 min; the second segment used a gradient steepness of 6% per modulation cycle, starting with 1% ACN and increasing to 26% ACN over last 72 min. The choice of the gradient steepness is obviously related to the chemical properties of the solutes: for compounds eluting from 8 to 80 min, a greater gradient steepness was investigated in the ^{2}D in order in order to avoid wrap-around phenomena. Figure 2 shows the RP-LC×RP-LC plots of four pistachio samples from different geographical origin, namely Bronte, Turkey, Iran, and California, whose 1D-LC profile is illustrated in Fig. 1.

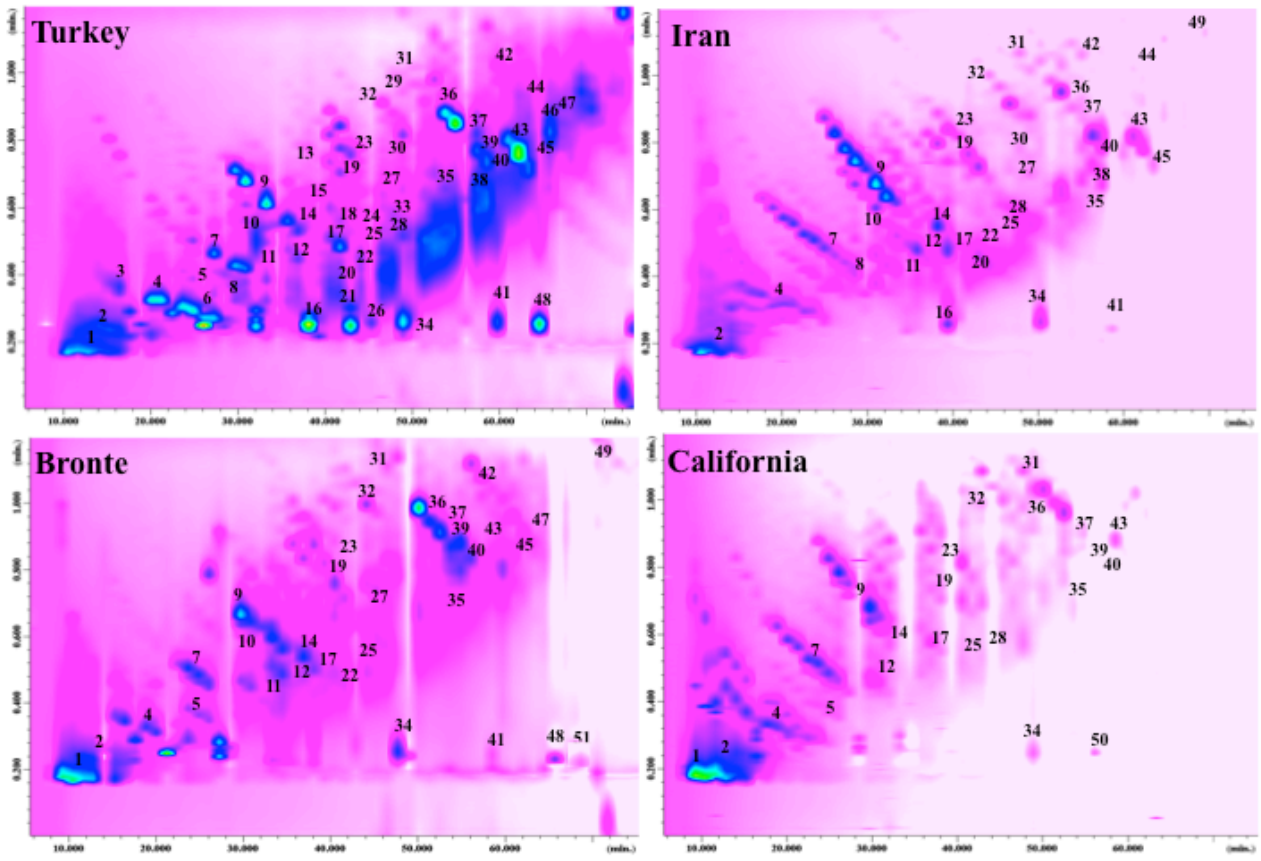

Figure 2: LC×LC-PDA chromatograms of the same samples illustrated in Fig. 1

As can be seen a great coverage of the separation space was attained, with a no typical diagonal-line distribution usually experienced when using a typical full-in-fraction approach [32, 35]. Table 3 reports some of the figures of merit

regarding the peak capacity and the orthogonality of the RP-LC×RP-LC method investigated for the four pistachio samples. Orthogonality values, calculated according to Camenzuli and Schoenmakers [44], ranged from 53 to 68% for the California and Iran pistachios, respectively. In terms of corrected peak capacity, $^{2D}n_{C,corr}$, considering both undersampling [45] and orthogonality, it can be observed how the highest values were attained for the Iran pistachio (633), whereas the lowest were observed for the Turkey one (432). These values can be considered very satisfactory despite the use of the same separation mechanisms employed in both dimensions and are similar to other previous works employing RP-LC×RP-LC set-ups, *e.g.,* 347 in ref. [37], 756 in ref. [38], and 695 in ref. [35].

Table 3. Peak capacity and orthogonality values for the RPLC×RPLC analysis of the four pistachio samples investigated.

Parameter	Bronte	Turkey	Iran	California
^{1}D peak capacity, $^{1}n_C$	64	77	91	88
^{2}D Peak capacity, $^{2}n_C$	26	23	24	23
Theoretical peak capacity, $^{2D}n_C$	1683	1750	2197	2019
Effective peak capacity, $^{2D}n_C$	820	795	932	866
Orthogonality, A_0	61%	54%	68%	53%
Corrected peak capacity, $^{2D}n_{C,corr}$	498	432	633	461

A total of 51 baseline separated polyphenolic compounds were tentatively identified by combining the information obtained with PDA and MS detection and by comparison with literature data. When possible, compound identification was confirmed by comparison with commercially available standards. Turkey pistachio turned out to be the most complex one, with up to 48 different polyphenolic compounds identified. The identified compounds in all samples investigated belonged to different chemical classes, 15 of them to phenolic acids, 4 to flavan-3-ols, 2 to isoflavones, and 30 to flavonoids. MS spectra were acquired in negative ionization mode with $[M-H]^-$ being the main ion due to the presence of hydroxyl functional groups providing the best sensitivity for all polyphenolic compounds identified.

In order to highlight the differences between the various pistachio species, a 3D data comparison has been carried out by subtracting the RP-LC×RP-LC Bronte plot against the Turkey, Iran, and California ones (Fig. 3). The resulting 3D plots can be used for data handling so that only the peaks of interest are depicted. Notably, considering that also quantitative variation is attained, peaks labeled as #32 and #51, corresponding to luteolin-4-O-glucoside and apigenin, respectively, can be considered as representative of Bronte pistachio.

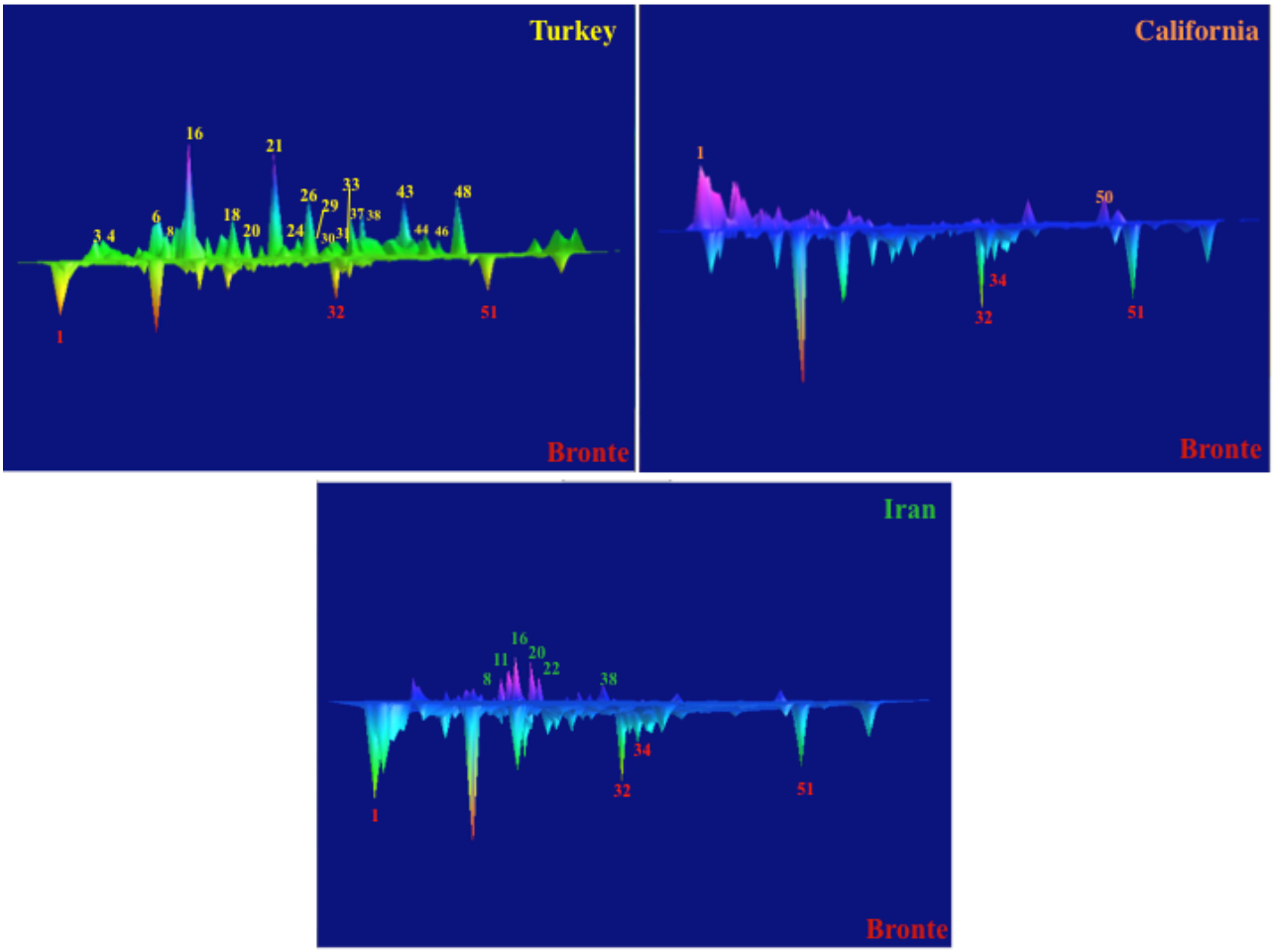

Figure 3: 3D subtraction plots of Bronte pistachio against Turkey, Iran, and California.

Luteolin hexoside was detected in Bronte pistachio with a content of 30 mg kg^{-1}; apigenin was detected only in the Bronte sample (20 mg kg^{-1}) and can be considered as a chemical marker of quality [12]. Peak #1, 1-O-galloyl β-D-glucopyranose, which

was detected in all samples with the exception of Iran, can be considered a marker of California pistachio along with luteolin diglucuronide (peak #50). One of the most abundant compounds which was detected in all samples was eriodictyol 7-glucoside (61 mg kg^{-1} in Turkey *vs.* 18 mg kg^{-1} in California, 52 mg kg^{-1} in Bronte, and 25 mg kg^{-1} in Iran). To further confirm the polyphenolic markers of Bronte pistachio, two more samples belonging to different lots were evaluated by LC-PDA/MS. As can be appreciated, the polyphenolic profile can be superimposed with little difference in the quantitative content. It is worth mentioning that to actually propose biomarkers of origin, a significantly higher amount of samples should be analyzed in order to provide the model with appropriate statistical strength [46].

4.8.3 Semi-quantification of the polyphenolic fraction of in Pistacia vera extracts by RP×RP-PDA-ESI-MS analysis

When dealing with complex food and natural real-world samples, conventional 1D-LC analysis does not often provide accurate quantification of interested analytes due co-elution issues and matrix effects. On the other hand, LC×LC, as a powerful separation technique, was considered for reliable quantification of target components. Since peaks for each analyte are distributed into several modulation cycles in the LC×LC system, single ^{2}D slides are usually summed for calculation [47, 48], making the process more complicated than 1D-LC. Therefore, in this study, a commercially available software, Chromsquare reported in the "Experimental" section, was employed allowing to easy recognize and quantify the target analytes in the contour plots. The developed RP-LC×RP-LC-PDA method was then validated to assess its quantitative reliability.

The standard curves, correlation coefficient (R_2), limits of detection (LoD) limits of quantification (LoQ), relative standard deviations (RSDs) of peak areas and accuracy values for each analyte for each analyte are displayed in Table 1. All 7-point calibration curves provided R_2 values ranging from 0.9993 to 0.9999 for all analytes, highlighting its feasibility and reliability for quantification purposes. LoQ and LoD were calculated

considering a signal-to-noise (S/N) ratio of 10 and 3, respectively. The LoQ/LoD values for the polyphenolic reference materials were extrapolated from the S/N value, observed at the lowest calibration level (0.1 ppm).

As can been observed in Table 1, sensitivity was in general satisfactory, much higher than that necessary for such an application-type. For example, LoD and LoQ values for the four of them were only 10 ppb and 30 ppb, respectively. The RSD values were lower than 0.5% showing the highly repeatability. Accuracy (A%) was determined as relative error deviation between the values observed in a spiked sample (California pistachio) (25 mg L^{-1} of each standard) and the expected values. Values below 10% were observed, except for catechin and eriodyctiol (10.5 and 11.3%, respectively).

All the figures-of-merits herein discussed are summarized in Table 1.

According to these procedures, all samples were analyzed and the calculated contents of target compounds are reported in Table 2. Among the identified compounds, 18 of them have never been reported in the pistachio kernels so far.

Notably, peak #34, eriodictyol 7-glucoside; peak #9, catechin hexoside; and peak #48, eriodictyol, turned out to be the most abundant ones in Bronte pistachios (52 mg kg^{-1}, 52 mg kg^{-1}, and 44 mg kg−1, respectively). Peak #9, catechin hexoside, was also the most abundant one in California and Iran (40 mg kg^{-1} *vs.* 51 mg kg^{-1}), whereas peak #34, eriodictyol 7-glucoside, was detected as the major polyphenolic content in Turkey one (61 mg kg^{-1}). Notably, catechin hexoside has never been reported in any of the so far investigated pistachio samples, apart from quercetin 3-glucoside [13, 16, 23, 26], eritrodyctiol [12–14, 25], and eriodictyol 7-glucoside [12–14, 18] already reported in previously published works.

In terms of bioactive content, Turkey and Bronte pistachios were the richest ones accounting for roughly 1123 mg kg^{-1} and 735 mg kg^{-1}, respectively. Considering chemical classes, these two pistachios showed the highest amount in flavonoids (595 mg kg^{-1} and 468 mg kg^{-1}), as well as in phenolic acids (436 mg kg^{-1} and 183 mg kg^{-1}) and flavan-3-ols derivates (132 mg kg^{-1} and 122 mg kg^{-1}).

4.9 Conclusion

In this contribution, a comprehensive two-dimensional liquid chromatography method was exploited for determination of the polyphenolic fraction of Pistacia vera extracts from different geographical origin. The employment of a shift gradient approach resulted in a significant increase in the separation space available, allowing to resolve several co-elution issues, thus leading to the detection of a higher number of compounds with respect the conventional one-dimensional LC analysis. A number of 51 polyphenolic compounds were tentatively identified, and, notably, 48 in the Turkish extract. The applied methodology can be advantageously applied to evaluate the health benefits associated to the consumption of pistachio kernels aiming to valorize the composition of refined ones, *i.e.*, Bronte.

References

[1] N. Goncüoğlu Taş; V. Gökmen. Curr Opin Food Sci 2017, 14, 103–109.

[2] F. Galvano; A. Pietri; B. Fallic; T. Bertuzzi; S. Scirè; M. Galvano. J. Food Protect. 1996, 59, 545–50.

[3] F. C. Lau; B. Shukitt-Hale; J. A. Joseph. Nutrition. 2006, 22, 295–302.

[4] A. Agouni; A. H. Lagrue-Lak-Hal; H.A. Mostefai; A. Tesse; P. Mulder; P. Rouet P. PLoS One. 2009, 4, e5557.

[5] G. Mazza. Ann Ist Super Sanità. 2007, 43, 369–74.

[6] D. Hou D; K. Kai; J. Li; S. Lin; N. Terahara; M. Wakamatsu M. Carcinogenesis. 2004, 25, 29-36.

[7] L. S. Wang; G. D. Stoner. GD. Cancer Lett. 2008, 269, 281–90.

[8] A. Basu; E. A. Lucas. Nutr Rev. 2007, 65, 361–75.

[9] K. J. Anderson; S. S. Teuber; A. Gobeille; P. Cremin; A. L. Waterhouse; F. M. Steinberg. J. Nutr. 2001, 131, 2837–2842.

[10] P. Velayutham; A. Babu; D. Liu. Curr. Med. Chem. 2008, 15, 1840–5180.

[11] S. Basaria; A. Wisniewski; K. Dupree. Endocrinol J. Invest. 2009, 32, 150–155.

[12] A. Tomaino; M. Martorana; T. Arcoraci; D. Monteleone; C. Giovinazzo; A. Saija A. Biochimie. 2010, 92, 1115–1122.

[13] G. Mandalari; C. Bisignano; A. Filocamo; S. Chessa; M. Sarò M; G. Torre G, Nutrition. 2013, 29, 338–344.

[14] D. Barreca; G. Laganà; U. Leuzzi; A. Smeriglio; D. Trombetta; E. Bellocco. Food Chem. 2016, 196, 493–502.

[15] I. Halil Kilic; C. Sarikurkcu; I. Didem Karagoz; M. C. Uren; M. Sefa Kocak; M. Cilkiz. RSC Adv. 2016, 6, 1203–1209.

[16] S. Erşan S; O. Gücü Ustündağ; R. Carle; R. M.Schweiggert. J. Agric Food Chem. 2016, 64, 5334–5344.

[17] M. P. Fabani; L. Luna; M. V. Baroni; M. V. Monferran; M. Ighnai; A. Tapia. J. Funct. Food 2013, 5, 1347–56.

[18] J. J. Rodríguez-Bencomo; H. Kelebek; A S. Sonmezdag; L. M. Rodríguez-Alcalá; J. Fontecha; S. Selli. J. Agric. Food Chem. 2015, 63, 7830–7839.

[19] C. Gentile; L. Tesoriere; D. Butera; M. Fazzari; M. Monastero; M. Allegra. J. Agric. Food Chem. 2007, 755, 643–648.

[20] Y. Liu; J. B. Blumberg; C. Y. Oliver Chen. J. Agric. Food Chem. 2014, 62, 1550–1556.

[21] A.S. Sonmezdag; H. Kelebek; S. Selli. J. Essent. Oil Res. 2017, 29, 262–270.

[22] F. Garavand; A. Madadlou; S. Moini. Int. J. Food Prop. 2017, 20, 19–29.

[23] S. Erşan; O. Güclü Ustündağ; R. Carle; R. M. Schweiggert. Food Chem. 2018, 253, 46–54.

[24] M. Saitta; G. L. La Torre; A. G. Potortì; G. Di Bella; G. Dugo. J. AmOil Chem. Soc. 2014, 91, 1595–603.

[25] G. Ballistreri; E. Arena; B. Fallico B. Molecules. 2009, 14, 4358–4369.

[26] S. Erşan S, O. Güclü Ustündağ; R. Carle; R. M. Schweiggert. J. Food Comp. Anal. 2017, 62, 103–114.

[27] F. Erni; R. W. Frei RW. J. Cromatogr. 1978, 149, 561–569.

[28] T. Hájek; V. Škeřiková; P. Česla; K. Výnhucalov; P. Jandera. J Sep Sci. 2008, 31, 3309–3328.

[29] L. Montero; V. Sáez; D. von Baer; A. Cifuentes; M. Herrero M. J. Chromatogr A. 2018, 1536, 205–215.

[30] F. Cacciola; P. Delmonte; K. Jaworska; P. Dugo; L. Mondello; J. I.Rader J. Chromatogr A. 2011, 15, 2012–2018.

[31] F. Cacciola; P. Donato; D. Giuffrida; G. Torre; P. Dugo; L. Mondello L. J. Chromatogr A. 2012, 1255, 244–251.

[32] G. Mazzi Leme; F. Cacciola; P. Donato; A. J. Cavalheiro; P. Dugo; L. Mondello L. Anal. Bioanal. Chem. 2014, 406, 4315–4324.

[33] P. Donato; F. Rigano; F. Cacciola; M. Schure; S. Farnetti; M. Russo; P. Dugo; L. Mondello. J Chromatogr. A. 2016, 1458, 54–62.

[34] F. Cacciola; D. Mangraviti; F. Rigano; P. Donato; P. Dugo; L. Mondello; L. H. J. Cortes 2018. Anal. Bioanal. Chem. 410, 3473–3482.

[35] Y. F. Wong; F. Cacciola; S. Fermas; S. Riga; D. James; V. Manzin; P. Dugo; L. Mondello. Electrophoresis. 2018, 39, 1993–2000.

[36] C. M. Willemse; M. A. Stander; A. G. J. Tredoux; A. de Villiers A. J. Chromatogr A. 2014, 1359, 189–201.

[37] D. Tomasini; F. Cacciola; F. Rigano; D. Sciarrone; P. Donato; M. Beccaria; P. Dugo; L. Mondello. Anal. Chem. 2014, 86, 11255–11262.

[38] E. Sommella; O. H. Ismail; F. Pagano; G. Pepe; C. Ostacolo; G. Mazzoccanti G, et al. J. Sep. Sci. 2017, 40, 2188–2197.

[39] E. Sommella; F. Pagano; E. Salviati; M. Chieppa; A. Bertamino; M. Manfra et al. J. Sep. Sci. 2018, 41, 1548–1557.

[40] G. Mandalari; A. Tomaino; T. Arcoraci; M. Martorana; V. Lo Turco; F. Cacciola et al. J. Food Comp. Anal. 2010, 23, 166–174.

[41] M. Fanzone; F. Zamora; V. Jofrè; M. Assof; A. Pena-Neira. J. Agric. Food Chem. 2011, 59, 6120–6136.

[42] R. Perestrelo; Y. Lu; S. A. O. Santos; A. J. D. Silvestre; C. P. Neto; J. S. Camara et al. Food Chem. 2012, 135, 94–104.

[43] R. E. Murphy; M. R. Schure; J. P. Foley. Anal. Chem. 1998, 70, 1585–1594.

[44] M. Camenzuli; P. J. Schoenmakers. Anal. Chim. Acta. 2014, 838, 93–101.

[45] X. Li; D. R. Stoll; P. W. Carr. Anal. Chem. 2009, 81, 845–850.

[46] F. Rigano; S. Stead; D. Mangraviti; R. Jandova; D. Petit; N. Marino et al. Food Anal. Meth. 2018.

[47] V. Elsner; V. Wulf; M. Wirtz; O. J. Schmitz. Anal. Bioanal. Chem. 2015, 407, 279–284.

[48] M. Kivilompolo; T. Hyotylainen. J. Chromatogr A. 2007, 1145, 155-164.

5.0 Quantitative analysis of aqueous phases of bio-oils resulting from pyrolysis of different biomasses by two-dimensional comprehensive liquid chromatography

Agrifood by-products are perfect candidates to be further processed under the concept of circular economy, in order to produce their valorization. Although significant amounts of food-related wastes that are discarded are produced worldwide, these might still be rich in valuable compounds. A strategy to further valorize agrifood-related by-products is based on pyrolysis processes. The result of this process is a liquid product termed bio-oil which is composed of an organic phase and an aqueous phase. This bio-oil is rich on a variety of components and its analysis implies several challenges. In this work, quantitative on-line comprehensive two-dimensional liquid chromatography (LC × LC) is proposed for the first time to characterize several aqueous phases of different bio-oils. Rice husk, peanut shell, spent coffee grounds, peach core and Eucalyptus sawdust biomasses were analyzed. The developed quantitative LC × LC method presented very good linearity, precision, reproducibility, recovery and LODs and LOQs as low as 0.05 g mL^{-1} and 0.16 g mL^{-1}, respectively. As much as 28 components were simultaneously separated and quantified in those samples. Our results found that the composition of these bio-oils was different but strongly related to the agrifood by-product submitted to pyrolysis. The developed methodology is foreseen as a valuable tool for the quantitative study of other bio-oils, considering the great complexity and high dimensionality of these samples

5.1 Introduction

Due to the increasing awareness on environmental protection, different strategies are constantly being developed in the frame of circular economy able to be implemented in biorefinery approaches. Agrifood by-products are perfect candidates to be further

processed following strategies directed to produce their valorization. Significant amounts of wastes related to foods and crops production and processing are generated worldwide. However, these by-products are often still rich in valuable compounds that could be re-utilized. The selective extraction of high value compounds is a feasible alternative, even more interesting when advanced green extraction techniques are employed [1]. However, other processes can be designed in order to avoid the generation of wastes and their contribution to environmental pollution. Pyrolysis is an example of this latter kind of processes. Pyrolysis is based on the application of high temperatures, typically around 500 °C in the absence of oxygen to produce the thermal decomposition of a particular biomass. In principle, any biomass composed of cellulose, hemicellulose and lignin is a good raw material for pyrolysis. Thus, agrifood wastes coming from vegetables may be used in this regard. As a result of pyrolysis, a liquid product termed bio-oil is produced. Bio-oils have been pointed out as starting materials for the production of biofuels as well as for high-added value chemicals. Deeper insight on the production of bio-oils by pyrolysis may be gained through different interesting review papers published elsewhere [2]. In general, the chemical composition of bio-oils is rather complex and it is composed by an organic phase (low-polarity components) and by an aqueous phase (highpolarity compounds). Components belonging to different chemical families, including hydrocarbons, esters, ethers, ketones, acids,aldehydes, phenols or sugars, among others may be present.

As the use and application of a bio-oil will strongly depend on its particular chemical composition, which in turn depends on the composition of the initial biomass, the chemical characterization of bio-oils is an essential step. Gas chromatography coupled to mass spectrometry (GC-MS) and, most notably, comprehensive two-dimensional gas chromatography (GC × GC), have been widely used as analytical tools to characterize the organic phase of different bio-oils [3–8]. However, the analysis of the aqueous phase using GC-based techniques is more challenging since a previous extraction step (usually performed with dichloromethane), is necessary due to the unsuitability of water samples in GC. This step can greatly affect the qualitative and

quantitative composition of the samples, due to the different solvent affinity for each chemical class present. In this context, liquid chromatography-based techniques allow the direct analysis of the aqueous phase without any further extraction step [9]. Thus, it is expected that LC is complementary to GC for the whole comprehensive chemical characterization of bio-oils, since compounds with low volatility, high polarities and poor thermal stabilities are found in this sample [10]. In this regard, comprehensive two-dimensional liquid chromatography (LC × LC) could be a useful tool in order to characterize the typical complex profiles of aqueous phase from bio-oil. Online LC × LC represents the most advanced two-dimensional liquid chromatography (2DLC) mode. It allows the combination of different separation mechanisms in each dimension through which the sample is analyzed. Typically, the sample is injected into the first dimension (^{1}D) where an initial separation is produced. Simultaneously, discrete fractions from the ^{1}D effluent are continuously collected and transferred to the second dimension (^{2}D) with the aid of a modulator or interface. The most-commonly used interface is based on the use of, at least, a switching valve equipped with two sampling loops with identical inner volume that change function upon valve actuation. Using this set-up, a fraction is collected in one of the sampling loops whereas the previous fraction is being injected using the other loop. This continuous procedure implies that slow separations are needed in the ^{1}D in order to produce effluent fractions at a relatively slow rate to allow enough time foreach subsequent fast ^{2}D separation.

By using on-line LC × LC, the separation potential and peak capacity are substantially improved compared to conventional one-dimensional separations. For this reason, comprehensive LC has already been demonstrated to be useful for the characterization very complex food and agrifood-related samples [11,12], although the separation of bio-oils has only scarcely been explored, being limited to tree-related bio-oils [10]. Most of the developed approaches based on the use of on-line LC × LC in this field are focused on qualitative analyses. In fact, there are just few papers dealing with the quantification of, at least, part of the separated compounds [13–18]. Still, it is widely

accepted that further developments are necessary to demonstrate the quantitative capabilities of LC × LC [11], even more if routine analysis is targeted.

Considering the analytical challenges related to the study of the aqueous phase of bio-oils derived from pyrolysis, the aim of the present work was to optimize a new quantitative LC × LC method for the separation and identification of compounds present on different bio-oils produced from important agrifood by-products, including rice husk, spent coffee grounds, peanut shell, peach core and Eucalyptus sawdust.

5.2 Materials and methods

5.2.1 Reagents and standards

All the solvents employed (acetonitrile, ethanol, methanol) were of HPLC-grade and acquired from VWR Chemicals (Barcelona, Spain). Ultrapure water was obtained from a Milli-Q apparatus (Millipore system, Billerica, MA, USA) and used for the preparation of all solutions and mobile phases. Reference standards used were at least 98% of purity and were purchased from Sigma–Aldrich (Saint. Louis, MO, USA). A stock solution (1000 mg L−1) was prepared in water containing 21 reference standards: 3 ketones (3-methyl-1,2-cyclopentanedione, 4-hydroxyacetophenone,4-hydroxy-3-ethoxyacetophenone), 2 alcohols (homovanillylalcohol, 3-p-hydroxyphenylpropanol), 9 phenols (1,2-benzenediol,phenol, 4-methyl-1,2-benzenediol, 2-methoxyphenol (guaiacol), 4-methylphenol, 2,6-dimethoxyphenol, 4-ethylphenol,3,4-dimethylphenol, 2-acetyl-resorcinol), 6 aldehydes (5-hydroxymethyl furfural, furfural, 4-hydroxybenzaldehyde, 5-methylfurfural, vanillin, syringaldehyde) and an alkaloid (caffeine). The stock solutions were stored at 5°C.

5.2.2 Biomass samples

Five biomass samples, which are agro-industrial wastes generated in large amounts per year in Brazil were investigated in this study. Rice husk was provided by Adib Peixoto Ltda (Pelotas, Brazil),peach core was supplied by Scharann Food Industry (Pelotas,Brazil), Eucalyptus sawdust was acquired from CMPC Cellulose Industry (Guaíba, Brazil), whereas peanut shell and spent coffee grounds were both obtained from a local market in Porto Alegre, Brazil. All samples were milled to particle sizes between 40–60 mesh and dried in an oven at 105◦C, until constant weight, before bio-oil production.

5.2.3 Bio-oils production

Intermediate pyrolysis of biomass samples was performed in a homemade vertical furnace containing a tubular fixed-bed reactor of quartz glass. A schematic diagram of the pyrolysis system is illustrated in Figure 1 and described elsewhere in detail [3]. The pyrolysis conditions were based on previous studies [4,19] and were as follows: 6.5 g of biomass (particle size 40–60 mesh) were used as starting material. N_2 flow of 100 mL min^{-1}, and a heating rate of 100°C min^{-1} up to a pyrolysis final temperature of 650°C were established. The system was then maintained for 10 min at the final temperature till no more vapors were formed. The condensable products were cooled through a condenser using ethylene glycol and water (1:1) at −10°C. The crude bio-oil produced (liquid product) from the pyrolysis of the different biomasses consisted of two immiscible phases: aqueous and organic phases. The phase separation was produced by decantation and the aqueous phase was collected without any further extraction or pretreatment. Aqueous phase samples were diluted in water, using a factor dilution of 1:30 *v/v* and 1:40 *v/v* according to the compounds concentration in the samples, and filtered through a 0.20 μm Chromafil PTFE membrane filter before qualitative and quantitative analysis by LC × LC/DAD-MS.

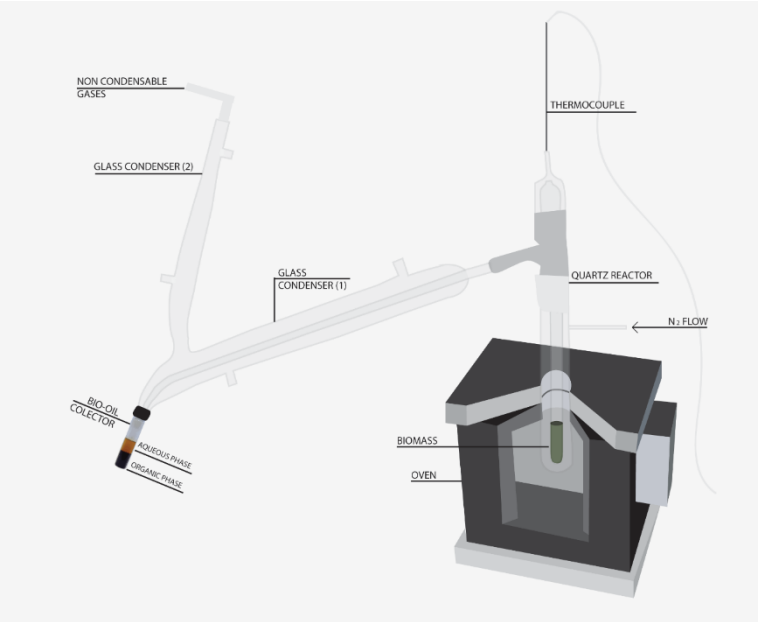

Figure 1. Scheme of the reactor employed for the pyrolysis processes.

5.3 LC × LC instrumentation

The first dimension (^{1}D) was operated using an Agilent 1200 series liquid chromatograph (Agilent Technologies, Waldbronn, Germany) equipped with an autosampler and a diode array detector (DAD) which was connected at the exit of the second dimension. The second dimension (^{2}D) was carried out using an additional LC pump (Agilent 1290 Infinity). An electronically-controlled 2-position 10-port switching valve (Rheodyne, Rohnert Park, CA, USA) was used to connect both dimensions. The interface between dimensions was based on two sampling loops of identical inner volume (30 μL). Separations were recorded at 280 nm although, in addition, UV–vis spectra were collected from 200 to 400 nm at a sampling rate of 20 Hz in the DAD. The wavelength (280 nm) chosen is suitable for the chemical families of compounds under investigation and has previously been used for analysis of aqueous phase samples by LC [5,9]. An Agilent 6320 ion trap mass spectrometer (Agilent Technologies, Waldbronn, Germany) was used for the identification of the separated compounds interfaced by an ESI ion source. The flow eluting from second dimension

was splitted via a T-piece in order to allow the introduction of a flow of ca. 600 µL min^{-1} in the MS. The instrument was operated under negative and positive ESI modes using the following conditions: mass spectra recorded from m/z50 to 200, according to the molecular weight of the compounds expected to be present in the bio-oils aqueous phase samples; capillary voltage: −3500 V; corona discharge: +4000 *n*A (positive)/-10000 *n*A (negative); nebulizer pressure, 60 psi; dry gas, 5 L min^{-1},and; dry temperature, 350°C; vaporizer temperature, 400°C. The ion trap mass analyzer was controlled by the 6300 series trap control software (Bruker Daltonik GmbH, V. 6.2).

5.3.1 LC × LC separation conditions

After optimization of each dimension, the final selected separation method was based on the coupling of two RP separations, using the following conditions:

^{1}D separation: a X-Bridge amide (150 × 2.1 mm, 3.5 µm d.p.,141˚A, Waters, Milford, MA, USA) column was employed in the ^{1}D, eluted using acidified water (0.1% formic acid, *v/v*, A) and acetonitrile (0.1% formic acid, *v/v*, B). Under optimum conditions, the linear gradient employed was: 0 min, 2% B; 3 min, 10% B; 50 min, 60% B;61 min, 100% B. The flow rate was set at 25 µL min^{-1}, the column temperature at 30°C and the injection volume was 10 µL.

^{2}D separation: a short partially-porous column (Poroshell EC-C18 30 × 4.6 mm, 2.7 µm, Agilent, Santa Clara, CA, USA) was selected. Gradient, flow rate, temperature, type of acid and sol-vents used were optimized separately. The optimum conditions were achieved using acidified water (0.1% formic acid, solvent A) and acetonitrile (0.1% formic acid, solvent B) as mobile phases. The optimum linear gradient was as follow: 0 min, 10% B; 0.85 min, 90% B; 0.86 min, 100% B; 0.9 min, 100% B; 0.91 min, 10% B and re-equilibrium at starting conditions until 1 min. The flow rate was set at 2.5 mL min^{-1}. Once these parameters were optimized, the coupling between both dimensions was achieved employing 1 min repetitive second dimension separations;

thus, the modulation time was 1 min. Other columns tested in both dimensions are described in Table 1.

Table 1. Columns tested for the ^{1}D and ^{2}D separations.

	Stationary phase	Dimensions	Particle size	Pore (Å)	Commercial brand
^{1}D Separations	Cyano	150 × 1.0 mm	3 μm	175 Å	Thermo Fisher Scientific (Waltham, MA, USA)
	PEG	150 × 2.1 mm	5 μm	120 Å	Supelco (Bellefonte, PA, USA)
	Amino	150 × 1.0 mm	3 μm	175 Å	Thermo Fisher Scientific (Waltham, MA, USA)
	ZIC-HILIC	150 × 1.0 mm	3.5 μm	100 Å	Merck (Darmstadt, Germany)
	Diol	150 × 1.0 mm	5 μm	100 Å	Hichrom (Markham Centre, RG, UK)
	Amide	150 × 1.0 mm	3.5 μm	141 Å	Waters Corporation (Milford, MA, USA)
^{2}D Separations	C18	50 × 4.6 mm	2.7 μm	90 Å	Supelco (Bellefonte, PA, USA
	PFP	50 × 4.6 mm	2.6 μm	100 Å	Phenomenex (Torrance, CA, USA)
	C18	30 × 4.6 mm	2.7 μm	120 Å	Agilent Technologies (Santa Clara, CA, USA)

5.4 Validation of the quantitative method

For the first time, an accurate quantitative analysis method using LC × LC has been developed and implemented on the analysis of the aqueous phase from bio-oils. Evaluation of method´s performance was accomplished through the assessment of the main figures of merit, namely: linearity, dynamic range, determination coefficients (R_2), limit of detection (LOD), limit of quantification (LOQ), precision (intra and inter-day precision) and recovery. The validation protocol followed the guidelines established by ANVISA [20].

Calibration curves were constructed by the triplicate injection of eight different concentration levels of a standards mixture. Linearity was estimated in the concentration range between 1–250 mg L^{-1} according the values of determination coefficients (R_2). LODs and LOQs were obtained based on the calibration curve parameters, being the standard deviation of the response at the lowest level of the

intercept of the corresponding calibration curve divided by the average slope multiplied by a factor of 3 and 10, respectively. Precision was evaluated by intra and inter-day precision. Intra-day precision was expressed as the relative standard deviation (% RSD) of peak volumes obtained for a 50 mg L^{-1} standard solution (intermediate level) injected three times on the same day, while inter-day precision was calculated by repeating those injections on three consecutive days (n = 9). System accuracy was evaluated by a spike recovery method, in which the aqueous phase from rice husk bio-oil was diluted by a factor 1:100 and quantified. Later on, this sample was spiked with a standard solution containing all the studied components at a final concentration of 100 mg $L^{-1}$and analyzed in triplicate. Recoveries (%) for each compound were calculated using these quantitative data.

5.5 Other calculations

5.5.1 Peak capacity

Individual peak capacity for each dimension was calculated according to Eq. 1:

$$n_c = 1 + \frac{t_G}{\bar{w}} \quad \textbf{(1)}$$

where t_G is the gradient time and $\bar{w}$ is the average peak width (4σ). For ^{1}D individual ^{1}D and ^{2}D peak capacity calculations, the average peak width was obtained from all the quantified peaks. For each two-dimensional set-up, different peak capacity values were estimated, starting from the, theoretical peak capacity (^{2D}nc). This value was calculated following the so-called product rule, using Eq. 2:

$$^{2D}\mathrm{nc} = {}^1n_c \times {}^2n_c \quad \textbf{(2)}$$

As eq. 2 does not take into consideration the deleterious effects due to the modulation process as well as possible ^{1}D under sampling, a more realistic peak capacity value was obtained from the equation proposed by Li et al. [21], denominated effective peak capacity (Eq. 3):

$$^{2D}n_{c,practical} = \frac{^{1}n_c \times {}^{2}n_c}{\sqrt{1 + 3.35 \times \left(\frac{^{2}t_c \ {}^{1}n_c}{^{1}t_g}\right)^2}} \quad \textbf{(3)}$$

Being ^{2}tc, the ^{2}D separation cycle time, which is equal to the modulation time. This latter equation includes the <β> parameter accounting for under sampling. Moreover, to more precisely com-pare among set-ups and in order to evaluate possible peak clusters along the 2D analysis and, thus, to estimate 2D space coverage, the orthogonality degree (A_0) was considered to offer the denominated 2D corrected peak capacity, as follows:

$$^{2D}n_{c,effective} = {}^{2D}n_{c,practical} \times A_0 \quad \textbf{(4)}$$

5.5.2 Orthogonality

System orthogonality (A_0) for each sample was calculated according to the method proposed by Camenzuli and Schoenmakers [22], taking into account the spread of each peak along the four imaginary lines that cross the 2D space forming an asterisk, that is Z_1, Z_2(vertical and horizontal lines) and Z_-, Z_+ (diagonal lines of the asterisk). Z parameters describe the use of the separation space with respect to the corresponding Z line, allowing to semi-quantitatively diagnose areas of the separation space where sample components are clustered, thus, reducing in practice orthogonality. For the determination of each Z parameter, the S_{Zx} value was calculated, as the measure of

spreading around the Z_x line, using the retention times of all the separated peaks in each 2D analysis

5.6 Results and discussion

5.6.1 LC × LC method optimization

Considering the aim of the present research directed towards the quantification of interesting compounds in different aqueous phases of bio-oils from several biomasses, the optimization of a LC × LC methodology able to provide with good separation capabilities is the first critical step. The first approach consisted on the screening of several stationary phases under both HILIC and RP conditions to test the potential for the ^{1}D separation. Aqueous phase of rice husk bio-oil was selected as a model matrix to perform these experiments. Among the stationary phases studied, cyano, PEG, amino, ZIC-HILIC, diol and amide particles were included in combination with typical mobile phases. Table S1 summarizes the physical characteristics of the compared columns. In any case, HILIC conditions did not produce any appropriate distribution of the sample components, whereas RP conditions were demonstrated to be more suitable for some columns. Combining the information from this screening and keeping in mind the possible differential selectivity with the ^{2}D, PEG and amide columns were selected as the most promising for the ^{1}D. Figure 2 shows RP separations attainable using these columns. As it can be observed, comparable results were obtained, although the amide column provided slightly more evenly separated peaks and, thus, it was selected for further optimization. Once the column for the ^{1}D was selected, the separation conditions were re-optimized, adjusting a slower flow rate. In view of the column dimensions, 25 μL min^{-1} was considered the target flow rate in order to produce discrete fractions for the ^{2}D separations.

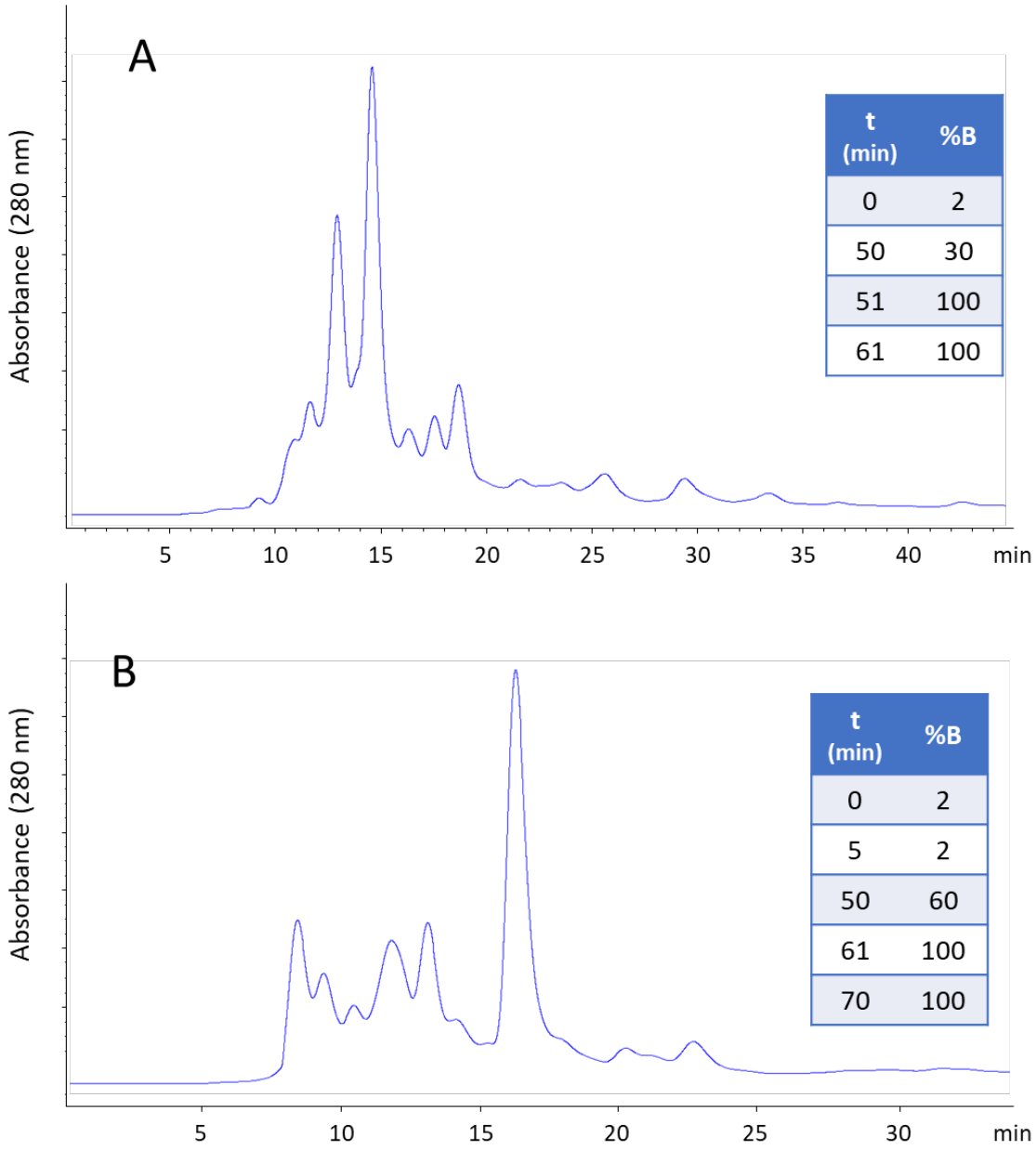

Figure 2. Chromatograms (280 nm) obtained for the separation obtained by reversed phase using PEG (A) and amide (B) columns of the aqueous phase of rice husk bio-oil. Flow rate 50 µL min^{-1}. Tables give indication of the gradient profiles employed using water (0,1% formic acid, solvent A) and acetonitrile (0,1% formic acid, solvent B) as mobile phases.

Keeping this flow rate constant, the gradient was adapted to provide wide peaks that could be appropriately sampled to the ^{2}D. Figure 3 shows the separations obtained for the 5 bio-oils studied in the present work under the ^{1}D optimum conditions selected. These conditions involved the use of an amide column in combi-nation with water (0.1% formic acid) and acetonitrile (0.1% formic acid) as mobile phases eluting under

RP conditions. For the ^{2}D optimization, rice husk bio-oil was directly injected in the candidate columns. In this case, a RP separation mode was straightforwardly selected, because RP has been repeatedly shown as the most appropriate separation mechanism to provide fast (<2 min) and efficient separations with short column re-equilibration times [3].

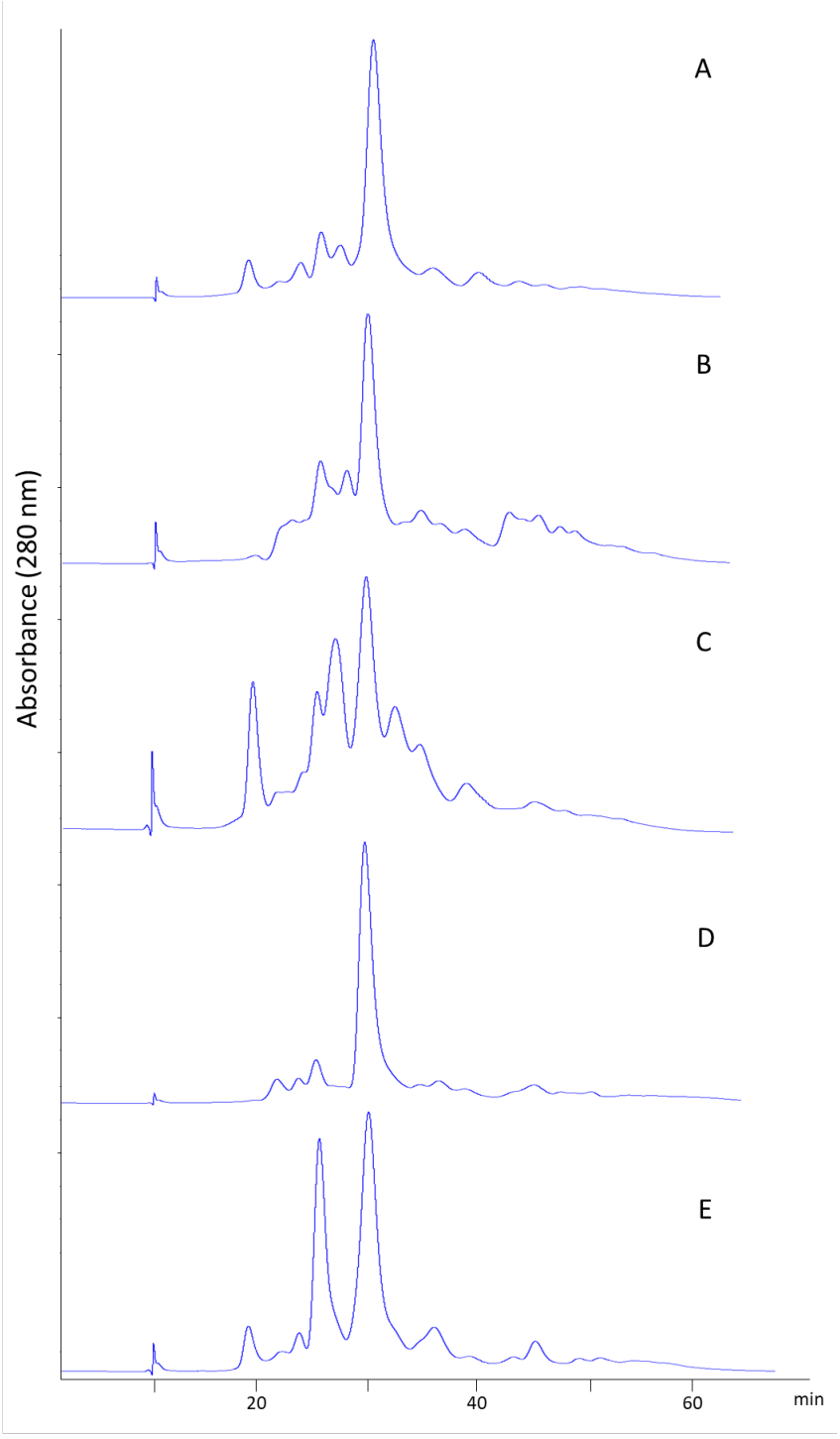

Figure 3. Chromatograms (280 nm) obtained by reversed phase using the amide column under the optimized conditions for the ^{1}D for the separation of aqueous phases of bio-oils produced from rice

husks (A), peanut shell (B), spent coffee grounds (C), peach core (D) and Eucalyptus sawdust (E). Flow rate 25 μL min^{-1}. Elution using water (0,1% formic acid, solvent A) and acetonitrile (0,1% formic acid, solvent B) as mobile phases, following the gradient program: 0min, 2% B; 3 min, 10% B; 50 min, 60% B; 61 min, 100% B; 76 min, 100% B.

These characteristics are strongly appreciated for ^{2}D separations in LC × LC. In order to seek for a different selectivity compared to the ^{1}D, C18 (30 and 50 mm × 4.6 mm,2.7 μm) and PFP (50 × 4.6 mm, 2.7 μm) short partially porous columns were tested in the ^{2}D, establishing a target total time cycle of 1 min. This time would be the allotted time for each modulation and, thus, it should include the gradient and separation as well as the column re-equilibration. The optimization was performed trying to maintain a flow rate as low as possible to minimize sample dilution. In this sense, 2.5 mL min^{-1} was the lowest possible flow rate that allowed proper separation and column reconditioning in 1 min. Figure 4 shows a comparison among the three tested columns under identical separation conditions (optimized gradient and flow rate). As it can be observed, albeit good separation of the sample components was possible using both stationary phases, C18 columns provided better peak shapes. Moreover, using the shorter alternative (Fig. 4C), faster separations and more resolved peaks were attained. Thus, the 30 mm long column was selected for further LC × LC analyses. Subsequently, all the studied samples were analyzed using the previously optimized conditions without previous ^{1}D separation, confirming the potential of those experimental conditions to be used in the ^{2}D (see Figure 5).

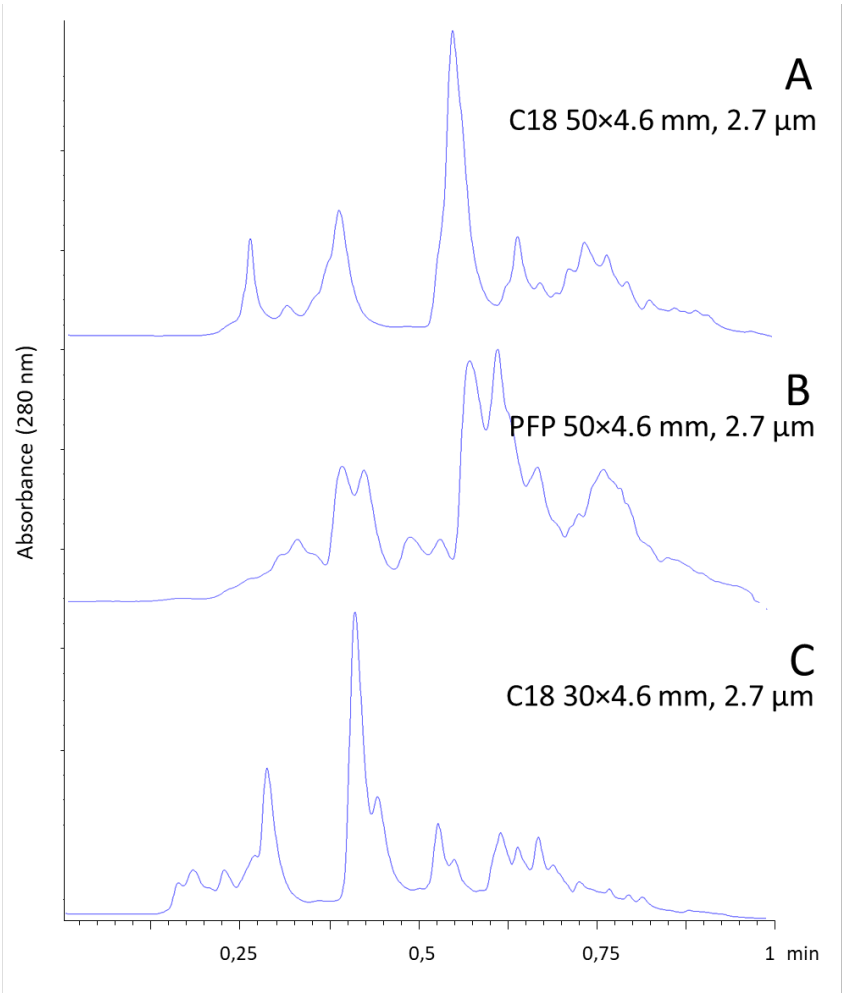

Figure 4. Chromatograms (280 nm) obtained for the separation obtained by reversed phase using the indicated partially-porous columns of the aqueous phase of rice husk bio-oil. Flow rate 2.5 mL min^{-1}. Elution using water (0,1% formic acid, solvent A) and acetonitrile (0,1% formic acid, solvent B) as mobile phases, with the following gradient: 0min, 10% B; 0.85 min, 90% B; 0.86 min, 100% B; 0.9 min, 100% B; 0.91 min, 10% B.

After individual optimization, the selected conditions were implemented in the new RPLC × RPLC method, setting 1 min as the modulation time. Two-dimensional plots (280 nm) of the five bio-oils analyzed (aqueous phase) using this method are shown in Figure 6. All the samples were characterized by the presence of a good number of components, which were distributed in the available separation space. Table 2 summarizes some of the figures of merit of the qualitative method for each sample studied. As it can be observed, orthogonality degree ranged from 33% corresponding to spent coffee grounds to 50% for peanut shell and Eucalyptus sawdust. These orthogonality calculations are based on the use of the 2D plane as it is occupied by sample components [22].

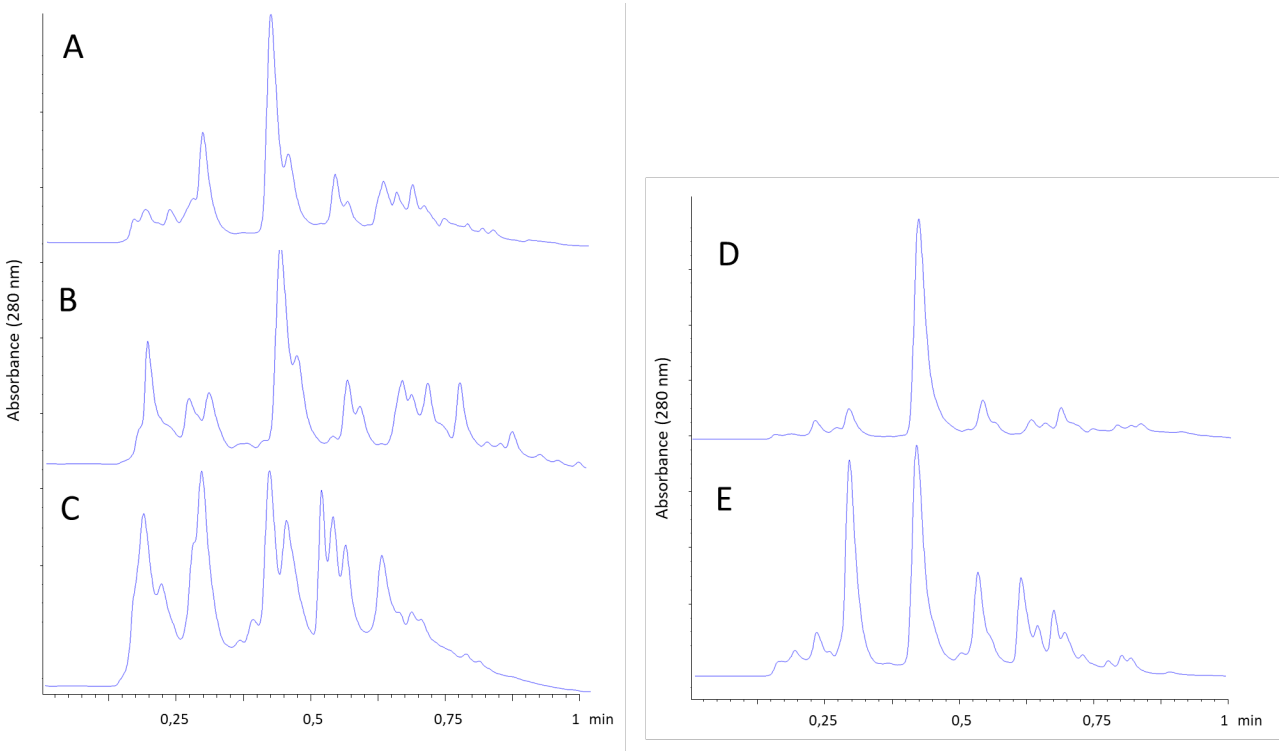

Figure 5. Chromatograms (280 nm) obtained by reversed phase using the 30×4.6 mm, 2.7 µm partially porous column under the optimized conditions for the ^{2}D for the separation of aqueous phases of bio-oils produced from rice husks (A), peanut shell (B), spent coffee grounds (C), peach core (D) and Eucalyptus sawdust (E). Flow rate 2.5 mL min^{-1}. Elution using water (0,1% formic acid, solvent A) and acetonitrile (0,1% formic acid, solvent B) as mobile phases, with the following gradient: 0min, 10% B; 0.85 min, 90% B; 0.86 min, 100% B; 0.9 min, 100% B; 0.91 min, 10% B.

Consequently, these values may be judged as good in spite of the use of the same separation mechanism in the two dimensions. This trend also corresponded to the corrected peak capacity reached, which considers the orthogonality to adapt $^{2D}n_c$ to provide more realistic figures. In any case, the obtained values were high, reaching peak capacities higher than 500 for Eucalyptus sawdust bio-oil, demonstrating the good separation capabilities of the developed method.

5.7 Development and validation of the quantitative method

Using the optimized LC × LC method, a wide group of 21 standard compounds that had been identified in other bio-oils were injected and analyzed. Ketones, alcohols, phenols, aldehydes and an alkaloid were included. As shown in Fig. 6F, the separation obtained for this group of components was very good. Calibration curves for each com-

pound were obtained by the triplicate injection and LC × LC analysis of eight different concentration levels after measuring their corresponding peak volume (Table 2). Determination coefficients (R^2) higher than 0.98 were obtained for all the tested compounds. Moreover, LODs obtained ranged from 0.05 μg mL^{-1} for caffeine and 2.08 μg mL^{-1} for phenol, whereas, LOQs values were lower than 6.29 μg mL^{-1}.

Besides, instrumental intraday and interday precision was assessed. For this purpose, a mixture (50 μg mL^{-1} each) of the 21 quantified components was consecutively injected three times in the same day (n = 3) and also in three consecutive days (n = 9). RSD values obtained were in the range between 0.30 and 9.14% for peak volumes in the same day. Interday RSD values ranged between 0.30 and 14.56% for peak volumes although were below 10% for 18 out of 21 quantified compounds. Accuracy was also estimated through analyte recovery (Table 3). Most of the standard compounds showed excellent accuracy (recovery range 90%–115%), except furfural and 2.6-dimethoxyphenol which show recovery of 85.2% and 88.5%, respectively. Since accuracy assays were performed using real samples, possible overlooked matrix effect-related issues were avoided. Regarding to the RSD% for accuracy data, all compounds analyzed showed values lower than 15%.Taken together, these values demonstrate the good capabilities of the quantitative LC × LC method developed, even more considering the analytical challenges commonly associated to this methodology such as: low response and low sensitivity, low reproducibility in the ^{1}D due to different cuts and, difficulties in the accurate determination of peak volumes [13,16,23].

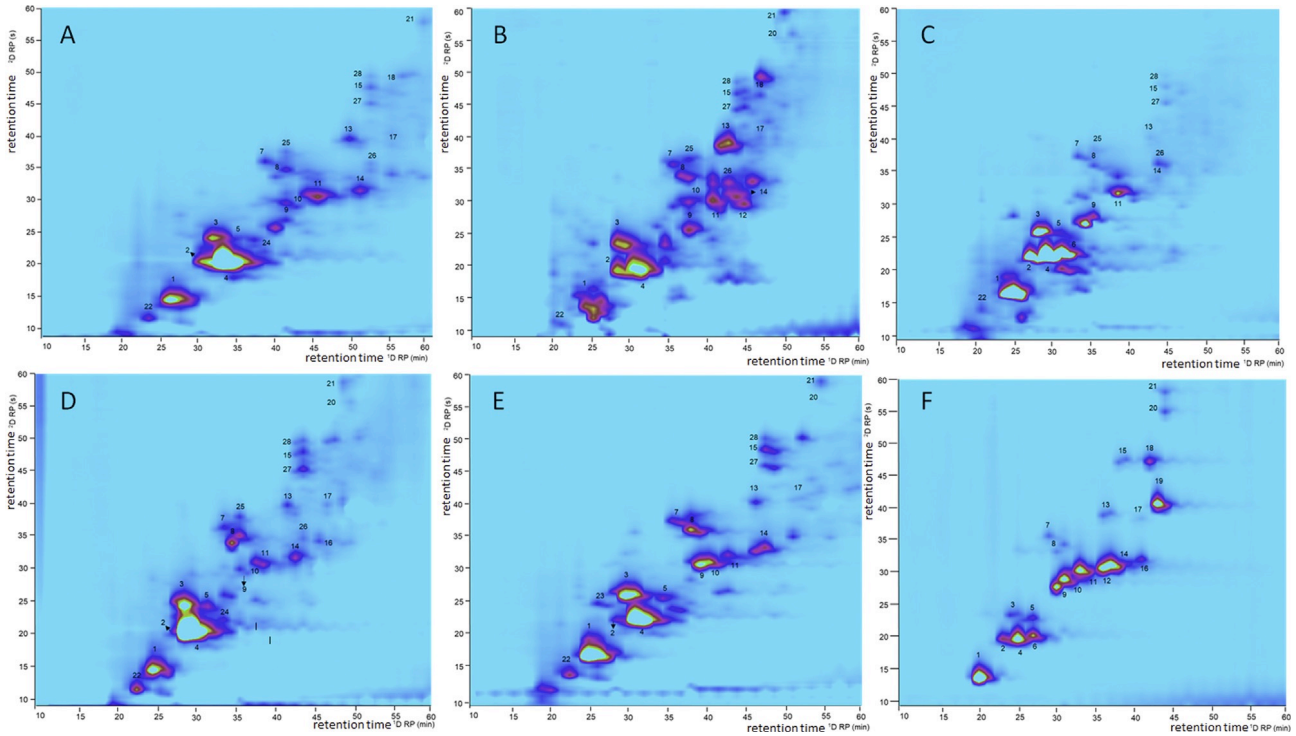

Figure 6. 2D contour plots (280 nm) obtained using the optimized LC × LC methodology for the analysis of the different bio-oil aqueous phases produced by pyrolysis from:rice husk (A), peanut shell (B), spent coffee grounds (C), peach core (D) and Eucalyptus sawdust (E). Panel F shows the separation obtained for the mixture of commercialstandards analyzed (50 µg mL^{-1} each). For peak identification see Table 4.

Table 2. Peak capacity and orthogonality values calculated for the RPLC×RPLC analysis of the five bio-oils studied.

Parameter	Rice husk	Peanut shell	Spent coffee grounds	Peach core	*Eucalyptus* sawdust
^{1}D peak capacity, $^{1}n_c$	33	37	32	37	36
^{2}D Peak capacity, $^{2}n_c$	35	43	38	40	48
Theoretical peak capacity, $^{2D}n_c$	1155	1591	1216	1480	1728
Effective peak capacity, $^{2D}n'_c$	675	924	735	858	1013
Orthogonality, A_0	47%	50%	33%	44%	50%
Corrected peak capacity, $^{2D}n_{c,corr}$	318	461	244	374	505

A_O, orthogonality; $^{2D}n_c = {}^{1}n_c \times {}^{2}n_c$; $^{2D}n'_c$: calculated according to [16]; $^{2D}n_{c\ corr.}$: $^{2D}n'_c \times A_O$;

5.8 Analysis of bio-oils

The already validated LC × LC quantitative method was applied to the characterization of aqueous phase samples from 5 different bio-oils produced by pyrolysis from diverse agrifood by-products, namely, rice husk, peanut shell, spent coffee grounds, peach core and Eucalyptus sawdust. The potential of the utilization of these biomasses to obtain bio-oils, has been already studied in the literature. Many reports have shown the characterization of the organic phase of similar bio-oils, especially using GC × GC [3,5,8,24], identifying high-value compounds in the samples. In this line, LC × LC can be a good choice that can be considered complementary to GC × GC to obtain a comprehensive characterization of these bio-oils, focused on the aqueous phases. However, the use of on-line LC × LC to this aim has been only scarcely explored [10]. Each sample was analyzed by LC × LC in triplicate and examined thanks to the use of DAD and MS detectors connected in series. This way, some tentative identifications for the separated compounds could be obtained, in addition to those for which

commercial standards were available. Table 4 summarizes the information collected from the quantification of all the assigned peaks. Twenty-eight compounds, including the major compounds, were identified and quantified in the aqueous phase samples. Twenty-one were positively identified by authentic standard injections, whereas seven were tentatively identified based on their UV and mass spectra. For the quantitative analysis, the concentration of analytes identified in the samples for which authentic standards were not available was estimated using the closest commercial standard from a chemical structure point of view. It was important to achieve good quantification of the most important compounds in the sample in order to define the potential use of the bio-oil. In a previous study [5], the quantification of aqueous phase from rice husk bio-oil using HPLC-DAD was reported; however, in that application, by means of conventional one-dimensional LC just 10 compounds could be identified and quantified, due to the great sample complexity.

As demonstrated in the present contribution, LC × LC is able to offer enhanced analytical performance for the analysis aqueous phase samples from bio-oils, in terms of resolving power, sensitivity and selectivity. LC × LC analyses evidenced the presence of polar compounds in bio-oils aqueous phases in high concentration. As a matter off act, if GC techniques were used for the analysis of these samples, as commonly occurs, the most polar compounds would have not been totally removed.

Table 3. Calibration data for the quantification of interesting compounds in the studied bio-oils using the new RPLC×RPLC method developed.

ID	Compound	Rt ^{1}D (min)	Rt ^{2}D (s)	Concentration range tested (µg/mL)	Slope (n = 8)	Intercept (n =8)	R^2
1	5-(hydroxymethyl)furfural	24	16.40	1-250	879.84	558.4	1.0000
2	3-methyl-1,2-cyclopentanedione	28	21.50	5-150	85.885	359.99	0.9816
3	1,2-benzenediol	29	25.95	5-250	99.393	56.289	0.9985
4	furfural	30	21.90	1-250	916.53	4618.3	0.9937
5	homovanillyl alcohol	33	25.15	1-150	136.73	311.46	0.9957
6	caffeine	33	22.60	1-150	169.34	223.3	0.9976
7	phenol	33	36.85	25-250	53.425	128.14	0.9972
8	4-methyl-1,2-benzenediol	35	37.95	1-150	85.07	463.38	0.9909
9	3-p-hydroxyphenyl propanol	38	30.35	1-150	271.96	680.22	0.9989
10	4-hydroxybenzaldehyde	37	30.75	1-150	495.49	441.18	0.9936
11	5-methylfurfural	40	31.75	1-150	607.44	1147.4	0.9957
12	4-hydroxyacetophenone	43	32.85	1-150	516.58	41.262	0.9990
13	2-methoxyphenol (guaiacol)	43	40.55	1-150	71.189	89.862	0.9996
14	vanillin	43	33.00	1-150	696.8	2129.4	0.9972
15	4-methylphenol	45	48.15	1-150	64.696	71.253	0.9995
16	syringaldehyde	47	33.70	1-150	17.895	76.638	0.9855
17	2,6-dimethoxyphenol	47	39.60	5-150	130.84	481.87	0.9925
18	4-hydroxy-3-methoxyacetophenone	48	48.00	5-150	170.32	952.36	0.9948
19	2-acetyl-resorcinol	49	41.70	1-150	595.41	356.58	1.0000
20	4-ethylphenol	49	55.40	5-150	59.237	77.089	0.9997
21	3,4-dimethylphenol	49	58.20	5-150	69.468	252.35	0.9982

Table 4. Validation data of the quantitative RPLC×RPLC method developed for the characterization of bio-oils.

ID	Compound	LOD (mg L^{-1})	LOQ (mg L^{-1})	Intraday precision, RSD (%) (n = 3)	Interday precision, RSD (%) (n = 9)
1	5-(hydroxymethyl)furfural	0.17	0.51	0.30	0.30
2	3-methyl-1,2-cyclopentanedione	1.30	3.92	7.93	8.18
3	1,2-benzenediol	1.19	3.62	1.48	9.93
4	Furfural	0.08	0.25	5.70	3.59
5	Homovanillyl alcohol	0.16	0.48	1.96	12.14
6	Caffeine	0.05	0.16	5.05	8.72
7	Phenol	2.08	6.29	1.71	5.09
8	4-methyl-1,2-benzenediol	0.10	0.30	2.73	1.72
9	3-p-hydroxyphenyl propanol	0.18	0.54	2.53	3.66
10	4-hydroxybenzaldehyde	0.05	0.15	5.38	10.27
11	5-methylfurfural	0.18	0.54	1.78	7.61
12	4-hydroxyacetophenone	0.16	0.49	9.14	3.82
13	2-methoxyphenol (guaiacol)	0.17	0.52	0.96	0.42
14	Vanillin	0.16	0.50	2.24	3.98
15	4-methylphenol	0.35	1.07	1.58	1.50
16	syringaldehyde	0.11	0.34	7.03	8.13
17	2,6-dimethoxyphenol	1.01	3.05	3.68	1.44
18	4-hydroxy-3-methoxyacetophenone	0.75	2.28	6.56	14.56
19	2-acetyl-resorcinol	0.20	0.62	0.77	0.81
20	4-ethylphenol	0.87	2.64	1.51	5.38
21	3,4-dimethylphenol	0.14	0.42	1.83	1.84

from water in the extraction step. Consequently, their actual concentration in the bio-oil would have been underestimated. Moreover, other compounds, such as 5-(hydroxymethyl)-furfural, which cannot be detected by GC × GC without a derivatization step, as previously reported [6], were properly separated and quantified by LC × LC. As can be observed in figure 7, 1,2-benzenediol is the main compound in all samples except for peanut shell where is the second highest, with concentration values ranging from 2.07 to 7.86 mg mL^{-1}, followed in absolute values by furfural

(4.44 mg mL^{-1} in peach core), 4-methyl benzenediol (3.61 mg mL^{-1} in peach core), guaiacol (2.99 mg mL^{-1} in peanut shell), 2-hydroxy-3-methyl-2-cyclopenten-1-one (1.98 mg mL^{-1} in Eucalyptus saw-dust) and caffeine (1.58 mg mL^{-1} in spent coffee grounds). Regarding chemical classes, table 5 shows the contribution of each group in terms of summed concentration values (mg mL^{-1}) in the 5 bio-oils (aqueous phase) analyzed. Phenols were majority in the samples, corresponding to the 65% of the quantified com-pounds in peach core and Eucalyptus sawdust. Among phenols, benzendiols were the most abundant class. Aldehydes, mainly furfurals, are also present as major components in the bio-oils from peach core (6.31 mg mL^{-1}), rice husk (4.66 mg mL^{-1}) and Eucalyptus sawdust (4.88 mg mL^{-1}). The high amount of benzenediols and furfurals found in the samples is in accordance with studies previously reported for other biomasses (coconut fibers, sugar cane straw and bagasse) representing a high proportion in terms of total peak volumes, although not quantitative information was included [9]. In the case of ketones, all identified components were cyclic ketones; the richest bio-oil on these components was Eucalyptus sawdust (3.75 mg mL^{-1}). Nitrogen compounds only appear in spent coffee grounds; this sample is characterized by high amount of caffeine representing 16% of the total quantified compounds. On the other hand, alcohols showed overall concentrations between 0.11 and 1.67 mg mL^{-1}, being peanut shell bio-oil the sample with the lowest concentration while Eucalyptus sawdust bio-oil was the richest. The differences in the composition of bio-oil aqueous phases is totally related to the distinct chemical compositions of the biomasses processed by pyrolysis. Cellulose, hemicellulose and lignin, together with other components, appear in different pro-portions in the biomasses; this proportion influences the final composition of the obtained bio-oil by pyrolysis [25]. Thus, the predominant phenolic composition of peach core and Eucalyptus sawdust bio-oils is due to the high content of lignin in these biomasses. Lignin is composed of three phenylpropane units, which by depolymerization leads to a variety of phenols, such as benzendiols, methoxyphenols and alkylphenols [26]. Benzenediols, due their higher polarity, remain mainly in the aqueous phase while metoxyphenols and alkylphenols

Table 5 Quantification of the identified compounds present in the aqueous phases of the studied bio-oils. Amounts provided as mg mL^{-1} of aqueous phase.

ID	Compounds	Chemical family	$[M+H]^+$/ $[M-H]^-$	Rice husk mg mL^{-1}	Peanut Shell mg mL^{-1}	Spent coffee grounds mg mL^{-1}	Peach core mg mL^{-1}	*Eucalyptus* sawdust mg mL^{-1}
1	5-(hydroxymethyl)furfural[a]	Aldehyde	127 / 125	0.76	0.35	0.56	0.81	1.78
2	3-methyl-1,2-cyclopentanedione[a]	Ketone	114 / -	1.94	1.33	1.61	0.55	0.80
3	1,2-benzenediol[a]	Phenol	- / 109	3.55	2.68	2.07	7.86	7.41
4	Furfural[a]	Aldehyde	-	2.88	1.04	0.68	4.44	1.83
5	Homovanillyl alcohol[a]	Alcohol	151 / -	0.34	-	0.31	0.83	0.60
6	Caffeine[a]	Alkaloid	195 / -	-	-	1.58	-	-
7	Phenol[a]	Phenol	-	1.33	0.64	0.54	1.37	1.92
8	4-methyl-1,2-benzenediol[a]	Phenol	- / 123	1.09	0.99	0.41	3.61	3.22
9	3-p-hydroxyphenyl propanol[a]	Alcohol	153 / 151	0.24	0.11	0.25	0.17	0.47
10	4-hydroxybenzaldehyde[a]	Aldehyde	123 / 121	0.25	0.15	-	0.13	0.84
11	5-methylfurfural[a]	Aldehyde	111 / -	0.48	0.23	0.22	0.36	0.22
12	4-hydroxyacetophenone[a]	Ketone	137 / 135	-	0.13	-	-	0.29
13	2-methoxyphenol (guaiacol)[a]	Phenol	125 / 123	1.15	2.99	0.14	0.81	0.78
14	Vanillin[a]	Aldehyde	153 / 151	0.29	0.25	0.05	0.32	0.21
15	4-methylphenol[a]	Phenol	-	0.38	0.42	0.10	0.91	1.80
16	Syringaldehyde[a]	Aldehyde	- / 181	-	-	-	0.25	-
17	2,6-dimethoxyphenol[a]	Phenol	-	1.11	0.51	-	0.65	1.13
18	4-hydroxy-3-methoxyacetophenone[a]	Ketone	- / 149	0.33	0.25		-	-
20	4-ethylphenol[a]	Phenol	-	0.35	0.15	-	0.23	<LOQ
21	3,4-dimethylphenol[a]	Phenol	-	-	0.30	-	0.47	0.52
22	2-hydroxy-3-methyl-2-cyclopenten-1-one-[b,c]	Ketone	114 / 111	1.00	0.34	0.66	1.96	1.98
23	3-ethyl-2-hydroxy-5-dimethylcyclopenten-2-en-1-one[b,c]	Ketone	- /137	-	-	-	-	0.68
24	Homovanillyl alcohol isomer[b,d]	Alcohol	151 / -	0.24	-	-	0.33	0.60
25	Methyl-benzenediol isomer[b,e]	Phenol	- / 123		0.55	0.31	0.67	1.20
26	Hydroxyacethophenone isomer[b,f]	Ketone	137 / 135	0.06	0.10	0.09	0.09	-
27	Methylphenol isomer[b,g]	Phenol	-	0.50	0.48	0.15	1.67	0.96
28	Methylphenol isomer[b,g]	Phenol	-	0.17	0.13	0.05	0.42	0.45

are commonly found in higher concentration in organic phase of the bio-oil. In contrast, the amount of aldehydes in aqueous phase samples is due to the cellulose content in the starting biomass. Aldehydes are derived from cellulose depolymerization, leading to a high amount of anhydro-saccharides and anhydro-oligosaccharides which formed aldehydes such as 5-(hydroxymethyl)-furfural, 5-methylfurfuraland furfural [26] by different reactions. These three compounds were identified in all aqueous phases analyzed. Regarding ketones, cyclopentenones and other cyclic ketones are derived mainly from hemicellulose and cellulose degradation [7]. Finally, the significant amount of caffeine in the aqueous phase from spent coffee grounds is due to its presence in high amounts in the raw biomass. Caffeine possibly does not suffer thermo-degradation to a great extent during pyrolysis, which makes possible its determination in spent coffee grounds bio-oil [8]. Many of the separated and quantified compounds in the studied bio-oil aqueous phase samples, might be a viable alternative feed-stocks within the chemical industry. As an example, benzenediols have many important applications as antiviral and antioxidants with application in skin whitening products. Other phenols (alkyl and methoxy compounds) could be used as substitutes for phenols in phenolic resins [27,28]. On the other hand, furfurals have potential as liquid biofuels and in biopolymers production, whereas ketones can be applied in chemical synthesis

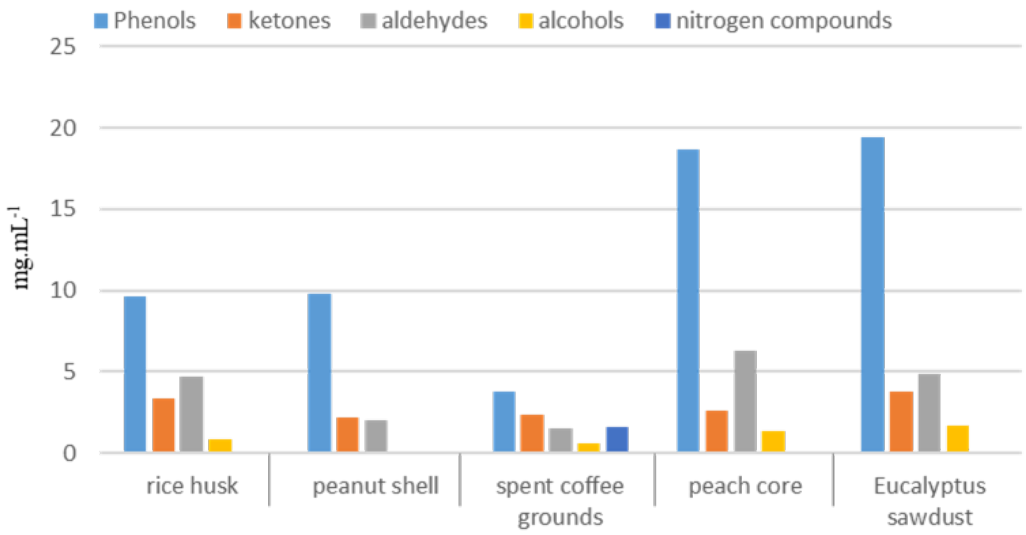

Figure 7. Quantitative contribution of the different compound families (phenols, ketones, aldehydes, alcohols and nitrogen compounds) in each of the analyzed aqueous phase samples by LC × LC.

5.9 Conclusion

Since pyrolysis has been confirmed as a viable alternative to valorize important industrial wastes, appropriate analytical methods to provide accurate elucidation of their products com-position, are needed. This work reports the development of anew RPLC × RPLC-based methodology to quali- and quantitatively assess the composition of aqueous phases of five different bio-oils produced by pyrolysis from interesting agrifood by-products namely, rice husk, peanut shell, spent coffee grounds, peach core and Eucalyptus sawdust. Albeit previous studies also explored the application of 2DLC the characterization of other different bio-oil aqueous phases, this is the first time where a quantitative methodology is implemented. The quantitative RPLC × RPLC developed method presented very good linearity, precision, reproducibility, recovery, and LODs and LOQs as low as 0.05 µg mL^{-1} and 0.16 µgmL^{-1}, respectively. By using this procedure, 28 different components separated and detected in the aqueous phases studied were quantified. The composition of these bio-oils was different but strongly related to the composition of the agrifood by-product sub-mitted to pyrolysis. The development of this methodology opens the door for the quantitative study of other bio-oils by LC × LC, as the complexity of these samples makes comprehensive LC an ideal alternative for their analysis.

References

[1] M. Herrero; E. Ibánez. J. Supercrit. Fluids 2018, 134, 252–259.

[2] A.V. Bridgwater. Biom. Bioenergy (2012), 38, 68–94.

[3] C.S. Faccini; I.D. Vecchia; D. Ribeiro; C.A. Zini; E.B. Caramão. J. Braz. Chem. Soc. 2013, 24, 1085–1098.

[4] E. Lazzari; T. Schena; C.T. Primaz; G.P. da Silva Maciel; M.E. Machado; C.A.L. Cardoso; R.A. Jacques, E.B. Caramão. Ind. Crops. Prod. 2016, 83, 529–536.

[5] E. Lazzari; A. dos Santos Polidoro; B. Onorevoli; T. Schena; A.N. Silva; E. Scapin; R.A. Jacques; E.B. Caramão. Renew. Energ. 2019, 135, 554–565.

[6] C. Michailof; T. Sfetsas; S. Stefanidis; K. Kalogiannis; G. Theodoridis; A. Lappas. J. Chromatogr. A 2014, 1369, 147–160.

[7] R.V.S. Silva; N.S. Tessarolo; V.B. Pereira; V.L. Ximenes; F.L. Mendes; M.B.B. de Almeida; D.A. Azevedo. Talanta 2017, 164, 626–635.

[8] T. Primaz, T. Schena, E. Lazzari, E. Caramão, R.A. Jacques. Fuel 2018, 232, 572–580.

[9] D. Tomasini; F. Cacciola; F. Rigano; D. Sciarrone; P. Donato; M. Beccaria; E.B. Caramão; P. Dugo; L. Mondello. Anal. Chem. 2014, 86, 11255–11262.

[10] A. Le Masle; D. Angot; C. Gouin; A. D'Attoma; J. Ponthus; A. Quignard; S.Heinisch. J. Chromatogr. A 2014, 1340, 90–98.

[11] F. Cacciola; S. Farnetti; P. Dugo; P.J. Marriott; L. Mondello. J. Sep. Sci. 2017, 40, 7–24.

[12] F. Cacciola; P. Dugo; L. Mondello. TrAC – trend, Anal. Chem. 2017, 96, 116–123.

[13] D.W. Cook; M.L. Burnham; D.C. Harmes; D.R. Stoll; S.C. Rutan. Anal. Chim. Acta 2017, 961, 49–58.

[14] M. Kivilompolo; T. Hyötyläinen. J. Chromatogr. A 2007, 1145, 155–164.

[15] M. Kivilompolo; V. Oburka; T. Hyötyläinen. Anal. Bioanal. Chem. 2008, 39, 373–380.

[16] P. Dugo; F. Cacciola; P. Donato; D. Airado-Rodriguez; M. Herrero; L. Mondello. J. Chromatogr. A 2009, 1216, 7483–7487.

[17] D.N. Bassanese; X.A. Conlan; N.W. Barnett; P.G. Stevenson. J. Sep. Sci. 2015, 38, 1642–1648.

[18] L. Mondello; M. Herrero; T. Kumm; P. Dugo; H. Cortes; G. Dugo. Anal. Chem. 2008, 80, 5418–5424.

[19] E. Lazzari; T. Schena; M.C.A. Marcelo; C.T. Primaz; A.N. Silva; M.F. Ferrão; T. Bjerk; E.B. Caramao. Ind. Crops Prod. 2018, 111, 856–864.

[20] ANVISA - Agência Nacional de Vigilância Sanitária, Resolution - 899 of May 29th, 2003, Brazil, 2003.

[21] X. Li; D.R. Stoll; P.W. Carr. Anal. Chem. 2009, 81, 845–850.

[22] M. Camenzuli; P.J. Schoenmakers. Anal. Chim. Acta 2014, 838, 93–101.

[23] J.M. Davis; D.R. Stoll. J. Chromatogr. A 2018, 1537, 43–57.

[24] M.S.A. Moraes; M.V. Migliorini; F.C. Damasceno; F. Georges; S. Almeida; C.A. Zini; R.A. Jacques; E.B. Caramao. J. Anal. Appl. Pyrolysis 2012, 98, 51–64.

[25] A. Sharma; V. Pareek; D. Zhang. Renew. Sust. Energ. Rev. 2015, 50, 1081–1096.

[26] F.-X. Collard; J. Blin. Renew. Sust. Energ. Rev. 2014, 38, 594–608.

[27] S. Czernik; A.V. Bridgwater. Energ. Fuel. 2004, 18, 590–598.

[28] J. Kim, Production, separation and applications of phenolic-rich bio-oil – areview, Bioresour. Technol. 2015, 178, 90–98.

6.0 Comprehensive two-dimensional liquid chromatography-based quali-quantitative screening of aqueous phases from pyrolysis bio-oils

Pyrolysis processes are an alternative to minimize the environmental problem associated to agrifood industrial wastes. The main product resulting from these processes is a high value liquid product, called bio-oil. Recently, the use of comprehensive two-dimensional liquid chromatography (LC × LC) has been demonstrated as a useful tool to improve the characterization of the water-soluble phases of bio-oils, considering their complexity and high water content. However, the precise composition of bio-oils from different agrifood byproducts is still unknown. In the present study, the qualitative and quantitative screening of eight aqueous phases from different biomasses, not yet reported in the literature, using LC × LC is presented. The two-dimensional approach was based on the use of two reverse phase separations. An amide column in the first dimension together with a C18 column in the second dimension were employed. Thanks to the use of diode array and mass spectrometry detection, 28 compounds were identified and quantified in the aqueous phase samples with good figures of merit. Samples showed a distinct quali-quantitative composition and a great predominance of compounds belonging to aldehydes, ketones and phenols, most of them with high polarity.

6.1 Introduction

Byproduct biomasses, as cheap and abundant renewable sources, can reduce the dependency on fossil fuels [1]. Nowadays, agrifood industrial wastes are an important biomass source worldwide due to the large amount of these materials generated annually and the environmental problem associated with them. Only for cassava, sugarcane, and coffee crops, Brazil was responsible in 2018 for more than 675, 20, and

2.6 million tons, respectively [2]. For every ton of cassava and coffee processed, approximately 500 kg of waste is generated, whereas sugarcane processing generates 250 kg of waste per ton [3–5]. Brazil also is known as one of the largest producers of fruit crops; their industrial processing generates a high amount of byproducts such as seeds, leaves, and stalks [2]. Pyrolysis can be an efficient choice for the processing of these agrifood-industrial wastes, producing high-value products. Pyrolysis is a process where the biomass suffers thermal decomposition at high temperatures, ranging approximately from 300°C to more than 800°C, in the complete absence of oxygen to obtain three products: a liquid product (bio-oil), a solid product (biochar), and a gas [6,7]. Recently, bio-oils have received a lot of attention due to their potential uses as biofuels (after upgrading process) or as added-value chemicals for different industrial applications [8]. A bio-oil is a very complex mixture that contains water and the depolymerization products of cellulose, hemicellulose, and lignin (biomass constituents). Most of the compounds in the bio-oil are oxygenated polar organic components that exhibit a wide range of chemical functionalities divided into two phases according to their water solubility [9]. On one side, the water-soluble phase, commonly called aqueous phase, consists of water generated mainly on the dehydration reactions, and high-polarity compounds, especially benzenediols, ketones, furfurals, and low-molecular-weight acids [8,9]. Usually, the aqueous phase represents 15–30 wt% of the bio-oil, although depending on the pyrolysis operating conditions and the particular biomass composition, the yield can reach up to 70 wt% [10]. Due to the high water content, the aqueous phase cannot be directly used as biofuel, and if discarded the bioenergy use rate is reduced as well as the overall sustainability of the pyrolysis process [11]. Research on the aqueous phase uses usually involves uses in hydrogen/biogas generation [12,13] or extraction of high-value chemicals [14,15]. In this regard, a wide range of chemicals with recognized industrial importance can be obtained from aqueous phase. In both cases, strategies for the chemical characterization allowing a comprehensive knowledge of their composition (quali-quantitative) are needed.

GC and, most notably, comprehensive two-dimensional gas chromatography (GC × GC) have been widely used for the characterization of bio-oils, specifically, for the organic phase analysis. However, for aqueous phase characterization, different pretreatments are required before analysis due to the unsuitability of high water content samples to be analyzed by GC. This preparation step can affect the native chemical composition of the aqueous phases, even more, when quantitative analysis is aimed [16]. To overcome this problem, comprehensive two dimensional liquid chromatography (LC × LC) may be a useful analytical tool, considering that aqueous phases are normally composed of a high number of compounds, some of them closely related and, thus, very difficult to be separated [16–19]. Besides, LC × LC allows the injection of the whole sample without any sample preparation steps, and retains a significantly higher separation power providing very high peak capacity compared to conventional one-dimensional LC separations [20–22]. The analytical power of LC × LC is related to the coupling of two dimensions each providing different separation selectivity. Briefly, the sample is injected in the ^{1}D (first dimension) where the first and slow separation occurs. Subsequently, discrete fractions of ^{1}D effluent are continuously collected and transferred with the aid of a modulator or interface into the ^{2}D (second dimension), where a fast separation occurs. Commonly, the interface is based on one or more switching valves equipped with two sampling loops with identical inner volume. In this way, the sample fraction from ^{1}D is collected in one of the sampling loops whereas the previous sample fraction is being injected into the ^{2}D using the other loop [20–24]. Comprehensive LC has been scarcely studied for the characterization of bio-oil aqueous phases, being limited to a few types of samples [16,17]. Recently, a novel approach for the quantitative characterization of bio-oil aqueous phases using LC × LC was developed and applied [18]. As a continuation of that study, the aim of the present contribution is to chemically characterize eight additional aqueous phases generated from diverse biomasses, including almond of mango seed, coconut fibers, pineapple leaves, sugarcane bagasse, cottonseed, coffee

silver skin, cassava peel, and crambe seed, to assess their potential to be valorized for interesting chemical industrial uses. Besides, the composition of most of these aqueous phases have not been reported before. Two dimensional LC is proposed as an important tool in the bio-oils characterization field.

6.2 Materials and methods

6.2.1 Chemicals and standards

Solvents used were acetonitrile and methanol purchased from VWR Chemicals (Barcelona, Spain) and the ultrapure water used for all solutions and mobile phase preparation was obtained from a Milli-Q apparatus (Millipore system, Billerica, MA, USA). All reference standards were at least 98% of purity and were acquired from Sigma–Aldrich (Saint Louis, MO, USA). A stock solution (1000 mg/L) was prepared in methanol containing the following 21 reference standards: 2 alcohols (homo vanillyl alcohol, 3-p-hydroxyphenylpropanol), 3 ketones (3-methyl-1,2-cyclopentanedione, 4-hydroxyacetophenone, 4-hydroxy-3-methoxyacetophenone), 6 aldehydes (5-(hydroxymethyl) furfural, furfural, 4-hydroxybenzaldehyde, 5-methylfurfural, vanillin, syringaldehyde), 9 phenols (1,2-benzenediol, phenol, 4-methyl-1,2-benzenediol, 2-methoxyphenol (guaiacol), 4-methylphenol, 2,6-dimethoxyphenol, 4-ethylphenol, 3,4-dimethylphenol, 2-acetyl-resorcinol), and one nitrogen compound (caffeine). Different concentration levels (1 to 250 mg/L) were prepared in ultrapure water from the stock solution and stored at 5°C.

6.3 Biomass samples

Eight biomasses were investigated in this study, namely: almond of mango seed, coconut fibers, pineapple leaves, sugarcane bagasse, cottonseed, coffee silver skin, cassava peel, and crambe seed. These biomasses, except crambe, are agrifood wastes

and represent a considerable environmental issue in Brazil, due to the large amounts produced per year. Crambe seed is not an agrifood waste, although is an interesting nonfood source of seed oil with a potential to generate bio-oil [25,26].

Among the biomasses studied, sugarcane bagasse, cassava peel, and almond of mango seed were obtained from the food industry located in Dourados and Porto Alegre, Brazil. Coconut fibers were provided by Embrapa (Aracaju, Brazil), coffee silver skin was acquired from Marata Industry (Aracaju, Brazil), cotton seed was provided from Planalto Farm (Costa Rica, Brazil), whereas pineapple leaves were obtained from a local supermarket (Porto Alegre, Brazil). The samples were milled to a particle size between 40 and 60mesh and dried in an oven at 105°C for 24 hr prior pyrolysis.

6.4 Pyrolysis process and aqueous phase samples

Intermediate pyrolysis of biomasses was performed in a homemade vertical furnace containing a tubular fixed-bed quartz reactor. The schematic diagram of the instrument has already been described in detail elsewhere [18]. A quartz reactor was heated by an electrical furnace, and N2 was used as carrier gas of the pyrolysis vapors which were directed through the condenser cooled with a mixture of ethylene glycol and water (1:1) at −10°C. All pyrolysis conditions were based on previous studies [27,28] and were as follow: 6.5 g of biomass (40–60 mesh), heating rate of 100°C/min, N_2 flow of 100 mL/min, and pyrolysis final temperature of 650°C with 10 min of residence time.

After the pyrolysis process, a liquid product consisting of two phases with different densities was obtained composed of an organic phase called bio-oil and an aqueous phase, which were separated by simple decantation. The aqueous phase was collected without any further pretreatment, diluted in water (using a dilution factor from 1:10 v/v to 1:40 v/v according to the concentration of compounds in the samples), filtered through a 0.20 μM Chromafil PTFE membrane, and directly analyzed by LC × LC-DAD-ESI-MS.

6.5 LC × LC analysis

6.5.1 Equipment

An Agilent 1200 series liquid chromatograph (Agilent Technologies, Waldbronn, Germany), equipped with an autosampler was used for the ^{1}D. The diode array detector (DAD) was connected at the exit of the ^{2}D, which was carried out using an additional LC pump (Agilent 1290 Infinity). The two dimensions were connected by an electronically controlled two position ten-port switching valve (Rheodyne, Rohnert Park, CA, USA), equipped with two identical 30 μL sampling loops. The wavelength used to monitor the separation was 280 nm, although UV-vis spectra were recorder from 200 to 400 nm using a sampling rate of 20 Hz in the DAD. The LC × LC data were elaborated using LC image software (Zoex Corp. Houston, TX, USA).
An Agilent 6320 ion trap mass spectrometer (Agilent Technologies) interfaced through an electrospray ionization (ESI) ion source was connected in series at the exit of the DAD. The total effluent flow from the ^{2}D was splitted before the MS instrument via a Tee union and the flow rate entering the MS detector was approximately 600 μL/min. The ion trap mass spectrometer was operated in both ESI positive and ESI-negative modes using the following parameters: mass range, *m/z* 50 to 200; corona discharge, +4000 nA (positive)/−10000 nA (negative); capillary voltage, −3500 V; nebulizer pressure, 60 psi; dry gas, 5 L/min; dry temperature, 350°C and; vaporizer temperature, 400°C. The ion trap was controlled using the 6300 series trap control software (Bruker Daltonik GmbH, V. 6.2).

6.5.2 Chromatographic conditions

The LC× LC analyses were performed coupling two RP separations. For the ^{1}D, a X-Bridge amide column (150 × 2.1mm I.D., 3.5 μm d.p., Waters, Milford, MA, USA) was employed, using as mobile phase acidified water (0.1% formic acid, v/v, solvent

A) and acetonitrile (0.1% formic acid, v/v, solvent B) under the following linear gradient elution: 0 min, 2% B; 3 min, 10% B; 50 min, 60% B; 61 min, 100% B. The flow rate was set at 25 μL/min. Ten microlitre of aqueous phase solutions were injected and the column temperature was kept at 30°C. In the ^{2}D, a short partially porous column (Poroshell EC-C18, 30 × 4.6 mm I.D., 2.7 μm d.p., Agilent, Santa Clara, CA, USA) was selected. The mobile phase was the same used in the ^{1}D, although, the flow rate was set at 2.5 mL/min. The optimum linear gradient selected was: 0 min, 10% B; 0.85 min, 90% B; 0.86 min, 100% B; 0.9 min, 100% B; 0.91 min, 10% B with re-equilibrium at starting conditions until 1 min. This 1-min gradient was repeated during the whole analysis time being, therefore, 1 min is the modulation time.

6.5.3 Calculations

In order to assess the separation performance of the system, the corrected peak capacity and the degree of orthogonality were evaluated. Corrected peak capacity is a more realistic value for peak capacity in a LC × LC system, since it takes in account both the deleterious effects due to the modulation process as well as the degree of orthogonality. Corrected peak capacity ($^{2D}n_{c,\,corrected}$) was determined by multiplying the effective peak capacity ($^{2D}n_{c,\,effective}$) by the degree of orthogonality (A_0). The effective peak capacity calculation (Eq. (1)), includes the (β) parameter, accounting for possible ^{1}D undersampling effect respecting, thus, the effective number of fractions transferred from the first to the second dimension.

$$^{2D}n_{c,practical} = \frac{^{1}n_c \times {}^{2}n_c}{\sqrt{1 + 3.35 \times \left(\frac{^{2}t_c \; ^{1}n_c}{^{1}t_g}\right)^2}} \quad \textbf{(1)}$$

where $^{1}t_G$ is the gradient time in the ^{1}D; $^{2}t_c$ is the ^{2}D separation time cycle which is equal to the modulation time; and the $^{1}n_c$ and $^{2}n_c$ correspond to the ^{1}D and ^{2}D theoretical peak capacity ($^{2D}n_c$), respectively, calculated according to Neue [29]. The A_0, was

estimated using the asterisk equations proposed by Camenzuli and Schoenmakers [30]. Such method allows the evaluation of the spread of each peak along the four imaginary lines in the 2D space forming an asterisk, that is Z_1, Z_2 (vertical and horizontal lines) and $Z_–$, Z_+ (diagonal lines of the asterisk), based solely on the experimentally peak retention times measured. Briefly, for the determination of each Z parameter, the S_{ZX} value was calculated, as the measure of spreading around the Z_x line, using the retention times of all the separated peaks in each 2D analysis. Z parameters described the separation space use according to the corresponding Z line, allowing to semi quantitatively diagnose areas of the separation space where sample components are clustered.

6.5.4 Quantitative method

All identified compounds in the aqueous phase samples were quantified using calibration curves constructed for 21 commercial standards compounds (see Section 2.1). Eight different concentration levels prepared in water were injected in triplicate in the LC × LC system, and the calibration curves were plotted using the peak volumes, based on DAD data recorded at 280 nm using LC Image software. The concentration of the analytes in the bio-oil samples was estimated in milligrams per litre. Method performance was evaluated through the assessment of the main figures of merit: dynamic range, linearity, limits of detection and quantification, precision (intra- and interday) and accuracy (by recovery). All the validation procedure was according ANVISA [31] protocols as previously reported in detail [18].

6.6 Results and discussion

6.6.1 LC × LC analysis of bio-oil aqueous phases

All the biomasses studied in the present research exhibit potential for the bio-oil production via pyrolysis as described in studies of almond of mango seed [32], crambe seed [25,26], spent coffee grounds [33], cassava peel [34], coconut fiber [35,36], coffee silverskin [28], and sugarcane bagasse [35,14]. However, these previous studies were exclusively focused on the screening of bio-oil composition (organic phase) by GC techniques. Even when the attention has been directed to aqueous phase characterization, it was carried out using a pretreatment step or a semiquantitative approach. For this reason, in the present contribution the quali-quantitative characterization of the aqueous phases from the mentioned bio-oils is targeted using comprehensive two-dimensional liquid chromatography.

Various columns, solvents, gradients, as well as flow rates have been tested and optimized to select the most appropriate LC × LC method configuration, as described in detail in our previous study [18]. The two-dimensional approach was based on the use of two RP separations; an amide column was used in the ^{1}D together with a C18 column in ^{2}D. The 2D contour plots, extracted at 280 nm for each aqueous phase analyzed using the RPLC × RPLC-DAD method are presented in Fig. 1.

As can be observed, all the samples are characterized by the presence of a relatively high number of compounds, involving a great chemical complexity, although they could be satisfactorily separated using the RPLC × RPLC-DAD optimized method. As a matter of fact, a great number of compounds that coeluted in the ^{1}D were successfully resolved in the ^{2}D, for instance, peaks 3 and 4, peaks 13 and 14, and peaks 24 and 6. Even if the separation mechanism selected in both dimensions is based on RP, the combination of different stationary phase chemistries provided different selectivity in each dimension. Table 1 summarizes some of the method performance parameters for the different studied samples.

Orthogonality values expressed in Table 1 allow evaluating the occupation of the 2D plane by the sample components. As can be observed, good degrees of orthogonality up to 70% were achieved for the aqueous phases from crambe seed, cottonseed, and coffee silver skin, confirming a good distribution of the compounds observed in the available 2D space. Even though the separation space is not entirely utilized, the orthogonality values were still relatively high, ranging from 43 to 46% for the aqueous phases from sugarcane bagasse, pineapple leaves, and coconut fiber samples, considering that two RP separations are employed. In the case of corrected peak capacity, values between 176 and 332 were found for the aqueous phases from pineapple leaves and crambe seed, respectively. This parameter takes into account the degree of orthogonality and possible deleterious effects due to the modulation process, providing a more realist values than the classical theoretical peak capacity ($^{2D}n_c$) provided by the product rule ($^{2D}nc = {}^{1}n_C \times {}^{2}n_c$).

In any case, these figures of merit demonstrated the good separation capacity for the RPLC × RPLC method higher than those found in the literature for some samples. Effective peak capacity and orthogonality values reaching 347 and 47%, respectively, were previously reported for aqueous phase samples from three lignocellulose biomasses [16] which would imply a corrected peak capacity of 163, lower that the one obtained in the present contribution.

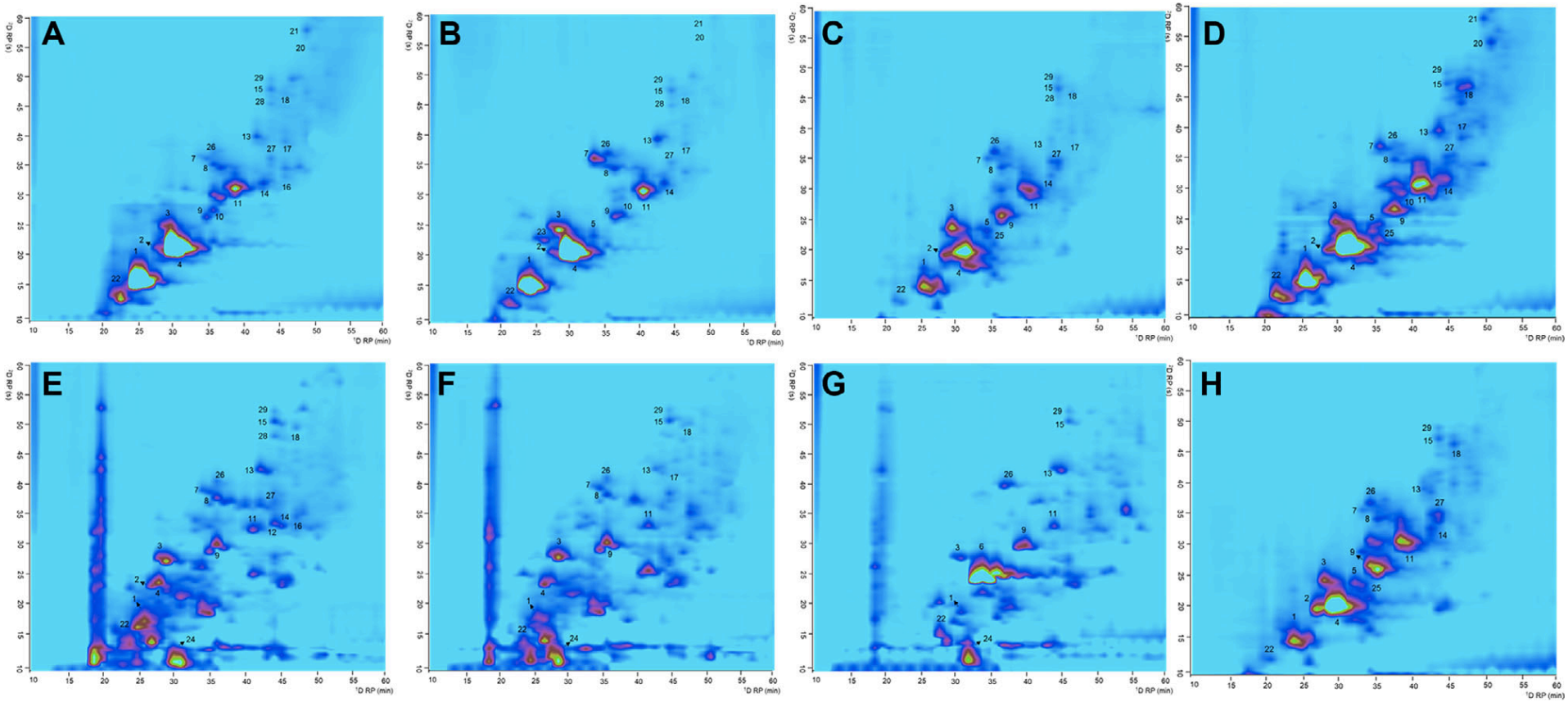

Figure 1. Resulting 2D contour plots (280 nm) for the different aqueous phases, analyzed using the RPLC×RPLC-DAD method, obtained by pyrolysis from (A) sugarcane bagasse; (B) coconut fiber; (C) almond of mango seed; (D) pineapple leaves; (E) crambe seed; (F) cottonseed; (G) coffee silverskin; and (H) cassava peel. For peak identification, see Table 3.

Table 1. Peak capacity values and orthogonality degree obtained for each studied biomass under optimum RPLC×RPLC analysis conditions.

	Sugarcane bagasse	Coconut fiber	Almond of mango seed	Pineapple leaves	Crambe seed	Cotton seed	Coffee silveskin	Cassava peel
${}^{2D}n_c$	644	619	660	584	643	709	647	735
${}^{2D}n_{c,\ effective}$	426	423	429	404	436	438	413	479
${}^{2D}n_{c,corrected}$	182	193	240	176	332	325	302	271
A_0	43	46	56	43	76	74	73	56

6.6.2 Qualitative and quantitative chemical characterization

Using the optimized RPLC × RPLC-DAD method, a wide group of 21 standard compounds considered as representative of the main group of compounds present in the aqueous phase samples were injected and analyzed. Phenols, aldehydes, ketones, alcohols, and a nitrogen compound were included; their chemical structures are presented in Fig. 2. Moreover, this figure also shows the good degree of separation attained using the 2D method for their separation.

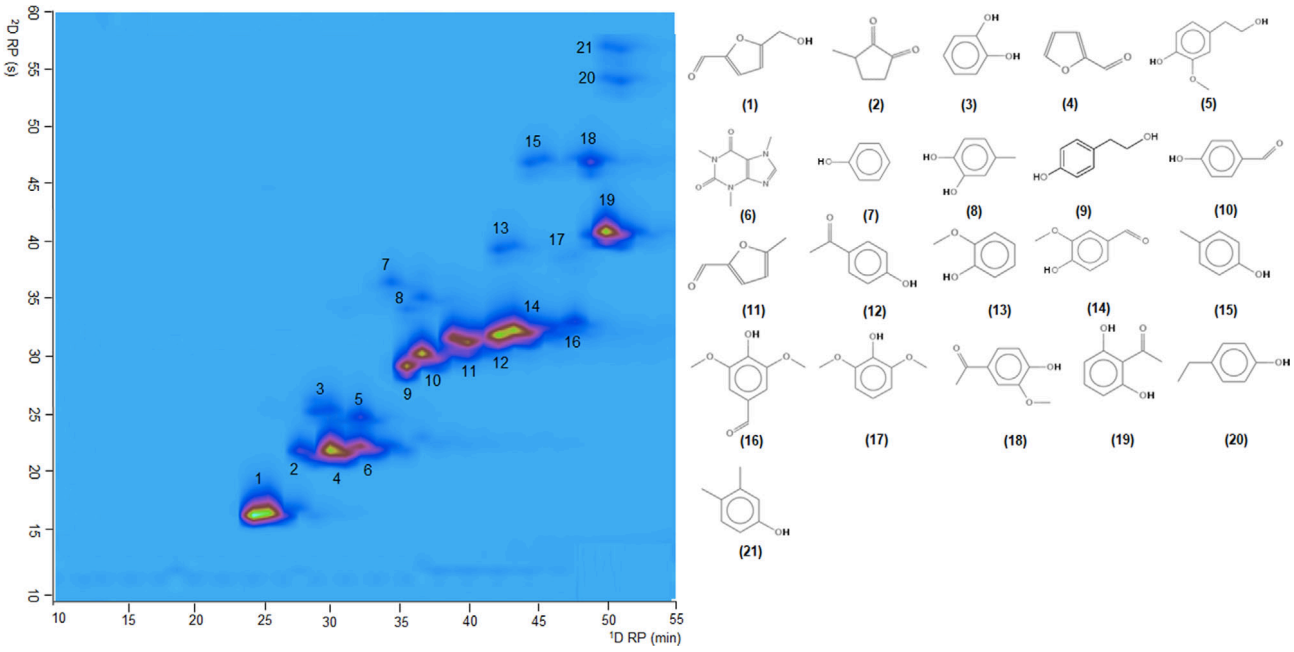

Figure 2. Chemical structures and two-dimensional contour plots (280 nm) of the separation obtained for the calibration standards mixture (50 mg/L each). For peak identification, see Table 2.

To increase the identification potential of the method, an ion trap MS was also connected in series at the exit of the ^{2}D, after the DAD. The MS was operated in both positive and negative ionization modes using an electrospray interface.

Table 2 reports the MS information collected from the standard compounds injected as well as their corresponding retention times in each dimension. As expected, negative ESI mode was more appropriate for acids and phenolic compounds, whereas positive ESI mode was preferred for ketones, furans and alkaloids. However, most of the target compounds could be detected in both ionization modes. For quantitative purposes, calibration curves for each standard compound, using the peak volumes obtained in the 2D plots (DAD data at 280 nm) after triplicate injections at each concentration level were employed. The validation of the method was performed according to ANVISA [31], showing good figures of merit.

Table 2. Molecular ions (m/z) detected using positive and negative ESI ionization modes and retention data for each compound contained in the commercial standard compounds mixture

	Compounds	Retention time (^{1}D min)		Retention time (^{2}D s)		$[M+H]^+$	$[M-H]^-$
		mean (SD)	RSD (%)	mean (SD)	RSD (%)		
1	5-(hydroxymethyl) furfural	24.67 (0.67)	2.70	16.36 (0.18)	1.09	127	125
2	3-methyl-1,2-cyclopentanedione	27.44 (0.83)	3.03	21.92 (0.30)	1.35	114	-
3	1,2-benzenediol	28.78 (0.79)	2.73	25.69 (0.11)	0.44		109
4	Furfural[1]	29.67 (0.94)	3.18	22.03 (0.13)	0.60	-	-
5	Homovanillyl alcohol	31.89 (1.10)	3.45	24.91 (0.14)	0.55	151	-
6	Caffeine	32.00 (0.94)	2.95	22.33 (0.14)	0.64	195	-
7	Phenol[1]	33.78 (1.03)	3.05	36.81 (0.20)	0.55	-	-
8	4-methyl-1,2-benzenediol	35.44 (0.83)	2.35	35.65 (0.21)	0.60	125	123
9	3-p-hydroxyphenyl propanol	35.33 (2.11)	5.97	29.76 (0.28)	0.93	153	151
10	4-hydroxybenzaldehyde	35.33 (0.67)	1.89	30.76 (0.09)	0.30	123	121
11	5-methylfurfural	38.44 (1.34)	3.49	31.95 (0.15)	0.46	111	-
12	4-hydroxyacetophenone	40.78 (0.92)	2.25	32.35 (0.36)	1.10	137	135
13	2-methoxyphenol (guaiacol)	41.22 (0.92)	2.22	40.22 (0.18)	0.45	125	123
14	Vanillin	41.56 (0.83)	2.00	32.77 (0.08)	0.24	153	151
15	4-methylphenol[1]	43.22 (0.63)	1.45	47.98 (0.16)	0.33	-	-
16	Syringaldehyde	44.89 (0.74)	1.64	33.43 (0.21)	0.61	183	181
17	2,6-dimethoxyphenol	45.33 (0.47)	1.04	39.42 (0.15)	0.39	155	
18	4-hydroxy-3-methoxyacetophenone	46.33 (0.47)	1.02	47.79 (0.21)	0.43	153	151
19	2-acetyl-resorcinol	47.33 (0,47)	1.00	41.53 (0.08)	0.19	151	149
20	4-ethylphenol[1]	48.22 (0.42)	0.86	55.33 (1.02)	1.84	-	-
21	3,4-dimethylphenol[1]	48.11 (0.31)	0.65	57.71 (0.13)	0.23	-	-

[1]Identified according Uv-Vis spectra and retention times.
SD, standard deviation for n = 9; RSD (%) relative standard deviation.
Peak numbers as in Fig. 2.

Intermediate precision of the applied procedure was also calculated. This parameter is relevant, since some compounds, such as alkylphenols, did not ionize properly in the MS and were identified by comparing their retention times and UV-Vis spectra with those from commercial standards. A mixture containing all the studied standards at 50 μg/mL was injected three times in three consecutive days (n = 9). As can be observed in Table 2, the RSD values obtained ranged from 0.65% for 3,4-dimethylphenol to 5.97% for 3-*p*-hydroxyphenyl propanol in the ^{1}D, and from 0.19 to 1.84% for 2-acetylresorcinol and 4-ethylphenol, respectively, in the ^{2}D. These values demonstrated a good instrumental reproducibility. The validated LC × LC-DAD-ESI-MS qualitative and quantitative method was implemented for the comprehensive characterization of the eight aqueous phase samples obtained from the bio-oils resulting from the pyrolysis from almond of mango seed, cassava peel, cottonseed, crambe seed, coffee silverskin, coconut fiber, sugarcane bagasse, and pineapple leaves. Each aqueous phase was analyzed by triplicate on the LC × LC system in order to confirm the injection reproducibility samples, evaluating retention times and peak volumes. Combining the information provided by both DAD and MS detectors, a total of 28 compounds were identified in the aqueous phase samples. Among them, eight compounds were not available as commercial standards and were assigned based on their corresponding mass spectra, UV-Vis information, presented in Table 3. Each identified compound was classified into one of the following categories: ketones, nitrogen compounds, alcohols, benzenediols, methoxy and alkyl phenols, furfurals and aldehydes (which includes aldehydes other than furfurals). A great predominance of compounds belonging to aldehydes, ketones, and phenols were evidenced in the aqueous phases, most of them with high polarity. In fact, if GC would have been used for aqueous phase analysis, a preliminary extraction step, commonly performed with Dichloromethane, would be required and all these polar components would have not been totally extracted from water. This approach was previously used by others.

Almeida et al. [36] characterized a coconut fiber aqueous phase employing a dichloromethane liquid-liquid extraction following by GC × GC coupled to time-of-

flight mass spectrometry (TOF-MS) analysis. Sixty-eight compounds were identified, with a high predominance of phenolic compounds, mainly alkylphenols. However, other more polar compounds, such as furfurals, were not present probably because they were not extracted from the water sample. Likewise, Maciel et al [14] applied GC × GC-TOFMS in the characterization of organic extracts from the aqueous phase of sugarcane straw obtained by liquid-liquid and SPE. More than 180 compounds were tentatively identified in the extract and based on semiquantitative analysis, phenols, mainly benzenediols, were majority. Lyophilization has also been used as pretreatment step coupled to GC-MS to study the chemical composition of an aqueous phase from rice husk [37]. Once more phenols were the most abundant compounds followed by sugars. Silva et al [26] employed a lyophilization together a GC × GC-TOFMS and high-resolution MS analysis for the characterization of the aqueous phase from crambe seeds bio-oil. Both techniques allowed the tentative identification of more than 100 compounds.

Table 3. Qualitative and quantitative results of eight aqueous phase analysis by LC × LC-DAD-ESI-MS

	Compounds	ESI (+)/ESI(-)	Chemical classes	Sugarcane bagasse (mg L^{-1})	Coconut fiber (mg L^{-1})	Almond of mango seed (mg L^{-1})	Pineapple leaves (mg L^{-1})	Crambe seed (mg L^{-1})	Cotton seed (mg L^{-1})	Coffee silveskin (mg L^{-1})	Cassava peel (mg L^{-1})
1	2-hydroxy-3-methyl-2-cyclopenten-1-one-[b]	114/111	ketone	6.68	3.02	0.34	4.26	0.91	0.28	0.30	0.30
2	5-(hydroxymethyl)furfural[a]	127/125	furfural	7.54	2.86	0.45	1.67	0.13	0.04	0.01	0.29
3	3-ethyl-2-hydroxy-5-dimethylcyclopenten-2-en-1-one[b]	-/137	ketone	-	1.26	-	-	-	-	-	-
4	3-methyl-1,2-cyclopentanedione[a]	114/-	ketone	1.73	0.49	1.15	2.77	0.19	-	-	1.01
5	1,2-benzenediol[a]	-/109	benzenediol	5.36	4.66	2.49	2.42	0.73	0.56	0.04	1.32
6	3-methyl-2-cyclopenten-1-one[b]	96/-	ketone	-	-	-	-	2.35	1.73	0.84	-
7	Furfural[a]	-	furfural	7.91	5.31	1.14	4.02	0.11	0.10	-	1.35
8	Caffeine[a]	195/-	nitrogen compound	-	-	-	-	-	-	2.30	-
9	Homovanillyl alcohol[a]	151/-	alcohol	-	0.60	0.44	0.57	-	-	-	0.50
10	Homovanillyl alcohol isomer[b]	151/-	alcohol	-	-	0.15	0.38	-	-	-	0.14
11	Phenol[a]	-	alkylphenol	1.21	4.70	< LOQ	1.03	0.20	0.14	-	< LOQ
12	3-p-hydroxyphenyl propanol[a]	153/151	alcohol	0.40	0.63	0.87	1.08	0.17	0.19	0.37	0.65
13	4-hydroxybenzaldehyde[a]	123/121	aldehyde	0.46	0.08	0.11	0.17	-	-	-	0.16
14	4-methyl-1,2-benzenediol[a]	-/123	benzenediol	1.87	1.07	0.54	0.43	0.33	0.14	-	0.46
15	Methyl-benzenediol isomer[b]	-/123	benzenediol	0.80	0.82	0.75	0.54	0.15	0.12	0.14	0.50
16	5-methylfurfural[a]	111/-	furfural	1.13	0.93	0.43	1.07	0.06	0.04	0.09	0.45
17	2-methoxyphenol (guaiacol)[a]	125/123	methoxyphenol	1.17	1.08	0.10	1.13	0.32	0.10	0.13	0.19
18	Vanillin[a]	153/151	aldehyde	0.31	0.22	0.12	0.23	0.05	-	-	0.10
19	4-hydroxyacetophenone[a]	137/135	ketone	-	-	-	-	0.01	< LOQ	-	-
20	Hydroxyacethophenone isomer[b]	137/135	ketone	0.07	0.05	0.08	0.13	0.01	0.04	-	0.10
21	Methylphenol isomer[b]	-	alkylphenol	0.49	0.36	0.11	-	0.08	0.03	-	-
22	4-methylphenol[a]	-	alkylphenol	0.48	0.42	0.25	0.13	0.11	0.07	0.04	0.13
23	Methylphenol isomer[b]	-	alkylphenol	0.24	0.13	0.12	0.19	0.03	0.03	0.02	0.06
24	2,6-dimethoxyphenol[a]	-	methoxyphenol	3.17	1.03	0.28	2.31	0.14	0.14	-	
25	4-hydroxy-3-methoxyacetophenone[a]	-/149	ketone	0.35	0.21	0.19	0.96	0.07	0.07	-	0.23
26	Syringaldehyde[a]	-/181	aldehyde	0.34	-	-	-	0.41	0.12	-	-
27	4-ethylphenol[a]	-	alkylphenol	0.85	< LOQ	-	0.48	0.04	< LOQ	-	-
28	3,4-dimethylphenol[a]	-	alkylphenol	0.44	0.22	-	0.90	0.04	-	-	-

On the other hand, 26 compounds in aqueous phases from coconut fiber, bagasse, and straw of sugarcane were identified by LC × LC-DAD-MS [16]; among them, compounds with high polarity, such as benzenediols, furfurals, alcohols, and ketones, were found. These results are in agreement with those described in the present article.

As observed in Table 3, furfural, 3-methyl-2-cyclopenten-1-one, and 1,2-benzenediol appeared as the main compounds in most of the samples (seven out of eight aqueous phases), with concentration values ranging from 0.10 to 7.91 mg/L, from 0.84 to 2.35 mg/L, and from 0.04 to 5.36 mg/L, respectively.

These compounds are followed in absolute values by 5-(hydroxymethyl) furfural (7.54 mg/L in sugarcane bagasse), phenol (4.70 mg/L in coconut fiber), 2-hydroxy-3-methyl-2-cyclopenten-1-one (4.26 mg/L in pineapple leaves), and caffeine
(2.30 mg/L in coffee silver skin).

With regards to the chemical classes, Fig. 3A shows the distribution of each group in terms of summed concentration values (mg/L) in the eight aqueous phases analyzed. In order to better investigate some similarities and differences among the aqueous phases composition, multivariate analysis based on principal component analysis (PCA) was performed. The PCA was performed using the chemostat software [38] and the concentration values for each chemical class identified by LC × LC-DAD-ESI-MS analysis. Before multivariate analysis, the data were autoscaled. The results are presented in Fig. 3B as a biplot in the plane of the first and second principal components (PCs) which together account for 76.39% of the total variability. The PCA separation was obtained according the sample compositions (Fig. 3A); thus, aqueous phases with similar chemical class distributions are closer in the plot.

As observed in Fig. 3A and B, aqueous phases from coconut fiber and sugarcane bagasse (inside the blue line in PCA) are characterized by a large concentration of phenols which represent 51 and 46% of the quantified compounds in these samples, respectively; among phenols, benzenediols were the most abundant components. Significant amounts of aldehydes, mainly furfurals are also present.

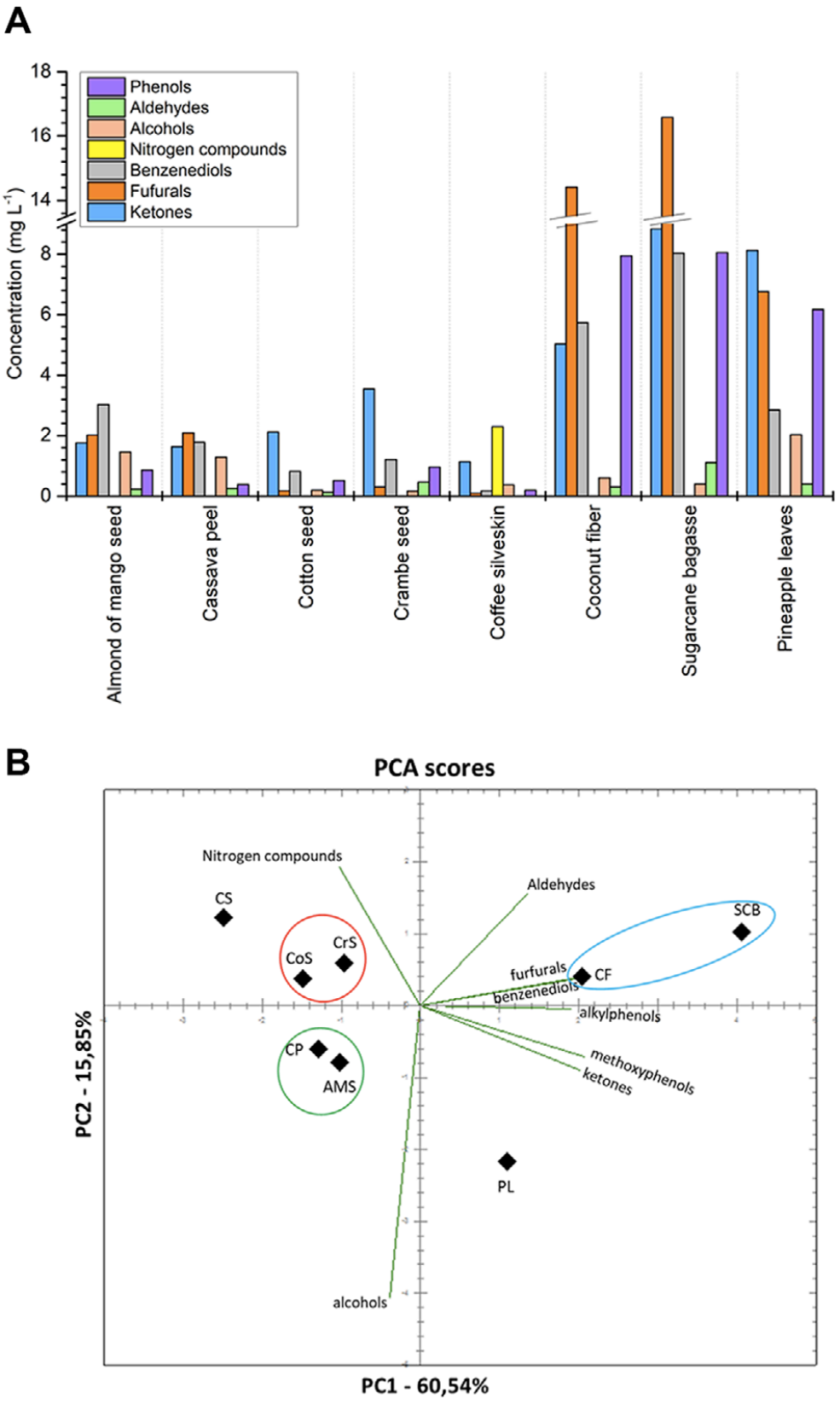

Figure 3. Distribution of the chemical classes in each aqueous phase analyzed samples by LC × LC -DAD-ESI-MS: (A) Quantitative contribution of the different chemical classes and (B) Biplot of PC1 (60.54%) versus PC2 (15.85%) resulting of PCA; CS, coffee silverskin; CrS, crambe seed; CoS, cottonseed; CP, cassava peel;AMS, almond of mango seed; PL, pineapple leaves; CF, coconut fiber; SCB, sugarcane bagasse.

Phenolic compounds and aldehydes are mainly derived from lignin and cellulose degradation, respectively [39]. Benzenediols, derived from lignin degradation, remain mainly in the aqueous phase while other phenols, such as alkyl and methoxyphenols, are commonly found in higher concentration in the bio-oils [18,40]. 5-(Hydroxymethyl) furfural, 5-methylfurfural, and furfural are the main compounds formed from cellulose thermal degradation [39] and were identified in all aqueous samples, though with different concentrations levels.

In the case of aqueous phases from cottonseed and crambe seeds (inside the red line in PCA), a composition consisting predominantly of ketones and benzenediols, which together represent more than 70% of the total quantified compounds in the samples, was found. All ketone compounds quantified corresponded to cyclic ketones which derive from thermal degradation of cellulose and hemicellulose [6]. In contrast, aqueous phases from almond of mango seed and cassava peel (inside the green line in PCA), showed a similar concentration of all chemical classes, with the highest contribution of ketones, furfurals, and alcohols. Lastly, aqueous phases from coffee silverskin and pineapple leaves showed different chemical class distribution profile; the first one is characterized for a high amount of nitrogen compounds, due to caffeine concentration that represents 53% of the total quantified compounds. Caffeine is present in coffee silverskin raw biomass and possibly does not suffer a great extent degradation during pyrolysis [33].

In the other hand, aqueous phase from pineapple leaves showed the highest concentration of alcohol compounds (2.03 mg/L). Considering the determined chemical compositions, the aqueous phases studied might be viable alternative feedstock within the chemical industry. As aqueous phases are normally considered as byproducts from the pyrolysis process, their further use would be highly interesting to increase the sustainability of the whole process. Thus, the valorization of those biomasses by pyrolysis could be an option. Many identified and quantified compounds by LC × LC-DAD-ESI-MS have important industrial uses; for example, furfurals may

be employed as adhesives, lubricants, plastics, and nylons whereas ketones can be applied in chemical syntheses [8]. Others have been pointed out by possessing some bioactivities such as the antiviral and antioxidant activities attributed to benezenediols [8,41]. Besides, the use of aqueous phases possesses some advantages as alternative chemical sources compared to bio-oil organic phases, based on a lower chemical complexity and relatively high concentration of interesting compounds solubilized in an aqueous matrix.

6.7 Conclusions

In this study, a quantitative analytical methodology based on the use of LC × LC is optimized and applied to the screening and chemical characterization of eight aqueous phases from different agrifood waste bio-oils, most of them not yet reported in the literature. Two RP-based separations were coupled providing relatively high separation capacities with degree of orthogonality up to 76%. These applications further demonstrate the possibility of using correlated separation mechanisms appropriately optimized for the separation of complex natural samples by LC × LC. Thanks to the coupling of DAD and ESI-MS detection in series, 28 compounds were identified and quantified with good merit figures in the studied samples. A great predominance of compounds belonging to phenols, ketones, and aldehydes were evidenced, although the bio-oils showed distinct compositions which were discriminated through multivariate analysis, specifically PCA. The implemented LC × LC method retains a good potential for the complete characterization of aqueous phases from bio-oils, given their complex nature as well as the diversity of functionalities and high water content present on those matrices, and permitted to obtain a first insight on the composition of these under studied fractions.

References

[1] M. Jahirul; M. Rasul; A. Chowdhury; N. Ashwath. Energies 2012, 5, 4952–5001.

[2] IBGE. Instituto Brasileiro de Geografia e Estatística, Available at https://www.sidra.ibge.gov.br/bda/prevsaf.

[3] M. K. D. Rambo; F. L. S. Schimidt; M. M. C. Ferreira. Talanta 2015, 144, 696–703.

[4] P. Esquivel; V. M. Jiménez. Food Res. Int. 2012, 46, 488–495.

[5] Pattiya, A. S. J. Suttibak. J. Anal. Appl. Pyrolysis 2012, 95, 227–235.

[6] A. V. Bridgwater. Biomass Bioenergy 2012, 38, 68–94.

[7] C. Zhang; Z. Zhang; L. Zhang; Q. Li; C. Li; G. Chen; S. Zhang; Q. Liu; X. Hu. Biores. Technol. 2020, 304, 123002.

[8] S. Czernik; A. V. Bridgwater. Energy Fuels 2004, 18, 590–598.

[9] A. Effendi; H. Gerhauser; A.V. Bridgwater. Renewable Sustainable Energy Rev. 2008, 12, 2092–2116.

[10] Q. Lu; L. Wen-Zhi, Z. Xi-Feng. Energy. Conv. Manag. 2009, 50, 1376 1383.

[11] S. Zhang; X. Li; Q. Li; Q. Xu; Y. Yan. J. Anal. Appl. Pyrolysis 2011, 92, 158–163.

[12] C. Pan; A. Chen; Z. P. Liu; H. Lou; X. Zheng. Bioresource Technol. 2012, 125, 335–339.

[13] J. Xie; D. Su; X. Yin ; C. Wu; J. Zhu. Int. J. Hydrogen Energy 2011, 36, 15561–15572.

[14] G. P. S. Maciel; M.E. Machado; J.A. Barbará; D.D. Molin; E.B. Caramão; R.A. Jacques. Biomass Bioenergy 2016, 85, 198–206.

[15] S. Ren; X. P. Ye; A. P., J. Borole. Anal. Appl. Pyrolysis 2017, 123, 16–18.

[16] D. Tomasini; F. Cacciola; F. Rigano; D. Sciarrone; P. Donato; M. Beccaria; E. B. Caramão; P. Dugo; L. Mondello. Anal. Chem. 2014, 86, 11255–11262.

[17] A. Le Masle; D. Angot; C. Gouin; A. D'Attoma; J. Ponthus; A. Quignard; S. Heinisch. J. Chromatogr. A 2014, 1340, 90–98.

[18] E. Lazzari; K. Arena; E.B. Caramão; M. Herrero. J. Chromatogr. A 2019, 1602, 359–367.

[19] M. Sarrut; A. Corgier; G. Grétier ; A. Le Masle ; S. Dubant; S. Heinish. J. Chromatogr. A 2015, 1402, 124–133.

[20] F. Cacciola; T. Kumm; G. Dugo; L. Mondello. J. Chromatogr. A 2008, 1184, 335–368.

[21] M. Herrero; E. Ibáñez; A. Cifuentes; J. Bernal. J. Chromatogr. A 2009, 1216, 7110–7129.

[22] F. Cacciola; F. Rigano; P. Dugo; L. Mondello. TrAC Trends Anal. Chem. 2020, 127, 115894.

[23] D.R. Stoll; P. W. Carr. Anal. Chem. 2017, 89, 519–581.

[24] L. Monteiro; M. Herrero; Anal. Chim. Acta 2019, 1083, 1–18.

[25] Onorevoli, B., Machado, M. E., Dariva, C., Franceschi, E., Krause, L. C., Jacques, R. A., Caramão, E. B., Ind. Crops Prod. 2014, 52, 8–16.

[26] R.V.S. Silva; V.B. Pereira; K.T. Stelzer; T.A. Almeida; G.A. Romeiro; D.A. Azevedo. Biomass Bioenergy 2019, 123, 78–88.

[27] E. Lazzari; A. dos S. Polidoro; B. Onorevoli; T. Schena ; A.N. Silva; E. Scapin; R.A. Jacques; E.B. Caramão. Renewable Energy 2019, 135, 554–565.

[28] A dos S. Polidoro; E. Scapin; E. Lazzari; A. N. Silva; A. L. Santos; E. Caramão; R. A. Jacques. J. Anal. Appl. Pyrol. 2018, 129, 43–52.

[29] U. W. Neue. J. Chromatogr. A 2005, 1079, 153−161.

[30] M. Camenzuli; P. J. Schoenmakers. Anal. Chim. Acta 2014, 838, 93–101.

[31] ANVISA. Agência Nacional de Vigilância Sanitária, Resolution-899 of May 29th, 2003, Brazil, 2003.

[32] E. Lazzari; T. Schena; C. T. Primaz; G. M. P. Silva; M.E. Machado; C. A. L. Cardoso; R.A. Jacques; E. B. Caramão. Ind. Crops Prod. 2016, 83, 529–536.

[33] C. T. Primaz; T. Schena; E. Lazzari; E. B. Caramão; R.A. Jacques. Fuel 2018, 232, 572–580.

[34] A. Pattiya. Biores. Technol. 2011, 102, 1959–1967.

[35] M. D. Bispo; J. A. S. Barros; D. Tomasini; C. T. Primaz; E. B. Caramão; C. Dariva; L.C. Krause. J. Earth Sci. Eng. 2016, 6, 235–244.

[36] T. M. Almeida; M. D. Bispo; A. R. T. Cardoso; M. V. Migliorini; T. Schena; M. C. V. de Campos; M. E. Machado; J. A. López; L. C. Krause ; E. B. Caramão ; J. Agric. Food Chem. 2013, 61, 6812–6821.

[37] Filho, P. J. S., Silveira, L. A., Betemps, G. R.,Oliveira, P. K., Sampaio, D. M., Santos, D. F., Microchem. J. 2019, 152, 1–10.

[38] G. A. Helfer; F. Bock; L. Marder; J. C. Furtado; A. B. da Costa; M. F. Ferrão. Quim. Nova 2015, 38, 575–579.

[39] F-X. Collard; J. Blin. Ren Sustainable Ene Rev. 2014, 38, 594–608.

[40] E. Lazzari; T. Schena; M. C. A. Marcelo; C. T. Primaz; A. N. Silva; M. F. Ferrão; T. Bjerk; E. B. Caramão. Ind. Crops Prod. 2016, 111, 856–864.

[41] J. Kim. Bioresour. Technol. 2015, 178, 90–98.

7.0 Application of compressed fluid–based extraction and purification procedures to obtain astaxanthin-enriched extracts from *Haematococcus pluvialis* and characterization by comprehensive two-dimensional liquid chromatography coupled to mass spectrometry

The green microalga *Haematococcus pluvialis* has been widely studied due to its capacity to accumulate great amounts of astaxanthin, a high-value carotenoid with biological activities. In the present work, two green compressed fluid–based processes, pressurized liquid extraction (PLE) and supercritical antisolvent fractionation (SAF), are integrated to obtain an astaxanthin-enriched extract from this microalga. PLE was carried out using pressurized ethanol as solvent, for 20 min, at 10 MPa, and 50 °C as extraction temperature.

Subsequently, the obtained extract was processed by SAF to further purify the carotenoid fraction. The SAF process was optimized using a 3-level factorial experimental design and considering three experimental variables: (i) CO_2 pressure (10–30 MPa), (ii) percentage of water in the PLE extract (20–50%), and (iii) PLE extract/supercritical-CO_2 flow rate ratio (0.0125–0.05).

Total carotenoid content was evaluated in both extracts and raffinates. Best results were obtained at 30 MPa, 0.05 feed/SC-CO_2 mass flow rate, and 20% (*v/v*) of water in the feed solution, achieving values of 120.3 mg g−1 carotenoids in extract (in the SAF extract fraction), which were significantly higher than those obtained in the original PLE extract. In parallel, a new fast two-dimensional comprehensive liquid chromatography (LC×LC) method was optimized to get the full carotenoid profile of these extracts in less than 25 min. This is the first time that the use of a C30 column is reported in an on-line LC×LC system.

7.1 Introduction

Microalgae are widely considered as a potential source of bioactive compounds with beneficial properties for human health.

These photosynthetic organisms are used in several fields such as nutraceutical, cosmetic, and food industries, mainly thanks to their high content in natural pigments [1]. Biologically, carotenoids have an important role in many physiological functions, including light-harvesting and protection against oxidation and excess of light, and even they can also contribute as growth regulators. It is known that carotenoids are commonly associated with other natural compounds including fatty acids, sugars, or proteins, which can also influence their chemical and biological properties [2]. Astaxanthin, β-carotene, lutein, canthaxanthin, and lycopene are the most commercially used carotenoids [1].

Among these, astaxanthin from *Haematococcus pluvialis* is one of the most demanded products due to its biological activities such as antioxidant, UV-light protection, and anti-inflammatory.

Besides, natural astaxanthin is preferred over its synthetic counterpart.

There are many natural sources of astaxanthin, such as salmon, trout, red sea bream, shrimp, lobster, and fish eggs, but *Haematococcus pluvialis* is considered the richest source of natural astaxanthin. In fact, accumulation of up to 30 mg of astaxanthin and derivatives per gram of dry biomass has been reported at an industrial scale [3].

Due to the huge interest in carotenoids, their extraction from natural matrices, specifically microalgae, is a hot research topic. Traditionally, the recovery of these compounds implied the use of high volumes of organic solvents and required long extraction times. Nowadays, these techniques are being replaced bymore advanced and environmentally friendly processes such as supercritical fluid extraction (SFE) or pressurized liquid extraction (PLE) [4]. PLE is based on the use of solvents at high temperatures and pressures, which helps to maintain the solvent in its liquid state and provides a fast and efficient extraction process. Moreover, generally recognized as safe

(GRAS) solvents such as ethanol, water, or ethyl lactate are preferred [5]. One of the most influential parameters when dealing with PLE is the extraction temperature.

It is known that high temperatures, along with high pressures, increase solubility and mass transfer rates since the solvent penetrates deeper and easier into the matrix. This way, a significant enhancement on the extraction rates is observed; on the other hand, high extraction temperatures could directly affect the stability of thermolabile compounds.

Regarding carotenoids, as they are natural antioxidants, most extraction studies reveal that very high temperatures may induce their degradation [6], although good results have been reported for the extraction of carotenoids from *Porphyridium cruentum* using PLE with ethanol at 125 °C [7]. Green compressed fluid–based extraction techniques, including PLE, SFE, and gas-expanded liquids (GXL), have been previously reported for the extraction of astaxanthin from *H. pluvialis* [8, 9]. PLE has the advantage of offering high extraction yields and faster extraction processes compared with the other mentioned techniques and its usefulness for the extraction of carotenoids from other microalgae has also been demonstrated [10]. However, the selectivity offered by PLE towards those compounds is not extremely high. For this reason, purification protocols may be needed to obtain fractions enriched in target compounds for further applications.

In this regard, supercritical antisolvent fractionation (SAF) has already been demonstrated to be useful for the fractionation and concentration of different bioactive compounds [11–14]. Briefly, SAF is based on the selective precipitation of target compounds depending on their polarity and solubility between an organic solvent and supercritical CO_2.

During the process, continuous contact between a relatively polar liquid extract with supercritical CO_2 is established. During this period, supercritical CO_2 is able to solubilize the less polar fraction (including solvents and compounds) of the liquid extract that is recovered by downstream pressure reduction (called SAF extract). Meanwhile, more polar compounds not soluble in supercritical CO_2 precipitate in the

so-called raffinate [5]. Thus, SAF is a feasible green alternative to further enrich liquid extracts thanks to the solvent properties obtained under pressurized conditions, although its use has not been reported so far for natural carotenoid purification.
Moreover, it provides the additional advantage of producing a dried extract.
To monitor the performance of extraction and purification procedures, appropriate analytical methods are needed to get proper information about the composition of the generated fractions. In this regard, the use of liquid chromatography coupled to mass spectrometry (LC–MS) may be the ideal analytical tool considering the nature of carotenoids. However, there are highly complex samples for which the use of multidimensional approaches to obtain higher separation power may be justified. In this regard, on-line two-dimensional comprehensive liquid chromatography (LC×LC) has already been used for the characterization of carotenoids present in different food-related samples [15–18]. These applications benefit from the increased separation performance provided by the coupling between a normal phase (NP) separation in the first dimension and a reversed-phase (RP) separation in the second dimension, using cyano and C18 columns, respectively. The separation performance of those developments was by far better than the attainable by conventional LC, although relatively long analysis times (ca. 100 min) should be assumed [15–18].
Here, a new approach is studied thanks to the use of amino and C30 columns in the first and second dimensions, respectively, looking for a significant reduction in overall ^{2}D analysis time. C30 is the stationary phase of choice when dealing with the carotenoid analysis from complex samples by conventional LC [19], although there are no previous reports related to its use in LC×LC.
Thus, the present work aimed to develop an integrated compressed fluid–based process combining PLE and SAF to efficiently obtain for the first time an astaxanthin-enriched fraction from *H. pluvialis* microalgae. In parallel, a new LC×LC method was also established for the separation and identification of the carotenoids, both free and esterified, contained in the produced fractions.

7.2 Materials and methods

7.2.1 Samples and Reagents

Freeze-dried Haematococcus pluvialis were kindly provided by Microphyt (Baillargues, France) and stored at 4 °C until use. HPLC-grade solvents including methyl tert-butyl ether (MTBE), methanol, acetone, and ethanol were purchased from VWR (Leuven, Belgium). Sea sand (0.25–0.30-mm particle diameter) was acquired from Panreac (Castellar del Vallés, Spain). Butylated hydroxytoluene (BHT), canthaxanthin, and β-carotene (from Anacystis nidulans algae) were obtained from Sigma–Aldrich (St. Louis, MO, USA). Lutein (from Echinacea purpurea) was purchased from Chengdu Biopurify Phytochemicals Ltd. (Chengdu, China).
Astaxanthin was purchased from Acros Organics (Geel, Belgium), whereas zeaxanthin was acquired from Carbosynth Limited (Berkshire, UK). Ultrapure water used was obtained from a Milli-Q system (Millipore, Billerica, MA, USA). For supercritical antisolvent fractionation experiments, carbon dioxide (99%purity) was supplied by Carburos Metálicos (Barcelona, Spain).

7.3 Pressurized liquid extraction

Pressurized ethanol extractions of dried biomass were carried out using an accelerated solvent extractor (ASE 200, Dionex, Sunnyvale, CA, USA), equipped with a solvent controller unit. Firstly, an optimization of PLE conditions was performed employing different extraction temperatures (50 to 200 °C, Electronic Supplementary Material (ESM) Table S1). For those extractions, 1.0 g of dried algal biomass was loaded into an 11-mL stainless steel extraction cell sandwiched between 4.0 g of sea sand. Pressure and extraction time were set at 10.5 MPa and 20 min, respectively, and pure ethanol was chosen as the extraction solvent, based on previous experience. All experiments

were performed in duplicate. The extracts obtained were dried using a gentle stream of nitrogen, protected from light, and stored at − 20 °C until further analysis.

Extraction yield (% extract dry weight/initial biomass dry weight) and total carotenoids (mg g^{-1} carotenoids in extract) were quantified to select the optimum extraction conditions.

Under those extraction conditions, successive extractions were performed to obtain 500 mL of extract, to continue with the purification step.

7.4 Supercritical antisolvent fractionation

SAF of the optimum PLE extract was carried out in a Speed Helix supercritical fluid extractor (Applied Separations, Allentown, PA, USA). A scheme of the SAF process is shown in Fig. 1. The PLE extract obtained under optimum conditions was diluted properly to obtain different percentages of water needed according to the planned experimental design (20, 35, and 50% *v/v* or 24, 40.5, and 55.8% *w/w*, respectively). These extract solutions were kept in the dark at − 20 °C to avoid degradation until their use for the antisolvent fractionation experiments. The fractionation process was accomplished as follows (Fig. 1): the feed (PLE extract with water) from the extract reservoir (1) was continuously pumped by a high-pressure pump (2) at a selected flow rate (0.1 to 0.5 mL min^{-1}) and reached a T-tube device where it was mixed with CO_2. CO2 was provided from a pressurized cylinder (3), subcooled, and pumped using another high-pressure pump (4) at a constant flow rate (8.244 mL min^{-1} or 8 g min^{-1}). Then, the mixture (feed and CO_2) reached the separation chamber (6), in which the compounds that were not soluble in supercritical CO_2 + EtOH mixture precipitated and were collected at the bottom of the separator (this non-soluble fraction is called raffinate).

During the separation process, the temperature was fixed at 40 °C and it was controlled by an oven (5). An upstream backpressure valve (7) kept constant the fractionation pressure throughout the experiment. Finally, the compounds soluble in supercritical

CO_2 + EtOH mixture proceeded to the next vessel where CO_2 pressure was decreased to turn CO_2 into gas to allow the recovery of those components in the second separation chamber (the soluble fraction is called extract) (8), which was kept at room temperature (25 °C). Both raffinate and extract were collected separately in plastic bottles and dried. The SAF process time was set at 120 min for each experiment.

All dried fractions were stored at − 20 °C until analysis. The recovery was determined gravimetrically, as the ratio of the mass of dry extract or raffinate recovered and the mass of dry PLE extract fed and expressed as a percentage.

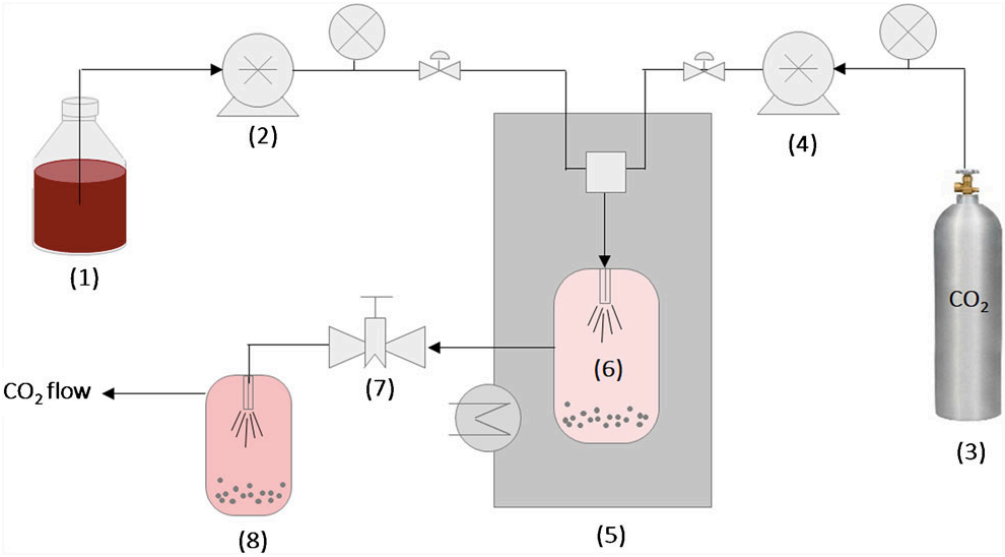

Figure 1: Scheme of the supercritical antisolvent fractionation equipment: 1, PLE extract reservoir; 2, high-pressure liquid pump; 3, CO_2 cylinder; 4, high-pressure CO_2 pump; 5, oven; 6, separator 1 (raffinate collection cell); 7, back pressure regulator; 8, separator 2 (extract collection cell).

7.5 Experimental design

An experimental design was applied to optimize the supercritical antisolvent fractionation process. A 3-level factorial experimental design 23 (including three center points) was proposed based on three factors: pressure (10 to 30 MPa), flow rate ratio (*w/w*) of feed (PLE extract) and supercritical CO_2 (0.01–0.05), and percentage of water in feed (20 to 50%, *v/v*). The response variables studied were recovery (% dry

weight of extract or raffinate/dry weight of PLE extract), total carotenoids (mg g^{-1} carotenoids in extract or raffinate), and total astaxanthin content (mg g^{-1} astaxanthin in extract or raffinate). The described experimental design involved 11 experimental runs. Both raffinate and extract from the application of each process condition, as well as the original PLE extract, were studied. Data analysis was performed using response surface methodology (RSM) using Statgraphics Centurion XVI software (StatPoint Technologies, Inc., Warrenton, VA, USA). The influence of independent parameters on the response variables was studied at a 95% level of confidence. Moreover, a linear regression model for each parameter (Yi) was proposed. The equation was:

$$Y_i = k_0 + k_1 \times P + k_2 \times F + k_3 \times W + k_{1,2} \times P \times F + k_{1,3} \times P \times W + k_{2,3} \times F \times W + k_{1,2,3} \times P \times F \times W + error \quad (1)$$

where P is the pressure, F is the feed/supercritical-CO_2 flow rate ratio, W is the percentage of water in feed (v/v), κ_0 is a constant, κ_1, κ_2, and κ_3 are the independent linear effects, $\kappa_{1,2}$, $\kappa_{1,3}$, and $\kappa_{2,3}$ are the linear effects of two factors, and $\kappa_{1,2,3}$ is the effect of the three-factor interaction. The effect of each factor and its statistical significance, for each of the response variables, were analyzed from the standardized Pareto chart. The response surfaces of the respective mathematical models were also obtained, and the significances were accepted at $p \leq 0.05$. A multiple response optimization was performed by the combination of the three experimental factors to maximize the desirability function for the response variables in the extract since the goal was to obtain an astaxanthin-enriched fraction.

Nevertheless, both extracts and raffinates were analyzed in terms of recovery (% dry weight of extract or raffinate/dry weight PLE extract), total carotenoid content (mg carotenoid per g extract or raffinate) by using a spectrophotometric method, and total astaxanthin content (mg astaxanthin per g extract or raffinate) determined by HPLC

7.6 Total carotenoid determination

A spectrophotometric method was used to determine the total carotenoid content, based on their characteristic absorbance, as previously described [7]. PLE extracts and fractions obtained from the SAF process were dissolved in ethanol at a concentration of 0.1 mg mL^{-1} and their absorbance was recorded at a specific wavelength (470 nm). The calibration curve was constructed using astaxanthin as an external standard (0.16–10.00 μg mL^{-1}). Results were expressed as milligram carotenoids per gram extract or raffinate.

7.7 Chemical characterization of *H. pluvialis* extracts and SAF fractions by liquid chromatography coupled to diode array detection

The profiles of carotenoids of the H. *pluvialis* extracts and the different SAF fractions were firstly determined using HPLC–DAD, according to a previously developed method [20], with some modifications. An Agilent 1100 series liquid chromatograph (Santa Clara, CA, USA), coupled to a diode array detector (DAD) was used to analyze all samples. The analytical conditions included the use of a YMC-C30 reversed-phase column (250 × 4.6 mm, 5 μm; YMC Europe, Schermbeck, Germany) and a YMC-C30 pre-column (10 × 4 mm, 5 μm), using the following mobile phases: methanol–MTBE–water (90:7:3, *v/v/v*) as solvent A and methanol–MTBE (10:90, *v/v*) as solvent B. A linear gradient was employed for elution as follows: 0 min, 0% B; 20 min, 30% B; 35 min, 40% B; 45 min, 80%B; 50min, 100%B; 52min, 0%B. The injection volume was 10 μL while the flow rate was 0.8 mL min^{-1}. The diode array detector was set at 280, 450, and 660 nm, although spectra from 240 to 770 nm were recorded (peak width 0.1 min (2 s), slit 4 nm). The instrument was controlled by LC ChemStation 3D Software Rev. B.04.03 (Agilent Technologies, Santa Clara, CA, USA). This method was also employed to estimate astaxanthin amounts in the extracts and SAF fractions. All

samples were dissolved in pure ethanol at an appropriate concentration (1–10 mg mL^{-1}) and filtered using 0.45-µm nylon filters before analysis. External standard calibrations were performed using at least five different concentrations of astaxanthin (3.1 to 50.0 µg mL^{-1}) dissolved in ethanol that were analyzed in triplicate. Good linearity was obtained in the mentioned range ($R_2 = 0.986$). Moreover, appropriate limits of detection (LOD = 0.28 µg mL^{-1}) and limits of quantification (LOQ = 0.93 µg mL^{-1}) calculated as a concentration giving a signal to-noise ratio equal to 3 and 10, respectively, were obtained. Results were expressed as mg g^{-1} astaxanthin in extract or raffinate.

7.8 Chemical characterization of *H. pluvialis* extracts and SAF fractions by comprehensive two-dimensional liquid chromatography

For the characterization of the specific carotenoids contained in *H. pluvialis* extracts and SAF fractions, a new LC×LC method was developed. The instrumentation consisted of a first dimension (^{1}D) composed by an Agilent 1200 series liquid chromatograph (Agilent Technologies, Santa Clara, CA) equipped with an autosampler. The second dimension (^{2}D) separation was performed using an additional LC pump (Agilent 1290 Infinity). Both dimensions were connected by an electronically controlled two-position ten-port switching valve (Rheodyne, Rohnert Park, CA, USA) acting as a modulator equipped with two identical 30-µL sampling loops. The modulation time of the switching valve was 1.0 min. The separation was recorded through the DAD at 450 nm (maximum sampling rate selected, 20 Hz), although the system was also connected to an Agilent 6320 Ion Trap mass spectrometer equipped with an atmospheric pressure chemical ionization (APCI) interface. MS detection was performed using the following settings using positive ionization mode: capillary voltage, − 3.5 kV; drying temperature, 350 °C; vaporizer temperature, 400 °C; drying gas flow rate, 5 L min^{-1}; nebulizer gas pressure, 60 psi; corona current, 4000 nA; and m/z 150 to 1300. The LC data were elaborated and visualized using LC Image software (version 1.0, Zoex Corp., Houston, TX).

The finally optimized normal phase × reversed phase (NP×RP) method involved the use of the following separation conditions:

^{1}D separation: A Hypersil Gold Amino column (150 × 1.0 mm, 3 μm, Thermo Scientific, Waltham, MA, USA) was used, eluted under isocratic conditions using hexane as mobile phase at 20 μL min^{-1}.

^{2}D separation: A Thermo Accucore C30 partially porous column (50 × 4.6 mm, 2.6 μm, Thermo Scientific, Waltham, MA, USA) was used using water/acetonitrile (20:80, *v/v*, solvent A) and 2-propanol (solvent B) as mobile phases eluted following full-in-fraction repetitive gradients as follows: 0 min, 10% B; 0.6 min, 90% B; 0.75, 90% B; 0.76 min, 10%B; 1.0 min, 10% B. The flow rate employed was 3.0 mL min−1 and the column temperature was held at 60 °C. The effluent from the ^{2}D column was split before entering the MS instrument so that the flow rate introduced in the MS detector was ca. 0.6 mL min^{-1}.

Practical peak capacity values were determined using the approach proposed by Li et al. [21] whereas method orthogonality was estimated following the asterisk equations [22].

7.9 Results and discussion

7.9.1 Extraction of carotenoids from *H. pluvialis* and purification by supercritical antisolvent fractionation process

Astaxanthin is present in H. pluvialis both in its free form and in a more stable esterified form bound to different fatty acids [3]. Moreover, astaxanthin can form mono- and di-esterified derivatives, thus, increasing the complexity of the whole carotenoid composition naturally present in the microalgae.

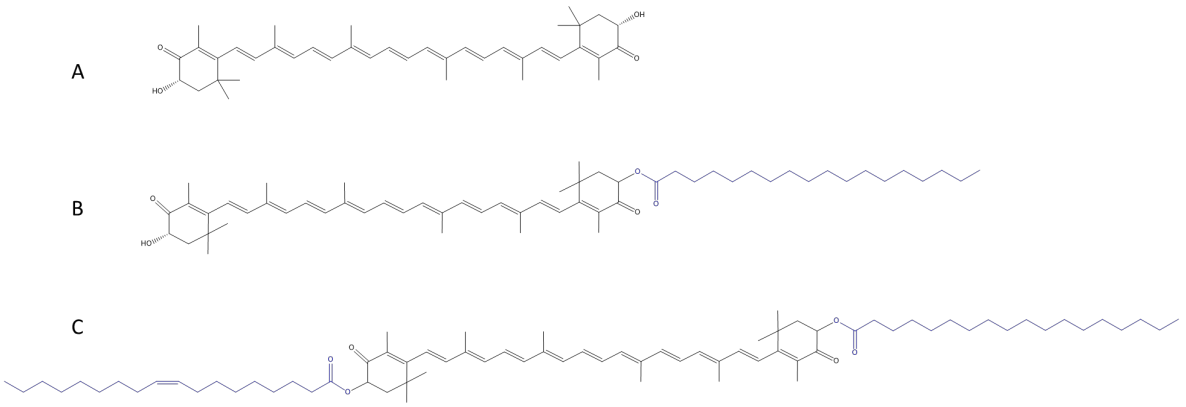

Figure 2: Chemical structures of A) astaxanthin, B) astaxanthin monoester (C18:0), and C) astaxanthin diester (C18:1/C18:0)

In this sense, the extraction of carotenoids from *H. pluvialis* is challenging considering that the complex chemical composition also implies very different polarities of its carotenoids. Based on our previous experience, PLE using ethanol as a solvent was considered as the most suitable GRAS alternative to extract carotenoids from *H. pluvialis*.

The combined use of PLE and SAF provides higher selectivity towards the compounds of interest whereas the use of PLE in the first step allows obtaining high extraction yields. Fast optimization of the extraction temperature at constant pressure (10.5 MPa) and time (20 min) was performed. As shown in Table 1, the use of 50 °C was considered optimum since it allowed working with a more carotenoid-enriched extract.

Table 1. Extraction yield and total carotenoids content (mean ± sd) obtained in *H. pluvialis* extracts using pressurized ethanol at 50, 100, 150 and 150 ºC. Other PLE extraction conditions: pressure, 10.5 MPa; extraction time, 20 min. Different superscript letters indicate statistically significant differences ($p < 0.05$) within the same column. CE: conventional extraction.

Temperature *ºC*	Extraction yield *%*	Total carotenoids *mg g^{-1} extract*	Total carotenoids *mg g^{-1} biomass*
50	5.44 ± 0.17 ^{d}	91.57 ± 6.83 ^{a}	4.97 ± 0.21
100	8.28 ± 0.40 ^{c}	67.52 ± 6.52 ^{b}	5.61 ± 0.81
150	11.69 ± 0.35 ^{b}	47.14 ± 9.75 ^{c}	5.49 ± 0.97
200	26.42 ± 1.79 ^{a}	24.65 ± 5.26 ^{d}	6.51 ± 0.95

To track the effect of the subsequent SAF process on the chemical composition of the extract, an LC–DAD method previously employed to reveal the carotenoid pattern of other microalgae was applied to the optimum PLE extract. ESM Fig. 3 shows the profile obtained. As can be observed, the extract was relatively complex with multiple peaks belonging to carotenoids according to their UV–Vis spectra.

Astaxanthin, canthaxanthin, lutein, and β-carotene could be identified in the extract by coelution with commercial standards.

Moreover, a high number of peaks possessed typical UV–Vis spectra with a maximum around 474 nm, compatible with astaxanthin. According to their retention windows [23], these compounds were tentatively considered as astaxanthin monoesters and astaxanthin diesters. Once the most suitable conditions for the pressurized extraction of carotenoids from *H. pluvialis* were selected, a relatively high volume of extract was generated to be employed as feed for the SAF process optimization. Up to 500 mL of extract was prepared with a total concentration of solids of 3.12 g L^{-1} of extract solution. To study the most important variables influencing the SAF process using supercritical CO_2 (sc-CO2) as the antisolvent, an experimental design was devised and applied. Feed to supercritical CO_2 ratio, process pressure and the amount of water in

the feed have repeatedly been shown as the factors that have the greatest impact on fractionation performance [13, 14, 24].

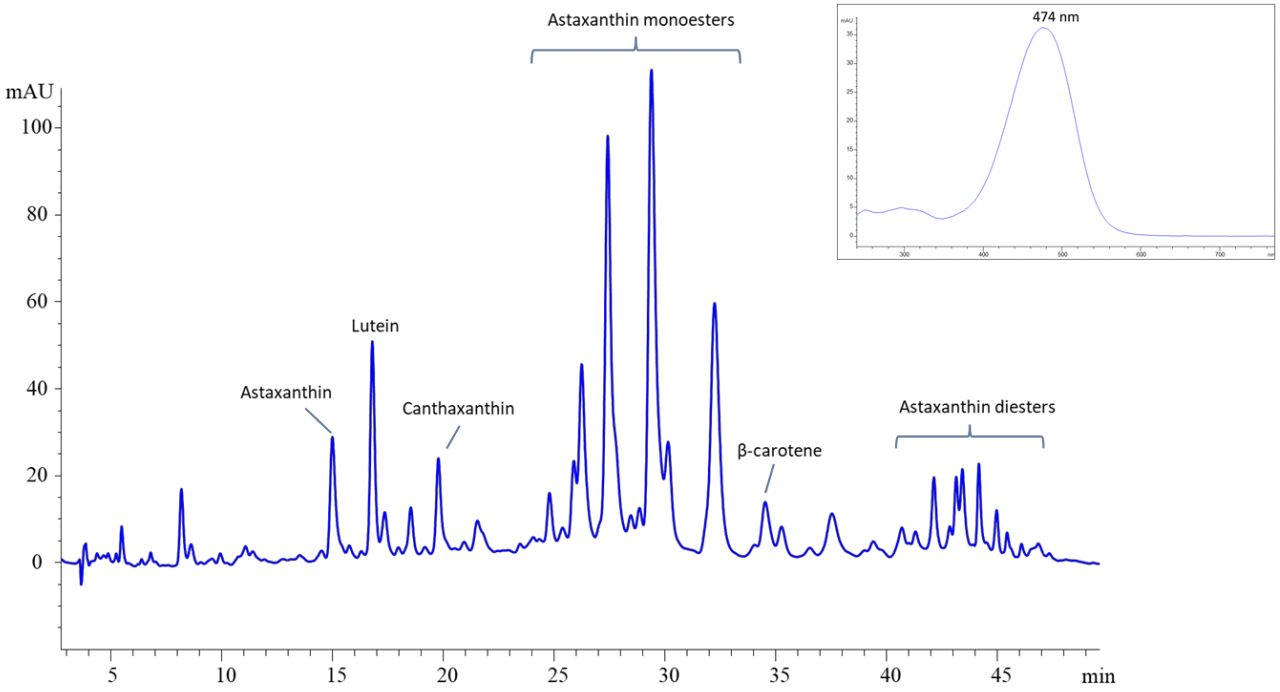

Figure 3: Chromatogram (450 nm) obtained by HPLC-DAD from the optimum Haematococcus pluvialis PLE extract obtained using pressurized ethanol at 50 °C and UV-Vis spectrum of astaxanthin and astaxanthin-esters

The performance of the process was monitored in terms of recovery, total carotenoid, and astaxanthin content in both SAF extract and raffinate.

Astaxanthin content was determined as the sum of the concentration of all the peaks contained in the LC–DAD chromatograms possessing the typical astaxanthin UV–Vis spectra.

Table 2 shows the results obtained under each process condition for extracts and raffinates. As can be observed, the recovery of total carotenoids in the raffinates was generally lower than that in the extracts, as could be expected from the diverse solubility of carotenoids between the water-soluble fraction (raffinate) and the ethanol + SC-CO_2 fraction (extract). For this reason, the analysis of the fractionation performance is focused on the extracts, since this fraction was the most suitable to maximize the recovery of carotenoids. As can be seen in Table 2, the total recoveries

obtained in the extract fractions were very variable, from 17.8 to 88.4%, which implies that there is a significant effect of the studied parameters on the solubility of the components present in the PLE extract on the supercritical CO_2 + ethanol mixture.

Figure 4 shows the standardized Pareto charts for the three response variables studied, together with their corresponding response surfaces. Different bar shadings indicate if the effect is positive or negative over the response variables, whereas the vertical line marks the significance of the effects at the 95% confidence level. As can be observed, for the total recovery (Fig. 4a), the individual influence of the percentage of water in feed and the PLE extract/SC-CO_2 ratio showed a negative effect, although only the first one was significant. The pressure showed a non-significant positive effect. It can be noted that the percentage of water in feed was the most influencing factor, followed by its interaction with the feed/SC-CO_2 ratio, as it can be also observed in their corresponding response surfaces (Fig. 4b, c). In terms of total carotenoid content as well as total astaxanthin content, both pressure and PLE extract/SC-CO_2 ratio exhibited a positive and significant effect, with small differences in terms of influence, whereas the content of water in the feed showed a negative effect, as it is shown in Fig. 4d, g. These two factors, pressure and PLE extract/SC-CO2 flow rate ratio, are strongly related to mass transfer and, thus, the use of higher pressures and feed ratios meant that more carotenoids would be available to be extracted. Figure 4e, f, h, i show the response surfaces of total carotenoid and total astaxanthin content, respectively, when percentage of water in feed is fixed. In terms of percentage of water in feed, as expected, compounds from PLE extract were more soluble in ethanol than in water; thus, as the proportion of ethanol (and less % water) in the feed was increased, a higher amount of compounds were recovered in the mixture SC-CO_2 + EtOH (extract).

Table 2. Experimental design of the factors and values of the response variables studied for the *extract* and *raffinate*.

Exp.	P (bar)	Feed/SC-CO_2	Water in feed	***Extract***			***Raffinate***		
				Recovery	Total carotenoids	Astaxanthin	Recovery	Total carotenoids	Astaxanthin
			(% v/v)	(wt %)	(mg g^{-1})	content (mg g^{-1})	(wt %)	(mg g^{-1})	content (mg g^{-1})
1	100	0.05000	20	36.5	31.5	29.0	63.5	11.2	6.0
2	300	0.05000	20	42.4	120.3	103.3	57.6	9.8	5.6
3	100	0.01250	20	66.5	9.7	9.6	33.5	11.5	6.8
4	300	0.01250	20	88.4	47.7	39.8	11.6	2.3	0.4
5	200 (CP)	0.03125	35	31.6	47.8	24.9	68.4	3.7	0.7
6	200 (CP)	0.03125	35	47.8	62.7	43.1	52.2	1.3	0.6
7	200 (CP)	0.03125	35	31.7	52.6	30.1	68.3	1.1	0.5
8	100	0.05000	50	25.6	13.7	10.9	74.4	48.9	47.4
9	300	0.05000	50	24.7	69.7	63.3	75.3	48.1	47.5
10	100	0.01250	50	17.8	12.4	8.2	82.2	18.2	17.1
11	300	0.01250	50	24.6	54.7	45.7	75.4	20.6	20.2

CP: experimental design central point.

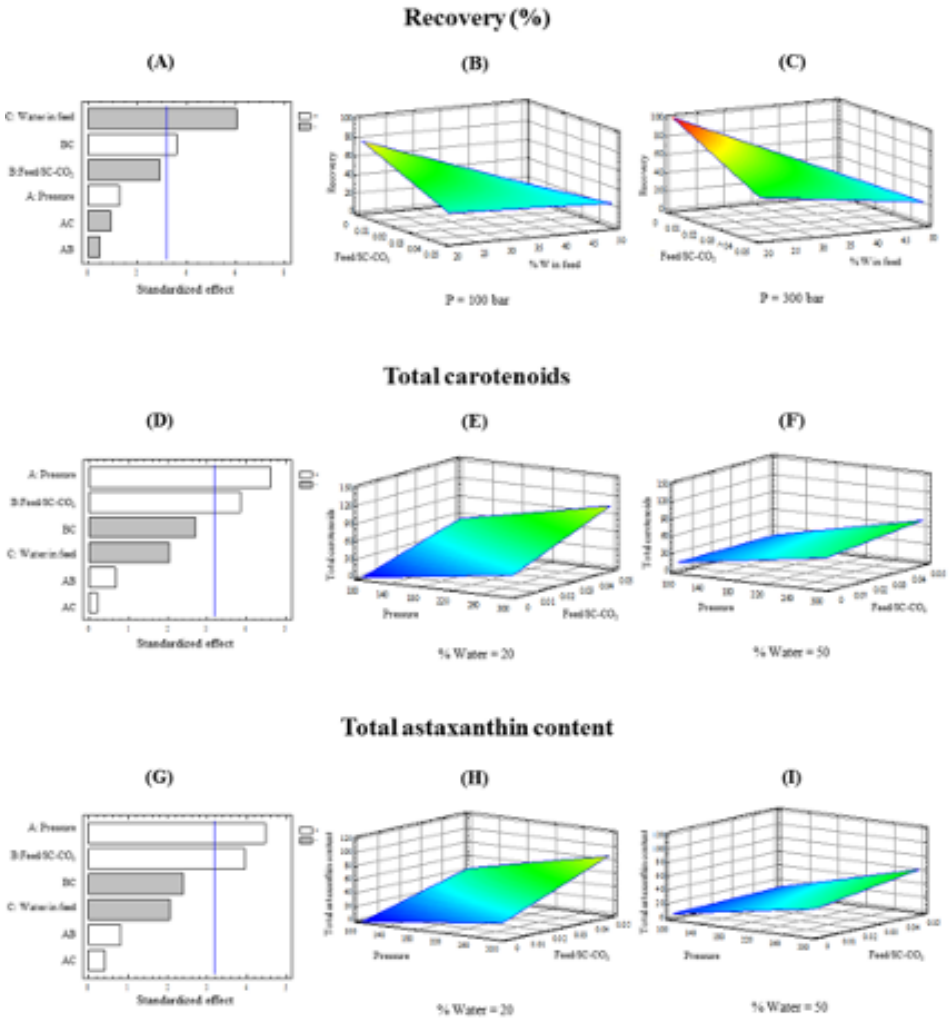

Figure 4: Standardized Pareto charts obtained for recovery (A), total carotenoids content (D) and total astaxanthin content (G) for *extract* fraction (white bars and grey bars show positive and negative effects, respectively), and their corresponding response surfaces, keeping constant the response variable that influences the least (pressure for recovery and % water in feed for carotenoid and astaxanthin content).

In general, the increase in fractionation pressure always increased the recovery of carotenoids in the extracts, as can be deduced from Table 2. Moreover, when the pressure was fixed, higher feed/SC-CO_2 ratios were more favorable. Lastly, the percentage of water in the feed influenced the total amount of carotenoids recovered depending on the extraction pressure.

At higher pressures (30 MPa), smaller ratios provided better carotenoid recoveries, whereas at lower pressures (10 MPa), the opposite trend was found. An ANOVA of

the experimental design was employed to statistically assess the recovery of total carotenoids in the SAF extract. Apart from the confirmation of the statistical influence of pressure and feed to SC-CO2 ratio at the 95% confidence level, the model presented an R-squared (R_2 = 0.97) and adjusted R squared (R_2 = 0.90) values that indicated a close agreement between the experimental results and theoretical values.

To determine the extraction conditions to obtain the most purified SAF fraction with the highest possible recovery, a multiple response optimization was performed to maximize all the studied variables simultaneously. The estimated response surface obtained for the multiple optimization can be observed in Fig. 5. Additionally, the optimum conditions and the estimated responses proposed by the model, along with those obtained experimentally at those conditions, are shown in Table 3. Consistently, the experimental results for the extraction performed according to the optimum conditions were similar to those predicted.

Overall, the SAF fraction obtained in SC-CO_2 + ethanol mixture (extract) was effectively enriched in carotenoids (up to 1.3-fold compared with the PLE original extract) when the process was performed at 30 MPa, and 20% (v/v) of water in the mixture and 0.05 PLE extract/SC-CO2 flow rate ratio.

Under those conditions, the carotenoid content was 120.3 mg g^{-1} carotenoids in extract. These results show the first application of SAF for the purification of natural carotenoids.

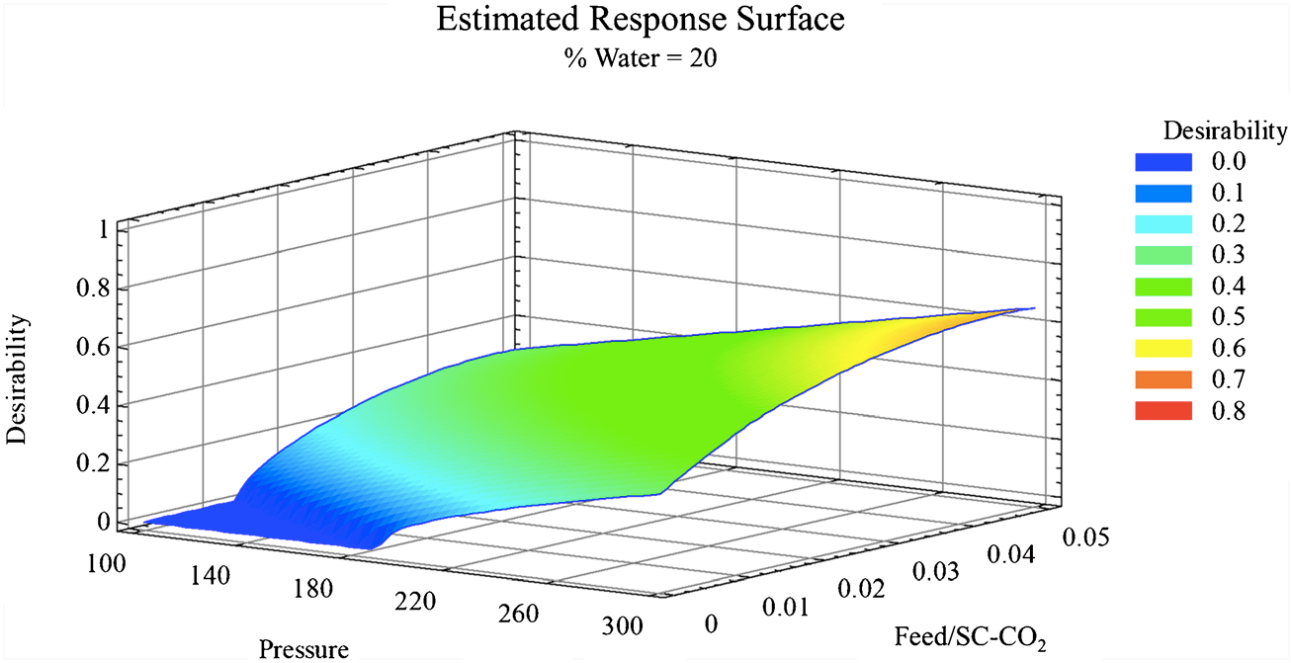

Figure 5: Estimated response surface obtained for the multiple response optimization for SAF extract fraction.

Table 3. Optimum and experimental factor and response values obtained for the multiple response optimization for extract fraction.

Factors			**Responses**		
Factor	*Optimum*	*Experimental*	*Response*	*Optimum*	*Experimental*
Pressure (MPa)	30	300	Recovery (%)	50.5	42.4
Feed/SC-CO_2 flow rate ratio	0.046	0.05	Total carotenoid content (mg g^{-1})	97.8	120.3
% Water in feed	20.0	20.0	Total astaxanthin content (mg g^{-1})	81.2	103.3

7.9.2 Characterization of extracts using comprehensive two-dimensional liquid chromatography coupled to mass spectrometry detection

Up to now, the characterization of carotenoids present in microalgae extracts has been carried out by conventional HPLC using C30 columns. However, even if this type of column is very well suited for the separation of carotenoids; very complex samples cannot be completely resolved. As can be observed in Fig. 3, the chemical composition present in the optimum *H. pluvialis* PLE extract (50 °C) could be considered complex enough to justify the use of multidimensional approaches to improve the separation of its components and to resolve some of the coelutions found. In this line, the use of on-line comprehensive two-dimensional LC (LC×LC) has been previously demonstrated as very powerful for the separation of carotenoids from other natural sources [15–18, 25]. For this reason, the use of a new LC×LC–MS method for the separation of carotenoids contained in H. pluvialis is proposed here for the first time.

The proposed method was optimized combining NP in the ^{1}D and RP in the ^{2}D. A new column combination, not used before for carotenoid analysis by LC×LC, was selected involving the use of a microbore amino column in the ^{1}D and a short partially porous C30 column in the ^{2}D. A separate optimization of the separation conditions of each dimension was performed. ^{1}D separation conditions were studied including different mobile phases and gradients although, finally, the isocratic elution using hexane as mobile phase provided with proper retention and rapid elution of the carotenoids contained in the sample into the ^{1}D amino column. On the other hand, considering the lack of previous reports including the use of a C30 column in LC×LC setups, different mobile phase compositions and gradients were also tested in the ^{2}D. One minute was established as the target modulation time. The finally selected separation conditions are reported in the "Chemical characterization of *H. pluvialis* extracts and SAF fractions by comprehensive two-dimensional liquid chromatography" section.

Figure 6a shows the separation attainable of the *H. pluvialis* PLE extract using this configuration. Peak assignment is shown in Table 4. As can be observed, a good

resolution between the different components was obtained, being able to separate free carotenoids (including carotenes and xanthophylls) as well as other mono- and di-esterified carotenoids derived from astaxanthin. The main compound found was the astaxanthin-C18:0 monoester (peak 19), although relevant amounts were also found of its C18:1 monoesters (peaks 14, 20, 21), presenting different isomers. Regarding astaxanthin diesters, the C18:1/C18:1 was the most intense (peak 8) together with the C18:0/C18:0 diester (peak 7). Free carotenoids were also detected and tentatively identified, including astaxanthin (peak 24), canthaxanthin (peak 15), lutein (peak 16), and β-carotene (peak 3).

This separation was characterized by a practical peak capacity of 268 while orthogonality degree was estimated at 40%. Although these figures-of-merit are interesting by themselves, it is worth to mention that the whole analysis took less than 25 min, which was nearly half than the original conventional HPLC method, as can be inferred from a comparison between Fig. 3 and Fig. 6.

Thus, the peak capacity achieved is rather high for a 25- min analysis (ca. 11 peaks min^{-1}). This analysis time can be considered as very fast compared with other LC×LC methods applied for carotenoid analysis which are typically around 90–100 min [15–18, 25], and it is, indeed, a significant analytical advantage over the use of conventional LC. The application of this method also allowed establishing a comparison between the original PLE extract used as feed for the SAF process and the enriched extract obtained after purification. As can be observed in Fig. 6 a, b, the chemical composition was not the same comparing both fractions, although astaxanthin derivatives were clearly the main components. Although astaxanthin monoesters were still the main compounds found, the proportions between the whole carotenoid pattern were modified, indicating a possible difference in the solubility of individual components under the SAF processing conditions.

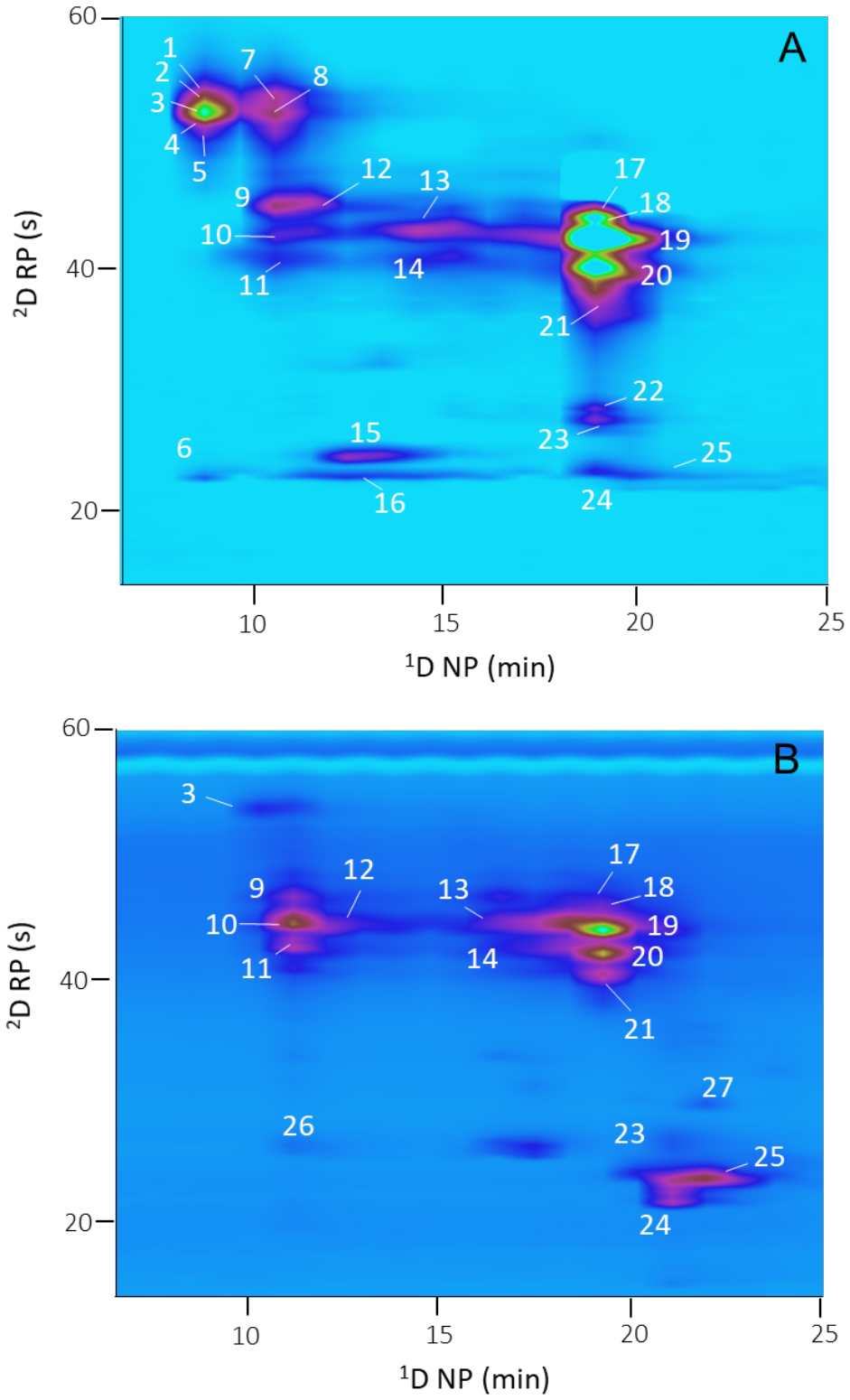

Figure 6: 2D plots (450 nm) of the NP×RP separation of the H. pluvialis PLE extract obtained at 50 °C (a) and the fraction obtained after SAF purification (b). Peak assignment as in Table 3 (for detailed separation conditions, see the "Chemical characterization of H. pluvialis extracts and SAF fractions by comprehensive two-dimensional liquid chromatography" section)

Table 4. Peak assignment, UV–Vis maxima and MS information of the separated peaks and contents of the quantified compounds in the H. pluvialis PLE and SAF extracts.

Peak #	Identification	UV-Vis maxima (nm)	$[M + H]^+$ *m/z*
1	Ast DE ($C_{18:0}/C_{18:1}$)	474	1127.0
2	Ast DE ($C_{18:1}/C_{18:1}$)	474	1125.9
3	β-carotene*	420s, 450, 480	537.0
4	Ast DE ($C_{18:1}/C_{18:2}$)	474	1123.9
5	Ast DE ($C_{18:2}/C_{18:3}$)	474	1119.9
6	Zeaxanthin	420s, 445, 476	569.0
7	Ast DE ($C_{18:0}/C_{18:0}$)	478	1129.2
8	Ast DE ($C_{18:1}/C_{18:1}$)	478	1125.0
9	Astacin-$C_{18:2}$	478	855.9
10	Astacin-$C_{18:3}$	478	853.0
11	Astacin-$C_{18:4}$	478	851.0
12	Ast ME ($C_{18:3}$)	478	857.0
13	Ast ME ($C_{18:0}$)	475	863.3
14	Ast ME ($C_{18:1}$)	475	861.7
15	Canthaxanthin*	474	565.7
16	Lutein*	422, 446, 474	568.9
17	Pheophytin a	412, 666	872.1
18	n.i.	478	865.3
19	Ast ME ($C_{18:0}$)	478	863.3
20	Ast ME ($C_{18:1}$)	478	861.7
21	Ast ME ($C_{18:1}$)	478	861.0
22	Ast ME ($C_{18:2}$)	478	859.8
23	Ast ME ($C_{18:2}$)	478	859.0
24	Astaxanthin*	478	597.6
25	n.i.	420s, 446, 474	
26	n.i.	475	
27	n.i.	420s, 446, 474	

* Identified with a commercial standard; s, spectral shoulder; Ast: astaxanthin; ME: monoester; DE: diester.

This fact could be expected considering the large differences in relative polarity among the carotenoids present in the original PLE extract. In this regard, fewer amounts of β-carotene, as well as astaxanthin diesters, were evident. Moreover, the possibility of different reactions, including isomerization or even degradation, taking place during the SAF process might not be ruled out.

Indeed, astacin derivatives were more prominent in the SAF extract compared with the PLE extract (peaks 9–11). Besides, new peaks appeared (peaks 26, 27) that could not be properly assigned although they could correspond to newly formed compounds. Unfortunately, due to the lack of commercial standards, no precise quantification of each separated compound was possible either by LC×LC or conventional LC.

7.10 Conclusion

The combination of compressed fluid–based processes for extraction and purification of target fractions has been demonstrated as a feasible environmentally green alternative for the recovery of astaxanthin and other carotenoids from *H. pluvialis* microalgae. Specifically, a PLE process performed with ethanol at 50 °C and 10.5 MPa for 20 min was demonstrated to be useful for the extraction of carotenoids from *H. pluvialis* biomass. Subsequently, this extract was used as feed for a SAF process targeting the further purification of carotenoids. An experimental design, studying different process parameters, including CO_2 pressure (10–30 MPa), percentage of water in the PLE extract (20–50%), and PLE extract/SC-CO_2 flow ratio (0.0125–0.05), was useful to select the optimum purification conditions allowing the recovery of a carotenoid-enriched fraction as SAF extract. By using 30 MPa, 0.05 feed/SC-CO_2 mass flow rate, and 20% (*v/v*) of water in the feed solution, a purified extract containing 120.3 mg g^{-1} carotenoids in the extract was produced. Thus, the possibility of using SAF to purify carotenoids from natural extracts was demonstrated. Moreover, a new fast LC×LC method based on the coupling of NP and RP separations has been optimized and applied in order to get the full carotenoid profile of these extracts in less than 25 min. Astaxanthin mono- and diesters were the most important compounds present, although other free carotenoids including canthaxanthin, lutein, and β-carotene were also detected. Interestingly, although the SAF process was able to produce an enrichment on total carotenoids, the application of this LC×LC method confirmed that the profiles obtained were qualitatively different compared with the original *H. pluvialis* PLE extract.

References

[1] C. Vílchez; E. Forján; M. Cuaresma; F. Bédmar; I. Garbayo; J. M.Vega. Mar Drugs. 2011, 9, 319–33.

[2] M. Rodriguez-Concepcion; J. Avalos; M. L. Bonet; A. Boronat; L. Gomez-Gomez; D. Hornero-Mendez et al. Prog. Lipid. Res. 2018, 70, 62–93.

[3] M. Guerin; M. E. Huntley; M. Olaizola. Trends Biotechnol. 2003, 21, 210–216.

[4] A. P. Sánchez-Camargo; E. Ibáñez; A. Cifuentes; M. Herrero In: Ibáñez E, Cifuentes A, editors. Comprehensive analytical chemistry, vol. 76. Amsterdam:Elsevier; 2017. p. 27–51.

[5] R. Gallego; M. Bueno; M. Herrero. TrAC-Trends Anal Chem. 2019, 116, 198–213.

[6] R. K. Saini; Y. S. Keum. Food Chem. 2018, 240, 90–103.

[7] R. Gallego; M. Martínez; A. Cifuentes; E. Ibáñez; M. Herrero. Molecules 2019, 24, 1564.

[8] F. A. Reyes; J. A. Mendiola; E. Ibañez; J. M. Del Valle. J. Supercrit. Fluids. 2014, 92, 75–83.

[9] L. Jaime; I. Rodríguez-Meizoso; A. Cifuentes; S. Santoyo; S. Suarez; E. Ibáñez; et al. Food Sci. Technol. 2010, 43, 105–112.

[10] R. Gallego; L. Montero, A. Cifuentes; E. Ibáñez; M. Herrero. J. Anal. Test. 2018, 2, 109–123.

[11] A. Visentín; M. Cismondi; D. Maestri. Innov. Food Sci. Emerg. Technol. 2011, 12, 142–145.

[12] A. Gonzalez-Coloma; L. Martín; A. M. Mainar; J. S. Urieta; B. M. Fraga; V. Rodríguez-Vallejo et al. Phytochem. Rev. 2012, 11, 433–446.

[13] A. P. Sánchez-Camargo; J. A. Mendiola; A. Valdés; M. Castro-Puyana; V. García-Cañas; A. Cifuentes et al. J. Supercrit. Fluids. 2016, 107, 581–589.

[14] P. Kraujalis; P. R. Venskutonis; E. Ibáñez; M. Herrero. J. Supercrit. Fluids 2015, 104, 234–242.

[15] F. Cacciola; P. Donato; D. Giuffrida; G. Torre; P. Dugo; L. Mondello. J. Chromatogr. A 2012, 1255, 244–251.

[16] P. Dugo; D. Giuffrida; M. Herrero; P. Donato; L. Mondello L. J. Sep. Sci 2009, 32, 973–980.

[17] P. Dugo; D. Giuffrida; G. Dugo; L. Mondello; M. Herrero; T. Kumm. J. Agric. Food Chem. 2008, 56, 3478–3485.

[18] F. Cacciola; D. Giuffrida; M. Utczas; D. Mangraviti; P. Dugo; D. Menchaca et al. Food Anal. Methods. 2016, 9, 2335–234.

[19] D. Giuffrida; P. Donato; P. Dugo; Mondello L. J. Agric. Food Chem. 2018, 66, 3302–3307.

[20] B. Gilbert-López; J. A. Mendiola; L. A. M. van den Broek; B. Houweling-Tan; L. Sijtsma; A. Cifuentes A, et al. Algal Res. 2017, 24, 111–121.

[21] X. Li; D. R. Stoll; P. W. Carr. Anal. Chem. 2009, 81, 845–850.

[22] M. Camenzuli; P. J. Schoenmakers. Anal. Chim. Acta. 2014, 838, 93–101.

[23] K. Holtin; M. Kuehnle; J. Rehbein; P. Schuler; G. Nicholson; K. Albert. Anal. Bioanal. Chem. 2009, 395, 1613–1622.

[24] O. J. Catchpole; J. B. Grey; K. A. Mitchell; J. S. Lan. J. Supercrit. Fluids 2004, 29, 97–106.

[25] P. Dugo; M. Herrero; T. Kumm; D. Giuffrida; G. Dugo; L. Mondello L. J. Chromatogr. A 2008 1189, 196–206.

8.0 Determination of the Metabolite Content of *Brassica juncea* Cultivars Using Comprehensive Two-Dimensional Liquid Chromatography Coupled with a Photodiode Array and Mass Spectrometry Detection

Plant-based foods are characterized by significant amounts of bioactive molecules with desirable health benefits beyond basic nutrition. The Brassicaceae (Cruciferae) family consists of 350 genera; among them, Brassica is the most important one, which includes some crops and species of great worldwide economic importance. In this work, the metabolite content of three different cultivars of *Brassica juncea*, namely ISCI Top, "Broad-leaf," and ISCI 99, was determined using comprehensive two-dimensional liquid chromatography coupled with a photodiode array and mass spectrometry detection. The analyses were carried out under reversed-phase conditions in both dimensions, using a combination of a 250-mm microbore cyano column and a 50-mm RP-Amide column in the first and second dimension, respectively. A multi (three-step) segmented-in-fraction gradient for the ^{2}D separation was advantageously investigated here for the first time, leading to the identification of 37 metabolites. In terms of resolving power, orthogonality values ranged from 62% to 69%, whereas the corrected peak capacity values were the highest for B. juncea ISCI Top (639), followed by *B. juncea* "Broad-leaf" (502). Regarding quantification, *B. juncea* cv. "Broad-leaf" presented the highest flavonoid content (1962.61 mg/kg) followed by *B. juncea* cv. ISCI Top (1002.03 mg/kg) and *B. juncea* cv. ISCI 99 (211.37 mg/kg).

8.1 Introduction

Vegetables from the Brassicaceae or Cruciferae family represent the most commonly consumed vegetables worldwide. This family includes brussels sprouts, broccoli, cabbage, cauliflower, and others. Such vegetables do contain high levels of bioactive compounds, *e.g.,* polyphenols, carotenoids, tocopherols, glucosinolates, and ascorbic

acid [1 –4]. Epidemiological data have demonstrated the ability of Brassica vegetables to decrease the risk of cardiovascular diseases and several types of cancer, *e.g.,* such as in the gastrointestinal tract [5]. All these effects have been associated with the presence of bioactive molecules with antioxidant and free radical scavenging properties, with potential effects on gene expression, cell signaling, and cell adhesion [6].

Among the bioactive compounds that occur in the Brassicaceae family, polyphenols represent a group of secondary plant metabolites comprising diverse families [7]. Among them, the most common subclass of polyphenols is represented by flavanols, and the most abundant aglycones are quercetin and kaempferol, which often occur as a complex conjugated via glycosilation and acylation of the aglycone [7]. Frequently, these compounds occur in acylated forms with hydroxycinnamic acids; among them, the most abundant are p-coumaric acid, caffeic acid, ferulic acid, and sinapic acids. These complex compositions are influenced by many factors, e.g., cultivar, climate, postharvest treatments, and agricultural and environmental variables [8–11].

Belonging to the Brassicaceae family, *Brassica juncea* L. is an amphiploid species, mainly grown as a food crop but is also used for medicinal purposes. It is one of the richest sources of iron, vitamin A, and vitamin C but also contains potassium, calcium, thiamine, riboflavin, and β-carotene. It has antiseptic, diuretic, emetic, and rubefacient properties. It has been reported to contain antioxidants like flavonoids, carotenes, lutein, indoles, and zeaxanthin [12].

The metabolite profiling of *Brassica juncea* L. has up until now been carried out using high- or ultra-high-performance liquid chromatography (HPLC, UHPLC) coupled with photodiode array (PDA) and/or MS detection [13–18]. However, due to its complexity, related to the simultaneous presence of isobaric molecules, a single separation system *viz.* one-dimensional LC (1D–LC) hampers a full profiling of such complex samples, thus negatively affecting quantification data [14–16]. An alternative expedient for overcoming such an issue could be the use of advanced analytical tools, *e.g.,* comprehensive two-dimensional LC (LC×LC). The latter, which comprises two

orthogonal separation mechanisms, can provide higher resolving power, which is the peak capacity (n_C) multiplicative of the peak capacity values in both dimensions [19–32]. The likelihood of achieving "orthogonal" separation mechanisms in LC×LC separations is quite high considering the hydrophobicity, polarity, size and charge; however, some technical difficulties can arise as a result of the chosen coupling. As an example, a combination of normal phase (NP) and reversed phase (RP) may lead to the precipitation of buffers or salts due to the mobile phase immiscibility [26,27]. On the other hand, when dealing with RP-LC×RP–LC separations, no solvent compatibility issues are usually observed. The main issue for such a set-up, using a conventional "full in fraction" in the second dimension (^{2}D) gradient, is the limited orthogonality due the similarity of the stationary phases employed. In fact, the analytes tend to align themselves along the diagonal line in the ^{2}D contour plot. To ameliorate such an issue, some expedients (tailored gradient programs) have been exploited in recent years [19–21,25,30–32]. A first type of gradient is called a "segmented gradient," where at least two different gradient segments are employed throughout the whole RP–LC×RP–LC run. As a result, a remarkable bandwidth suppression effect is achieved and the likelihood of the "wrap-around" phenomena is toned down [19,21,22]. A second type of gradient, a parallel gradient mode, involves a single ^{2}D gradient run matching the ^{1}D one. In this case, a longer ^{2}D elution time can be used since a post-gradient equilibration is not necessary [19,21]. Also, the use of "shift gradients" for the 2D run has been proposed with the aim to adopt a (changing) narrower gradient program for the entire RP-LC×RP-LC analysis time. This approach turned out to be a very effective one in various natural product and food applications [20,25,30–32].

In this contribution, a newly developed RP-LC×RP–LC system coupled with PDA and MS detection for the untargeted metabolite content of three different cultivars of *Brassica juncea*, namely ISCI 99, ISCI Top and "Broad-leaf," is reported. Separations were conducted using a combination of a first dimension (^{1}D) microbore cyano column, and a ^{2}D superficially porous RP-Amide column. A novel ^{2}D gradient mode,

namely a multi (three-step) segmented-in-fraction gradient, was proposed and successfully demonstrated, leading to an improved expansion of metabolic coverage.

8.2 Materials and methods

8.2.1 Chemical and Reagents

LC-MS-grade water, methanol, acetonitrile, and acetic acid were obtained from Merck Life Science (Merck KGaA, Darmstadt, Germany). Km 3-O-glucoside, Is 3-O-glucoside, and Qn 3-O-glucoside were obtained from Merck Life Science (Merck KGaA, Darmstadt, Germany). Stock solutions of 1000 mg L^{-1} were prepared for each standard by dissolving 10 mg in 10 mL of methanol. 1D-LC separations were performed on an Ascentis Express C18 column (Merck Life Science, Merck KGaA, Darmstadt, Germany; 150×4.6 mm I.D., 2.7 μm dp). LC×LC separations were conducted by using a ^{1}D Ascentis ES-Cyano (ES-CN) column (Merck Life Science, Merck KGaA, Darmstadt, Germany; 250×1.0 mm I.D., 5 μm dp) and a ^{2}D Ascentis Express RP-Amide column (Merck Life Science, Merck KGaA, Darmstadt, Germany; 50 ×4.6 mm I.D., 2.7 μm dp).

8.2.2 Sample and Sample Preparation

Brassica juncea L. Czern&Coss *cv*. ISCI 99, ISCI Top, and "Broad-leaf" leaf selections were provided from the Brassica collection of Consiglio per la ricerca in agricoltura e l'analisi dell'economia agraria – Centro di Ricerca Cerealicoltura e Colture Industriali) (CREA-CI) [39]. Samples were immediately frozen and freeze-dried for storage in glass vacuum desiccators. Lyophilized tissues were finely powdered to 0.5 μm size for analysis. Compound extraction was carried out based on the following protocol [16] with some modifications. The powder of the leaves of the

three different *B. juncea* cultivars were weighed into 100 mg samples. The samples were extracted twice with 5 mL of a mixture of methanol:water (60:40, *v/v*) for 30 min in a sonicator and centrifuged at 1000×g for 15 min, followed by filtration of the supernatants through a 0.45 µm nylon filter (Merck Life Science, Merck KGaA, Darmstadt, Germany). The prepared organic extracts were subjected to evaporation in a EZ-2 evaporator and then redissolved in 1 mL of the same solvent extraction mixture of methanol:water (60:40, *v/v*).

8.3 Instrumentation

LC and LC×LC analyses were performed on a Nexera-e liquid chromatograph (Shimadzu, Kyoto, Japan), consisting of a CBM-20A controller, one LC-Mikros binary pump, two LC-30AD dual-plunger parallel-flow pumps, a DGU-20A5R degasser, a CTO-20AC column oven, a SIL-30AC autosampler, and an SPD-M30A PDA detector (1.0 µL detector flow cell volume). The two dimensions were connected by means of two high-speed/high-pressure, two-position, six-port switching valves with a micro electric actuator (model FCV-32 AH, 1.034 bar; Shimadzu, Kyoto, Japan), placed inside the column oven, and equipped with two 10 µL stainless steel loops. The Nexera-e liquid chromatograph was hyphenated to an LCMS-8050 triple quad mass spectrometer through an ESI source (Shimadzu, Kyoto, Japan).

8.4 Analytical Conditions

8.4.1 LC Separations

1D-LC separations were run on the Ascentis Express C18 column. Mobile phases: (A) 0.15% acetic acid in water (pH 3), (B) 0.15% acetic acid in ACN. Gradient: 0 min, 5% B; 5 min, 5% B; 15 min, 10% B; 30 min, 20% B; 60 min, 50% B; 80 min, 100%. Mobile phase flow rate: 1 mL min^{-1}. Column oven: 30 °C. Injection volume: 10 µL.

8.4.2 LC×LC Separations

For ^{1}D separations, the Ascentis ES-CN column was used. Mobile phases: (A) 0.15% acetic acid in water (pH 3), (B) 0.15% acetic acid in ACN. Gradient: 0 min, 2% B; 5 min, 2% B; 30 min, 30% B; 60 min, 40% B; 80 min, 100% B. Flow rate: 10 µL min^{-1}. Column oven: 30 °C. Injection volume: 1 µL.

For ^{2}D separations, an RP-Amide column was used. The mobile phases employed were (A) 0.15% acetic acid in water (pH 3), (B) 0.15% acetic acid in ACN. Multi (three-step) segmented-in-fraction gradient conditions: I) 10 to 32 min (cycle: 0.01–0.80 min, 3–8% B; 0.81–1.0 min, 3% B); II) 32 to 43 min (cycle: 0.01–0.80 min, 10–44% B; 0.81–1.0 min, 10% B); III) 43 to 60 min (cycle: 0.01–0.80 min, 20–60% B; 0.81–1.0 min, 20% B). Flow rate: 2 mL min^{-1}, modulation time of the switching valves: 1.00 min, loop internal volume: 10 µL, and column oven: 30 °C.

8.4.3 Detection Conditions

PDA range: 200–450 nm; sampling rate: 12.5 Hz (1D-LC analyses), 40 Hz (LC×LC analyses); time constant: 0.08 sec (1D-LC analyses), 0.025 sec (LC×LC analyses).

Interface: ESI-MS in negative ionization mode. Mass spectral range in full scan mode: m/z 100–1200; event time: 0.5 (1D-LC analyses), 0.2 sec (LC×LC analyses); nebulizing gas (N_2) flow: 3 L min^{-1}; drying gas (N_2) flow: 15 L min^{-1}; heating gas flow (air): 10 L min^{-1} same; heat block temperature: 400 °C; desolvation line (DL) temperature: 250 °C; interface temperature: 300 °C; interface voltage 3.50 kV; detector voltage: 1.80 kV.

8.4.4 Data Handling

The LC×LC-LCMS-8050 system and the switching valves were controlled using the Shimadzu Labsolution software (ver. 5.93) (Kyoto, Japan). LC×LC-Assist software (ver. 2.00) (Shimadzu, Kyoto, Japan) was used for setting up the multi (three-step) segmented-in-fraction gradient analyses. The LC×LC data were visualized and elaborated into two and three dimensions using Chromsquare ver. 2.3 software (Shimadzu, Kyoto, Japan).

8.4.5 Construction of Calibration Curves

For flavonoid determination, due to the lack of commercial standards, Km 3-O-glucoside, Is 3-O-glucoside, and Qn 3-O-glucopyranoside, as representatives of the distinct chemical classes under evaluation, were selected. Standard calibration curves were prepared in the concentration range 0.1–100 mg L^{-1} with five different concentration levels, run in triplicate. The amount of the compound was finally expressed in mg kg^{-1} of extract.

8.5 Results and Discussion

The analysis of the three different cultivars of B. juncea L. was first run using a conventional LC-PDA-MS approach on a C18 column. As illustrated in the following section, a considerable number of compounds overlapped; consequently, an RP-LC×RP–LC system was adopted in order to attain higher separation power, thus providing a thorough overview of the overall metabolites pool, which is beneficial for quantification purposes.

8.5.1 Elucidation of Brassica juncea Cultivars Using RP-LC×RP-LC-PDA-MS

RP-LC×RP–LC separations have proved to be quite effective for the analysis of the metabolite content of food and natural products [19–22,25,30–32]. Before running an RP-LC×RP–LC analysis, a careful optimization of the independent separations must be carried out [26,27,29]. A low mobile phase flow rate is preferred in the 1D in order to decrease the fraction volume onto the ^{2}D and augment the ^{1}D sampling rate. Usually, this is achieved by employing a microcolumn in the ^{1}D; however, since most commercial LC pumps are not capable of delivering a stable and repeatable flow rate, a higher flow rate is commonly employed and split up before entering the ^{1}D column. A scheme of the RP-LC×RP–LC employed is reported in Figure 1. In this work, a robust and easy-to-use micropump with a completely new direct-drive engineering was advantageously employed and was capable of delivering micro- to semi-micro flow rates ranging from 1 to 500 µL/ min.

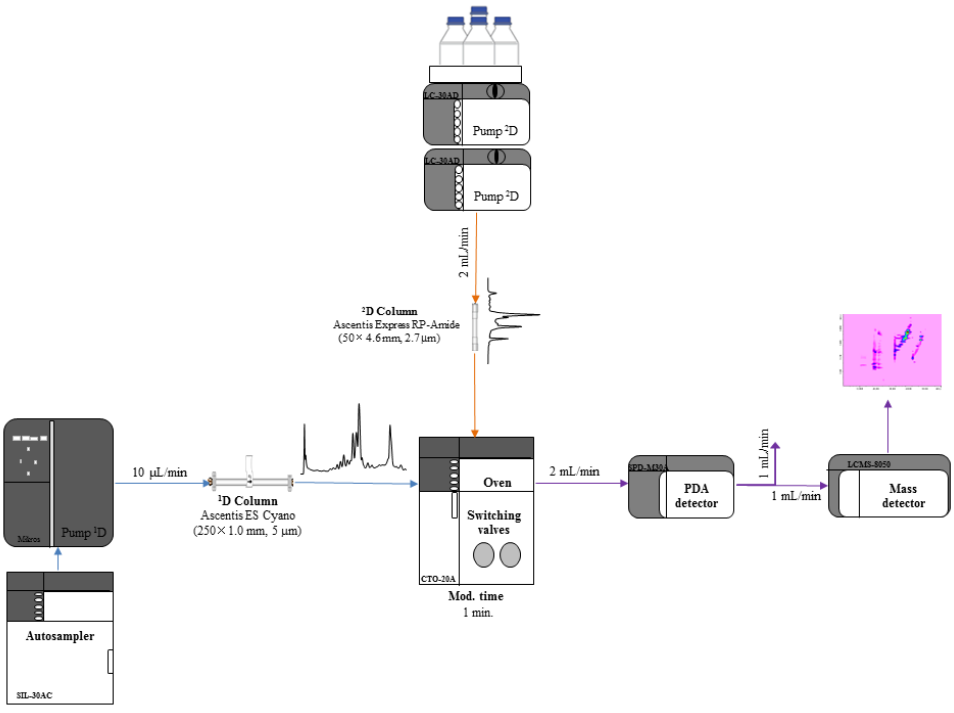

Figure 1. Scheme of the reversed-phase liquid chromatography RP-LC×RP-LC system employed for the investigated work. PDA: Photodiode array.

Repeatability data obtained on four selected peaks are displayed in Table 1. Relative standard deviation (RSD, %) values lower than 0.02 were attained in the case of mean retention times (min), whereas RSD (%) values lower than 1.21 were determined in case of mean areas. With regard to the ^{2}D, a fast separation is commonly employed in order to increase the ^{1}D sampling to lower the risk of incurring wrap-around phenomena. Consequently, a microcyano column was chosen in the ^{1}D, whereas a 4.6-mm I.D. partially porous RP-Amide column was employed in the ^{2}D and operated at 2 mL min^{-1}. For fraction transfer, two high-speed, six-port, two-position switching valves equipped with two 10 μL sampling loops were chosen.

Table 1. Repeatability data calculated from four selected peaks of the RP-LC×RP-LC plots shown in Figure 2.

Peak	Compound	Mean Tt_R	RSD (%) n=3	Mean Area	RSD (%) n=3
1	Malic acid	19.32	0.02	59664	0.78
2	Km -3-diglucoside-7-glucoside	34.54	0.02	159713	1.21
3	Sinapoyl-feruloyl-triglucose	42.73	0.01	95465	0.55
4	Disapoylgentiobiose	47.79	0.01	1481389	1.02

In this context, the optimization of the gradient programs, especially for the ^{2}D, is also necessary for an adequate separation and is mainly related to the chemical properties of the solutes. Late eluting compounds that are retained more in the ^{2}D require a greater gradient steepness in order not to incur wrap-around effects. In the case of closely related compounds, *e.g.*, early-eluting compounds, which are subjected to co-elutions, a lower gradient of steepness is preferable in order to permit stronger retention.

Following this strategy, a newly developed RP-LC×RP-LC system was investigated. In particular, a multi segmented-in-fraction gradient approach was employed, as illustrated in Figure 2. In particular, three different full-in-fraction gradients were considered for the ^{2}D analysis. The first gradient was from 10 to 32 min, where %B ranged from 3% to 8% (D%B: 5) for the analysis of early eluting organic acids; in the

second gradient step (from 32 to 43 min), %B ranged from 10% to 44% (D%B: 34) for the analysis of (acetylated) tri- and tetrasaccharides, whereas in the last one (from 43 to 60 min), %B ranged from 20% to 60% (D%B: 40) for the analysis of late eluting (acetylated) mono- and disaccharides. The modulation time of the switching valves was 1.00 min. Figure 2 shows the contour plots for the RP-LC×RP–LC analysis of the three cultivars of *Brassica juncea*, where a total of 37, 34, and 31 metabolites were positively separated using the optimized multi segmented-in-fraction gradient approach.

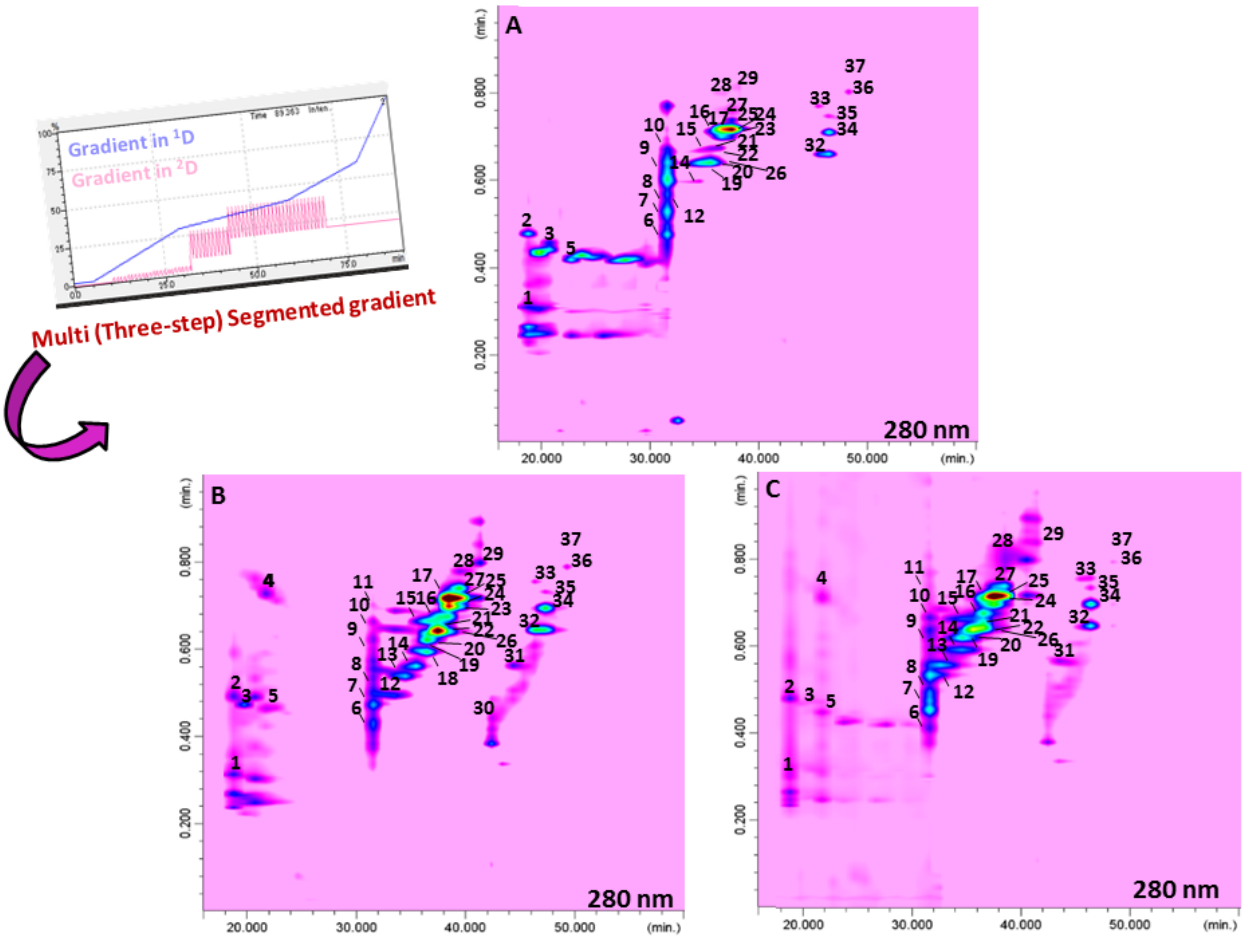

Figure 2. RP-LC×RP-LC contour plots of the system employed for ISCI Top (A), "Broad-leaf" (B), and ISCI 99 (C).

Concerning the performance of the developed RP-LC×RP-LC system, Table 2 reports the values attained for both peak capacity and orthogonality [33]. The highest theoretical peak capacity values, which are multiplicative of the peak capacity of the

two single dimensions [34], were attained for the cultivar ISCI Top (1734), whereas the lowest was obtained for the cultivar ISCI 99 (932).

The orthogonality values ranged from 62% to 69% for ISCI Top and "Broad leaf", respectively [33]. The corrected peak capacity values, which considered, both undersampling [35] and orthogonality values, were 639, 404, and 502 for ISCI Top, ISCI 99, and "Broad leaf", respectively. Considering the similarity of the two separation systems employed in both dimensions, such values can be considered quite remarkable and are in agreement with previously published findings on similar set-ups exploited for polyphenolic characterization in licorice (695 in Wong et al. [30]) and pistachio (461–633 in Arena et al. [31]) samples.

Table 2. Peak capacity and orthogonality values for the RPLC×RPLC analysis of the three *Brassica juncea* extracts

Parameter	Brassica j. ISCI TOP	Brassica j. ISCI 99	Brassica j. Broad leaf
^{1}D peak capacity, $^{1}n_C$	51	34	46
^{2}D Peak capacity, $^{2}n_C$	34	28	29
Theoretical peak capacity, $^{2D}n_C$	1734	952	1334
Effective peak capacity, $^{2D}n_C$	926	652	772
Orthogonality, A_0	69%	62%	65%
Corrected peak capacity, $^{2D}n_{C,corr}$	639	404	502

As an example, the benefits associated with the employment of the developed RP-LC×RP–LC with the multi segmented-in-fraction gradient program over the conventional RP-LC separation are highlighted in Figure 3.

A selected chromatographic region of the Brassica ISCI Top extract (Figure 3A) clearly shows how the 1D-LC did not provide enough peak capacity for unambiguous characterization of the chemical profile of the three occurring metabolites, due to compound overlapping. However, when the RP-LC×RP–LC analysis was employed, the three different bioactive compounds were conveniently separated and characterized via inspection of the respective MS spectra (Figure 3B). As a result, the better

resolution of the RP-LC×RP–LC separation (with the ^{2}D operated under the multi (three-step) segmented-in-fraction gradient mode) over the conventional 1D-LC led to a greater metabolite expansion in the RP-LC×RP–LC space, which was essential for improving the reliable identification of compounds with complexity and/or various polarities.

8.5.2 Semi-Quantitative Determination of the Flavonoid Content of Brassica juncea Cultivars

Tentative identification of the *Brassica juncea* extracts, illustrated in Figure 2, was performed based on their PDA, MS, and literature data [1,2,9–11,14–16,36–38]. Among the major classes of compounds identified, organic acids, (acetylated) tri- and tetrasaccharides, and (acetylated) mono- and disaccharides, were recognized (Table 3). Due to the lack of commercial standards, quantification of *Brassica* spp content has so far been carried out after acidic and/or alkaline hydrolysis [36–38].

In this work, a quantification of the native flavonoid composition of the three cultivars of *Brassica juncea* was carried out by RP-LC×RP–LC system coupled to PDA detection for the first time. Toward such an aim, and considering the unavailability of corresponding standard references, an established approach in the field of food and natural product analysis was followed. Basically, three standards, as representatives of the distinct chemical classes, i.e., Km 3-O-glucoside, Isorhamnetin (Is) 3-O-glucoside, and Qn 3-O-glucopyranoside, were chosen and calibration curves were prepared, as reported in Section 8.4.5.

Results are shown in Table 4, which reports all the standard curves, correlation coffecients (R_2), limits of detection (LoDs) and limits of quantification (LoQs), and relative standard deviations (RSDs) of the peak areas for each standard selected. The five-point calibration curves provided R_2 values ranging from 0.9993 to 0.9997, whereas for LoQ and LoD, values as low as only 30 ppb and 90 ppb, respectively, were found. Finally, RSD values lower than 0.89% were obtained, demonstrating valuable method repeatability.

Subsequently, all three samples were analyzed and the contents of the target compounds were calculated using commercially-available software, as reported in Table 3. *B. juncea* cv. "Broad-leaf" presented the highest flavonoid content (1962.61 mg/kg), followed by *B. juncea* cv. ISCI Top (1002.03 mg/kg) and *B. juncea* cv. ISC

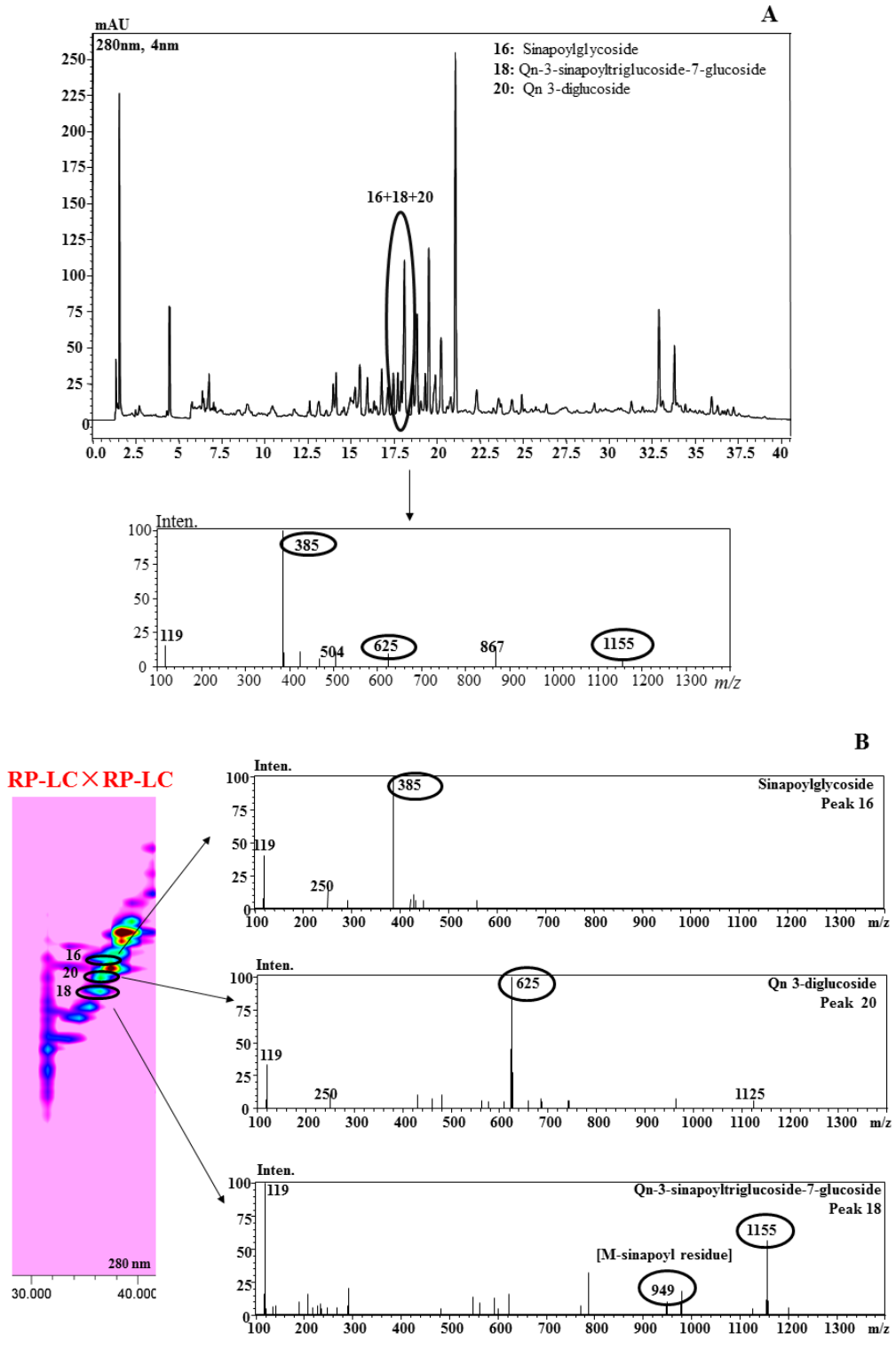

Figure 3. RP-LC (A) vs. RP-LCRP-LC (B) analysis of metabolites in B. juncea cv. ISCI Top. Qn: Quercetin.

Table 3. Semi-quantitative analysis (mg/kg) of the flavonoid content of Brassica spp extracts. Results are expressed as mean S.D. of three replicates

	Componds	$[M-H]^-$	λ max (nm)	B. Juncea ISCI TOP	B. Juncea Broad leaf	B. Juncea ISCI TOP99
1	Malic acid	133	215; 260	n.q.	n.q.	n.q.
2	Citric acid	191	215; 260	n.q.	n.q.	n.q.
3	Dihydrocaffeic acid 3-O-glucoside	357	250; 323	n.q.	n.q.	n.q.
4	Km 3-dicoumaryl-glucoside	739	202; 257	14.6±2.1	13.1±1.5	-
5	1-methoxyspirobrassin	279	198; 259	n.q.	n.q.	n.q.
6	Qn 3-caffeoylsophoroside-7-glucoside	949	250; 336	5.30±0.1	2.91±0.1	3.01±2.2
7	Qn 3-sophoroside-7-glucoside	787	254; 350	11.02±0.2	23.96±1.0	1.44±0.3
8	Sinapoyl-gentiobiose	547	238; 320	n.q.	n.q.	n.q.
9	Rhamnosyl-ellagic acid 1	447	238; 304	n.q.	n.q.	n.q.
10	Rhamnosyl-ellagic acid 2	447	238 ; 304	n.q.	n.q.	n.q.
11	Feruloylglucose 1	355	243 ; 328	n.q.	n.q.	-
12	Km3-O-diglucoside-7-O-glucoside	771	263 ; 330	33.56±0.4	27.70±5.0	3.67±1.9
13	Km 3-sophoroside-7-glucoside	771	266 ; 343	45.77±1.5	80.29±4.2	-
14	Km 3-caffeoyl-triglucoside-7-glucoside	1095	250, 335	15.97±0.4	21.34±1.4	7.39±0.6
15	Qn 3-hydroxyferuloylsophoroside-7-glucoside	979	250; 337	10.47±0.1	26.62±1.1	4.25±0.9
16	Sinapoylglycoside	385	239, 329	n.q.	n.q.	n.q.
17	Feruloylglucose 2	355	243 ; 329	n.q.	n.q.	n.q.
18	Qn 3-sinapoyltriglucoside-7-glucoside 1	1155	249 ; 336	11.05±0.1	-	-
19	Km 3-hydroxyferuloylsophoroside-7-glucoside	963	264 ; 334	21.21±0.5	8.55±0.3	1.52±1.1
20	Qn 3-diglucoside	625	255 ; 345	35.75±0.3	61.97±1.9	13.59±1.5
21	Km 3-O-caffeoyldiglucoside-7-O-glucoside 1	933	249 ; 335	64.78±0.4	80.29±4.2	7.39±0.6
22	Km 3-sinapoylsophorotrioside-7-glucoside	1139	249 ; 335	248.54±8.1	174.38±1.9	10.88±0.3
23	Km 3-hydroxyferuloylsophoroside-7-glucoside 2	963	250; 333	27.88±0.6	-	10.57±0.3
24	Km 3-sinapoylsophoroside-7-glucoside	977	266; 333	63.36±0.9	32.92±1.8	1.65±0.2
25	Is-3,7-diglucoside	639	264 ; 336	309.48±0.4	1321.50±6.3	130.2±4.2
26	Km 3-sinapoylsophorotrioside-7-glucoside	1139	241 ; 335	29.85±1.7	20.13±1.4	1.88±0.3
27	Km 3-feruloylsophoroside-7-glucoside	947	267 ; 330	28.57±0.1	19.32±0.7	6.89±0.2
28	Kaempferol-3-O-coumaroyldiglucoside-7-O-glucoside	917	267;318	4.56±0.1	2.22±0.2	0.41±0.2
29	Sinapoylferuloyltriglucose	885	262 ; 325	n.q.	n.q.	n.q.
30	Sinapic acid	223	270 ; 326	n.q.	-	-
31	Sinapoyhydroxyferuloyldiglycoside	739	273 ; 329	n.q.	n.q.	-
32	Disapoylgentiobiose	753	240 ; 330	n.q.	n.q.	n.q.
33	Isorhamnetinglycoside	477	254 ; 348	20.31±0.7	45.41±3.9	6.63±1.3
34	Sinapoyl-feruloylgentiobiose	723	240 ; 330	n.q.	n.q.	n.q.
35	Diferuloyldiglucoside	693	245 ; 329	n.q.	n.q.	n.q.
36	Trisinapoylgentiobiose	959	243 ; 326	n.q.	n.q.	n.q.
37	Feruoyl-disapoyl-gentiobiose	929	246 ; 329	n.q.	n.q.	n.q.

Table 4. Quantitative performance of the polyphenolic reference materials used in this study using the RP-LC×RP-LC system coupled to PDA detection

Reference material	Standard curve	R^2	LoD (µg/mL)	LoQ (µg/mL)	Precision (RSD%)
Quercetin-3-O-glucopyranoside	y = 13239x - 9234.3	0.9993	0.03	0.09	0.80
Isorhamnetin-3-O-glucopyranoside	y = 1990.7x + 188.37	0.9997	0.12	0.39	0.72
Kaempferol-3-O-glucopyranoside	y = 4625.7x + 4475.7	0.9994	0.03	0.12	0.89

99 (211.37 mg/kg). Is 3,7-diglucoside turned out to be the most abundant flavonoid in each cultivar investigated (ISCI Top: 309.48 mg/kg; "Broad-leaf": 1321.50 mg/kg; "ISCI99": 130.2 mg/kg), followed by Km 3-sinapoylsophorotrioside-7-glucoside (ISCI Top: 284.54 mg/kg; "Broad leaf": 174.38 mg/kg; ISCI 99: 10.88 mg/kg). Considering the three different flavonoid classes, isorhamnetin derivates were the most abundant flavonoids in the cultivars "Broad-leaf" and "ISCI 99" (1366.91 mg/kg *vs.* 136.83 mg/kg); on the other hand, with regard to the cultivar ISCI Top, kaempferol derivates were detected in the highest amount (598.65 mg/kg). Interestingly, as an example, looking at the quercetin derivates, by using the LC×LC technique, it was possible to quantify all of them, unlike the conventional LC, in which some of the compounds could not be determined due to either co-elutions or matrix interferences (Figure 4).

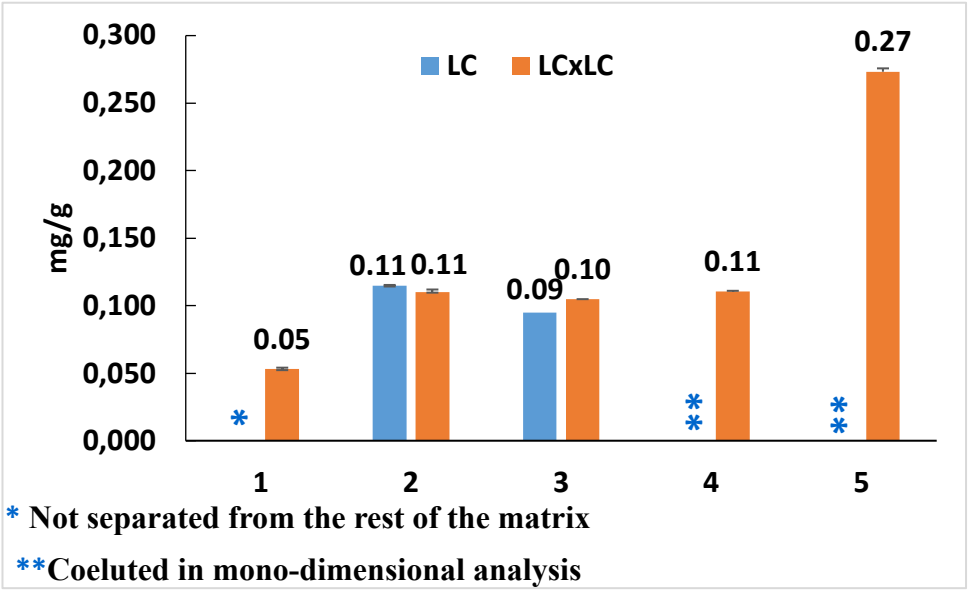

Figure 4. Semi-quantitative results (mg/g) for quercetin derivates by RP-LC and RP-LC×RP-LC PDA

8.6 Conclusion

In this contribute, the benefits associated with the use of a multi (three-step) segmented-in-fraction gradient in the RP-LC×RP-LC-PDA-MS analysis of three *Brassica juncea* cultivars are demonstrated. The coupling of a microcyano and an RP-Amide columns, in the first and second dimension, respectively, provided a characteristic metabolite pattern of the extracts, leading to the identification of 37 bioactives of different chemical nature, *i.e.,* organic acids, (acetylated) tri- and tetrasaccharides, and (acetylated) mono- and disaccharides. Interestingly, the employment of a micro LC pump in the first dimension of the RP-LC×RP-LC-PDA-MS systems allowed for high repeatability and stable retention times and areas. The investigated approach can be advantageously employed for RP-LC×RP-LC metabolic analyses of other complex plant derived extracts.

References

[1] M. E. Cartea; F. Marta; P. Soengas; P. Velasco. Molecules 2011, 6, 251–280.

[2] A. Podsedek. LWT Food Sci. Technol. 2007, 40, 1–11.

[3] A. C Kurilich; G. J. Tsau; A. Brown; L. Howard; B.P. Klein; E.H. Jeery; M. Kushad; M. A Wallig; J. A Juvik. J. Agric. Food Chem. 1999, 47, 1576–1781.

[4] J. Nilsson; K. Olsson; G. Engqvist; J. Ekvall; M. Olsson; M. Nyman; B. Åkesson. J. Sci. Food Agric. 2006, 86, 528–538.

[5] C.W Beecher. Am. J. Clin. Nutr. 1994, 59, 1166–1170.

[6] P. Kroon; G. Williamson. J. Sci. Food Agric. 2005, 85, 1239–1240.

[7] Ø. M Andersen; K. R., Markham, Eds.; Taylor & Francis Group: Boca Raton, FL, USA, 2006.

[8] B. Winkel-Shirley. Curr. Opin. Plant. Biol. 2002, 5, 218–223.

[9] S. F. Hagen; G. I. A Borge; K. A Solhaug; G. B. E Bengtsson. Postharvest Biol. Technol. 2009, 51, 36–42.

[10] M. Zietz; A. Weckmuller; S. Schmidt; S. Rohn; M. Schreiner; A. Krumbein; L. W. Kroh, J. Agric. Food Chem. 2010, 58, 2123–2130.

[11] S. Schmidt; M. Zietz; M. Schreiner; S. Rohn; L. W. Kroh; A. Krumbein.

Food Chem. 2010, 119, 1293–1299.

[12] K. Shekhawat; S. S. Rathore; O. Premi; B. K. Kandpal; J. S. Chauhan. Int. J. Agron. 2012, 408284. [CrossRef]

[13] U. Thiyam-Holländer; F. Aladedunye; A. Logan; H. Yang; B. W. K. Diehl, B.W.K. Eur. J. Lipid Sci. Technol. 2014, 116, 1664–1674.

[14] B. Harbaum; E. M. Hubbermann; Z. Zhu; K. Schwarz. J. Agric. Food Chem. 2008, 56, 148–157.

[15] L. Z. Lin; J. Sun; P. Chen; J. Harnly. Agric. Food Chem. 2011, 59, 12059–12072.

[16] J. Sun; Z. Xiao; L. Lin; G. E. Lester; Q. Wang; J. M. Harnly; P. Chen. J. Agric. Food Chem. 2013, 61, 10960–10970.

[17] S. Oh; C. Tsukamoto; K. Kim; M. Choi. J. Food Biochem. 2017, 41, 12366.

[18] R. Khattab; M. Eskin; M. Aliani; U. Thiyam. J. Am. Oil Chem. Soc. 2010, 87, 147–155.

[19] P. Jandera; T. Hájek; P. Cesla, P. J. Chromatogr. A 2011, 1218, 1995–2006.

[20] D. Li; O. J. Schmitz Anal. Bioanal. Chem. 2013, 405, 6511–6517.

[21] G. M. Leme; F. Cacciola; P. Donato; A. Cavalheiro; P. Dugo; L. Mondello. Anal. Bioanal. Chem. 2014, 406, 4315–4324.

[22] D. Tomasini; F. Cacciola; F. Rigano; D. Sciarrone; P. Donato; M. Beccaria; E. B. Caramão; P.Dugo, L. Mondello. L. Anal. Chem. 2014, 86, 11255–11262.

[23] C. Willemse; M. A. Stander; J. Vestner; A. G. J. Tredoux; A. De Villiers. Anal. Chem. 2015, 87, 12006–12015.

[24] L. Montero; E. Ibáñez; M. Russo; L. Rastrelli; A. Cifuentes; M. Herrero. J. Chromatogr. A 2016, 1428, 115–125.

[25] P. Donato; F. Rigano; F. Cacciola; M. Schure; S. Farnetti; M. Russo; P. Dugo; L. Mondello, L. J. Chromatogr. A 2016, 1458, 54–62.

[26] F. Cacciola; P. Donato; D. Sciarrone; P. Dugo; L. Mondello. Anal. Chem. 2017, 89, 414–429.

[27] F. Cacciola; P. Dugo; L. Mondello. Anal. Chem. 2017, 96, 116–123.

[28] E. Sommella; O. H. Ismail; F. Pagano; G. Pepe; C. Ostacolo; G. Mazzoccanti; M. Russo; E. Novellino; F. Gasparrini; P. Campiglia. J. Sep. Sci. 2017, 40, 2188–2197.

[29] B. W. J. Pirok; A. F. G. Gargano; P. J. Schoenmakers. J. Sep. Sci. 2018, 41, 68–98.

[30] Y. F. Wong; F. Cacciola; S. Fermas; S. Riga; D. James; V. Manzin; B. Bonnet; P. J. Marriott; P. Dugo; L. Mondello. Electrophoresis 2018, 39, 1993–2000.

[31] K. Arena; F. Cacciola; D. Mangraviti; M. Zoccali; F. Rigano; N. Marino; P. Dugo; L. Mondello. Anal. Bioanal. Chem. 2019, 411, 4819–4829.

[32] M. Russo; F. Cacciola; K. Arena; D. Mangraviti; L. de Gara; P. Dugo; L. Mondello, L. Nat. Prod. Res. 2019. [CrossRef]

[33] M. Camenzuli; P. J. Schoenmakers. Anal. Chim. Acta 2014, 838, 93–101.

[34] U. D. Neue. J. Chromatogr. A 2005, 1079, 153–161.

[35] H. Gu; Y. Huang; P. W. Carr. J. Chromatogr. A 2011, 1218, 64–73.

[36] B. Harbaum; E. M. Hubbermann; C. Wol; R. Herges; Z. Zhu; K. Schwartz. J. Agric. Food Chem. 2007, 55, 8251–8260.

[37] H. Olsen; K. Aaby; G. I. A. Borge. Food Chem. 2009, 57, 2816–2825.

[38] H. Olsen; K. Aaby; G. I. A. Borge. J. Agric. Food Chem. 2010, 58, 11346–11354.

[39] L. Lazzeri; L. Malaguti; M. Bagatta; L. D'Avino; L. Ugolini; G. R. De Nicola; N. Casadei;S. Cinti;R. Matteo; R. Iori. Acta Hortic. 2003, 1005, 331–33

9.0 Polyphenolic compounds with biological activity in guabiroba fruits (*Campomanesia xanthocarpa* Berg.) by comprehensive two-dimensional liquid chromatography

This study aimed to evaluate the polyphenolic composition along with the biological activity of guabiroba (*Campomanesia xanthocarpa* Berg.) fruits using comprehensive two-dimensional liquid chromatography (LC × LC). A simplex centroid design comprising three solvents (methanol, 2% acetic acid, and acetonitrile) was used to optimize the extraction mixture for polyphenols from ripe and unripe guabiroba fruits. A quantitative LC × LC platform was proposed to characterize the guabiroba extracts using a RP-Amide column and a C18 column in the first and second dimensions, respectively. Antidiabetic properties, using in vitro enzyme assay models and in vivo antioxidant activity with the eukaryote model Saccharomyces cerevisiae, was measured. Total phenolics compounds were more efficiently extracted with 2% acetic acid solution and acetonitrile (50:50, *v/v*). A total of 37 different compounds were identified and quantified using the proposed LC × LC method (linearity ranging from 0.9990 to 0.9994, intra- and interday precision from 0.40 to 10.57% and, accuracy from 81.89 to 108.98%). Significant differences were observed between ripe and unripe guabiroba fruits, especially for the compounds geraldone and methyl galangin isomer. Guabiroba fruits showed significant antidiabetic and antioxidant properties and may be potentially adopted as part of dietary strategies in the management of early stages of type 2 diabetes and associated complications.

9.1 Introduction

The Brazilian flora, due to its high species diversity, provides to the country a prominent position in relation to the diversity of native species with the potential of technological use [1]. In the Southern region of Brazil, there are still parts of the Atlantic Forest. These areas are rich in biodiversity, highlighting the occurrence of

native species of small fruits such as pitanga, araçá, uvaia, butiá, jabuticaba, and guabiroba.

Among them, the fruit of guabiroba (*Campomanesia xanthocarpa* Berg.), which belongs to Myrtaceae family, has a great potential for commercial cultivation, mainly on family-based farms, due to its desirable agronomic characteristics, high yield, abundant and succulent pulp, besides the characteristic flavor and aroma. It also presents interesting nutritional properties, such as high content of vitamin C, mineral salts and phenolic compounds, and thus for these reasons it is considered a functional food [2,3].

Some studies were carried out approaching different technologies for the use of guabiroba in the food industry. When using guabiroba to make jam, it was demonstrated that the processed food still presents considerable nutritional value with high levels of vitamin C, phenolic compounds, carotenoids, as well as a good content of β-carotene [4]. In addition, the fruit contain different types of pectins that allow the elaboration of several products, highlighting the plant as a native resource with technological and economic potential.

According to Valillo et al. [5], guabiroba stands out for its water content (81.4%), total carbohydrates (8.9%), and fibers (6.3%). Santos et al. [4] evaluated the levels of minerals present in the pulp of *C. xanthocarpa*. In particular, the levels found for calcium (28.45 mg/100 g) and phosphorus (25.3 mg/100 g) are higher than those reported for strawberry and watermelon. The iron content (3.52 mg/100 g) is similarto that found in the fruit of the same family, but higher than those found in banana (0.4 mg/100 g), apple (0.1 mg/100 g), and beef (2.8 mg/100 g) [6]. Furthermore, Czaikoski et al. [7] reported the supercritical extraction of bioactive compounds from guabiroba, identifying numerous compounds of the terpene class in their composition. The extract obtained in this study was evaluated for its antimicrobial and antioxidant activity, proving to present action against Staphylococcus aureus, Escherichia coli, Pseudomonas aeruginosa, and Salmonella typhimurium, in addition to the high antioxidant capacity values.

The characterization of the polyphenolic content of *C. xanthocarpa* Berg. is somewhat limited since so far only a few works on this fruit were carried out by HPLC-PDA focusing on selected compounds. Considering the potential complexity of the sample, in this work comprehensive two-dimensional LC (LC×LC), which combines two distinct separation modes was employed. Compared to conventional one-dimensional LC (1D-LC), LC×LC provides higher resolving power since sample components are spread out in the LC×LC space according to chemical specificity of retention patterns. Briefly, the whole sample is initially analyzed in the first dimension (^{1}D) and afterwards the ^{1}D effluent is transferred into the second dimension (^{2}D) through a modulator or interface, equipped with identical sample loops thus achieving a "comprehensive" separation [8–13]. Besides the polyphenolic composition, the antidiabetic and antioxidant properties of guabiroba fruits were evaluated.

Knowing the composition and biological activity, it will be possible to expand the possibilities of using this fruit that is highly perishable. In addition, native fruits such as guabiroba lack studies about their beneficial health potential considering the few data present in the literature.

9.2 Materials and Methods

9.2.1 Sample

Guabiroba fruits (C. xanthocarpa Berg.) were collected in populations of plants native from the West of Santa Catarina, Brazil (latitude 27.09'46"S, longitude 51.22'58"W). The collections were made after obtaining the required authorizations (Sisgen A4D350D). The fruits were harvested manually and randomly in various positions and orientations of the plants. The unripe fruits were harvested with green colored epidermis, with an average total acidity of 0.68% citric acid and 1.1 °Brix. The ripe fruits had orange skin, average total acidity of 0.47% citric acid, and 16.2 °Brix.

The guabirobas were selected by the uniformity of color and absence of injuries, were cleaned with tap water and freeze-dried (LIOTOP, L101, S.o Carlos, Brazil) at −46ÅãC, with pressure from 15 to 30 μHg.

9.2.2 Chemicals

LC-MS grade water, methanol, acetonitrile, and acetic acid were attained from Merck Life Science (Merck KGaA, Darmstadt, Germany). Gallic acid, catechin, hesperidin, epicatechin, sinapic acid, isoquercetin, isorhamnetin-3-O-glucoside, naringenin, quercetin, apigenin, and kaempferol were obtained from Merck Life Science (Merck KGaA). Stock solutions for each standard were prepared at a concentration of 1000 mg/L by dissolving 10 mg in 10 mL of methanol.

Porcine pancreas α-amylase (Type VI-B), Saccharomyces cerevisiae α-glycosidase (Type I), p-nitrophenyl-α- d-glycopyranoside, dinitrosalicylic acid, Folin–Ciocalteu reagent were obtained from Sigma-Aldrich (St.Louis, MO, EUA). Wild type strain of Saccharomyces cerevisiae EG103 (MATα leu2Δ0 his3-Δ1 trp1-289 ura3-52) was acquired from Euroscarf (Frankfurt, Germany). Their stocks were maintained in 2% YPD solid culture medium (1% yeast extract, 2% glucose, 2% peptone, and 2% agar).

9.3 Extraction of polyphenolic compounds and experimental design

Polyphenols were extracted from freeze-dried ripe guabiroba fruits using a simplex-centroid design comprising three pure solvents (x1 = methanol; x2 = 2% acetic acid solution; x3 = acetonitrile), three binary mixtures, six ternary mixture, with three replicates from the central point (Table 1). The response function was expressed as concentration of polyphenolic compounds (mg GAE/100 g).

Twelve experiments were generated and executed in random order.

Table 1. Simplex-centroid design and response function expressed in the freeze-dried ripe guabiroba fruits.

Extraction	Methanol (x_1)	2% acetic acid solution (x_2)	Acetonitrile (x_3)	Total phenolic content (mg GAE.100 g^{-1})
1	1	0	0	152.33
2	0	1	0	241.56
3	0	0	1	251.61
4	0.5	0.5	0	226.58
5	0.5	0	0.5	224.32
6	0	0.5	0.5	274.49
7	0.66	0.17	0.17	229.68
8	0.17	0.66	0.17	246.80
9	0.17	0.17	0.66	258.17
10	0.33	0.33	0.33	243.80
11	0.33	0.33	0.33	238.84
12	0.33	0.33	0.33	269.10

GAE = gallic acid equivalent

Prior to the extraction of total polyphenolic compounds, the freeze-dried ripe fruits were grounded in an electric grinder. Approximately, 1.5 g of each sample was used with 15 mL of solvent according to the experimental design (Table 1). The mixtures were then shaken on an orbital shaker (Solab, SL 180/D, Piracicaba, SP, Brazil) for 15 min at 100 rpm. Thereafter, the mixtures were placed in an ultrasonic bath (Cristófoli, Campo Mourão, PR, Brazil) at 25 °C for 5 min at a frequency of 42 kHz, centrifugated (Centribio, 80–2B, São Paulo, SP, Brazil) for 10 min at 4400 rpm. The organic phase was separated and evaporated in a rotatory evaporator (Quimis, Q344B, Diadema, Sp, Brazil) with controlled temperature at 28°C. The extract was resuspended in methanol and filtered through a 0.45 μm Acrodisc nylon membrane (Merck Life Science, Merck KGaA).

9.4 Determination of total phenolic content

Total phenolic content was measured by the Folin-Ciocalteu colorimetric method [14] using gallic acid. Total phenolic content was expressed as mg of gallic acid equivalents per 100 grams of fresh sample.

9.5 Determination of polyphenolic compounds by LC×LC

9.5.1 Chromatographic columns

Different columns in the ^{1}D were tested during the method development, namely Ascentis ES Cyano (250 × 1 mm; 5 μm dp,Merck Life Science,Merck KGaA), Ascentis Phenyl (250 × 1 mm; 5 μm dp, Merck Life Science, Merck KGaA), and Ascentis RP-Amide (250 × 1 mm; 5 μmdp,Merck Life Science, Merck KGaA).
^{2}D separations were carried out on an Ascentis Express C18 column (Merck Life Science,Merck KGaA; 50 × 4.6mm I.D., 2.7 μm dp).

9.5.2 Instrumentation and software

LC×LC analyses were carried out on a Nexera-e liquid chromatograph (Shimadzu, Kyoto, Japan), equipped with a CBM-20A controller, a LC-Mikros binary pump, two LC-30AD dualplunger parallel-flow pumps, a DGU-20A5R degasser, a CTO-20AC column oven, a SIL-30AC autosampler, an SPD-M30A photodiode array (PDA) detector (1.0 μL detector flow cell volume). Two high speed/high pressure two-position, six-ports switching valves with microelectric actuator (model FCV-32 AH, 1.034 bar; Shimadzu, Kyoto, Japan), placed inside the column oven and equipped with two 10 μL stainless steel loops, were employed for connecting the two dimensions. For peak identification, the Nexera-e liquid chromatograph was connected to an LC-MS-

8050 triple quadruple mass spectrometer, equipped with an ESI source (Shimadzu, Kyoto, Japan).

The LC×LC-LCMS-8050 system and the switching valves were controlled by the Shimadzu Labsolution software (version 5.93). LC×LC-Assist software (version 2.00) was used for setting up the 2D gradient analyses. The LC×LC data were visualized and elaborated using Chromsquare version 2.3 software (Shimadzu, Kyoto, Japan).

9.5.3 Analytical conditions

For ^{1}D separations, the Ascentis RP-Amide column was employed. The mobile phases were (A) 0.1% formic acid in water (pH 3) and (B) 0.1% formic acid in acetonitrile, with gradient conditions: 0 min, 2% B; 5 min, 2% B; 40 min, 40% B; 50 min, 60% B; 60 min, 100% B; 90 min, 100% B. The mobile phase flow rate was 10 μL min^{-1} with oven temperature of 30 °C and injection volume of 5 μL.

For ^{2}D separations, a RP-C_{18} column was used. The mobile phases were (A) 0.1% formic acid in water (pH 3), (B) 0.1% formic acid in acetonitrile. Multi (four-step) segmented-in-fraction conditions were: I) 10 to 40 min (cycle: 0.01-0.80 min, 10-16% B; 0.81-1.0 min, 10% B); II) 40 to 60 min (shifted from 16%B to 26%B; gradient height 6%; III) 60 to 70 min (cycle: 0.01-0.80 min, 30-50% B; 0.81-1.0 min, 30% B); IV) 70 to 105 min (cycle: 0.01-0.80 min, 50-90% B; 0.81-1.0 min, 50% B). The mobile phase flow rate was 2.5 mL.min^{-1}. The modulation time of the switching valves was 1.00 min. The loop internal volume was 10 μL and the column oven was 30 °C.

PDA detection range was 200-450 nm, with a sampling rate of 40 Hz and a time constant of 0.025 sec.

Electrospray ionization mass spectrometry (ESI-MS) was used in negative ionization mode. The mass spectral range in full scan mode was *m/z* 100-1200 with an event time of 0.2 sec. The nebulizing gas (N_2) flow was 3 L.min^{-1}; drying gas (N_2) flow was 15 L.min^{-1}; heating gas flow (air) was 10 L.min^{-1}; heater block temperature was 400 ºC;

desolvation line (DL) temperature was 250 ºC; interface temperature was 300 ºC; interface voltage was 3.50 kV; and detector voltage was 1.80 kV.

For quantification, eleven standards representatives of the chemical classes under study were selected, as reported in section 2.2. Standards calibration curves were prepared in a concentration range from 1.0 to 100 mg L^{-1}. The calibration curves with the external standards were obtained using concentrations (mg L^{-1}) with respect to the area obtained from the integration of the PDA peaks at a wavelength of 280 nm for benzoic acid-like and flavan-3-ol-like compounds, 320 nm for cinnamic acid-like compounds, 336 nm for flavone-like compounds, 346 nm for flavanone-like compounds and 360 nm for flavonol-like compounds. The compounds for which there was no standard available were semi-quantified based on the analytical curves of compounds with similar chemical structure.

9.5.4 Validation of the quantitative method

The method was validated by employing eleven polyphenolic compounds according to the ANVISA guidelines. Specifically, the LC×LC method was validated by considering the following parameters: linearity, limit of detection (LOD), limit of quantification (LOQ), intra (6 analyses) and interday (18 analyses within three consecutive days) precision and accuracy. For the evaluation of linearity, a calibration curve using six different concentrations of the standards in the matrix free of phenolic compounds (exhausted extract) was built in order to emulate the matrix effects related to the real sample. The square coefficient of determination (R^2) and the significance of the slope ($p \leq 0.05$) were also determined.

LODs and LOQs were calculated as follows: the standard deviation (SD) at the lowest level of the intercept of each calibration curve (0.1 mg.L^{-1}) was divided by the average slope multiplied by a factor of 3 and 10, respectively.

The precision was obtained considering the relative standard deviation (% RSD) of peak areas at 10 mg L^{-1} injected on the same day (n = 6) (intraday precision) and three

consecutive days (n=18) (interday precision). The accuracy (%) was determined by the recovery method, by the addition of a standard solution of each phenolic compound in three concentrations (5, 10 and 25 mg L^{-1}) in the matrix of freeze-dried guabiroba fruit. The recovery was expressed as the percentage of deviation between the calculated value and the nominal value.

9.5.5 Peak capacity and orthogonality

System orthogonality (A_0) for each sample was calculated according to the method proposed by Camenzuli and Schoenmakers, taking into account the spread of each peak along the four imaginary lines that cross the ^{2}D space forming an asterisk, that is Z_1, Z_2 (vertical and horizontal lines) and ,Z--., ,Z-+. (diagonal lines of the asterisk). Z parameters describe the use of the separation space with respect to the corresponding Z line, allowing to semi-quantitatively diagnose areas of the separation space where sample components are clustered, thus, reducing in practice orthogonality. For the determination of each Z parameter, the S_{Z_x} value was calculated, as the measure of spreading around the Z_x line, using the retention times of all the separated peaks in each ^{2}D analysis.

Individual peak capacity (,n-c.) for each dimension was calculated according to Eq. (1):

$$n_c = 1 + \frac{t_G}{w} \quad \textbf{(1)}$$

where t_G is the gradient time and $\overline{w}$ is the average peak width, equivalent to 4σ. For ^{1}D individual ^{1}D and ^{2}D peak capacity calculations, the average peak width was obtained from all the quantified peaks. For each two-dimensional set-up, different peak capacity values were estimated, starting from the, theoretical peak capacity ($^2D_{n_c}$). This value was calculated following the so-called product rule, using Eq. (2):

$$^{2D}\mathrm{nc} = {}^{1}n_c \times {}^{2}n_c \quad \textbf{(2)}$$

As Eq. (2) does not take into consideration the deleterious effects due to the modulation process as well as possible ^{1}D undersampling, a more realistic peak capacity value was obtained from the equation proposed by Li et al. [3], denominated effective peak capacity (Eq. 3):

$$^{2D}n_{c,practical} = \frac{{}^{1}n_c \times {}^{2}n_c}{\sqrt{1 + 3.35 \times \left(\frac{{}^{2}t_c \; {}^{1}n_c}{{}^{1}t_g}\right)^2}} \quad \textbf{(3)}$$

where $^{2}t_c$ the ^{2}D separation cycle time, which is equal to the modulation time. This latter equation includes the <β> parameter accounting for undersampling. Moreover, to more precisely compare among set-ups and in order to evaluate possible peak clusters along the ^{2}D analysis and, thus, to estimate ^{2}D space coverage, the orthogonality degree (A_0) was considered to offer the denominated ^{2}D corrected peak capacity, as follows:

$$^{2D}n_{c,effective} = {}^{2D}n_{c,practical} \times A_0 \quad \textbf{(4)}$$

9.6. Biological activity

9.6.1 α-amylase inhibitory activity

The α-amylase inhibitory activity was measured as described by Fujita et al. [4]. A total of 500 µL of sample extract was mixed with 500 µL of α-amylase enzyme solution (0.5 mg mL^{-1}) in 0.02 M sodium phosphate buffer, pH 6.9 with 0.006 M NaCl) and was incubated at 25 °C for 10 min. After 10 min preincubation, 500 µL of a 1% starch solution in 0.02 M sodium phosphate buffer (pH 6.9 with 0.006 M NaCl) was added to

each tube. After additional 10min incubation the reaction was stopped with 1.0 mL of dinitrosalicylic acid color reagent. The test tubes were then placed in boiling water (100 °C water bath for 10 min) and later cooled down to room temperature. The reaction mixture was then diluted to optimize the reading of control (only enzyme and substrate) to 1.0 at 540 nm absorbance. Absorbance of all samples at 540 nm was recorded using a Quimis UV–vis spectrophotometer (Quimis, Q898U2M5, Diadema, SP, Brazil). The readings were compared with the controls, containing buffer instead of sample extract. The results were expressed as percent α-amylase inhibition and calculated according Eq. (5). The concentration of inhibitors required for inhibiting 50% of the α-amylase activity under the assay conditions was defined as the ,IC-50. value.

$$\alpha\text{-amylase inhibition } (\%) = \frac{\text{Abs control -(Abs sample-Abs sample blank)}}{\text{Abs control}} \times 100 \quad \textbf{(5)}$$

9.6.2 α-glucosidase inhibitory activity

The α-glucosidase enzyme inhibitory assay was performed according to the Fujita et al. A total of 500 µL of sample extracts was added in 500 µL of 0.1 M phosphate buffer (pH 6.9) and mixed with 1000 µL of α-glucosidase enzyme (1unit/ mL) and incubated at 25 °C for 10 min. After 10 min incubation, 500 µL of 5mM p-nitrophenyl-α-D-glucopyranoside solution prepared in 0.1 M phosphate buffer (pH 6.9) was added. The reaction mixtures were then incubated at 25 °C for 5 min. Absorbance readings were recorded at 405 nm before and after 5 min incubation by using a Quimis UV-Vis spectrophotometer (Quimis, Q898U2M5, Diadema, SP, Brazil) and compared to a control that had 500 µL of buffer solution instead of the sample extract. The results were expressed as percent of α-glucosidase inhibition and calculated according to the Eq. (6). The concentration of inhibitors required for inhibiting 50% of the α-amylase activity under the assay conditions was defined as the ,IC-50. value.

$$\alpha\text{-glucosidase inhibition (\%)} = \frac{(\Delta \text{ Abs control} - \Delta \text{ Abs sample})}{\Delta \text{ Abs control}} \times 100 \quad (6)$$

9.6.3 Antioxidant analysis by survival assay

This assay was performed using cells of wild type strain of *Saccharomyces cerevisiae* EG103 from Euroscarf (Frankfurt, Germany), according Baroni et al. Cells were grown in liquid YPD medium, using an orbital shaker at 28 ºC and 160 rpm (Solab, SL 180/D, Piracicaba, SP, Brazil). Yeast cells at the exponential phase were transferred to fresh medium, containing H_2O_2 (2 mmol.L^{-1}) with either presence or absence of sample extract at final concentration (1:25, v/v). After transferring, yeast cells were incubated 1 h at 28 ºC at 160 rpm. Two control groups were used: a control Petri dish (untreated cells) and sample extract control Petri dish (yeast exposed to sample extract alone, without addition of H_2O_2).

Cell viability was analyzed by plating on solid YPD medium, after proper dilution. Petri dishes were incubated at 28 ºC for 72 h. One hundred percent survival was considered the number of colonies observed in the control plate (untreated cells). The number of colonies in each plate was between 150 and 200. All assays were carried out in triplicate.

9.7. Statistical analysis

A Scheffé quadratic model was expressed for response function from the simplex centroid design. The mathematical model was subjected to analysis of variance (ANOVA) and regression analysis using Statistica 10.0 software (Statsoft, Tulsa, OK, USA). Response surface and contour plots of the response was generated from adjusted model. The optimization of the response variables was based on the overall desirability function. Model was validated using Student's t-test ($p \leq 0.05$), where the average ($n = 3$) of the experimental values were compared with the estimated response of the model.

Regarding the validation of the LC×LC analytical method, the homogeneity of the variances of the data was tested using the Cochran test, defining the exclusion of outliers using the Grubbs test. The adjustment of the analytical curves was performed using ANOVA and R test. The data about method validation were analyzed using Excel software (Microsoft, Redmond, WA, USA). Data on phenolic composition and biological activity were expressed as mean ± standard deviation, averaged over at least three independent experiments. Pearson's linear correlations at $p \leq 0.05$ were evaluated using Statistica 10.0 software

9.8. Results and discussion

9.8.1 Effects of the solvent system on phenolic compounds extraction

The quadratic model fitted to the experimental data had determination coefficients (R_2) of 92% (Table 2).

Table 2. ANOVA of the quadratic model adjusted to the experimental data.

Source	Df	SS	F-value	*p*-value
Model	6	8958.65	9.54	0.01
Total error	5	782.23		
Lack of fit	3	255.64	0.32	0.81
Pure error	2	526.59		
Total adjusted	11	9740.88		

df = degrees of freedom; SS = sum of squares

Regarding the phenolic compounds extraction from freeze-dried ripe guabiroba fruits, the binary interaction coefficients (methanol/2% acetic acid solution, methanol/acetonitrile, and 2% acetic acid solution/ acetonitrile) and ternary (methanol/2% acetic acid solution/acetonitrile) were not significant ($p \leq 0.05$).

However, the factors methanol (x1; regression coefficient = 156.05), 2% acetic acid solution (x2; regression coefficient = 239.29), and acetonitrile (x3; regression coefficient = 251.70) were significant ($p \leq 0.05$) for the total phenolic compounds concentration response function (Fig. 1A).

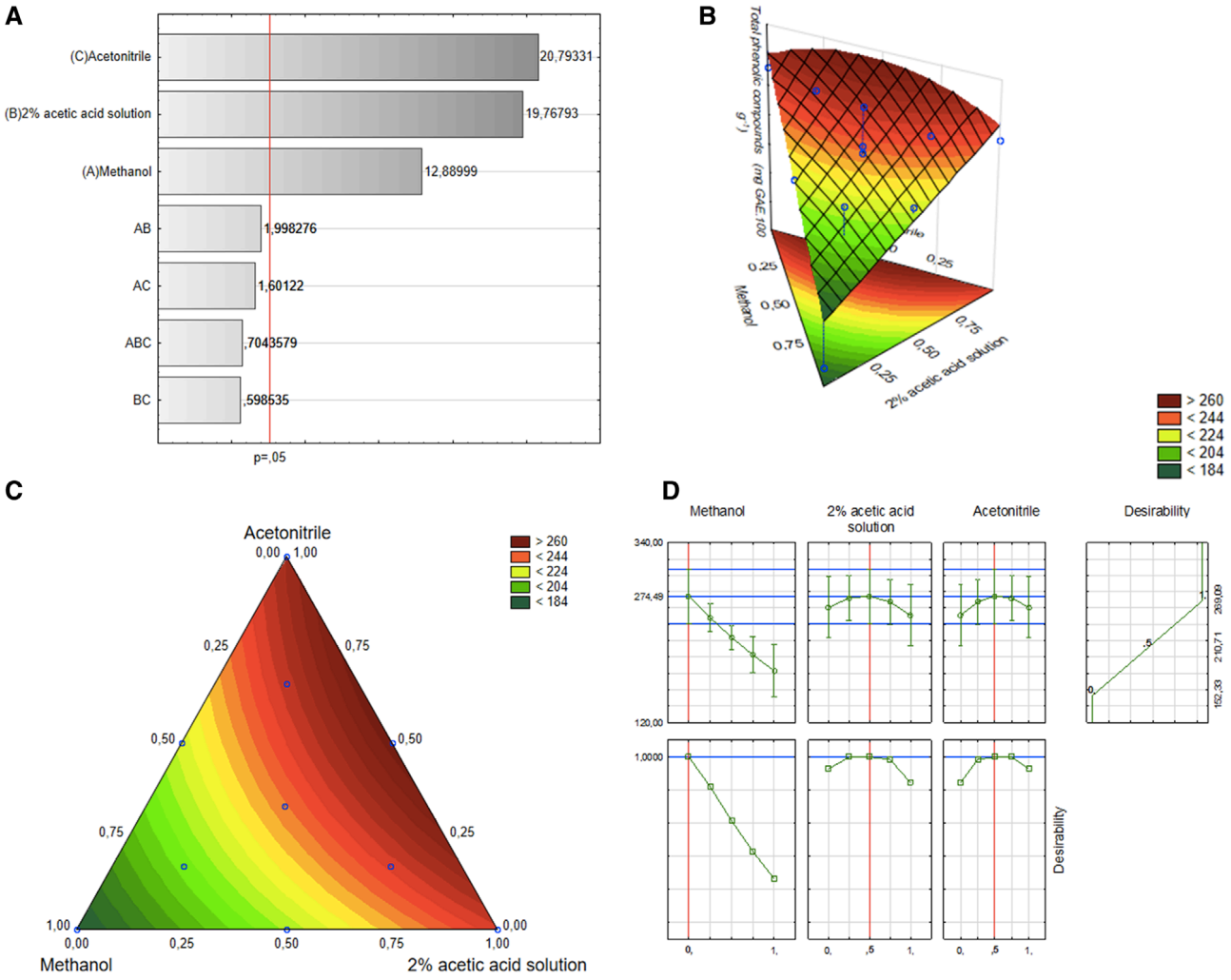

Figure 1. Pareto chart (A), response surface plot (B), contour plot (C), and profiles for the predicted values and overall desirability as a function of the solvent system (D) for extraction of polyphenolic compounds from freeze-dried guabiroba fruits.

The combination of solvent used to obtain the highest value for total phenolic compounds (274.49 mg GAE/100g) was 0:0.5:0.5 (*v/v/v*, methanol:2% acetic acid solution: acetonitrile), as seen in the response surface plot (Fig. 1B), contour plot (Fig. 1C), and profiles for the predicted values and overall desirability as a function of the solvent system (Fig. 1D).

The extraction of polyphenolic compounds from different matrices is influenced by the polarity of the solvents and the solubility of the molecules [15]. The polarity index of water is 9.0, while methanol is 6.6 and acetonitrile is 6.2. By using aqueous solvent mixtures like methanol and acetonitrile, the solvent system is able to extract phenolic compounds from high and medium range of polarity [16].

Polyphenolic compounds occur as soluble conjugates and insoluble forms. The sugars are quite common in the soluble forms, whereas the insoluble forms are covalently bound to cellulose, hemicellulose, lignin, pectin, and structural proteins.

Phenolic acids are found in insoluble or bound forms, whereas flavonoids typically occur as soluble forms [17]. The solubility of flavonoids in aqueous media is primarily associated the presence of glucose and hydroxyl groups in the chemical structure, whereas methyl and acetyl radicals decrease the polarity of the flavonoids [18]. The solvent viscosity can also affect the extractability of bioactive compounds from plant materials. Considering that the viscosity of methanol and acetonitrile is 0.60 and 0.37 mPa s (20°C), respectively, aqueous mixtures containing acetonitrile show greater extraction capacity since a low solvent viscosity enables greater diffusion into the pores of the matrix, improving the extraction [19].

Thus, the solvent system (v/v, 0.5:0.5, 2% acetic acid:acetonitrile) was used do validate the model. The model was verified to be significant (Table2) and appropriate for estimative finalities because the experimentally observed value (276.68 mg GAE/100 g) was not significantly different ($p \leq 0.05$) from the estimated value of the model (274.49 mg GAE/100 g).

9.8.2 LC×LC method optimization

The first step in determining the polyphenolic compounds ocurring in guabiroba fruits was the optimization of the LC×LC methodology, to provide a good separation capability [20]. The first approach consisted on the careful selection of several stationary phases to test the potential for the ^{1}D separation. Unripe guabiroba fruits

were selected as a model matrix for the development of these experiments, using the extraction method previously optimized in this study. Different conditions have been tested independently, firstly looking at the performance achievable by three different stationary phases in the ^{1}D and then, studying their potential when combined with a C18 column in the ^{2}D. Ascentis ES Cyano (250 × 1 mm; 5 μm dp), Ascentis Phenyl (250 × 1 mm; 5 μm dp), and Ascentis RP-Amide (250 × 1 mm; 5 μm dp) stationary phases were studied, using the appropriated mobile phases. Taking this screening into account and considering the possible different selectivity with columns in 2D, RP-amide was selected as the most promising for 1D. As it can be observed, a good peak distribution was obtained with the three tested columns, but the Ascentis RP-Amide column provided more separated peaks and better peak shape and, thus, it was therefore selected for definitive optimization. Once the column for the ^{1}D was selected, the separation conditions were optimized adjusting the gradient to provide wide peaks that could be appropriately sampled into the ^{2}D.

For the ^{2}D optimization, the extract obtained from the matrix model was injected directly into the C18 column (50 × 4.6 mm; 2.7 μm dp). In this case, an RP separation mode was selected because it has been shown as the most suitable separation mechanism to provide fast (<2 min) and efficient separations with shorter column equilibrium times [21], characteristics highly appreciated for 2D separations in LC×LC. Target total time cycle of 1 min was established, corresponding to the allotted time for each modulation and, it included besides the separation gradient, the column re-equilibration (20 s). Keeping inmind that the coupling of two RP-LC phases provides less resolving power due to apparent similarity of the separation mechanisms in both dimensions, a tailored ^{2}D elution gradient was developed to improving the diffusion of the solutes in the ^{2}D separation space [22]. A ^{2}D multisegmented gradient approach, gradually increasing the concentration of organic solvent was investigated. Due to the polarity range of polyphenolic compounds, four gradients were used: the first segment used a gradient slope of 6% per modulation cycle, starting with 10% ACN in the first 40 min and increasing to 16% in 40 min; the second segment used a slope

of 10% per modulation cycle, starting with 16% ACN and increasing to 26% ACN in 60 min; the third segment used a slope of 20% per modulation cycle, starting with 30% ACN and increasing to 50% ACN in 70 min; the fourth segment used a slope of 40% per modulation cycle, starting with 50% and increasing to 90% ACN in the last 105 min.

Subsequently, unripe and ripe guabiroba samples were analyzed using the previously optimized conditions. Two dimensional plots (280 nm) of the samples analyzed using this method are shown in Fig. 2.

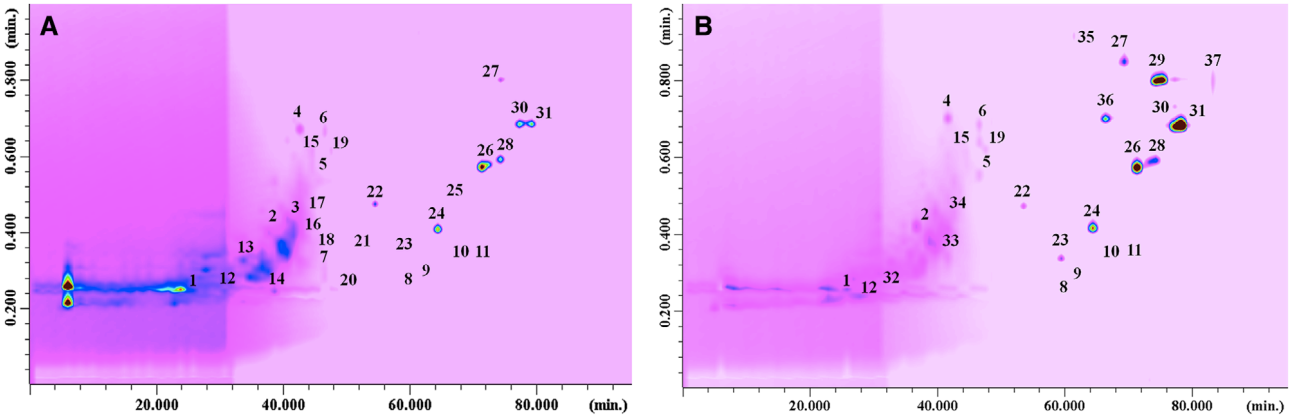

Figure 2. Contour plots (280 nm) obtained using the optimized LC×LC methodology for the analysis of unripe (A) and ripe (B) guabiroba extracts.

Orthogonality calculations are based on the use of the ^{2}D plane, as it is occupied by sample components [23]. As can be observed, the orthogonality degree was 65% for unripe guabiroba and 52% for ripe guabiroba (Table 3). Consequently, these values can be considered satisfactory considering the same selection mechanism in the two dimensions. Values of theoretical peak capacity as high as 2826 and 2331 were attained for unripe and ripe samples, respectively and are shown in Table 3. However, to provide more realistic values, the "effective" peak capacity, was also calculated considering the effects of undersamplig which can cause the remix of already separated compounds in the ^{1}D during the collection of the ^{1}D effluent in the sample loops [24]. Using this approach, values of 803 and 808 for unripe and ripe guabiroba, respectively, were obtained. Finally, calculate the "corrected" peak capacity achieved, considering both orthogonality and undersampling, the maximum limit of 522 peaks for unripe

guabiroba and 418 peaks for ripe guabiroba, were attained. Similar values were obtained by Montero et al. [25], Arena et al. [26], and Lazzari et al. [27] employing RP-LC×RP-LC.

Table 3. Peak capacity and orthogonality values for the RP-LC×RP-LC analysis of unripe and ripe guabiroba samples investigated.

Parameter	Unripe guabiroba	Ripe guabiroba
^{1}D peak capacity, $^{1}n_c$	111	89
^{2}D peak capacity, $^{2}n_c$	26	26
Theoretical peak capacity, $^{2D}n_c$	2826	2331
Effective peak capacity, $^{2D}n'_c$	803	808
Orthogonality, A_0	65%	52%
Corrected peak capacity, $^{2D}n_{c,corr}$	522	418

9.8.3 Development and validation of the quantitative method

Using the optimized LC×LC method, a group of 11 standards belonging to several polyphenolic classes, namely, hydroxybenzoic acid, cinnamic acid, flavanol, flavanone, flavone, and flavonols, were injected and analyzed. Calibration curves for each compound were obtained by the quintuplicate injection and LC×LC analysis of six different concentration levels after measuring their corresponding peak area (Table 4). Homoscedasticity was verified by the Cochran test, including the residual graph, in which the data were randomly dispersed and could be treated by the Ordinary Least Squares Method.

For the 11 compounds analyzed, the data were heteroscedastic. ANOVA and R test showed that linear regression was significant for the studied concentration ranges ($p \leq 0.05$), and thatmathematical models did not show evidence of lack of fit ($p > 0.05$). Determination coefficients (R2) higher than 0.999 were obtained for all the tested compounds.

Furthermore, the values of LODs obtained ranged from 0.24 mg/L to 0.39 mg/L for apigenin and epicatechin, respectively; whereas, LOQs values were lower than 1.13 mg/L (Table 4). It has been demonstrated that LODs values in LC×LC are higher than 1D-LC, due to chromatographic dilution [28]. However, the LODs results attained in this work by LC×LC-PDA are comparable with the ones reported by a recent work at least for five compounds, namely catechin, epicatechin, quercetrin, quercetin, and kaempferol, analyzed by LC-UV [29]. Moreover, instrumental intra- and interday precision was assessed. For this purpose, a mixture (10 mg/L each) of the 11 quantified standards was consecutively injected six times in the same day (n = 6) and in three consecutive days (n = 18).

RSD (%) values obtained were in the range between 0.40 and 9.41% in the same day. Interday RSD values ranged between 3.97 and 10.57% in consecutive days. Accuracy was also estimated through recovery (Table 4), by addition of 11 standard compounds in the exhaustive matrix. After the extraction and analysis of the 11 phenolic compounds studied, recovery results of the range between 81.89% and 108.98% were obtained for kaempferol and isorhamnetin-3-O-glucoside, respectively.

Regarding to the RSD% for accuracy data, all compounds analyzed showed values lower than 10%. These results are considered suitable since they do not exceed the nominal value by 20%, as recommended by ANVISA [30].

Table 4. Validation parameters of the quantitative of the polyphenolic standards used in this study by using the RP-LC×RP-LC system.

Compound	Chemical class	Standard curve	R^2	LOD (mg L^{-1})	LOQ (mg L^{-1})	Intraday precision RSD (%) (n=6)	Interday precision RSD (%) (n=18)	Accuracy (%) ± S.D.		
								5 mg L^{-1}	10 mg L^{-1}	25 mg L^{-1}
Gallic acid	Hydroxybenzoic acid	y = 41277x - 44503	0.9992	0.33	1.00	6.07	8.03	96.09±1.66	96.41± 2.00	93.35±1.78
Catechin	Flavonol	y = 45581x - 98563	0.9992	0.36	0.98	9.41	10.57	95.74±2.73	98.17±0.84	93.46±0.68
Hesperidin	Flavanone	y = 20722x -4626.6	0.9992	0.34	1.03	9.08	9.95	87.21±3.15	90.04±1.46	91.03±1.80
Epicatechin	Flavanol	y = 28801x + 12521	0.9990	0.39	1.12	0.40	7.09	93.55±0.73	99.41±3.55	93.50±0.71
Quercetin 3-O-glucoside	Flavonol	y = 32036x + 40064	0.9992	0.32	0.97	8.67	9.03	87.88±4.46	97.69±2.53	87.33±1.59
Isorhamnetin 3-O-glucoside	Methoxyflavonol	y = 38886x - 59650	0.9990	0.37	1.13	6.70	8.10	101.75±2.29	106.71±0.66	108.98±1.40
Sinapic acid	Methoxycinnamic acid	y = 30177x - 150483	0.9991	0.31	0.95	4.32	6.50	93.21±0.29	102.81±1.44	103.01±5.34
Naringenin	Flavanone	y = 79810x + 156698	0.9990	0.35	1.06	2.03	7.11	92.38±3.88	92.00±6.52	86.06±3.80
Quercetin	Flavonol	y = 65078x - 15699	0.9994	0.26	0.79	8.66	9.84	94.94±4.55	83.27±1.10	88.43±4.12
Kaempferol	Flavonol	y = 71092x + 2335.5	0.9992	0.31	0.95	1.43	3.97	81.89±6.32	90.46±2.76	92.91±3.80
Apigenin	Flavone	y = 86300x - 74422	0.9990	0.24	0.73	5.51	8.00	90.57±4.79	103.25±0.97	106.83±1.59

9.8.4 Profiling of polyphenolic compounds in guabiroba fruits

Through the evaluation of the quantitative analysis of the polyphenolic compounds, it was possible to obtain an evident discrepancy between the ripe and unripe fruit. Thirty-seven compounds, through LC×LC method, were positively identified (Table 5) and quantified by combining the information obtained with PDA and MS detection and literature data. Eleven compounds were quantified by authentic standard; on the other hand, when the reference standards were not available, each compound was quantified with the commercial standard belonging to the same chemical family. The compounds occurring in the samples can be clustered in different chemical classes, 10 out of them to flavonols, 9 to flavones, 6 to phenolic acids, 5 to flavan-3-ols, 4 to phenones, 2 to flavanones, and 1 to another class.

As observed in Fig. 3, methyl galangin isomers (no. 29,30) are the most abundant in ripe samples (151.66 and 142.24 mg/100 g). Galangin and methyl galangin were previously reported in fruits of the Myrateceae family such as Eugenia catharinensis [31] and Eugenia brasiliensis [32]. They are formed by the phenylpropanoid pathway; thus, they are derived from the amino acid phenylalanine. Phenylpropanoids are some of the most important sets of secondary metabolites in plants, especially in fruit ripening, which explains the considerable increase in the methyl galangin concentration in ripe fruits. The production of this flavonol has as its precursor cinnamic acid, which is converted to cinnamoyl-CoA by 4- coumaroyl-CoA ligase (4CL), forming pinocembrin, which is converted to methyl galangine by the action of flavanol synthase (FLS) [33]. According to Lee et al. [34], galangins may be promising therapeutic agents against inflammation. The other most abundant compounds are represented by geraldone (no. 26) (133.36 and 50.31 mg/100 g in ripe fruit and ripe fruit) and cirsimaritin (no. 36) (49.48 mg/100 g in ripe fruit).

Quantitative analysis showed a high content of polyphenolic compounds previously reported in guabiroba such as quercetin, gallic acid, kaempferol [35–38]. All these compounds are found in greater concentration in ripe fruits. Betta et al. [39] found similar behavior for quercetin and gallic acid, when analyzing Brazilian fruits during ripening stages.

Higher concentration of quercetin and kaempferol in the mature fruits may be related to the protective function of the photosynthetic apparatus of the plant. Higher content of gallic acid in the mature stage could be related to the gallotannins, which are more concentrated in immature fruit stages, and during ripening, the ester bonds are hydrolyzed. This statement is consistent with the fact that epicatechin gallate was detected only in unripe fruits, although other gallotannins have been quantified in the ripe fruits.

Other compounds, such as hesperidin, sinapic acid, 5-p-coumaroylquinic acid, quercetin 3-O-arabinopyranoside, epicatechin gallate, quercetin 3-O-xyloside (reynoutrin), myricetin-3-O-rhamanoside, ellagic acid-rhamnoside, isorhamnetin 3-O-rhamnoside, arbutin were found in unripe fruits; however, they were not found in ripe fruits.

This trend of a decrease during ripening may be related to the association of phenolic compounds with other components through stable covalent bonds [40], or polymerization of polyphenolic compounds that result in decreased astringency [39,41].

Table 5. Table S4. Polyphenolic compounds identified in the *Campomanesia xanthocarpa* Berg. fruits investigated by LC×LC-PDA-MS.

Peak numbering	Compound	[M-H]$^-$	λ max (nm)	^{1}tR (min)	^{2}tR (min)	Guabiroba unripe	Guabiroba ripened	Literature data
1	Gallic acid [a]	169	203, 272	26	0.256	X	X	-
2	Catechin [a]	289	203, 278	37	0.428	X	X	-
3	Hesperidin [a]	609	203, 276	42	0.443	X	-	-
4	Epicatechin [a]	289	206, 275	42	0.703	X	X	-
5	Quercetin 3-*O*-glucoside [a]	463	207, 256, 354	47	0.556	X	X	-
6	Isorhamnetin 3-*O*-glucoside [a]	477	206, 255, 354	47	0.685	X	X	-
7	Sinapic acid [a]	223	196, 255	48	0.289	X	-	-
8	Naringenin [a]	271	218, 293, 335	60	0.337	X	X	-
9	Quercetin [a]	301	204, 255, 371	66	0.383	X	X	-
10	Kaempferol [a]	285	220, 265, 367	67	0.384	X	X	-
11	Apigenin [a]	269	224, 336	69	0.377	X	X	-
12	Galloyl-bis-HHDP-hexoside (casuarinin) [b]	935	275	28	0.237	X	X	[8-10]
13	5-*p*-coumaroylquinic acid [b]	337	312	34	0.340	X	-	[6,7]
14	Quercetin 3-*O*-arabinopyranoside (guajaverin) [b]	433	255, 356	39	0.252	X	-	[2,4]
15	Myrciaphenone B [b]	481	271, 340	43	0.648	X	X	[9-11]
16	Epicatechin gallate [b]	441	203, 255, 367	44	0.413	X	-	[11]
17	Quercetin 3-*O*-xyloside (reynoutrin) [b]	433	258, 353	44	0.455	X	-	[7,9]

18	Myricetin 3-*O*-rhamnoside [b]	463	204, 275, 332	47	0.376	X	-	[8,10]
19	Kaempferol 3-*O*-glucoside [b]	447	262, 360	48	0.627	X	X	-
20	Ellagic acid-rhamnoside [b]	447	214, 278, 330	49	0.251	X	-	[8]
21	Isorhamnetin 3-*O*-rhamnoside [b]	461	254, 338	52	0.336	X	-	[7]
22	Guavinoside B [b]	571	216, 283, 348	54	0.476	X	X	[9-11]
23	7,3',4'-trihydroxyflavone [b]	269	214, 286	60	0.337	X	X	-
24	Biochanin A [b]	283	213, 261	65	0.419	X	X	-
25	Arbutin [b]	271	222, 290	67	0.495	X	-	-
26	Geraldone [b]	283	230, 333	72	0.580	X	X	[12]
27	Galangin [b]	269	214, 340	74	0.805	X	X	[13,14]
28	Hispidulin [b]	299	223, 272, 334	75	0.593	X	X	[14]
29	Methyl galangin isomer [b]	283	213, 255, 334	76	0.801	-	X	[14]
30	Methyl galangin isomer [b]	283	215, 257, 344	77	0.681	X	X	[14]
31	Sativol [b]	297	220, 338	79	0.684	X	X	-
32	*p*-Coumaric acid ethyl ester [b]	191	216, 294	29	0.276	-	X	[15]
33	Epigallocatechin [b]	305	271	40	0.361	-	X	[11]
34	Epigallocatechin 3-*O*-gallate [b]	457	211, 266	42	0.436	-	X	[10,11,13]
35	Hesperitin [b]	301	212, 364	62	0.919	-	X	-
36	Cirsimaritin [b]	313	276, 333	67	0.705	-	X	[14]
37	[6]-gingerol [b]	299	230, 279	84	0.805	-	X	[16]

[a] identified with commercial standards.
[b] identified using PDA, MS and literature data ("tentatively identified")

For hesperidin (no. 3), a concentration of 23.75 mg/100 g was found only in unripe guabiroba fruit. The aglycone (hesperitin, no. 35, 19.58 mg/100 g), in turn, was found in ripe fruits. A variation in polyphenolic compounds is mainly dependent on the biosynthesis and enzymatic regulation during the maturation. Some enzymes catalyze the breakdown of bonds between phenolic compounds and sugars, resulting in decreased concentration of glycosylated phenolics during maturation.

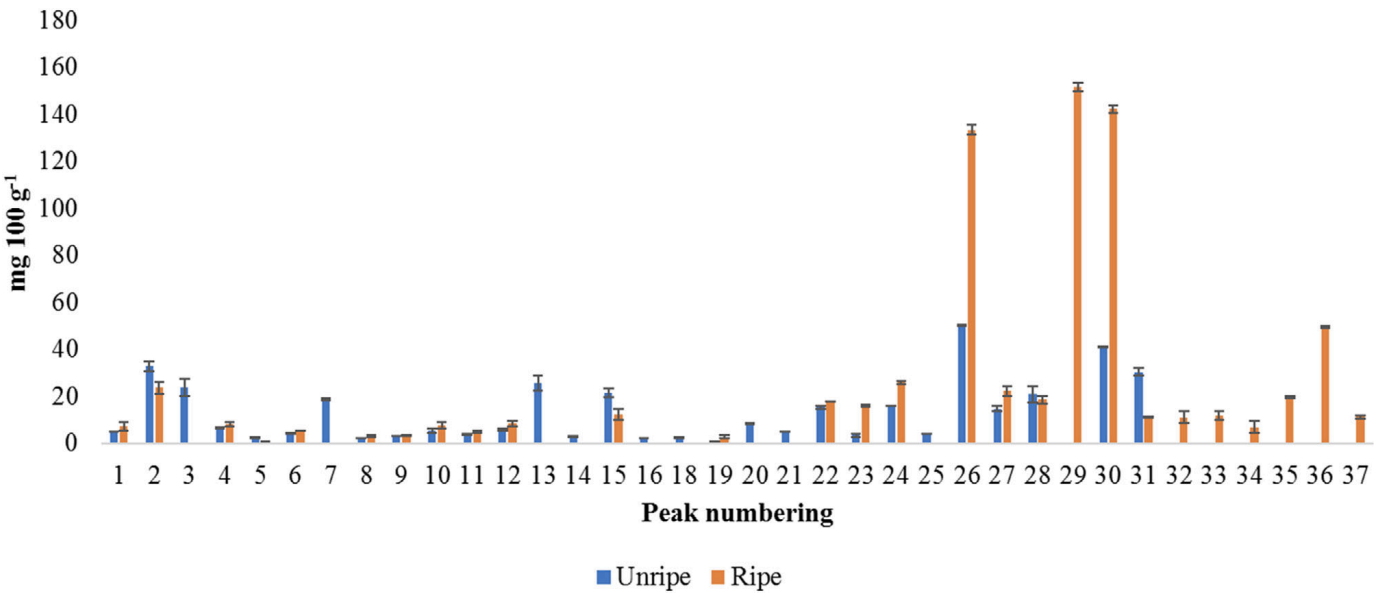

Figure 3. Quantitative analysis of the polyphenolic compounds in guabiroba extracts by LC×LC-PDA. Peak numbering in Table 5.

9.8.5 Antidiabetic and antioxidant properties

It is well-known that α-amylase and α-glucosidase are key enzymes linked to soluble carbohydrate digestion and associated glucose metabolism. Therefore, products with the capacity to inhibit these enzymes can be attractive for the treatment of postprandial hyperglycemia by slowing carbohydrate metabolism [42]. In this work, potential inhibitory activities of these two early stage digestive enzymes were investigated with extracts of freeze-dried ripe and unripe guabiroba.

In Figure 4 shows that the IC50 values of inhibition of α-amylase enzyme activity were 11.3 and 25.6 µg of unripe and ripe samples for millilitres of reaction, respectively.

During carbohydrate digestion, pancreatic α-amylases hydrlyze α-1-4 glucosidic linkages and, also release oligosaccharides with α-1-6-oligomers [42]. According to the literature [43,44], the analyzed samples were less efficient for α-amylase inhibition than acarbose (IC50 ≈ 3 μg/mL).

For α-glucosidase, the IC50 values were 117 and 169 μg of ripe and unripe guabiroba for millilitres of reaction, respectively (Figure 4A). During the carbohydrate digestion, α-glucosidase hydrolyze terminal α-1-4-linked glucose and release glucose in small intestine.

Therefore, it is necessary to inhibit this enzyme do decrease absorption of glucose in the small intestine [41]. Compared to acarbose, with IC50 ≈ 150 μg/mL [43,44], ripe and unripe guabiroba are regularly effective in inhibiting α-glucosidase.

For safe and effective management of postprandial hyperglycemia linked to type 2 diabetes, plant-based functional food should have moderate α-amylase and high α-glucosidase inhibitory activities [45]. This result clearly showed that guabiroba has the potential to be incorporated in functional foods or in dietary strategies for safe and cost-effective management of early stage type 2 diabetes and associated complications.

The inhibition capacity of the α-amylase enzyme showed by the guabiroba fruits have an inverse correlation to the 5-p-coumaroylquinic acid (−0.95), quercetin-3-Oglucoside (−0.94), epicatechin gallate (−0.96), myricetin-3-O-rhamnoside (−0.95), ellagic acid-rhamnoside (−0.97), sinapic acid (−0.97), arbutin (−0.95), and hispidulin (−0.93) content. On the other hand, the inhibition capacity of the α-glucosidase enzyme by the guabiroba fruits have an inverse correlation to the geraldone (−0.89), methyl galangin (−0.91), (-)-epigallocatechin 3-O-gallate (−0.89), cirsimaritin (−0.88), and [6]-gingerol (−0.89) content, suggesting that the presence of these polyphenolic compounds were responsible for the antidiabetic activity.

The ripe guabirobawas more active against α-glucosidase instead of unripe guabiroba, which was more active against α-amylase. These differences suggest that the inhibition of these enzymes depends on the nature of the phenolic compounds present in the fruits [43].

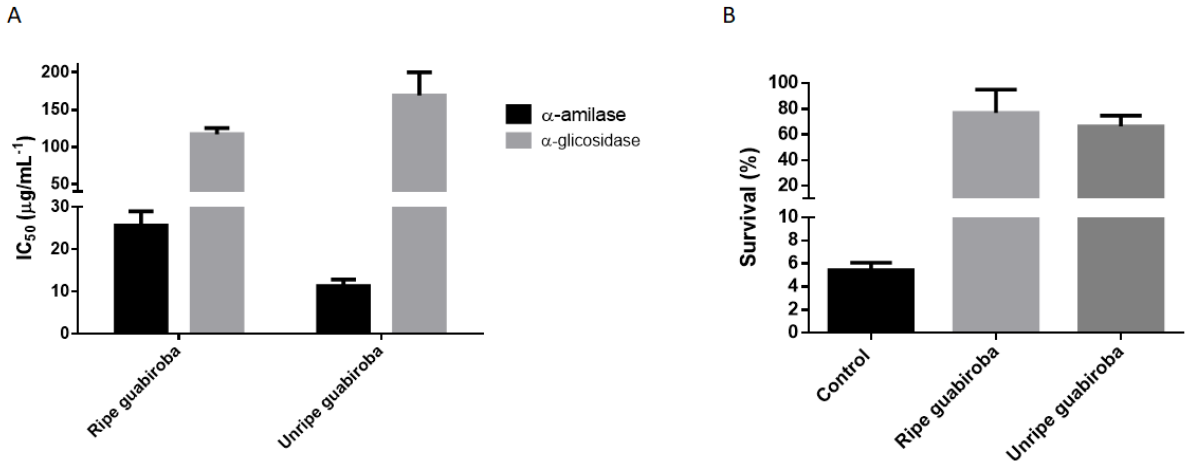

Figure 4. Half maximal inhibitory concentration (IC_{50}) of the α-amylase and α-glucosidase with ripe and unripe guabiroba extracts (A) and survival rates of Saccharomyces cerevisiae treated and untreated with guabiroba extracts and/or H_2O_2 (B).

The antioxidant effect of studied samples using yeast Saccharomyces cerevisiae as a simple cell model was also evaluated. Exponentially growing cells are very sensitive to oxidants due to catabolic repression exerted by glucose on the antioxidant defense system [46]. However, a previous treatment with an antioxidant would increase cell tolerance to oxidative stress. In this study, hydrogen peroxide (H_2O_2) was used, which generates oxidative stress, causes cell damage by the production of hydroxyl radicals via the Heber-Weiss/Fenton reaction. H_2O_2 is diffusible within and between cells in vivo, causing damage in membranes, organelles, and in cellular nucleus [47,48].

Thus, to analyze the capacity of guabiroba fruits to protect S. cerevisiae cells against damage, after inducing oxidative stress with H_2O_2, cell viability was determined with or without the presence of guabiroba extracts as chemoprotector.

Yeast cells showed sensibility to H_2O_2 (2 mmol/L) and only 5.4% were able to survive to the oxidative insult (Figure 4B). As shown in Fig. 2B, pretreatment with guabiroba extracts partially suppressed the damage triggered by H_2O_2. Especially ripe guabiroba increased 71% the survival rate compared to yeast cells exposed to H_2O_2 (without sample). Unripe guabiroba extract increased the survival rate by 61%.

The protective effect of polyphenols is supposed to be related to their large number of biological actions including antioxidant enzyme modulation [47]. In order to evaluate

the correlation between the phenolic profile and in vivo antioxidant activity, Pearson's linear correlations were applied. Significant correlations were not observed between the survival rate and the polyphenolic profile. This result indicates that the biological activity observed could be attributed to the mix of phenolic compounds present in studied samples, rather than to a single compound. According Baroni et al. [47], synergistic and antagonistic effects between different compounds could lead to different biological activities.

9.9. Conclusion

A simplex-centroid design proved to be an efficient tool for the optimization of the extraction of phenolics from guabiroba fruits. The extraction mixture comprised of aceteonitrile: 2% acetic acid (0.5:0.5, *v/v*) can be used to obtain extracts with high phenolics content from guabiroba. In addition, this is the first time that a quantitative LC×LC method has been implemented to characterize the phenolic fraction of ripe and unripe guabiroba fruits. The quantitative LC×LC developed method presented very good linearity, precision, reproducibility, recovery, and LODs and LOQs as low as 0.24 and 1.13 mg/L, respectively. By using this procedure, 37 different compounds separated and detected in the extracts studied were quantified. The polyphenolic composition of ripe and unripe guabiroba was strongly different, especially regarding the concentration of flavonoids.

Overall guabiroba showed regular α-amylase and high α-glucosidase inhibition that is potentially ideal for incorporation into dietary strategies for management of early stages of type 2 diabetes and its associated complications. This study suggests that guabiroba with its high antioxidant activity and rich phenolic profile potentially provides protection against microvascular complications. More research is needed to fully assess the real biological activity of polyphenols and other secondary metabolites presents in the fruits, especially as it was not possible to establish a correlation between the antioxidant effect of the fruit and its polyphenolic composition.

References

[1] A. M. Giulietti; R. M. Harley; L. P. De Queiroz; M. D. G. L. Wanderley; C. Van Den Berg. Conserv. Biol. 2005, 19, 632–639.

[2] E. P. da Silva; E. V. B. de Vilas Boas; L. J. Rodrigues; H. H. Siqueira. Ciência e Tecnol. Aliment. 2009, 29, 803–809.

[3] M. C. Pereira; R. S. Steffens; A. Jablonski; P. F. Hertz; A. De O. Rios; M. Vizzotto; S. Flôres. H., J. Agric. Food Chem. 2012, 60, 3061–3067.

[4] M. Silva Santos; J. J. De Lima; C. L. de Oliveira Petkowicz; L. M. Bileski Candido. Acta Sci. Agron. 2013, 35, 73–82.

[5] M. I. Valillo; P. R. H. Moreno; E. Oliveira; L. C. A. Lamardo, Ciência e Tecnol. Aliment. 2008, 28, 231–237.

[6] M. D. S. Santos; C. L. de O Petkowicz; G. Wosiacki; A. Nogueira; E. B. B. Carneiro; Acta Sci. Agron. 2007, 29, 617–621.

[7] K. Czaikoski; M. C. Mesomo; R. L. Krüger; C. L. Queiroga; M. L. Corazza. J. Supercrit. Fluids 2015, 98, 79–85.

[8] F. Cacciola; P. Donato; D. Sciarrone; P. Dugo; L. Mondello. Anal. Chem. 2017, 89, 414–429.

[9] F. Cacciola; P. Dugo; L. Mondello. TrAC Trends Anal. Chem. 2017, 96, 116–123.

[10] P. Cesla, J. Krenková. J. Sep. Sci. 2017, 40, 109–123

[11] B.W.J. Pirok; A.F.G. Gargano; P.J. Schoenmakers, J. Sep. Sci. 2018, 41, 68–98.

[12] L. Montero; M. Herrero. Anal. Chim. Acta 2018, 1083, 1–18

[13] F. Cacciola; F. Rigano; P. Dugo, L. Mondello. TrAC Trends Anal. Chem. 2020, 127, 115894.

[14] V. L. Singleton, J. A. J. Rossi. Am. J. Enol. Vinic. 1985, 16, 144–158.

[15] S. S. Abozed; M. El-kalyoubi, A. Abdelrashid, M. F. Salama. Ann. Agric. Sci. 2014, 59, 63-67.

[16] D. B. Uma; C.W. Ho; W. M. Wan Aida; SainsMalaysiana 2010, 39, 119–128.

[17] B. A. Acosta-Estrada; J. A. Gutiérrez-Uribe; S. O. Serna-Saldívar. Food Chem. 2014, 152, 46–55.

[18] C. L. Handa; F. S. De Lima; M. F. G. Guelfi; S. R. Georgetti; E. I. Ida. Food Chem. 2016, 197, 175–184.

[19] M. M. J. O. Wijekoon; R. Bhat; A. A. Karim. J. Food Compos. Anal. 2011, 24, 615–619.

[20] L. Montero; M. Herrero, M. Prodanov; E. Ibáñez, A. Cifuentes. Anal. Bioanal. Chem. 2013, 405, 4627–4638.

[21] Y. F. Wong; F. Cacciola; S. Fermas; S. Riga; D. James; V. Manzin; B. Bonnet; P. Marriott; P. Dugo; L. Mondello. Electrophoresis 2018, 39, 1993–2000.

[22] D. R. Stoll; P. W. Carr. Anal. Chem. 2017, 89, 519–531.

[23] M. Camenzuli; P. J. Schoenmakers. Anal. Chim. Acta 2014, 838, 93–101.

[24] X. Li; D. R. Stoll; P. W. Carr. Anal. Chem. 2009, 81, 845–850.

[25] L. Montero; V. Sáez; D. von Baer; A. Cifuentes; M. Herrero, J. Chromatogr. A 2018, 1536, 205–215.

[26] K. Arena; F. Cacciola; D. Mangraviti; M. Zoccali; F. Rigano; P. Dugo; L. Mondello. Anal. Bioanal. Chem. 2019, 411, 4819–4829.

[27] E. Lazzari; K. Arena; E. B. Caramão; M. Herrero, J. Chromatogr. A 2019, 1602, 359–367.

[28] K. Arena; F. Cacciola; F. Rigano, P. Dugo, L. Mondello. J. Sep. Sci. 2020, 43, 1781–1789.

[29] A. Marchelak; M. A. Olszewska; A. Owczare. J. Pharm. Biomed. Anal. 2020, 184, 113121

[30] ANVISA—Agência Nacional de Vigilância Sanitária, Resolution 166 of July 25th, 2017.

[31] S. C. Barauna; D. Delwing-Dal Magro; M. B. Brueckheimer; T. P.Maia; G. A. B. N. Sala; A. W. Döhler; M. C. Harger, D. F. M. de Melo; A. L. de Gasper; M. D. Alberton; D. A. Siebert; G. A., Micke; C. A. C. de Albuquerque, D. Delwing-De Lima, Metab. Brain Dis. 2018, 33, 1985–1994.

[32] F. F. de Araújo; I. A. Neri-Numa; D. de Paulo Farias; G. R. M. C. da Cunha; G. M. Pastore. Food Res. Int. 2019, 121, 57–72.

[33] A. Luque; S. C. Sebai; B. Santiago-Schübel; Y. Le Coz; D. Jenot; O. Ramaen; V. Sauveplane; R. Pandjaitan. Metab. Eng. 2014, 23, 123–135.

[34] H. N. Lee; S. A. Shin; G. S. Choo; H. J. Kim; Y. S. Park; B. S. Kim; S. K. Kim; S. D. Cho; J. S. Nam; C. S. Choi, J. H. Che; B. K. Park; J. Y. Jung. Int. J. Mol. Med. 2018, 41, 888–898.

[35] L. S. Sant'Anna; L. Merlugo; C. S. Ehle; J. Limberger; M. B. Fernandes; M. C. Santos; A. S. L. Mendez; F. R. Paula, C. M. Moreira; Evid. based Complement. Altern. Med. 2017, 2017, 1591762.

[36] J. A. De Sousa; L. S. da Prado; B. L. Alderete; F. B. M. Boaretto; M. C. Allgayer; F.M. Miguel; J. Y. De Sousa; N. P Marroni; M. L. B Lemes; D. S. Corrêa; A. de B. F. Ferraz; J. N. Picada. J. Toxicol. Environ. Health Part A 2019, 82, 62–74.

[37] J. Z. Klafke; R. L. D. Pereira; G. E. Hirsch; M. M. Parisi; F. G. Porto; A. S. de Almeida, F. H. Rubin; A. Schmidt; H. Beutler; S. Nascimento; G. Trevisan; I. Brusco; S. M. de Oliveira; M. M. M. F. Duarte; T. Duarte; P. R. N. Viecili. Phytomedicine 2016, 23, 1227–1234.

[38] T. Pastori; F. C. Flores; A. A. Boligon; M. L. Athayde; C. D. B. Da Silva; T. S. Do Canto-Dorow; S. B. Tedesco. Pharm. Biol. 2013, 51, 1249–1255.

[39] F. D Betta; P. Nehring; S. K. T. Seraglio; M. Schulz; A. C. Valese; H. Daguer; L. V. Gonzaga; R. Fett; A. C. O. Costa. Plant Foods Hum. Nutr. 2018, 73, 302–307.

[40] M. E. Arena; P. Postemsky; N. R. Curvetto. New Zeal. J. Bot. 2012, 50, 15–28.

[41] H. A. Bashir; A. B. A. Abu-Goukh. Food Chem. 2003, 80, 557–563.

[42] K. Hanhineva; R. Törrönen; I. Bondia-Pons; J. Pekkinen; M. Kolehmainen; H. Mykkänen, K. Poutanen. Int. J. Mol. Sci. 2010, 11, 1365–1402.

[43] L. Daniel Daza; A. Fujita; D. Granato; C. Silvia Fávaro-Trindade, M. Inés Genovese. Food Biosci. 2017, 18, 15–21.

[44] A. Fujita; D. Sarkar; S. Wu; E. Kennelly; K. Shetty; M. I. Genovese. Food Res. Int. 2015, 77, 194–203.

[45] M. D. S. Pinto; Y. I. Kwon; E. Apostolidis; F. M. Lajolo; M. I. Genovese; K. Shetty. J. Agric. Food Chem. 2008, 56, 4386–4392.

[46] M. D. Pereira; R. S. Herdeiro; P. N. Fernandes; E. C. A. Eleutherio; A. D. Panek. Biochim. Biophys. Acta Gen. Subj. 2003, 1620, 245–251.

[47] M. V. Baroni; R. D. Di Paola Naranjo; C. García-Ferreyra; S. Otaiza; D. A. Wunderlin. LWT - Food Sci. Technol. 2012, 47, 1–7.

[48] P. K. Wilmsen; D.S. Spada; M. J. Salvador. Agric. Food Chem. 2005, 53, 4757–4761.

10.0 Evaluation of matrix effect in one-dimensional and comprehensive two-dimensional liquid chromatography for the determination of the phenolic fraction in extra virgin olive oils

Olea europaea, meaning "European olive," is a small tree belonging to the family Oleaceae, occurring in the Mediterranean Basin. Olive oil is an essential component of a balanced diet because of its nutritional value. Among micronutrients, phenolic compounds did show important beneficial effects for human health. The majority of the research studies on the phenol content are carried out by liquid chromatography combined to photodiode array and/or mass spectrometry detection; however, because of matrix complexity, one-dimensional liquid chromatography cannot be sometimes sufficient to obtain rewarding separations, requiring more advanced analytical techniques. In this work, comprehensive two-dimensional liquid chromatography, incorporating RP-Amide and C18 stationary phases, in the first and second dimension, respectively, both under reversed phase conditions, was investigated for the determination of the phenolic fraction in extra virgin olive oil samples. As far as detection is concerned, triple quadrupole mass spectrometry was employed under multi reaction monitoring mode offering superior selectivity and sensitivity. The reduction of matrix effects, when using comprehensive two-dimensional liquid chromatography with respect to conventional one-dimensional liquid chromatography, was assessed by comparing the slopes of calibration curves built from standard solutions and spiked olive oil samples.

10.1. Introduction

Extra virgin olive oil (EVOO) is obtained from the fruits of the olive tree (*Olea europaea L.*) by cold mechanical pressing without further refining processes [1,2]. For commercial and health-related reasons, the authenticity of vegetable oils is of great importance, and chromatographic analysis of different compounds occurring in

vegetable oils, for example, fatty acids, triacylglycerols, waxes, and sterols, has been investigated [3].

EVOO is associated with the beneficial effects of a Mediterranean diet due to the presence of antioxidant molecules, including tocopherols (vitamin E), carotenoids, chlorophylls, and phenols [4]. The latter are minor EVOOs components and do show important features for the human health as they are known to reduce cardiovascular and atherosclerosis diseases, cancer risk, diabetes, obesity, and lung diseases; moreover, they display antimicrobial, antiinflammatory, and antioxidant properties that have been the topic of several studies [5,6]. Besides their nutritional benefits, phenolic compounds also protect the oil against autoxidation increasing shelf-life and are also responsible for the characteristic bitter and pungent taste of EVOOs [4,7]. The concentrations of phenolic compounds in EVOOs depend on many factors, for example, the olive cultivar, fruit ripening, geographic origin, and technological conditions [4,8,9].

Despite only the 2% of phenols are transferred from fruit to the EVOO, the phenolic fraction contains more than 36 structurally distinct phenolic compounds, including phenolic acids, phenyl ethyl alcohols, flavonoids, lignans, and secoiridoids [1,4,10]. Among the phenolic acids, gallic acid (GA), caffeic acid (CA), vanillic acid, sinapic acid, ferulic acid, and many others have been found in virgin olive oil [4, 11–13]. Phenolic ethyl alcohols are mainly represented by hydroxytyrosol (HTY) and tyrosol [4]. The intact olive fruit contains secoiridoids such as oleuropein (HTY-EA) and ligstroside. During mechanical pressing, hydrolysis reactions of the secoiridoids lead to the formation of the respective aglycons [4]. Oleuropein aglycon and ligstroside aglycone are present in EVOOs in the form of various isomers [2,14,15]; flavonoids are represented by apigenin (AP) and luteolin (LU), and, finally, lignans include pinoresinol and acetoxypinoresinol [4]. LC-MS is by far the most assessed analytical technique employed for EVOO phenolic fraction characterization; due to its high separation efficiency and short analysis time, capillary electrophoresis [16–18] has been used as well, even though information reported are quite meagre and limited.

Spectrophotometric methods were also employed for total phenolic content aswell as and various antioxidant tests, without providing any qualitative information about the phenolic compounds in the sample [19].

Due to the complexity of thematrix, 1D-LC could not completely resolve the hydrophilic phenols present in EVOOs, and the employment of more advanced analytical techniques would be beneficial especially if a proper quantification of such compounds in the EVOO samples is required [20].

As viable alternative for enhancing the overall separation capability, comprehensive 2D-LC (LC × LC) has been far employed for phenol determination in many food and natural products as witnessed by several recent research and review articles [21–34]. It was already reported that LC × LC minimize matrix interferences at the detector, because of the higher resolving power, *viz.* a minor number of coelutions [21,35]. Specifically, when dealing with atmospheric pressure ionization interface forMS, the effect of such interfering compounds on the detection of the target analytes is called matrix effect (ME). This aim of the work was the evaluation of the reduction in matrix-related signal suppression phenomena in LC × LC coupled to single and MS/MS detection; for the first time a direct comparison with conventional 1D-LC separation for the determination of the phenolic profile of EVOO samples is provided.

10.2 Materials and methods

10.2.1 Chemical and reagents

Commercial phenolic standards such as GA (purity > 98 %), CA (≥95 %), LU (≥90 %), and AP (≥98 %) were all purchased from Merck Life Science (Merck, Darmstadt, Germany). HTY (≥98 %) and HTY-EA (≥98 %) were attained from Extrasynthese (Genay, France). *n*-Hexane and methanol (MeOH) both reagent grade as well as acetonitrile (ACN), MeOH, ethanol (EtOH) and formic acid were all HPLC-MS

grade and were purchased from Merck Life Science (Merck KGaA, Darmstadt, Germany). Water (resistivity above 18 MΩ cm at 25 °C) was obtained from a Milli-Q SP Reagent Water System (Millipore, Bedford, MA, USA).

1D-LC separationswere carried out on an Ascentis Express C18 column (Merck Life Science (Merck KGaA, Darmstadt, Germany); 150 × 4.6 mm I.D., 2.7 μm d.p.). LC × LC separations were performed on an Ascentis RP-Amide column (150 × 2.1 mm I.D., 2.7 μm d.p., Merck Life Science (Merck KGaA, Darmstadt, Germany)) as first dimension (^{1}D) and an Ascentis Express C18 column (30 × 2.1 mm I.D., 2.7 μm d.p.; Merck Life Science (Merck KGaA, Darmstadt, Germany)) as second dimension (^{2}D).

10.2.2 Samples and sample preparation

Two extra virgin olive oils (EVOOs) samples produced in Sicily (Sample 1, Protected Denomination of Origin, Val di Mazara, Italy) and Apulia (Sample 2, Protected Denomination of Origin, Terra di Bari, Italy) were obtained from local producers.

Phenolic compounds were extracted from EVOOs by using a procedure reported by Klikarova et al. [15]. Briefly, 1.0 g (0.92 mL) of EVOO was diluted in 1 mL of n-hexane and mixed four times with 1 mL of MeOH/H2O (3:2, v/v) before centrifugation for 5 min at 4000 rpm. The polar phase was then collected and mixed with 2 mL of n-hexane. After centrifugation, the polar phase containing the extracted phenolic compounds were again separated, evaporated to dryness under vacuum, re-dissolved with 0.5 mL of MeOH, and filtered through a 0.45-μm nylon filter (Merck Life Science) prior to injection.

10.2.3 Instrumentation and software

Both LC and LC × LC analyses were carried out on a Nexera-e liquid chromatograph (Shimadzu, Kyoto, Japan), composed of a CBM-20A controller, one LC-Mikros binary

pump, two LC-30AD dual-plunger parallel-flow pumps, a DGU-20A5R degasser, a CTO-20AC column oven, and a SIL-30AC autosampler. Concerning detection, an LCMS- 8050 triple quadrupole mass spectrometer through an ESI source was employed (Shimadzu, Kyoto, Japan). For LC × LC analyses, the two dimensions were connected by means of two high speed/high pressure two-position, six ports switching valves with microelectric actuator (model FCV-32 AH, 1.034 bar; Shimadzu,Kyoto, Japan). Such valves were placed inside the column oven and equipped with two 50 µL stainless steel loops. A schematic of the Nexera-e liquid chromatograph system is displayed in Figure 1.

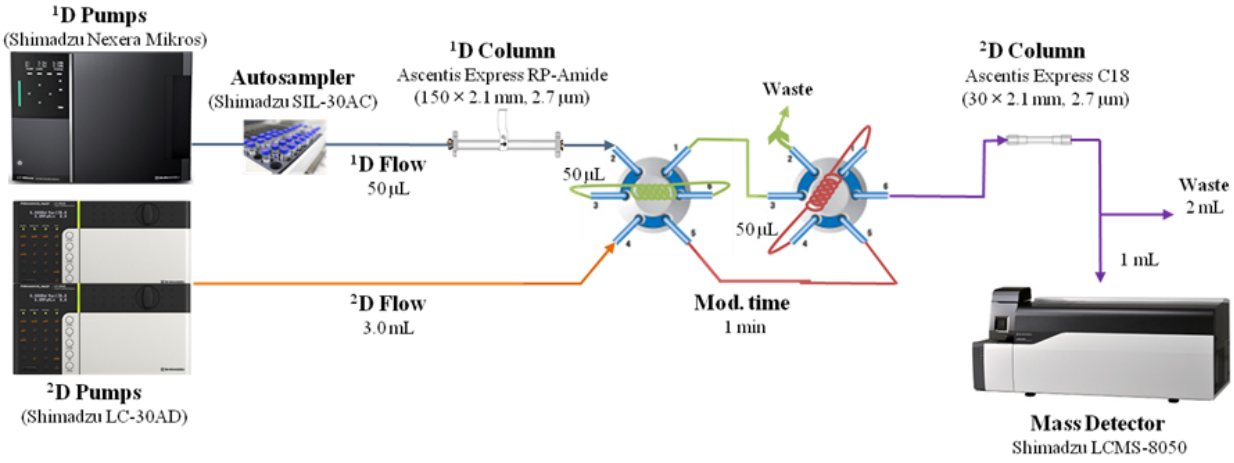

Figure 1. Schematic of the RP-LC×RP-LC system employed in this study.

10.3 Analytical conditions

10.3.1 LC separations

For 1D-LC separations run on the Ascentis Express C18 column, mobile phases consisted of (A) 0.1 % formic acid in water (pH 3), (B) 0.1 % formic acid in ACN, under the following gradient: 0 min, 10% B; 4 min, 35% B; 12 min, 47% B; 12.5 min,

60% B; 16 min, 75% B; 20 min, 100%. Mobile phase flow rate: 1 mL/min prior to MS detection. Column oven: 30 °C. Injection volume: 5 μL.

10.3.2 LC × LC separations

For ^{1}D separations, performed on the Ascentis RP-Amide column, mobile phases were as follows: (A) 0.1% formic acid in water (pH 3), (B) 0.1% formic acid in ACN. Gradient: 0 min, 2% B; 5 min, 2% B; 20 min, 30% B; 30 min, 50% B; 40 min, 50% B; 60 min, 70% B. Flow rate: 50 μL/min. Column oven: 30◦C. Injection volume: 5 μL. For ^{2}D separations, run on the Ascentis Express short C18 column, mobile phases were as follows: (A) 0.1% formic acid in water (pH 3), (B) 0.1% formic acid in ACN, under the following repetitive gradient: 0 min, 10% B; 0.70 min, 100% B; 0.80 min, 100% B; 0.81 min, 10% B. The flow rate employed was 3 mL/min split to 1.0 mL/min prior to MS detection. Modulation time of the switching valves: 1.00 min. Column oven: 30 °C.

10.3.3 Detection conditions

Interface: ESI-MS in negative ionization mode. Mass spectral range in full scan mode: *m/z* 50–800; event time: 0.25 s; nebulizing gas (N_2) flow: 3 L/min; drying gas (N_2) flow: 10 L/min; heating gas flow (air): 10 L/min; interface temperature: 300 °C; heat block temperature: 400 °C; desolvation line temperature: 250 °C.

The selected phenolic compounds were detected by selective ion monitoring (SIM) considering their anions produced in the negative ionization mode, further confirmed also, by comparison with the corresponding reference standard materials (Table 2). The transitions employed in the MS/MS experiments were selected on the basis of the product ion scan experiments, which provided the best and most intense daughter ions on the available standards using various collision energies (from −16 to −35 V) prior to be analyzed in the multiple reaction monitoring (MRM) mode (Table 2). The

selected ion form of the parent $[M-H]^-$ was transferred from the first quadrupole to the second one (collision chamber), and then the corresponding daughter ion was sent to the last quadrupole. The LCMS-8050 system was run simultaneously in both SIM and MRM modes.

Table 1. Phenols detected by ESI-MS/ analysis with Selected Ion Monitoring (SIM) *m/z* values, Multiple Reaction Monitoring (MRM) with quantifier (Q) and qualifier (q) transitions (Collision Energy V)

Compound	SIM^-	Qualifier	Quantifier
	m/z	MRM transition (CE) V	
GA	169	169> 73 (-23)	169> 125 (-16)
HTY	153	-	-
CA	179	179> 107 (-24)	179> 135 (-18)
HTY-EA	539	539> 307 (-22)	539> 377 (-18)
LU	285	285> 175 (-26)	285> 133 (-35)
AP	269	269> 150 (-25)	269> 117 (-35)

10.3.4 Data handling

The LC × LC-LCMS-8050 system and the switching valves were controlled by the Shimadzu Labsolution software (ver. 5.93). The LC × LC data were elaborated using Chromsquare ver. 2.3 software (Shimadzu).

Table 2. Figures of merit relative to the applied chromatographic methods for six standard compounds dissolved in pure solvent by LC-MS, LC-MS/MS, LC×LC-MS and LC×LC-MS/MS.

LC-MS									LC-MS/MS							
Compound	**Linearity range (mg L^{-1})**	**Slope**	**Intercept**	**R^2**	**LOD (mg L^{-1})**	**LOQ (mg L^{-1})**	**Intraday RSD (%) (n=3)**	**Interday RSD (%) (n=9)**	**Linearity range (mg L^{-1})**	**Slope**	**Intercept**	**R^2**	**LOD (mg L^{-1})**	**LOQ (mg L^{-1})**	**Intraday RSD (%) (n=3)**	**Interday RSD (%) (n=9)**
GA	0.1-5	7474296	543410	0.9982	0.017	0.056	0.73	1.52	0.005-10	1421783	46770	0.9992	0.001	0.003	0.10	1.54
HTY	0.1-5	5239288	187929	0.9994	0.030	0.099	1.87	3.24	-	-	-	-	-	-	-	-
CA	0.1-10	6985850	228103	0.9990	0.036	0.121	0.94	4.11	0.005-5	3989013	100186	0.9993	0.002	0.005	1.09	3.22
HTY-EA	0.01-2.5	26204898	400601	0.9991	0.002	0.006	1.04	4.25	0.001-5	7846212	27115	0.9998	0.0003	0.001	1.35	3.21
LU	0.01-2.5	31558531	2111431	0.9991	0.002	0.007	0.70	3.24	0.001-10	4587483	349681	0.9991	0.0003	0.001	0.62	2.54
AP	0.01-2.5	36051044	2898229	0.9993	0.002	0.008	0.17	2.58	0.001-10	5663229	45148	0.9997	0.0004	0.001	1.29	3.21
LC×LC-MS									**LC×LC-MS/MS**							
GA	1-25	2907089	1828626	0.9985	0.221	0.737	4.75	9.28	0.5-10	729558	267736	0.9992	0.054	0.180	1.33	4.21
HTY	1-25	1310083	2021733	0.9987	0.165	0.551	1.32	5.24	-	-	-	-	-	-	-	-
CA	0.5-25	4805541	314692	0.9990	0.110	0.367	2.20	5.31	0.1-10	1675583	163439	0.9991	0.015	0.048	0.17	3.12
HTY-EA	0.1-10	12082252	102596	0.9994	0.033	0.111	0.37	2.35	0.01-10	2706489	228212	0.9994	0.003	0.010	0.71	2.84
LU	0.1-10	15525498	1280434	0.9997	0.040	0.133	1.59	3.54	0.01-10	3435424	197535	0.9993	0.004	0.010	0.76	2.51
AP	0.5-10	17309209	8288064	0.9989	0.245	0.817	2.37	8.54	0.01-10	7378869	605208	0.9992	0.002	0.010	1.07	5.69

Table 3. Figures of merit relative to the applied chromatographic conditions for the six standard compounds dissolved in a blank sample by LC-MS and LC×LC-MS analyses.

Compound	Linearity range (mg L^{-1})	Slope	Intercept	R^2	LOD (mg L^{-1})	LOQ (mg L^{-1})	Intraday RSD (%) (n=3)	Interday RSD (%) (n=9)	Accuracy (%)
LC-MS									
GA	0.2-2.5	4397313	58775	0.9994	0.044	0.146	2.25	4.59	91.8
HTY	0.2-2.5	3502038	646229	0.9992	0.158	0.528	1.47	2.21	117.5
CA	0.2-2.5	6437483	457459	0.9997	0.110	0.369	0.29	1.28	116.6
HTY-EA	0.2-2.5	24737695	3117979	0.9994	0.037	0.124	2.04	5.26	119.4
LU	0.2-2.5	23393881	2213049	0.9998	0.082	0.274	0.57	1.58	86.5
AP	0.2-2.5	29134735	8801325	0.9994	0.159	0.529	0.51	1.56	124.5
LC×LC-MS									
GA	LOD>1	-	-	-	-	-	-	-	-
HTY	LOD>2.5	-	-	-	-	-	-	-	-
CA	0.2-2.5	3956322	135678	0.9992	0.027	0.089	2.60	6.24	93.7
HTY-EA	0.2-2.5	12497786	1255403	0.9982	0.021	0.068	3.76	7.24	126.1
LU	0.2-2.5	15624002	1337385	0.9967	0.034	0.112	5.48	7.85	88.8
AP	0.2-2.5	22494604	4890763	0.9990	0.053	0.176	2.58	4.58	126.7

Table 4. Figures of merit relative to the applied chromatographic conditions for the six standard compounds dissolved in a blank sample by LC-MS/MS and LC×LC-MS/MS analyses.

Compound	Linearity range (mg L^{-1})	Slope	Intercept	R^2	LOD (mg L^{-1})	LOQ (mg L^{-1})	Intraday RSD (%) (n=3)	Interday RSD (%) (n=9)	Accuracy (%)
LC-MS/MS									
GA	0.2-2.5	974905	6820	0.9987	0.011	0.037	3.34	3.36	71.1
HTY	LOD>0.2	-	-	-	-	-	-	-	-
CA	0.2-2.5	2641736	180623	0.9993	0.039	0.131	2.28	4.58	83.9
HTY-EA	0.2-2.5	2729742	437538	0.9998	0.078	0.259	0.48	3.25	64.7
LU	0.2-2.5	3470671	360411	0.9997	0.071	0.236	1.34	5.28	93.6
AP	0.2-2.5	3811789	1213292	0.9991	0.174	0.581	1.35	5.24	126.7
LC×LC-MS/MS									
GA	LOD>1	-	-	-	-	-	-	-	-
HTY	LOD>2.5	-	-	-	-	-	-	-	-
CA	0.2-2.5	1656180	105137	0.9994	0.349	1.16	6.89	11.51	108.7
HTY-EA	0.2-2.5	3182022	123672	1.0000	0.027	0.091	0.05	2.21	62.1
LU	0.2-2.5	2293243	249291	0.9999	0.015	0.051	2.92	4.15	96.9
AP	0.2-2.5	3206200	913228	0.9991	0.113	0.375	2.06	6.24	117.7

10.3.5 Method validation

The performance of the analytical method was accomplished through the assessment of different parameters, namely linearity, LOD, LOQ, precision (intra- and interday precision), and accuracy.

Stock solutions of each standard were prepared at a concentration of 1000 mg/L in EtOH. Calibration curves were constructed injecting each standard five times at a minimum of six different concentration levels between 0.001 and 25 mg/L, depending on the LOQ of eachmethod, and plotting peak area (1D-LC) or the area of 2D blob (LC × LC) against the concentration. In particular, the SIM chromatograms were used to validate the LC-MS and LC × LC-MS methods, while the MRM chromatograms, specifically the quantifier transitions corresponding to the most intense signals generated from the parent ions [M-H]−, were used to validate the LC-MS/MS and LC × LC-MS/MS methods. The monitored ions in SIM and the details about MRM transitions are provided in Table 1. Peak and blob were automatically integrated by Labsolution and Chromsquare software. Three different calibration curves were built for each analyte under each analytical condition (LC-MS, LC-MS/MS, LC × LCMS, and LC × LC-MS/MS) in an automatic way by the two software: one curve was built by injected pure standard dissolved in pure solvent, and another curve was obtained by injecting pure standards dissolved in a blank sample (cabbage oil was chosen as blank sample on the basis it does not contain the same phenolic compounds as EVOOs [36]) and one-third one was built by spiking the phenolic EVOO extracts with the standard compounds at the same concentration levels.

LODs and LOQs were calculated by using the calibration curve parameters: the SD of the response at the lowest level of the intercept of the corresponding calibration curve was divided by the average slope multiplied by a factor of 3 and 10, respectively [37]. Precision was evaluated considering the relative SD (% RSD) of peak areas obtained

for an intermediate level (2.5 mg/L) injected three times on the same day and three consecutive days (n = 9), for intra- and inter-day, respectively.

Accuracy (%) for each compound was calculated according to Eurachem guidelines [38] after addition of known amounts of all standards to the blank sample of cabbage oil. ME (%) was estimated by the following equation [39]:

$$ME(\%) = \left(\frac{B}{A}\right) \times 100 \quad \textbf{(1)}$$

where A is the slope of the calibration curve of the standards in pure solvent and B is the slope of the calibration curve of the standards spiked after the extraction of phenolic compounds from EVOO samples.

10.4 Results and discussion

10.4.1 RP-LC and RP-LC × RP-LC method validation

Taking into account that the aim of the present work was to highlight the benefits of the RP-LC × RP-LC technique over the conventional 1D-LC, both methods were optimized and subjected to method validation as reported in Section 10.3.5. For the 1D-LC separations performed on a partially porous C18 column, the profiles of the two EVOOs samples (along with one spiked sample) are illustrated in Figure 1. From a qualitative point of view, a similar profile in both cases was attained; particularly a sort of “mountain” at an analysis time from 3.5 to 10.5 min, more evident in Sample 2, Apulia, was observed probably due to matrix interferences. For this reason, in order to evaluate the ME, discussed previous, six different phenolic reference standards eluting in the all MS range were chosen. Notably, three out them, namely HTY-EA, LU, and AP are eluted in this specific region.

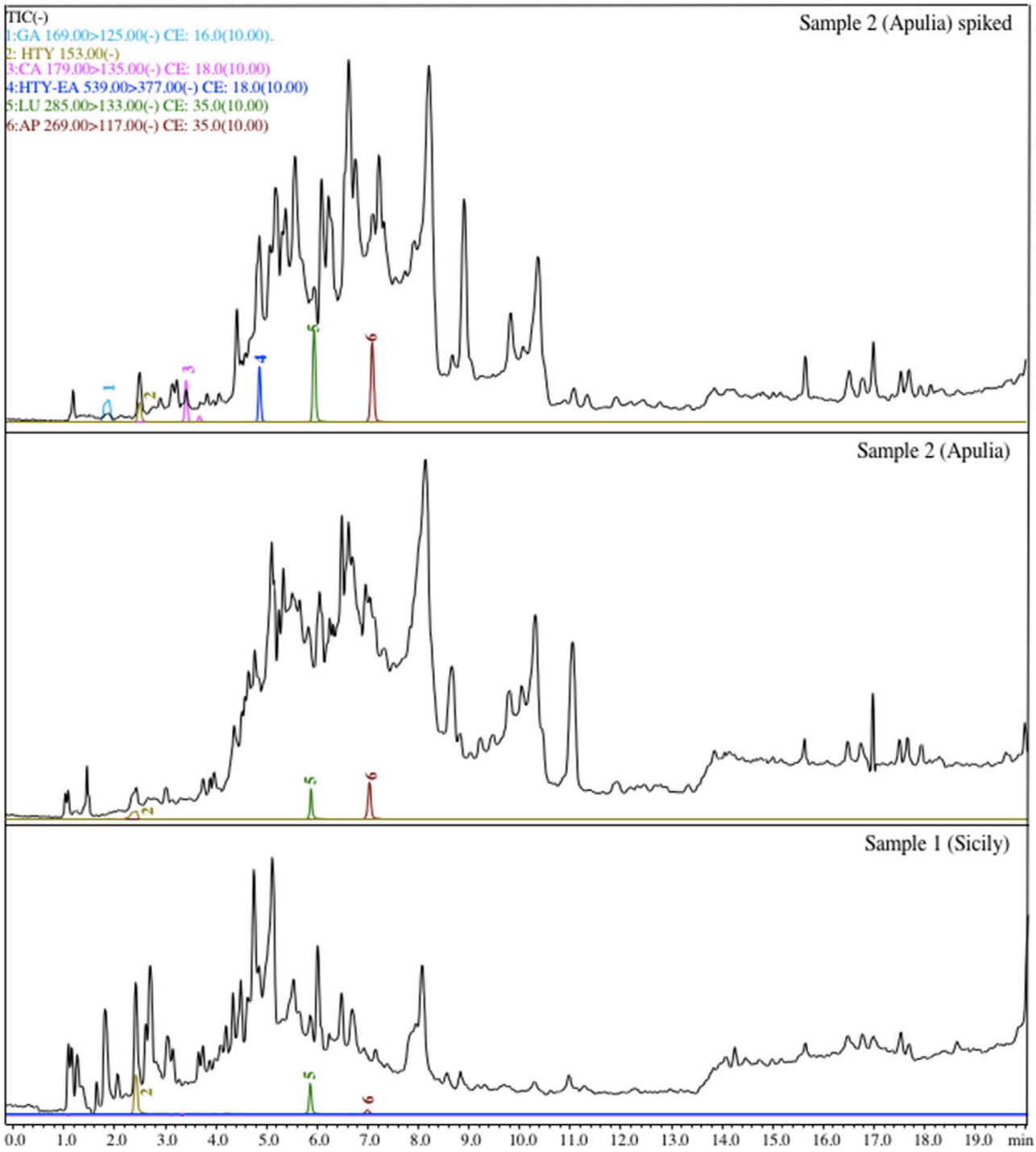

Figure 2. HPLC-MS chromatograms of the phenolic profile of EVOOs coming from Sicily (Sample 1) and Apulia (Sample 2, unspiked and spiked with six reference standards.

An RP-LC × RP-LC system, based on the use of RP conditions in both dimensions, was further investigated. In the ^{1}D, a flow rate of 50 µL/min ensured sufficient ^{1}D sampling, allowing not to impair the ^{1}D resolution. For the ^{2}D separations, the optimization was achieved by employing a fast gradient that was beneficial for

ensuring the elution of all sample components, thus avoiding "wrap-around" phenomena. First, based on the successful employment in the elucidation of various food samples [21,28,29,33], a "shift" gradient approach was employed. However, due to ineffective "peak focusing" this approach was not feasible for this kind of application (data not shown). As a consequence, a full-in-fraction gradient from 10 to 100%B from 0 to 0.80 min was employed and 12 sec was evaluated as sufficient for proper reconditioning time. All the validation parameters are reported in Table 1, Tables 2 and 3 considering calibration curves of six compounds dissolved in pure solvent and blank samples. One of them *viz.* hydroxytyrosol was not measured in MS/MS mode at concentration less than 1 and 2.5 mg/L, by 1D-LC and LC × LC, respectively, probably due to the small molecular structure and a certain degree of in-source fragmentation prior of the entrance in the MS analyzer. Then, only LC-MS and LC × LC-MS methods were validated for the determination of HTY. All calibration curves of the reference standards in pure solvent provided satisfactory linearity, with $R2$ values ≥0.9967 for all set-up tested, viz. by LC-MS, LC-MS/MS, LC × LC-MS, and LC × LC-MS/MS. Precision, evaluated as intra- and interday area repeatability at the lowest concentration level, was lower than 9.58% for all compounds dissolved in pure solvent (Table 2) and was still satisfactory in the blank sample (minor than 11.51%), as illustrated in Tables 3 and 4.

As for LOQs in pure solvent, the lowest values were observed for LC-MS and LC-MS/MS with an average of 50 ppb and 2.2 ppb, respectively. LC × LC-MS and LC × LCMS/ MS values for most of them were roughly 10 times higher (Table 2) compared to 1D-LC analysis, most likely due to chromatographic dilution as assessed in previous work [40].

In the blank sample, the influence of the chromatographic dilution can be counterbalanced by MEs, thus leading to comparable or even minor LOQs in the LC × LC set-up with respect to 1D-LC set-up. In our case, lower LOQs were achieved in LC × LC for HTY-EA, LU, and AP with both MS and MS/MS detection, whereas GA and HTY were never detected in LC × LC at concentrations lower than 1 and 2.5 mg/L,

respectively, due a prevalent chromatographic dilution. Then, the 1D-LC set-up should be chosen for their quantification and calibration curves at higher concentration levels were not build through the LC × LC set-up.

Finally, accuracy was also evaluated (Tables 3 and 4) showing for most of the standard compounds remarkable accuracy values ranging from 71.1 to 126.7 with the exception of HTYEA with values of 62.1 and 64.7 for compounds dissolved in blank sample as reported in Table 2.

10.4.2 Evaluation of MEs of the RP-LC×RP-LC method for determination of the phenolic compounds of extra virgin olive oils

ME may affect the signal response, resulting in either suppression or enhancement phenomena, thus leading to poor linearity, accuracy, and repeatability [41]. It has been established that a careful evaluation of ME is an essential step in any LC-MS based validation protocol. As a general approach, the whole analytical process must be optimized in each step in order to limit the effect of the interfering compounds occurring in the matrix. In fact, the interferences could increase the LOD and LOQ values and totally hamper analyte detection. Many authors have attempted to address such an issue with a meticulous sample-preparation step, especially with the use of new stationary phases [42]. Another approach consists of a different calibration strategy, for example, external calibration with internal normalization, through the addition of an internal standard, which should have a chemical structure and chromatographic retention as close as possible to those of the target analytes; specifically, isotopically labeled IS should be employed to achieve an accurate quantification. Unfortunately, their use is not widespread due to a lack of commercial standards or their high cost [39]. Other established approaches for overcoming such aspects are represented by the use of nano LC-EI-MS [43–45] and LC × LC-MS [21,35]. The former, born as an LC miniaturized technique, implies the use of flow rates in the ranges of nL/min, permitted a direct coupling to an electron ionization source without splitting requirements.

In the direct-EI-LC-MS interface, the ionization process occurs in the gas phase under high vacuum conditions without being influenced by co-eluted matrix compounds.

On the other hand, the LC × LC-ESI-MS technique, which has been constantly investigated in the last three decades, has in many cases outperformed the pitfalls of shotgun MS and LC-MS approaches for its selectivity and capability to eliminate matrix interferences, often under- or overestimated in quantitative determinations. Interestingly, the use of the MRM mode (in combination or not with chromatography) has become a valuable tool to ensure adequate analysis speed, low analysis costs, reduced sample volume, and common interferences without sample pretreatment. However, food and natural products matrices may contain interfering signals negatively influencing the accuracy/repeatability, leading sometimes to a total suppression of the signal. To this regard, the addition of a second LC separation dimension, as demonstrated in this work, can enhance the quantification capability in real-world samples. ME (%) was estimated by comparing the slopes of calibration curves built in pure solvent and matrix-matched according to the equation 1, and results are reported in Table 5. A value of 100% means the lack of ME, a value higher than 100% indicates a signal enhancement, while a value minor than 100% reveals signal suppression. In most cases, ion enhancement effects were observed especially for the sample 2 coming from Apulia with turned out to be the most complex in terms of matrix interferences (for instance, CA, LU, and AP, ME (%) = 137 by LC/MS and CA ME (%) = 153 by LC-MS/MS). Switching from the conventional LC to the LC × LC set-up, a significant reduction of ME% was attained as a result of the better analyte fractionation prior to either MS or MS/MS detection.

A peculiar behavior was attained for LC-MS/MS and LC × LC-MS/MS analysis of HTY-EA in both samples, which showed ME% values ranging from 44 to 57, probably due to a certain degree of in-source fragmentation that, besides being scarcely repeatable and highly affected by the matrix, decreases the intensity of the MRM transition, as previously observed for HYT.

Finally, ME% was out of a "normal" range (80–120%) also for GA that shows ion suppression by LC-MS in both Samples 1 (72%) and 2 (77%). The higher selectivity of MS/MS method increased ME% up to 89% and 83% in Samples 1 and 2, respectively. Then, the addition of a second dimension chromatographic separation allowed to obtain percentages very close to 100%, specifically a value of 104% was achieved in LC × LC-MS/MS in both samples. The attained results confirmed advantage arising from the use of a LC × LC set-up in minimizing matrix interferences.

Table 5. Matrix effect values (%) for each set-up investigated

	Sample 1				Sample 2			
Compound	**LC-MS**	**LC-MS/MS**	**LC×LC-MS**	**LC×LC-MS/MS**	**LC-MS**	**LC-MS/MS**	**LC×LC-MS**	**LC×LC-MS/MS**
GA	72	89	102	104	77	83	116	104
CA	104	81	100	102	137	153	106	107
HTY-EA	147	44	122	53	129	57	123	56
LU	113	103	102	100	137	80	93	110
AP	119	107	113	100	137	130	91	106

10.5 Conclusions

The developed application demonstrates how LC × LC can be used to significantly improve the separation of phenolic compounds contained in extra virgin olive oils compared to a 1D separation. The comparison of 1D-LC and LC × LC in combination with MS (single quadrupole) and MS/MS (multiple reaction monitoring) modes highlights how the LC × LC-MS/MS technique can be advantageously adopted for overcoming ME issues with minimal sample clean-up. Such methodology will be applied to a larger number of samples in order to highlight the differences between the phenolic compositions of extra virgin olive oils coming from different European Union (Italian) and non-European Union countries.

References

[1] Y. Ouni; A. Taamalli; A. M. Gomez-Caravaca; A. Segura-Carretero; A. Fernandez-Gutierrez; M. Zarrouk.Food Chem. 2011, 127, 1263–1267.

[2] S. Fu; A. Segura-Carretero; D. Arraez-Roman; J. A. Menendez; A. De La Torre; A. J. Fernandez-Gutierrez. Agric. Food Chem. 2009, 57, 11140–11147.

[3] R. Aparicio; R. Aparicio-Ruiz. J. Chromatogr. A 2000, 881, 93–104.

[4] M. El Riachy; F. Priego-Capote; L. Leon; L. Rallo; M. D. Luque de Castro. Eur. J. Lipid Sci. Technol. 2011, 113, 678–691.,

[5] M. I. Covas; K. Nyyssonen; H. E. Poulsen; J. Kaikkonen; H. J. f. Zunft; H. Kiesewetter; A, Gaddi; R, de la Torre; J. Mursu; H. Baumler; S. Nascetti; J. T. Salonen; M. Fito; J. Virtanen; J. Marrugat. Ann. Intern. Med. 2006, 145, 333–341.

[6] N. Kalogeropoulos; M. Z. Tsimidou. Antioxidants 2014, *3*, 387–413.

[7] G. Beltran; M. T. Ruano; A. Jimenez; M. Uceda; M. P. Aguilera. Evaluation of virgin olive oil bitterness by total phenol content analysis. Eur. J. Lipid Sci. Technol. 2007, 108, 193–197.

[8] C. Jimenez-Sanchez; J. Lozano-Sanchez; M. Bruggemann; M. Neves-Vieira; M. Rodriguez-Werner; E. Schmalfus; P. Winterhalter; A. Segura-Carretero ; A. Fernandez-Gutierrez. Eur. J. Lip. Sci. Technol. 2017, 119, 1500532.

[9] P. Reboredo-Rodriguez; E. Valli ; A. Bendini, G. Di Lecce; J. Simal-Gandara ; T. G. Toschi. (EU Reg. 432/2012). Eur. J. Lip. Sci. Technol. 2016, 118, 1593–1599.

[10] M. Bonoli; A. BendinI; L. Cerretani; G. Lercker; T. G. Toschi. J. Agric. Food Chem. 2004, 52, 7026–7032.

[11] A. Bianco; F. Buiarelli; G. Cartoni; F. Coccioli; R. Jasionowska; P. Margherita. J. Sep. Sci. 2003, 26, 409–416.

[12] A. Bianco; F. Buiarelli; G. Cartoni; F. Coccioli; R. Jasionowska; P. Margherita, P., J. Sep. Sci. 2003, 26, 417–424.

[13] A. Carrasco-Pancorbo; C. Neusus, M. Pelzing, A. Segura-Carretero, A., Fernandez Gutierrez. Electrophoresis 2007, 28, 806–821.

[14] G. Dierkes; S. Krieger; R.,Duck; A. Bongartz; O. J. Schmitz; H. J. Hayen. Agric. Food Chem. 2012, 60, 7597–7606.

[15] J. Klikarova; A. Rotondo; F. Cacciola; L. Česlova; P. Dugo; L. Mondello; F. Rigano. Food Anal. Meth. 2019, 12, 1759–1770.

[16] R. P. Monasterio; L. Fernandez Mde; M. F. Silva. J. Agric. Food Chem. 2013, 61, 4477–4496.

[17] R. Garcia-Villalba ; A. Carrasco-Pancorbo; A. Vazquez-Martin; C. Oliveras-Ferraros ; J. A. Menendez ; A. Segura-Carretero; A. Fernandez-Gutierrez. Electrophoresis 2009, 30, 2688–2701.

[18] A. Beutner; T. Herl; F. M. Matysik. Anal. Chim. Acta 2019, 1057, 18–35.

[19] G. Del Monaco; A. Officioso; S. D'Angelo; F. La Cara; E. Ionata; L. Marcolongo, G. Squillaci; L. Maurelli; A. Morana. Food Chem. 2015, 184, 220–228.

[20] A. Mastralexi; N. Nenadis; M. Z. Tsimidou. (EC Regulation 432/2012). J. Agric. Food Chem. 2014, 62, 2459–2461.

[21] P. Donato; F. Rigano; F. Cacciola; M. Schure; S. Farnetti; M. Russo; P. Dugo; L. Mondello. J. Chromatogr. A 2016, 1458, 54–62.

[22] F. Cacciola; S. Farnetti; P. Dugo; P. J. Marriott, P. J.; L. Mondello. J. Sep. Sci. 2017, 40, 7–24.

[23] F. Cacciola; P. Donato; D. Sciarrone; P. Dugo; L. Mondello. Anal. Chem. 2017, 89, 414–429.

[24] F. Cacciola; P. Dugo; L. Mondello. TrAC-Trends Anal. Chem. 2017, 96, 116–123.

[25] E, Sommella; O. Ismail; F. Pagano; G. Pepe; C. Ostacolo; G. Mazzoccanti; M. Russo; E. Novellino; F. Gasparrini; P. Campiglia. Sep. Sci. 2017, 40, 2188–2197.

[26] P. Česla ; J. Křenkova. J. Sep. Sci. 2017, 40, 109–123.

[27] B.W. J. Pirok; A. F. G. Gargano; P. J. Schoenmakers. J. Sep. Sci. 2018, 41, 68-98.

[28] Y. F. Wong; F. Cacciola; S. Fermas; S., Riga; D. James; V. Manzin; B. Bonnet, P. J. Marriott; P. Dugo; L. Mondello. Electrophoresis 2018, 39, 1993–2000.

[29] K. Arena; F. Cacciola; D. Mangraviti; M. Zoccali; F. Rigano; N. Marino; P. Dugo; L. Mondello. Anal. Bioanal. Chem. 2019, 411, 4819–4829.

[30] L. Montero; M. Herrero. Anal. Chim. Acta 2019, 1083, 1–18.

[31] P. F. Brandao; A. C. Duarte; R. M. B. O. Duarte. TrAC-Trend Anal. Chem. 2019, 116, 186–197.

[32] E. Lazzari; K. Arena; E. B. Caramao; M. Herrero. J. Chromatogr. A 2019, 1602, 59–367.

[33] M. Russo ; F. Cacciola ; K. Arena ; D. Mangraviti ; L. de Gara : P. Dugo, L. Mondello. Nat. Prod. Res. 2020, 34, 39–45.

[34] K. Arena; F. Cacciola; L. Dugo; P. Dugo; L.Mondello. Molecules 2020, 25, 1235–1246.

[35] R., Pascoe; J. P. Foley; A. I. Gusev. Anal. Chem. 2001, 73, 6014–6023.

[36] F. Cacciola; M. Beccaria; M. Oteri; M. Utczas; D. Giuffrida; N. Cicero; G. Dugo; P. Dugo; L. Mondello. Nat. Prod. Res. 2016, 30, 1646–1654.

[37] ANVISA-Agencia Nacional de Vigilancia Sanitaria, Resolution-899 of May 29, 2003, Brazil, 2003.

[38] Eurachem Guides. The Fitness for Purpose of Analytical Methods, 2nd Edition, Eurachem, Zug, Switzerland 2014.

[39] F. Gosetti, E. Mazzucco; D. Zampieri; M. C. Gennaro. J Chromatogr A 2010, 1217, 3929–3937.

[40] P. Dugo; F. Cacciola; P. Donato; D. Airado-Rodriguez; M. Herrero; L. Mondello. J. Chromatogr. A 2009, 1216, 7483–7487.

[41] H. Trufelli; P. Palma; G. Famiglini; A. Cappiello. Mass Spectrom. Rev. 2011, 30, 491–509.

[42] R. J. C. A. Steen; A. C. Hogenboom; P. E. G. Leonards; R. A. L. Peerboom; W. P. Cofino; U. A. Brinkman. J. Chromatogr. A 1999, 857, 157–166.

[43] M. Russo; F. Rigano; A. Arigo; D. Sciarrone; M. L. Calabro; S. Farnetti; P. Dugo;L. Mondello. J. Sep. Sci. 2016, 39, 2018–2027.

[44] F. Rigano; A. Albergamo; D. Sciarrone; M. Beccaria; G. Purcaro; L. Mondello. Anal. Chem. 2016, 88, 4021–4028.

[45] F. Rigano; P. Q. Tranchida; P. Dugo; L. Mondello. TrAC-Trends Anal. Chem. 20.

Annexes

Others articles/review not present in the thesis:

- Marina Russo, Francesco Cacciola, **Katia Arena**, Domenica Mangraviti, Laura de Gara, Paola Dugo, Luigi Mondello (2019)

"Characterization of the polyphenolic fraction of pomegranate samples by comprehensive two-dimensional liquid chromatography coupled to mass spectrometry detection."

Natural Product Research, 2020, Vol. 34(1), Pag. 39-45, DOI: 10.1080/14786419.2018.1561690 (I.F: 2.060).

- **Katia Arena**, Francesca Rigano, Domenica Mangraviti, Francesco Cacciola, Francesco Occhiuto, Paola Dugo, Luigi Mondello. (2020)

"Exploration of rapid evaporative-ionization mass spectrometry as a shotgun approach for the comprehensive characterization of Kigelia Africana (Lam) Benth. Fruit"

Molecules, 2020, Vol. 25(4), Pag. 962-981 DOI: 10.3390/molecules25040962 (I.F: 3.267)

- **Katia Arena**, Giuseppe Brancato, Francesco Cacciola, Francesco Crea, Salvatore Cataldo, Concetta De Stefano, Sofia Gama, Gabriele Lando, Demetrio Milea, Luigi Mondello, Alberto Pettignano, Silvio Sammartano. (2020)

"8-hydroxyquinoline-2-carboxylic acid as possible molybdophore: A multi-technique approach to define its chemical speciation, coordination and sequestering ability in aqueous solution."

Biomolecules, 2020, Vol. 10(6), Pag. 930-951 DOI: 10.3390/biom10060930 (I.F. 4.082)

- **Katia Arena,** Filippo Mandolfino, Francesco Cacciola, Paola Dugo, Luigi Mondello. (2020)

"Multidimensional liquid chromatography approaches for analysis of food contaminants."

Journal of Separation Science, 2020, Article in press.